

HYDROGRAPHIC OBSERVATIONS OF OXYGEN AND RELATED  
PHYSICAL VARIABLES IN THE NORTH SEA AND WESTERN  
ROSS SEA POLYNIA

INVESTIGATIONS USING SEAGLIDERS, HISTORICAL OBSERVATIONS AND  
NUMERICAL MODELLING



BASTIEN YVES QUESTE

PhD Candidate  
Centre for Ocean and Atmospheric Sciences  
School of Environmental Science  
University of East Anglia

SEPTEMBER 2013

This copy of the thesis has been supplied on condition that anyone who consults it is understood to recognise that its copyright rests with the author and that use of any information derived there from must be in accordance with current UK Copyright Law. In addition, any quotation or extract must include full attribution.

Bastien Yves Queste: *Hydrographic observations of oxygen and related physical variables in the North Sea and Western Ross Sea Polynya*, Investigations using Seagliders, historical observations and numerical modelling, © September 2013

**SUPERVISORS:**

Prof. Karen J. Heywood,  
Prof. Timothy D. Jickells,  
Dr. Liam Fernand

**LOCATION:**

Norwich, United Kingdom

## ABSTRACT

---

Shelf seas are one of the most ecologically and economically important ecosystems of the planet. Dissolved oxygen in particular is of critical importance to maintaining a healthy and stable biological community. This work investigates the physical, chemical and biological drivers of summer oxygen variability in the North Sea (Europe) and Ross Sea polynya (Antarctica). In particular, this work also focuses on the use of new autonomous underwater vehicles, Seagliders, for oceanographic observations of fine scale (a few metres) to basin-wide features (hundreds of kilometres).

Two hydrographic surveys in 2010 and 2011 and an analysis of historical data dating back to 1902 revealed low dissolved oxygen in the bottom mixed layer of the central North Sea. We deployed a Seaglider in a region of known low oxygen during August 2011 to investigate the processes regulating supply and consumption of dissolved oxygen below the pycnocline. Historical data highlighted an increase in seasonal oxygen depletion and a warming over the past 20 years. Regions showing sub-saturation oxygen concentrations were identified in the central and northern North Sea post-1990 where previously no depletion was identified. Low dissolved oxygen was apparent in regions characterised by low advection, high stratification, elevated organic matter production from the spring bloom and a deep chlorophyll maximum. The constant consumption of oxygen for the remineralisation of the matter exported below the thermocline exceeded the supply from horizontal advection or vertical diffusion. The Seaglider identified cross-pycnocline mixing features responsible for re-oxygenation of the bottom mixed layer not currently resolved by models of the North Sea. Using the data, we were also able to constrain the relative importance of different sources of organic matter leading to oxygen consumption.

From November 2010 to February 2011, two Seagliders were deployed in the Ross polynya to observe the initiation and evolution of the spring bloom. Seagliders were a novel and effective tool to bypass the sampling difficulties caused by the presence of ice and the remoteness of the region, in particular they were able to obtain data in the polynya before access was possible by oceanographic vessels. Seagliders were able to survey the region at a fraction of the cost and inconvenience of traditional ship surveys and moorings. We present observations of a large phytoplankton bloom in the Ross Sea polynya, export of organic matter and related fluctuations in dissolved oxygen concentrations. The bloom was found to be widespread and unrelated to the presence of Ross Bank. Increased fluorescence was identified through the use of satellite ocean colour data and is likely related to the intrusion of modified circumpolar deep water. In parallel, changes in dissolved oxygen concentration are quantified and highlight the importance of a deep chlorophyll maximum as a driver of primary production in the Ross Sea polynya. Both the variability of the biological features and the inherent difficulties in observing these features using other means are highlighted by the analysis of Seaglider data.

The Seaglider proved to be an excellent tool for monitoring shelf sea processes despite challenges to Seaglider deployments posed by the ice presence, high tidal velocities, shallow bathymetry and lack of accurate means of calibration. Data collected show great potential for improving biogeochemical models by providing means to obtain novel oceanographic observations along and across a range of scales.

## PUBLICATIONS

---

Some ideas and figures have appeared previously in the following publications:

- Smith Jr., W.O., Goetz, K., Kaufman, D., *Queste*, B.Y., Asper, V., Costa, D.P., Dinniman, M.S., Friedrichs, M.A.M., Hofmann, E.E., Heywood, K.J., Kohut, J.T., Lee, C.M. (2013) Multi-platform, Multi-disciplinary Investigations of the Ross Sea, Antarctica. *Oceanography, Breaking Waves (submitted)*.
- *Queste*, B.Y., Heywood, K.J., Kaiser, J., Lee, G.A., Matthews, A.J., Schmidtko, S., Walker-Brown, C., and Woodward, S.W. (2012) Deployments in extreme conditions: Pushing the boundaries of Seaglider capabilities. *Autonomous Underwater Vehicles (AUV)*, 2012 IEEE/OES, pp.1,7, 24-27 Sept. 2012. (*doi: 10.1109/AUV.2012.6380740*).
- *Queste*, B.Y., Fernand, L., Jickells, T.D., and Heywood, K.J. (2012) Spatial extent and historical context of North Sea oxygen depletion in August 2010. *Biogeochemistry (doi: 10.1007/s10533-012-9729-9)*.
- Asper, V., Smith, W., Lee, C., Gobat, J., Heywood, K., *Queste*, B.Y., Dinniman, M. (2011) Using gliders to study a phytoplankton bloom in the Ross Sea, Antarctica. *OCEANS 2011*, pp.1,7, 19-22 Sept. 2011.



## ACKNOWLEDGMENTS

---

The author thanks the crew, officers and scientists of the RV CEFAS Endeavour, RV Mytilus, the RV Roger Revelle, the RV Nathaniel B. Palmer and the RRS James Clark Ross as well all as the support staff on McMurdo base. Particular thanks also to Gareth Lee, Stephen Woodward, Dave Sivyer and Naomi Greenwood for technical training and support. Thanks also to Rodney Forster, Veronique Creach, Katy Owen and Andy Hind for help collecting samples during the North Sea surveys.

I am grateful for the support provided by iRobot, specifically Elizabeth Creed and the Maritime Support team, and members of the University of Washington, Fritz Stahr, Craig Lee, Jason Gobat and Geoffrey Shilling. Thanks also to the staff at the CSIC (Spain), Des Barton, SAMS (Scotland), Toby Sherwin and Estelle Dumont, Andy Thompson and the entire UEA Seaglider team.

These projects were funded through a Natural Environment Research Council (NERC) CASE studentship with CEFAS and the UEA through the NERC grant NE/H012532/1. Additional funding was provided through GENTOO NERC grant NE/H01439X/1 and European Union 7th Framework Programme (FP7 2007-2013), under grant agreement n.284321 GROOM. We are grateful for additional funding from CEFAS, and thank the UEA Science Faculty for the funding to purchase the 4 Seagliders. Additional funding was provided by an Antarctic Science bursary for the work in the Ross Sea. Antarctic Science Ltd. is a charitable company, registered in the UK (Charity Number 1090581), whose role is to promote Antarctic science nationally and internationally. The GOVARS project was funded by the US National Science Foundation's Office of Polar Programs (NSF-ANT-0838980).

ECMWF ERA-Interim data used in this study were obtained from the ECMWF data server (2011). Bathymetric data was obtained from General Bathymetric Chart of the Oceans (2010): The GEBCO\_08 Grid,

version 20100927 (<http://www.gebco.net>). Temperature, salinity, pressure and oxygen concentration data for the historical analysis were obtained from the International Council for the Exploration of the Sea Dataset on Ocean Hydrography (2011). Some of the research presented in this thesis was carried out on the High Performance Computing Cluster supported by the Research and Specialist Computing Support service at the University of East Anglia.

On a personal note, I wish to thank my supervisors, Prof. Karen Heywood, Prof. Tim Jickells and Dr. Liam Fernand, for the steadfast support provided during my PhD. Their enthusiasm and interest in this work, along with their patience and immense knowledge, made this thesis what it is now. Not only did they help me greatly during the research and writing of this thesis, but they encouraged me to explore all aspects of the topic and tangents that arose despite my tendency to get distracted. I would also like to thank my thesis examination committee, Dr. Martin White and Dr. Carol Robinson, for a very enjoyable and interesting examination and for taking the time and effort to carefully read this thesis.

I wish to thank my fellow work mates, particularly Ben and Nem, the Chrises, Nick, Rich, Phil, Sunke, Sian and Jenny. Thanks also to Manu, Claire, Becky and the whole CDO group for keeping me sane outside of the PhD. Finally, thanks to Sam and Josh, Seb and Agathe and Anne who played such important roles over the past four years for the continuous encouragement, patience and understanding. Last but not the least, I thank my parents and my sisters, without whom this thesis might not have been written, for their love, support and never-ending supply of critical and very necessary PhD survival kits. Merci !

# CONTENTS

---

i	INTRODUCTION	1
1	BACKGROUND AND MOTIVATION	3
1.1	Oxygen depletion in marine waters . . . . .	3
1.1.1	The importance of shelf seas . . . . .	3
1.1.2	Hypoxia . . . . .	4
1.1.3	Distribution of low oxygen systems . . . . .	6
1.1.4	Mechanisms regulating the decline and supply of dissolved oxygen . . . . .	7
1.1.5	Long-term impacts of severe oxygen depletion .	12
1.1.6	Recovery and return to normoxia . . . . .	13
1.2	Context . . . . .	16
1.2.1	The North Sea . . . . .	16
1.2.2	The Ross Sea . . . . .	19
1.2.3	Seagliders for ocean monitoring . . . . .	21
1.3	Rationale . . . . .	23
ii	SEAGLIDERS	25
2	SEAGLIDERS AS TOOLS FOR OCEANOGRAPHIC RESEARCH	29
2.1	The instrument . . . . .	29
2.2	Data correction method . . . . .	37
2.2.1	Influence of platform characteristics on data quality . . . . .	37
2.2.2	Timestamps . . . . .	39
2.2.3	Data flagging and binning . . . . .	40
2.2.4	Sensor lag correction . . . . .	40
2.2.5	Temperature, Conductivity and Chlorophyll <i>a</i> sensor calibration . . . . .	42
2.2.6	Dissolved Oxygen . . . . .	43
3	DEPLOYMENTS IN EXTREME CONDITIONS: PUSHING THE BOUNDARIES OF SEAGLIDER CAPABILITIES ( <i>published</i> )	47
3.1	Introduction . . . . .	47

3.2	Deployments . . . . .	48
3.2.1	Seagliders . . . . .	51
3.2.2	Scotland Trials . . . . .	54
3.2.3	GOPINA - Iberian upwelling . . . . .	55
3.2.4	North Sea Hypoxia . . . . .	59
3.2.5	Tropical DISGO - Indian Ocean . . . . .	60
3.2.6	GENTOO - Weddell Sea . . . . .	61
3.3	Dealing with data . . . . .	63
3.4	Summary . . . . .	66
iii	THE CENTRAL NORTH SEA	67
4	SPATIAL EXTENT AND HISTORICAL CONTEXT OF NORTH SEA OXYGEN DEPLETION IN AUGUST 2010 ( <i>published</i> )	69
4.1	Introduction . . . . .	69
4.2	Materials and methods . . . . .	75
4.2.1	Sample collection and analysis . . . . .	75
4.2.2	Historical data . . . . .	77
4.3	Results and Discussion . . . . .	78
4.3.1	Hydrography of the North Sea in August 2010 .	78
4.3.2	Historical records of oxygen concentrations in the North Sea . . . . .	84
4.3.3	Drivers of oxygen depletion in the central North Sea . . . . .	88
5	DRIVERS OF SUMMER OXYGEN DEPLETION IN THE CENT- RAL NORTH SEA	95
5.1	Introduction . . . . .	95
5.2	Methods . . . . .	100
5.2.1	Survey . . . . .	100
5.2.2	GOTM-BFM . . . . .	106
5.3	Results and discussion . . . . .	109
5.3.1	Supply of oxygenated water . . . . .	109
5.3.2	Sources of oxygen consumption . . . . .	123
5.3.3	Conclusion . . . . .	130
iv	THE WESTERN ROSS SEA POLYNIA	133
6	HYDROGRAPHY OF THE WESTERN ROSS POLYNIA	135

6.1	Introduction . . . . .	135
6.2	Methods . . . . .	138
6.2.1	Sampling . . . . .	138
6.2.2	Data Processing . . . . .	141
6.3	Results and Discussion . . . . .	155
6.3.1	Hydrography of the Ross Sea polynya . . . . .	155
6.3.2	Location and timing of phytoplankton bloom and production . . . . .	159
6.3.3	Controls on the timing of the austral spring bloom	165
6.3.4	Watermass properties and distribution of chlorophyll <i>a</i> . . . . .	168
6.3.5	Variability within the Ross Sea polynya . . . . .	171
6.3.6	Dissolved oxygen change within the water column	176
6.4	Conclusion . . . . .	181
V	CONCLUSIONS	183
7	SUMMARY AND OUTLOOK	185
7.1	The North Sea . . . . .	185
7.2	The Ross Sea . . . . .	187
7.3	Physical drivers of dissolved oxygen variability . . . . .	189
7.4	Seagliders as tools for ocean observation . . . . .	191
	BIBLIOGRAPHY	197

## LIST OF FIGURES

---

Figure 1.1	Median lethal oxygen concentration ( $LC_{50}$ , in $\mu\text{mol dm}^{-3}$ ) among four different taxa. The box runs from the lower ( $Q_1$ , 25%) to the upper ( $Q_3$ , 75%) quartile and also includes the median ( <i>thick vertical line</i> ). The range of data points not considered outliers is defined as 1.5 times the difference between the quartiles ( $Q_3 - Q_1$ ), also known as interquartile range (IQR). The whiskers show the location of the lowest and highest datum within this range, i.e., $1.5 * \text{IQR}$ . Shaded diamonds are outliers as per this definition. Redrawn after Vaquer-Sunyer and Duarte (2008). Copyright (2008) National Academy of Sciences, U.S.A. Figure and caption taken from Keeling et al. (2010). . . . .	5
Figure 1.2	Global distribution of 400-plus systems that have scientifically reported accounts of being eutrophication-associated dead zones. Their distribution matches the global human footprint [the normalized human influence is expressed as a percent] in the Northern Hemisphere. For the Southern Hemisphere, the occurrence of dead zones is only recently being reported. Details on each system are in tables S1 and S2 in Diaz and Rosenberg (2008). Figure and caption taken from Diaz and Rosenberg (2008) . . . . .	7

Figure 1.3 Schematic of interactions of open ocean oxygen minimum zones (Oxygen Minimum Zone (OMZ), red) with hypoxic shelf systems (Diaz and Rosenberg, 2008) on continental shelves of eastern ocean boundaries. Figure and caption taken from Stramma et al. (2010). . . . . 8

Figure 1.4 (a) Colours indicate O<sub>2</sub> concentrations at the depth of minimum O<sub>2</sub>. (b) Depth of the 60 μmol dm<sup>-3</sup> isoline in metres. Based on data from World Ocean Database, 2001 (Conkright et al., 2002). Figure and caption taken from Keeling et al. (2010). . . . . 8

Figure 1.5 Bathymetry of the North Sea and surrounding area. Depth contours have been added for the 20, 40, 80 and 160 m isobaths. A more detailed figure is provided in Ch. 4. Locations of Dogger Bank (DB) and the Norwegian Trench (NT) are also indicated. . . . . 17

Figure 1.6 Bathymetry of the Ross Sea and surrounding area. Depth contours have been added for the 200, 400, 600, 800 and 1000 m isobaths. A more detailed figure is provided in Ch. 6. . . . . 20

Figure 2.1 Four Seaglidors in their handling cradles being prepared for a trial launch in Puget Sound, WA USA. The Seaglidors are pointing nose down, with the red aerial extending towards the sky. The rudder is visible just below the antenna and the wings further below extending to either side. On the top side of the Seaglidors, in between both wings is the Seabird CT sail. . . . . 30

Figure 2.2	Schematic side view of a Seaglider with the wing shape provided above for reference and position of the sensors. The antenna mast is shown separately above the fairing and pressure hull. Figure and caption adapted from Eriksen et al. (2001). . . . .	31
Figure 2.3	UEA Seaglider system structure. The Seaglider data are processed in near real-time and feeds back to the pilots for adjustment of piloting and sampling commands. New orders are then downloaded by the glider for the following dive. Processing is automated on a central server hosted at the UEA, the basestation, and data are disseminated to national data centres for operational purposes and are displayed online for public outreach. . . . .	32
Figure 2.4	Canonical Seaglider dive. Figure taken from IRobot (2012). . . . .	35
Figure 2.5	Detail of the basestation data processing routines and data dissemination methods. . . . .	36
Figure 3.1	UEA Seaglider deployments and collaborations. 1-3: Scotland Trials. 4: GOPINA. 5: GOVARS, a collaboration with the Virginia Institute of Marine Science and the University of Washington (Asper et al., 2011). 6-7: North Sea. 8: Tropical DISGO. 9: GENTOO, also involving iRobot and the California Institute of Technology. 10: OSMOSIS (scheduled autumn 2012). . . . .	53
Figure 3.2	A thick algal mat covering the Seaglider upon recovery. Growth on the Aanderaa optode may also have contributed to the sensor drift. . . . .	56

Figure 3.3 Pre (top) and post (bottom) sensor drift correction output of the Aanderaa 4330F. A net time-dependent shift is visible indicating gradual sensor drift throughout the mission. The black line represents mean values. Sensors were calibrated against Winkler titrations performed at repeated CAIBEX transect stations. . . . . 58

Figure 3.4 Map of Seaglider GPS positions (red) and ARGOS positions (black) with significant dates during the GENTOO mission. . . . . 62

Figure 3.5 Successive sampling of devices with associated timelags and warm-up delays for a standard sensor payload on the Seaglider 1KA. . . . . 65

Figure 4.1 Bathymetry of the study area in metres (GEBCO, 2010). Circles mark the 88 sampling locations. The black line indicates the order of stations sampled, starting from the south and the dotted grey line the section used in Fig. 4.3. Depth contours have been added for the 20, 40, 80 and 160 m isobaths. Positions of the two SmartBuoy described by Greenwood et al. (2010) are indicated as North Dogger (ND) for the North Dogger site and Oyster Grounds (OG) for the Oyster Grounds site. A & B: Shetland and Orkney Isles. C: Humber estuary. D: the Channel. E: Dogger Bank. F: Norwegian Trench. G: German Bight. H: Skagerrak . . . . . 72

Figure 4.2	General circulation of the North Sea (adapted from Turrell et al., 1992 and Hill et al., 2008) overlaid on the density difference between the Surface Mixed Layer (SML) and Bottom Mixed Layer (BML) in $\text{kg m}^{-3}$ . FIC: Fair Isle Current, DC: Dooley Current, SCC: Scottish Coastal Current, CNSC: Central North Sea Current, SNSC: Southern North Sea Current. Hatch marks cover areas not subject to thermal stratification . . .	73
Figure 4.3	Results from surface and bottom waters sampled during all CTD casts from the shallowest 3m and the deepest 3m of the water column. (a) Deepest and (b) shallowest temperature ( $^{\circ}\text{C}$ ). (c) Deepest and (d) shallowest salinity. . . . .	79
Figure 4.2	<b>cont.</b> Results from surface and bottom waters sampled during all CTD casts from the shallowest 3m and the deepest 3m of the water column. (e) Deepest and (f) shallowest oxygen concentration ( $\mu\text{mol dm}^{-3}$ ). (g) Deepest oxygen saturation (%) and (h) temperature difference between surface and bottom mixed layers ( $^{\circ}\text{C}$ ). The 70% saturation contour line is included to highlight the similarity in spatial extent	80
Figure 4.3	North-south section of selected parameters: (a) potential temperature ( $^{\circ}\text{C}$ ), (b) oxygen concentration ( $\mu\text{mol dm}^{-3}$ ) and (c) oxygen saturation profiles (%). Section position is indicated by the grey dotted line in Fig. 1. Station positions are indicated by dotted lines in this section and by circles in Fig. 1. Density contours are depicted for reference. Stations nearest to the ND and OG sites are indicated as well as the position of the Dogger Bank . . . . .	81

- Figure 4.4 5-yearly values of an 11-year running mean of (a) summer BML temperature ( $^{\circ}\text{C}$ ), (b) oxygen concentration ( $\mu\text{mol dm}^{-3}$ ) and (c) oxygen saturation (%) in the stratified central North Sea, subdivided into ICES grid squares (Fig. 6). Only data from the months of June to September below 30 m, in regions deeper than 45m and in grid squares north of  $56^{\circ}\text{N}$  with over 5 data points were retained for analysis (total of 16250 measurements). Error bar length is equal to two standard errors. The horizontal line indicates the overall mean of the time-series. Standard deviation and number of grid squares retained are indicated below each data point . . . 85
- Figure 4.5 Mean summer bottom oxygen saturation values (%) from (a) 1900 to 1990 (10425 data points over 199 grid squares) and (b) 1990 to 2010 (21057 over 133 grid squares). Change in bottom oxygen saturation (c) and temperature (d) between the first and the second periods . . . 86
- Figure 5.1 BML oxygen saturation (%) and with the 70% saturation contour during the August 2010 (a) and August 2011 surveys (b), mean summer bottom oxygen saturation values (%) from 1900 to 2010 from the ICES database (c) and mean summer bottom oxygen saturation values (%) from 1958 to 2008 from the GETM-ERSEM model output using ERA interim reanalysis data (d). 99

Figure 5.2	<p>Bathymetry of the study area in metres (GEBCO, 2010). Depth contours have been added for the 20, 40, 80 and 160 m isobaths. The region where the glider was deployed is indicated by the large white dot at approximately 57° N 2°30' E. Major land marks are indicated as A &amp; B: Shetland and Orkney Isles. C: Humber estuary. D: the Channel. E: Dogger Bank. F: Norwegian Trench. G: German Bight. H: Skagerrak. The general circulation of the North Sea (adapted from Turrell et al., 1992 and Hill et al., 2008) is overlaid as arrows for FIC: Fair Isle Current, DC: Dooley Current, SCC: Scottish Coastal Current, CNSC: Central North Sea Current, SNSC: Southern North Sea Current. Hatch marks cover areas not subject to thermal stratification in summer. . . . .</p>	101
Figure 5.3	<p>Linear regression of TCPhase from the CEFAS Endeavour's oxygen optode and corresponding median Winkler titration triplicate pseudo-CalPhase back-calculated using the optodes's foil coefficients (<i>blue line</i>) and manufacturer's calibration (<i>dotted black line</i>). Due to poor experimental handling, many sets of replicates had high standard deviations. Blue dots indicate the 21 sets of replicates used in the linear regression (standard deviation less than <math>0.1 \text{ ml l}^{-1} / 4.47 \text{ } \mu\text{mol dm}^{-3}</math>). Phase coefficient 0 = -2.856, phase coefficient 1 = 1.0472. <math>R^2 = 0.87</math>. . . . .</p>	104

Figure 5.4 Temperature (a), salinity (b), potential density (c) and Dissolved Oxygen (DO) profiles (d) of the final dive for SG510. Glider observations as output by the iRobot processing are in red. Glider observations after calibration by the UEA toolbox are in blue. The dotted red line is iRobot processed DO offset for ease of comparison with calibrated data. The greatest difference between the iRobot processed data and the UEA toolbox data is located near the thermocline. The UEA toolbox provides additional corrections for thermal lag and inertia of sensors as well as corrects offsets in timestamps for each sensor providing synchronous temperature, conductivity and oxygen optode phase measurements for calculation of seawater properties. 105

Figure 5.5 Schematic representation of forcing and feedback between General Ocean Turbulence Model (GOTM) and European Regional Seas Ecosystem Model (ERSEM) (*top*) and schematic of the interactions between containers and functional groups within ERSEM (*bottom*). . . . . 108

Figure 5.6 3-day composite of MODIS Aqua daytime sea surface temperature at 11  $\mu\text{m}$  ( $^{\circ}\text{C}$ , a and b) and chlorophyll a concentration ( $\text{mg m}^{-3}$ , c and d) across the entire North Sea (*left*) and around the Seaglider deployment area (*right*) from the 20<sup>th</sup> to 22<sup>nd</sup> of August 2011. The colour scale for the North Sea map of chlorophyll a is logarithmic to highlight chlorophyll a distribution in the central North Sea where concentrations are low. Northward Seaglider track is indicated by the black line. . . . . 110

Figure 5.7 Seaglider section of salinity (PSU) sampled along the transect. . . . . 112

Figure 5.8	Seaglider section of DO saturation (%) sampled along the transect. . . . .	112
Figure 5.9	Seaglider section of chlorophyll a concentration ( $\text{mg m}^{-3}$ ) sampled along the transect. . .	115
Figure 5.10	Seaglider section of potential density ( $\text{kg m}^{-3}$ ) sampled along the transect. . . . .	115
Figure 5.11	Seaglider section of temperature ( $^{\circ}\text{C}$ ) sampled along the transect. . . . .	119
Figure 5.12	Seaglider temperature ( $^{\circ}\text{C}$ , a), salinity (PSU, b), chlorophyll a ( $\text{mg m}^{-3}$ , c) and DO concentration ( $\mu\text{mol dm}^{-1}$ , d) along isobars at 1 dbar intervals from 45 dbar to 71 dbar, coloured by pressure. Black vertical lines indicate the difference between minimum and maximum values at each time step. Binned data from the BML (45 dbar and below) are plotted against time and coloured by pressure. This highlights a vertical gradient in all four properties observed. Temperature and chlorophyll a were highest near the thermocline while salinity and DO increased with depth. Alongside, the extent of the vertical gradient for each property is shown by the black vertical lines. This illustrates changes in vertical gradients; a small value indicates a homogenous BML while a large value indicates a strong vertical gradient in the BML. We can clearly see events where the temperature gradient increases in the BML, showing injection of warmer surface water across the thermocline. . . . .	120

- Figure 5.13 Tidal velocities ( $\text{m s}^{-1}$ , a), 10 m wind speed ( $\text{m s}^{-1}$ , b), sea surface temperature ( $^{\circ}\text{C}$ , c) and sea surface salinity (PSU, d) and depth (m, e) at the Seaglider's location during the survey. Tidal data was obtained from the TMD tide toolbox and OTIS European Shelf Model (Egbert et al., 2010). Wind data was obtained from European Centre for Medium-Range Weather Forecasts (ECMWF) ERA-Interim reanalysis data. Bathymetry was gathered by the Seaglider's on-board acoustic altimeter. . . . . 121
- Figure 5.14 GOTM-Biogeochemical Flux Model (BFM) temperature ( $^{\circ}\text{C}$ , a), salinity (PSU, b), chlorophyll  $\alpha$  ( $\text{mg m}^{-3}$ , c) and DO concentration ( $\mu\text{mol dm}^{-1}$ , d) along isobars at 1 dbar intervals from 48 dbar to 76 dbar, coloured by pressure. Black vertical lines indicate the difference between minimum and maximum values at each time step. Binned data from the BML (45 dbar and below) are plotted against time and coloured by pressure. This highlights a vertical gradient in all four properties observed. Temperature and DO were highest near the thermocline while chlorophyll  $\alpha$  increased with depth. Salinity shows constant values as the model represented the BML with no salinity gradients. Alongside, the extent of the vertical gradient for each property is shown by the black vertical lines. This illustrates changes in vertical gradients; a small value indicates a homogeneous BML while a large value indicates a strong vertical gradient in the BML. . . . . 122
- Figure 5.15 Seaglider section of scattering at 650 nm ( $\beta(\theta_c) \text{ m}^{-1} \text{ sr}^{-1}$ ) sampled along the transect. . . . . 127

Figure 5.16	Seaglider scattering at 650 nm ( $\beta(\theta_c) \text{ m}^{-1} \text{ sr}^{-1}$ , <i>top</i> ) along isobars at 1 dbar intervals from 45 dbar to 71 dbar, coloured by pressure. Black vertical lines indicate the difference between minimum and maximum values at each time step. Discrete Fourier transform of the anomaly of the difference between the maximum and minimum values in the BML ( <i>bottom</i> ). This can identify dominating frequencies in the mixing events. Peaks indicate periodic mixing events at that frequency. There is no evident periodicity in the signal. . . . .	127
Figure 5.17	GOTM-BFM output relevant to resuspension of organic matter from the benthic layer. Bottom friction velocity ( $\text{m s}^{-1}$ , a), suspended sediment ( $\text{mg m}^{-3}$ , b) and particulate organic carbon ( $\text{mg C m}^{-3}$ , c) during model runs simulating the glider deployment period. . . . .	129
Figure 6.1	Seaglider survey locations. Crosses show every tenth dive by SG502, circles show every tenth dive by SG503. Dark shading corresponds to the 50% ice cover contour on the day SG502 crossed beneath the ice bridge (December 14th 2010) and entered Ross polynya. Contours correspond to bathymetry in metres (GEBCO, 2010). Contours are located at 200 m intervals down to 1000 m. A. McMurdo Sound, B. Central Basin, C. Crary Bank, D. Pennell Bank, E. Ross Bank, F. Ross Island. . . . .	139

- Figure 6.2 Calibration of temperature, salinity, potential density and DO profiles (*a to d*) for SG502. Ship calibration casts are in black. Glider observations as output by the iRobot processing are in red. Glider observations after calibration by the UEA toolbox are in blue. The dotted red line is iRobot processed DO offset by  $50 \mu\text{mol dm}^{-3}$  for ease of comparison with calibrated data to highlight reduced signal amplitude. . . . . 142
- Figure 6.3 Calibration of temperature, salinity, potential density and DO profiles (*a to d*) for SG503. Ship calibration casts are in black. Glider observations as output by the iRobot processing are in red. Glider observations after calibration by the UEA toolbox are in blue. The dotted red line is iRobot processed DO offset by  $-40 \mu\text{mol dm}^{-3}$  for ease of comparison with calibrated data to highlight reduced signal amplitude. . . . . 143
- Figure 6.4 *Left*: Linear regression of TCPhase from SG502's dive 701 and corresponding pseudo-CalPhase from the ship's CTD oxygen backcalculated using SG502's optode's foil coefficients. *Right*: Difference between the ship's calibration DO profile and recalculated glider DO profile with respect to potential density. . . . . 146
- Figure 6.5 *Left*: Linear regression of TCPhase from SG503's dive 919 and corresponding pseudo-CalPhase from the ship's CTD oxygen backcalculated using SG503's optode's foil coefficients. *Right*: Difference between the ship's calibration DO profile and recalculated glider DO profile with respect to potential density. . . . . 147
- Figure 6.6 Histogram of WetLabs ECO puck fluorometer counts. The vertical red line indicates the determined dark count value for the sensor. . . . 148

- Figure 6.7 Regression of the glider's fluorometer counts after dark count compensation against bottle chlorophyll a concentrations from the R/V Palmer vessel during recovery after dive 701. Scale factor =  $7.4517 \times 10^{-3}$ ,  $R^2 = 0.878$ . . . . . 148
- Figure 6.8 Comparison of bottle chlorophyll a concentrations from the R/V Palmer vessel during recovery after dive 701 (*black dots*) against the WetLabs ECO puck manufacturer calibration (*dotted line, blue*) and calibrated data (*solid line, red*). Mean difference =  $0.06 \text{ mg dm}^{-3}$ ; Root Mean Square (RMS) difference =  $0.39 \text{ mg dm}^{-3}$ . 151
- Figure 6.9 Decrease in DO concentrations per day ( $\mu\text{mol dm}^{-3} \text{ day}^{-1}$ ) for each potential temperature - salinity bin for SG502 (*left*) and SG503 (*right*). The most saline and coldest watermass is used as reference and the change in DO is assumed to be a linear drift affecting the optodes. This watermass identified by the black circle. . . . . 152
- Figure 6.10 Horizontal distance between SG502 and SG503 during the mission. The gliders passed within 6.8 km of each other on the 25-Dec-2010. Those profiles are used to validate the calibration performed based on the R/V Palmer observations. 153
- Figure 6.11 *a.* Temperature as observed by SG502 (*blue*) and SG503 (*red*) for their nearest profile in space and time as identified in Fig. 6.10 located 6.8 km apart on the 25-Dec-2010. *b.* All temperature measurements from SG502 (*blue*) and SG503 (*red*) against pressure around the centre of the bowtie pattern. This area was delimited as a box between  $174$  to  $178^\circ \text{ E}$  and  $76^\circ 15'$  to  $76^\circ 45' \text{ S}$ . *c.* Same as centre, but against potential density. 153

- Figure 6.12 *a.* Salinity as observed by SG502 (*blue*) and SG503 (*red*) for their nearest profile in space and time as identified in Fig. 6.10 located 6.8 km apart on the 25-Dec-2010. *b.* All salinity measurements from SG502 (*blue*) and SG503 (*red*) against pressure around the centre of the bowtie pattern. This area was delimited as a box between 174 to 178° E and 76°15' to 76°45' S. *c.* Same as centre, but against potential density. . . . . 154
- Figure 6.13 *a.* DO as observed by SG502 (*blue*) and SG503 (*red*) for their nearest profile in space and time as identified in Fig. 6.10 located 6.8 km apart on the 25-Dec-2010. *b.* All DO measurements from SG502 (*blue*) and SG503 (*red*) against pressure around the centre of the bowtie pattern. This area was delimited as a box between 174 to 178° E and 76°15' to 76°45' S. *c.* Same as centre, but against potential density. . . . . 154
- Figure 6.14 Special Sensor Microwave Imager / Sounder percentage sea ice cover data for either end of the mission, the 25<sup>th</sup> of November 2010 (*a*) and 30<sup>th</sup> of January 2011 (*b*). Mean sea ice cover during the deployment period (*c*). 0, 400 and 1000 m contours are in black (GEBCO, 2010). . . . . 156
- Figure 6.15 10 m windspeeds from ERA Interim reanalysis data (*a*) over each glider's position ( $\text{m s}^{-1}$ ; SG502: *blue*, SG503: *red*) and Seaglider density sections ( $\text{kg m}^{-3}$ ) from SG502 (*b*) and SG503 (*c*). Density contours are shown at  $0.1 \text{ kg m}^{-3}$  intervals from  $27.9 \text{ kg m}^{-3}$  (*solid line*) to  $27.6 \text{ kg m}^{-3}$  (*dash-dot line*). GEBCO\_o8 bathymetry is indicated by the grey shaded area (GEBCO, 2010). Alternating solid and dashed red bars at the bottom of section *b* delimit the regions labelled a to g and described in Fig. 6.22. . . . . 157

- Figure 6.16 DO sections ( $\mu\text{mol dm}^{-3}$ ) from SG502 (*a*) and SG503 (*b*) and oxygen saturation (%) sections from SG502 (*c*) and SG503 (*d*). Density contours are shown at  $0.1 \text{ kg m}^{-3}$  intervals from  $27.9 \text{ kg m}^{-3}$  (*solid line*) to  $27.6 \text{ kg m}^{-3}$  (*dash-dot line*). GEBCO\_o8 bathymetry is indicated by the grey shaded area (GEBCO, 2010). Alternating solid and dashed red bars at the bottom of graphs *a* and *c* delimit the regions labelled a to g and described in Fig. 6.22. . . . . 158
- Figure 6.17 Chlorophyll a concentration calibrated against fluorometer samples from the R/V Palmer (*a*,  $\text{mg m}^{-3}$ ), red optical backscatter counts at 700 nm (*b*), blue optical backscatter counts at 470 nm (*c*), and red/blue optical backscatter count ratio (*d*) sections from SG502's transect. Density contours are shown at  $0.1 \text{ kg m}^{-3}$  intervals from  $27.9 \text{ kg m}^{-3}$  (*solid line*) to  $27.6 \text{ kg m}^{-3}$  (*dash-dot line*). Alternating solid and dashed red bars at the bottom of each graph delimit the regions labelled a to g and described in Fig. 6.22. 160
- Figure 6.18 Mean (*a*) and maximum values (*b*) of a 21 day composite of MODIS ocean colour surface chlorophyll a concentrations ( $\text{mg m}^{-3}$ ) from the 14<sup>th</sup> of December to the 4<sup>th</sup> of January. This period corresponds to the SG502's observations of a large phytoplankton bloom over Ross Bank. White areas are devoid of data due to the continuous cloud and ice cover during the 21 day period. 161

- Figure 6.19 Timeseries of mean oxygen saturation (a. %) within the top 50 m of the water column for SG502 (*blue*) and SG503 (*red*). Panels b to e compare SG502 mean chlorophyll a concentration within the top 50 m of the water column ( $\text{mg m}^{-3}$ , *green*) with depth of the water column at SG502's position (b. m), ERA-Interim reanalysis winds at SG502's position (c.  $\text{m s}^{-1}$ ), mean sea-ice cover within the bloom region (d. %) and mean potential density of the top 50 m of the water column (e.  $\text{kg m}^{-3}$ ). . . . . 162
- Figure 6.20 Oxygen saturation (%) between 75 dbar and 200 dbar as recorded by SG502 between the 14<sup>th</sup> of December 2010 and the end of the survey. 163
- Figure 6.21 Potential Temperature - Salinity ( $\theta - S$ ) diagram of Ross Sea climatology (*black*) and data collected by Orsi and Wiederwohl (2009) (*red*) at water depths shallower than 2000 m. Solid traces show the 28.00 and 28.27  $\text{kg m}^{-3}$  neutral density  $\gamma^n$  surfaces. The white horizontal line shows the surface freezing point of seawater. Major water masses are labelled: Antarctic Surface Water (AASW), Modified Circumpolar Deep Water (MCDW/CDW), Modified Shelf Water (MSW/SW), and Antarctic Bottom Water (AABW). (For interpretation of the references to colour in this figure legend, the reader is referred to the web version of the Orsi and Wiederwohl (2009) article.). Figure and caption taken from Orsi and Wiederwohl (2009). . . . . 165
- Figure 6.22  $\theta - S$  diagrams of the 7 different sections identified from 502's observations coloured by chlorophyll a concentration ( $\text{mg m}^{-3}$ ). Each section is identified by the red bars on Figs. 6.15 to 6.17. 169

Figure 6.23	Location of the 7 different sections identified along SG502's track. 400 m isobaths are included to highlight the position of Ross Bank. . . . .	170
Figure 6.24	Empirical variogram of temperature (°C) recorded by SG502 and SG503 along different isobars (15, 50, 75, 100, 150, 200, 250, 300, 400 dbar). Due to the irregular spacing of the data and spatial sparseness, a proper statistical fit was not performed. Instead, a black line has been added to highlight the general location of the sill. This indicates the dominant spatial and temporal scales of variability. A red bar indicates poor significance of the plot due to aliasing, generally due to absence of data from one glider. Distance is in kilometres and time is in days. . . . .	172
Figure 6.25	Empirical variogram of salinity (PSS-78) recorded by SG502 and SG503 along different isobars (15, 50, 75, 100, 150, 200, 250, 300, 400 dbar). Due to the irregular spacing of the data and spatial sparseness, a proper statistical fit was not performed. Instead, a black line has been added to highlight the general location of the sill. This indicates the dominant spatial and temporal scales of variability. A red bar indicates poor significance of the plot due to aliasing, generally due to absence of data from one glider. Distance is in kilometres and time is in days. . . . .	173

- Figure 6.26 Empirical variogram of DO ( $\mu\text{mol dm}^{-3}$ ) recorded by SG502 and SG503 along different isobars (15, 50, 75, 100, 150, 200, 250, 300, 400 dbar). Due to the irregular spacing of the data and spatial sparseness, a proper statistical fit was not performed. Instead, a black line has been added to highlight the general location of the sill. This indicates the dominant spatial and temporal scales of variability. A red bar indicates poor significance of the plot due to aliasing, generally due to absence of data from one glider. Distance is in kilometres and time is in days. . . . . 174
- Figure 6.27 *a.* Mean temperature ( $^{\circ}\text{C}$ , *blue*) and salinity (PSS-78, *red*) profiles between the 14<sup>th</sup> of December 2010 and the end of the survey. *b.* Mean DO ( $\mu\text{mol dm}^{-3}$ , *blue*) and chlorophyll *a* (PSS-78, *red*) concentrations between the 14<sup>th</sup> of December 2010 and the end of the survey. *c.* Estimated daily change in DO concentration at each depth bin ( $\mu\text{mol dm}^{-3} \text{ day}^{-1}$ ). Data as recorded by SG502 between the 14<sup>th</sup> of December 2010 and the end of the survey. . . . . 177
- Figure 6.28 *a.* Mean temperature ( $^{\circ}\text{C}$ , *blue*) and salinity (PSS-78, *red*) profiles between the 14<sup>th</sup> of December 2010 and the end of the survey. *b.* Mean DO ( $\mu\text{mol dm}^{-3}$ , *blue*) concentrations between the 14<sup>th</sup> of December 2010 and the end of the survey. *c.* Estimated daily change in DO concentration at each depth bin ( $\mu\text{mol dm}^{-3} \text{ day}^{-1}$ ). Data as recorded by SG503 between the 14<sup>th</sup> of December 2010 and the end of the survey. . . 178

Figure 6.29	Oxygen solubility ( $\mu\text{mol dm}^{-3}$ ) of the top 20 m of the water column as recorded by SG502 between the 14 <sup>th</sup> of December 2010 and the end of the survey. . . . .	179
Figure 7.1	Seaglider mission trade-off triangle. When planning a Seaglider mission, the user must identify the requirements to answer the scientific question. . . . .	195

## LIST OF TABLES

---

Table 3.1	Commonly occurring issues during Seaglider deployments . . . . .	49
Table 3.2	Summary table of UEA Seaglider deployments. Median ( $\tilde{x}$ ) and mean ( $\bar{x}$ ) values included for several post-mission statistics. Estimated communication cost per dive includes pre-mission testing of Seagliders. * See Asper et al. (Asper et al., 2011) for more details on the GOVARS mission . . . . .	50

## ACRONYMS

---

$\tau$	Sensor Lag
AASW	Antarctic Surface Water
AIS	Automatic Identification System
AUV	Autonomous Underwater Vehicle
BFM	Biogeochemical Flux Model

BML	Bottom Mixed Layer
CDOM	Coloured Dissolved Organic Matter
Cefas	Centre for Environment, Fisheries and Aquaculture Science
DCM	Deep Chlorophyll Maximum
DO	Dissolved Oxygen
ECMWF	European Centre for Medium-Range Weather Forecasts
ERSEM	European Regional Seas Ecosystem Model
GETM	General Estuarine Ocean Model
GOTM	General Ocean Turbulence Model
GOVARS	Glider Observed Variations in the Ross Sea
ICES	International Council for the Exploration of the Sea
IEEE	Institute of Electrical and Electronics Engineers
LOEC <sub>C</sub>	Community Lowest Observable Effect Concentration
MCDW	Modified Circumpolar Deep Water
MSW	Modified Shelf Water
NAO	North Atlantic Oscillation
NAOI	North Atlantic Oscillation Index
ND	North Dogger
OG	Oyster Grounds
OMZ	Oxygen Minimum Zone
OSPAR	the Oslo and Paris Commission
RMS	Root Mean Square
SML	Surface Mixed Layer
SST	Sea Surface Temperature

$\theta - S$  Potential Temperature - Salinity

UEA University of East Anglia

UW University of Washington

VIMS Virginia Institute of Marine Science

Part I

INTRODUCTION

---



## BACKGROUND AND MOTIVATION

---

### 1.1 OXYGEN DEPLETION IN MARINE WATERS

#### 1.1.1 *The importance of shelf seas*

Shelf seas are both ecologically and economically important environments. They only represent around 7% of the world's marine waters but play a disproportionate role in providing economic and ecosystem services to human populations, including supporting unique biodiversity and bioremediation. They provide many resources (food, minerals, oil, construction materials) as well as space for industry (aquaculture, shipping and telecoms). Shelf sea waters play an important role in waste disposal and a growing importance in renewable energy production as well as being highly valued for recreation and tourism (Beaumont et al., 2007; Martínez et al., 2007).

Strong anthropogenic pressures, from waste disposal and eutrophication to fisheries, petrochemical and mineral extraction, have caused considerable changes in the functioning of these ecosystems. Dissolved Oxygen (DO) concentration is an important ecosystem quality indicator for assessing the impact of anthropogenic pressures and the health of these environments (Best et al., 2007; Painting et al., 2005; Tett et al., 2007). It is a critical component of most chemical cycles in the ocean and maintaining normoxic concentrations is imperative for sustaining macrofauna (Baden et al., 1990; Eriksson and Baden, 1997; Moodley et al., 2005; Vaquer-Sunyer and Duarte, 2008). This thesis will consider oxygen in two contrasting shelf sea environments, the North Sea and the Ross Sea, and the use of new autonomous underwater gliders in observing oxygen cycling in these environments.

### 1.1.2 Hypoxia

In the past decade, apprehension over the occurrence of low oxygen regions has increased to the point of becoming a major world concern and has led to the creation of the term “dead zones”. This first appeared in print in the early eighties designating the brackish waters of Lake Pontchartrain (LA, USA; Rabalais et al., 2010) and later reappeared in publications by Diaz (2001) and Diaz and Rosenberg (2008). Now the term has come to refer to coastal regions where hypoxia has occurred and caused mass visible effects on biota (death or migration). As discussed by Rabalais et al. (2010), the term is incorrect as microbiota remain present and it is often used inconsistently. Instead we prefer to use the term hypoxia.

Hypoxia is defined as oxygen concentrations below 4 to 6 mg dm<sup>-3</sup> (125 to 190 µmol dm<sup>-3</sup>) by the Oslo and Paris Commission (OSPAR) in the Ecological Quality Objective (EcoQO) for the North Sea (Painting et al., 2005). This threshold was selected as it is generally considered that organisms may suffer sub-lethal, and potentially lethal, effects below this oxygen concentration (Diaz and Rosenberg, 2008; Vaquer-Sunyer and Duarte, 2008). Nevertheless, higher concentrations than considered hypoxic by OSPAR may be lethal to marine organisms as shown in Fig. 1.1 (Keeling et al., 2010; Pörtner and Knust, 2007). Sublethal effects will be present at concentrations much lower than indicated in Fig. 1.1 but are difficult to quantify. Sedentary organisms are most affected due to their inability to avoid hypoxic regions (Rosenberg et al., 1991). Synergistic effects may also be observed when other environmental parameters are at suboptimal levels. In *Nephrops norvegicus*, low DO concentrations negatively affect their tolerance of temperature fluctuations (Baden et al., 1990; Eriksson and Baden, 1997). Low DO may also lead to habitat compression for many commercially important and sensitive species by reducing the vertical habitat when an Oxygen Minimum Zone (OMZ) expands or causing avoidance behaviour and reduction in potential spawning grounds in shelf seas (Ekau et al., 2010; Stramma et al., 2012, 2010).

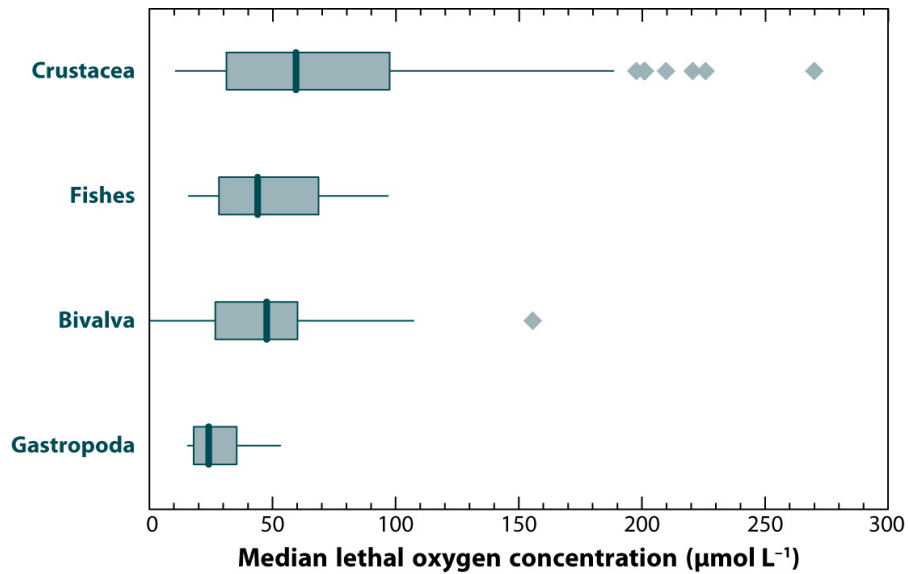


Figure 1.1: Median lethal oxygen concentration ( $LC_{50}$ , in  $\mu\text{mol dm}^{-3}$ ) among four different taxa. The box runs from the lower ( $Q_1$ , 25%) to the upper ( $Q_3$ , 75%) quartile and also includes the median (*thick vertical line*). The range of data points not considered outliers is defined as 1.5 times the difference between the quartiles ( $Q_3 - Q_1$ ), also known as interquartile range (IQR). The whiskers show the location of the lowest and highest datum within this range, i.e.,  $1.5 * \text{IQR}$ . Shaded diamonds are outliers as per this definition. Redrawn after Vaquer-Sunyer and Duarte (2008). Copyright (2008) National Academy of Sciences, U.S.A. Figure and caption taken from Keeling et al. (2010).

### 1.1.3 *Distribution of low oxygen systems*

Diaz (2001) provides a concise overview of the major anthropogenic eutrophication-induced hypoxic regions around the world (Figure 1.2). The majority of oxygen measurements in coastal waters date from the 1950s, although some datasets date back to the early 19th century. In the majority of cases, oxygen depletion began to be observed in the 1950s and 1960s (although many may have existed before but remained unrecorded). Some systems, such as the Baltic Sea, showed reducing DO as early as the 1930s and widespread hypoxia, expanding beyond isolated deep basins, starting in the 1950s (Conley et al., 2009a; Fonselius and Valderrama, 2003). The best data sets available come from the European seas and highlight a pattern between the presence of large human developments and reduced benthic DO; expansion of hypoxic regions was observed in the northern Adriatic in the 1960s, in the south-east Kattegat in the 1970s and in the 1980s for the north-western Black Sea (Baden et al., 1990; Diaz, 2001; Mee et al., 2005). Many of these systems showed natural hypoxia on account of their hydrographic and topographic properties, but the extent and intensity of hypoxia has increased with human influence. Similar patterns were found for major hypoxic systems around the United States of America with Chesapeake Bay (1930s) and the Gulf of Mexico (1970s) (Rabalais et al., 2010).

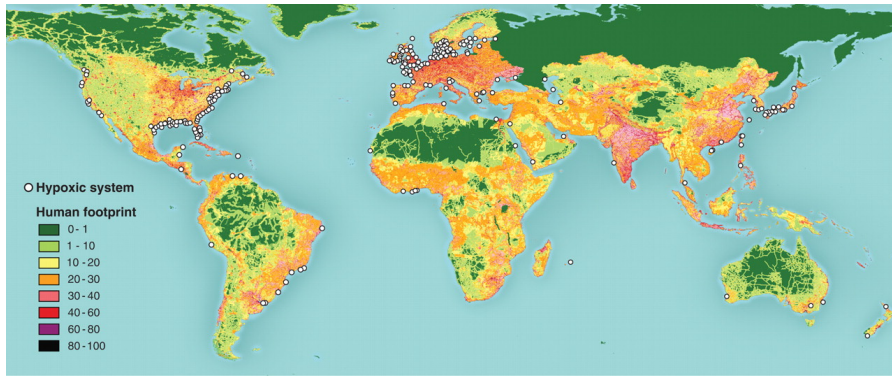


Figure 1.2: Global distribution of 400-plus systems that have scientifically reported accounts of being eutrophication-associated dead zones. Their distribution matches the global human footprint [the normalized human influence is expressed as a percent] in the Northern Hemisphere. For the Southern Hemisphere, the occurrence of dead zones is only recently being reported. Details on each system are in tables S1 and S2 in Diaz and Rosenberg (2008). Figure and caption taken from Diaz and Rosenberg (2008)

#### 1.1.4 *Mechanisms regulating the decline and supply of dissolved oxygen*

Low oxygen in marine waters can be a natural phenomenon and occurs in many areas regardless of anthropogenic nutrient inputs: shelf seas, deep basins and fjordic systems as well as eastern boundary upwelling areas. An OMZ is a vertical layer in the water column where oxygen concentration is at its lowest. It appears due to decay of settling organic matter with the majority being remineralised in the top 1000 m leading to the consumption of DO (Fig. 1.3). Surface waters are replenished in oxygen through air-sea interaction whilst the deep water is supplied with oxygen by cold deep water currents. The OMZ is located within the intermediate watermass, generally between 200 and 1000 m (Fig. 1.4). Fig. 1.4a shows that the main OMZ are located in the eastern Pacific, the northern Indian ocean (off the Bay of Bengal) and the south-eastern Atlantic ocean (Helly and Levin, 2004; Rabalais et al., 2010). Fig. 1.4b shows the depth at which these OMZ begin by showing the depth of the  $60 \mu\text{mol dm}^{-3}$  isoline; at this concentration, behavioural changes are observed in most marine organisms.

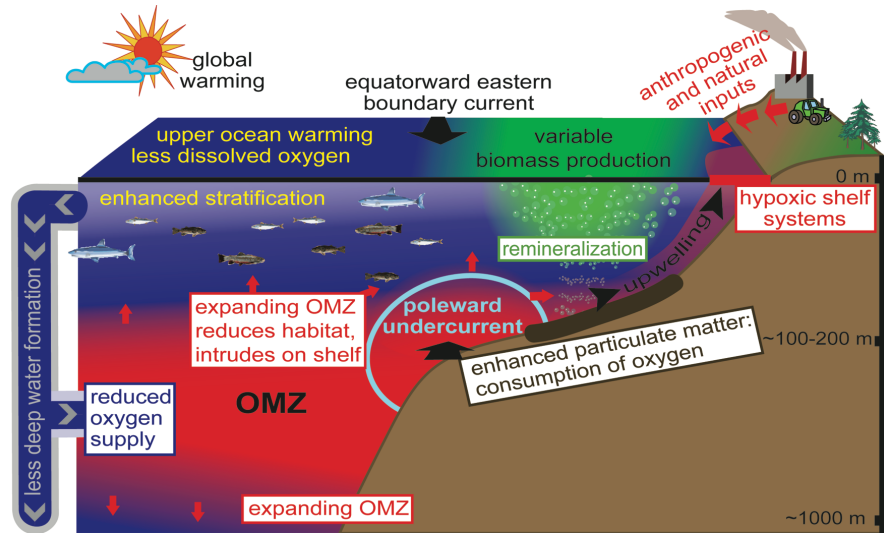


Figure 1.3: Schematic of interactions of open ocean oxygen minimum zones (OMZ, red) with hypoxic shelf systems (Diaz and Rosenberg, 2008) on continental shelves of eastern ocean boundaries. Figure and caption taken from Stramma et al. (2010).

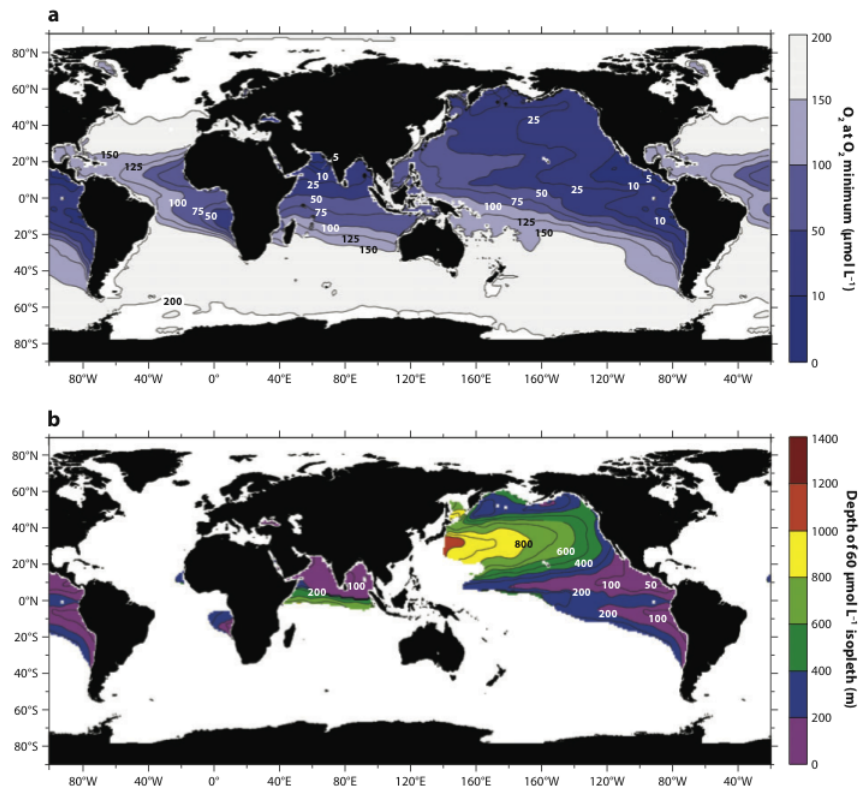


Figure 1.4: (a) Colours indicate  $O_2$  concentrations at the depth of minimum  $O_2$ . (b) Depth of the  $60 \mu\text{mol dm}^{-3}$  isoline in metres. Based on data from World Ocean Database, 2001 (Conkright et al., 2002). Figure and caption taken from Keeling et al. (2010).

Both deep basins and fjordic systems may suffer low oxygen in bottom waters due to their isolation from the atmosphere even under weak stratification; oxygen saturation may reach very low levels due to the prolonged stratification maintained by the system's natural morphology when supplied with sinking organic matter. Whilst in basins and fjords, oxygen depletion is dependent on geomorphological factors, the presence of low oxygen areas around eastern boundary upwelling areas is mainly driven by biological factors: the sustained supply of nutrients promotes continuous production which leads to oxygen consumption as organic matter sinks and is remineralised (Helly and Levin, 2004).

Although a mix of physical, chemical and biological processes are required for oxygen depletion to occur in shelf seas, they may be either mainly driven by increased biological consumption as a result of nutrient stimulation (e.g. the southern North Sea) or by isolation of bottom water masses through strong stratification (e.g. the Gulf of Mexico) (Pena et al., 2010; Rabalais et al., 2010, 2002; Scavia and Donnelly, 2007; Turner et al., 2006; Zhang et al., 2009b). Three main factors act in synergy to regulate the extent, severity, duration of the oxygen depletion: stratification, advection, and organic matter availability (Fig. 1.3). Each system reacts differently, reflecting their biological, chemical and physical structure (Jickells, 1998; Pena et al., 2010).

The major source of organic matter supplied to bottom waters is that produced in the Surface Mixed Layer (SML). The spring bloom is responsible not only for a large portion of that production, but also the highest increase in production rate, in temperate shelf seas. The onset of the bloom is regulated by stratification of the water column providing phytoplankton in the surface layer sufficient stability to facilitate growth within the photic zone (Gray et al., 2002; McQuatters-Gollop et al., 2007; Sharples et al., 2006). In shelf seas such as the North Sea, there can also be a Deep Chlorophyll Maximum (DCM) along the pycnocline caused by small scale injection of nutrients into the surface layer where phytoplankton receive enough light and vertical stability to develop. Production from the DCM is estimated to

contribute to as much as 60% of annual production in the North Sea (Fernand et al., 2013; Weston et al., 2005). The amount of organic matter exported to the Bottom Mixed Layer (BML) is dependent upon mixing and sinking rates whilst the lability of the organic matter and the delay before export to the BML is a product of cycling within the SML.

In the winter, consumption exceeds production leading to the net accumulation of remineralisation products. These nutrients are evenly distributed throughout the water column through convective overturning (Sharples et al., 2006). In spring, wind mixing decreases and surface temperatures increase leading to the appearance of a pycnocline separating a BML and SML. With longer days, increased vertical stability and elevated nutrient concentrations, phytoplankton populations bloom and consume nearly all surface nutrients rapidly; this occurs on a scale of weeks for the majority of shelf seas (Postma and Zijlstra, 1988). At the same time, the stratification effectively isolates the BML from the atmosphere halting replenishment of DO through air-sea interactions. In regions where pycnoclines do not limit vertical turbulent transfer, the constant mixing may help maintain phytoplankton in the euphotic zone by providing a constant supply of nutrients; at the same time, the lack of vertical stability will hinder phytoplankton adaptation to specific light levels making for reduced production rates.

More recently, a phenomenon other than the spring bloom has been deemed responsible for a large portion of organic matter export into the bottom layer in shelf seas; although the extent of its contribution remains highly debated, it is non-negligible (Fernand et al., 2013). The DCM which appears once the system becomes stratified is caused when the euphotic depth is deeper than the pycnocline or in cases where minor turbulence around the pycnocline sends small jets of nutrient rich water into the euphotic layer (Brown et al., 1999; Cullen, 1982). Weston et al. (2005) state that it is likely that mechanisms such as tidal and wave mixing govern the majority of transfers. The contribution of this DCM to total production is very difficult to assess due to the spatial and temporal heterogeneity of this feature

(Fernand et al., 2013; Weston et al., 2005). However its influence on BML oxygen depletion is non-negligible as all production occurs near the pycnocline. This limits the available water column where this organic matter may be consumed before entering the BML therefore exporting higher quantities of more labile organic matter.

Attempts to mitigate oxygen depletion in shelf seas and coastal areas has primarily focused on reducing excessive primary production by reducing nutrient input into the marine environment. The ratio of various nutrients will affect the plankton composition (McQuatters-Gollop et al., 2007) which in turn affects biomass production and nutrient cycling, as well as sinking rates and bioavailability of dead organisms both in the water column and in sediments. The relationship between nutrient availability and production is rarely linear due to potential limitations by other macro and micronutrients (Gray et al., 2002); in cases of nutrient reductions, there may be no ensuing reductions in primary production if phytoplankton growth was previously limited by another nutrient (de Jonge et al., 1996).

Stratification is the development of a strong vertical density gradient due to vertical differences in temperature and/or salinity. The most common form of stratification in marine waters is due to solar irradiation of the surface layer causing thermal expansion and hence a decrease in density. In coastal areas, especially near large estuaries, stratification may also occur based on salinity gradients, with a salt wedge penetrating towards the land and a thin layer of less saline water extending on the surface; this phenomenon rarely extends beyond 50 km from the coast (Lefort et al., 2012). Haloclines also form in tropical and polar regions. Less saline layers form from large amounts of rainfall or from land run-off, particularly in fjordic systems, and ice formation and melt. Wind, tide and wave-induced mixing all contribute to disrupting the pycnocline; the relative strength of each is dependent on the characteristics of the environment (hydrography, bathymetry, climate, etc.).

In the context of marine hypoxia, it is the development of a stable density gradient which gradually provides sufficient vertical stability to enable a rapid increase in primary production and subsequently

maintain an active phytoplankton community as a DCM. More importantly, stratification prevents BML interaction with either the SML or the atmosphere and therefore oxygen replenishment. Surface waters remain near oxygen saturation through air-sea exchanges. A break down of the stratification will replenish BML DO levels by injecting oxygen into the oxygen-depleted waters (Pena et al., 2010).

Horizontal transport processes generally contribute to the reoxygenation of hypoxic areas. Residual horizontal advection, on the order of days to weeks, will have limited impact in a hypoxic shelf sea system if it is advecting waters of similar oxygen concentrations as may be the case in laterally homogeneous systems with large oxygen depleted zones (Pena et al., 2010). However, in coastal areas characterised by small localised areas of hypoxia, advection may transport oxygen-rich waters back into hypoxic systems (Pena et al., 2010). Changes in horizontal transport velocities also affect deposition of organic matter; a reduction in horizontal transport velocities will promote settling of organic matter thereby increasing the supply of degradable organic matter in an area (Van Raaphorst et al., 1998). Tidal processes on the order of hours will cause vertical mixing in shallow systems which may cause cross-pycnocline exchange and injection of DO into the BML. At the same time, these processes contribute to maintaining DCMs in some systems (Weston et al., 2005, 2008).

#### 1.1.5 *Long-term impacts of severe oxygen depletion*

The effects of eutrophication, the leading cause of excessive organic matter production, may promote macrofaunal production thereby outweighing any detrimental effects of hypoxic events on fisheries yield (Caddy, 1993). However, once the ecosystem's ability to process this organic matter is exceeded, organic matter accumulates and facilitates the occurrence of hypoxic regions when stratification occurs. In situations where there is already a strong stratification, it enhances the severity and the extent of the hypoxic area.

In well oxygenated waters, organic matter is consumed by heterotrophic organisms, respired or remineralised and a small portion is

buried in the sediment. Hypoxia leads to increased anaerobic respiration based on nitrates, metal hydroxides and sulphates (Middelburg and Levin, 2009). The resulting reduced compounds are usually the greatest drain on oxygen budgets in sediments as they are rapidly re-oxidised, however as oxygen saturation decreases, less-efficient anaerobic pathways become more prevalent (Middelburg and Levin, 2009). This has the potential to increase lability and quantity of organic matter sequestered in the top layer of sediment by reducing oxygen consumption kinetics and oxygen penetration depth (Moodley et al., 2005). Reduced oxygen penetration depth is caused not only by decreased oxygen concentrations, but also by reduced bioturbation from benthic organisms which may be affected by oxygen levels and the greater concentrations of reduced compounds (Gray et al., 2002). Middelburg and Levin (2009) also put forward the idea that in regions suffering from occasional low oxygen saturation, in contrast to regions of permanent hypoxia, nitrates may accumulate in bottom waters. Accumulated nitrates could serve as a reservoir for additional nutrients which may be transferred into the euphotic zone in the case of resuspension events, further fuelling organic matter supply (Suratman et al., 2008; Van Raaphorst et al., 1998).

#### 1.1.6 *Recovery and return to normoxia*

Whilst the suspected majority of severely oxygen depleted regions have been identified in the past three decades and strong measures are now in place (Diaz, 2001; Diaz and Rosenberg, 2008), particularly aiming to reduce nutrient loads, less than half have shown clear trends of recovery. Analysis of historical data by Kemp and Testa (2009) suggested complex non-linear responses. Diaz and Rosenberg (2008) put forward the idea that ecosystem recovery would, on a biological level, go through separate stages during decline and recovery due to a hysteretic progression of successional dynamics. Nevertheless, whilst phosphorous inputs may have been reduced in many coastal areas, nitrogen release into the environment is still increasing and is difficult to regulate due to the diffuse nature of the inputs

into the environment (Conley et al., 2009b; Van Engeland et al., 2010). Also, the number of hypoxic regions (as opposed to the extreme examples of 'anoxia and extreme hypoxia) being recorded is increasing. This may be explained only in part by the evolution of methods and the increased observational efforts leading to the identification of occasional and small-scale hypoxic events. However the main concern revolves around the potential influence of climate trends (Behrenfeld et al., 2006; Hofmann et al., 2008; Keeling et al., 2010; Rabalais et al., 2009; Vaquer-Sunyer and Duarte, 2008). Weston et al. (2008) conjecture that climate change scenarios in the North Sea could see a decrease in BML DO due to increasing temperatures (a temperature increase of 2-3°C could decrease oxygen concentrations by 12  $\mu\text{mol dm}^{-3}$ ) with both a longer and earlier occurring stratification and enhanced primary production coupled to a decrease in summer storms disrupting the stratification.

According to Diaz (2001), there has been little change (positive or negative) in the intensity of hypoxia in affected regions since the 1980s, nor has the distribution and extent of hypoxic zones changed markedly. Diaz and Rosenberg (2008) also attempted to determine the proportion of zones showing signs of improvement. Only 4% exhibited positive developments caused by reductions in nutrient loading, less organic matter and weaker stratification (also regulated by freshwater run-off in coastal areas).

Due to the hysteretic pathways observed during recovery of many areas, it follows that the longer an area is exposed to abnormal oxygen depletion, the longer recovery will take, potentially leading to entire changes in community structure. Mature communities may demonstrate lower tolerance of hypoxia than opportunistic communities. Such a situation was observed in Gullmarsfjord, Sweden, where 6 months of severe oxygen-depletion led to a change in community structure and abundance which lasted 2 years (Rosenberg et al., 2002); yet sediment biochemistry was not severely affected and therefore larval recruitment was able to take place. This promoted rapid recovery of the site to previous conditions (Rosenberg et al., 2002). However, if similar conditions were to occur for prolonged periods, recovery

would be greatly prolonged; in the case of the Black Sea, the benthos is still undergoing changes and has yet to recover to a stable state since conditions deteriorated in the 1970s (Mee et al., 2005).

Similar patterns may be observed on physical and chemical levels, where prolonged severe hypoxia will lead to a shift in the redox levels of sediments and enhance the potential for hypoxia. Prolonged hypoxia leads to a shift in early diagenetic pathways and a potential shift towards anaerobic oxidation of secondary reduced compounds (ie. *amanox*) (Middelburg and Levin, 2009). Changes in sediment organic matter proportions and the impact on biota (ie. reducedurbation) lead to a decrease in oxygen penetration depth, sequestration of additional organic matter and the accumulation of dissolved reduced metals and nitrates (Middelburg and Levin, 2009; Moodley et al., 2005). The overall effect is the accumulation of labile organic matter in the sediment which is readily available for oxidation when DO becomes available. Such changes in sediment dynamics have long lasting effects and slow recovery to a steady state. First, because conditions are far from optimal for the habitual mature communities, this leads to the absence of the usual biotic functions (bioirrigation, bioturbation, and biotransportation of microscopic organisms; Rabalais et al., 2010). Secondly, by increasing the potential for low oxygen saturation and accumulation of labile organic matter, resuspension events can lead to sudden severe decreases in DO (Van Raaphorst et al., 1998). Additionally, in sediments and the benthic-pelagic interface, oxidation of compounds reduced in early diagenetic pathways may account for 75% of the oxygen consumption (Glud, 2008). The accumulation of these compounds will delay the return of oxygen saturation. However, it is thought that before significant accumulation leading to such effects could occur, nitrification would reduce in the water column reducing nitrate input into bottom waters (Kemp et al., 1990; Kemp and Testa, 2009). Therefore, this is likely only of importance in regions suffering from very severe hypoxia where reoxygenation is a slow process and not completely dominated by vertical overturning as in the North Sea.

The consequence of both the increased likelihood of oxygen depletion and the shift in community structure hinders recovery: in the case of prolonged hypoxia, sites may develop a mature community which will collapse slowly upon site recovery. It is unlikely that a return to normoxia would have severe negative impacts on the low-oxygen tolerant community; transition back to a stable normoxic community in these cases would occur through competition and gradual dominance. Additionally, the transition between hypoxia and normoxia is not a clearly defined threshold but is gradual. One year conditions may prove particularly severe, whereas the following year oxygen saturation may not drop below Community Lowest Observable Effect Concentration (LOEC<sub>C</sub>). Therefore factors which may increase the potential, severity or duration of hypoxia events will also delay the recovery. A highly variable system may also prevent settlement of early stages of mature communities until oxygen concentrations are well above LOEC<sub>C</sub>.

## 1.2 CONTEXT

### 1.2.1 *The North Sea*

The North Sea, located in western Europe, between Britain, France, Belgium, the Netherlands, Germany, Denmark and Norway is delimited according to ICES (1983) as a region covering 575 300 km<sup>2</sup> and containing 42 494 km<sup>3</sup> of water with an average depth of 74 m, increasing from south to north (Fig. 1.5). Two major topographical areas stand out from the general area; Dogger Bank is situated in the central North Sea, at depths of 15 to 20 m, and the Norwegian Trench is situated along the Norwegian coast, with depths reaching over 400 m (Lenhart et al., 2004; Postma and Zijlstra, 1988). In the southern half (south of Dogger Bank) with an average depth of 30 m, the water column is well-mixed throughout the year (Otto et al., 1990). The northern half, excluding Dogger Bank and the Norwegian Trench, gently slopes down to the edge of the continental shelf at a depth of 200 - 250 m and shows seasonal stratification and nutrient depletion

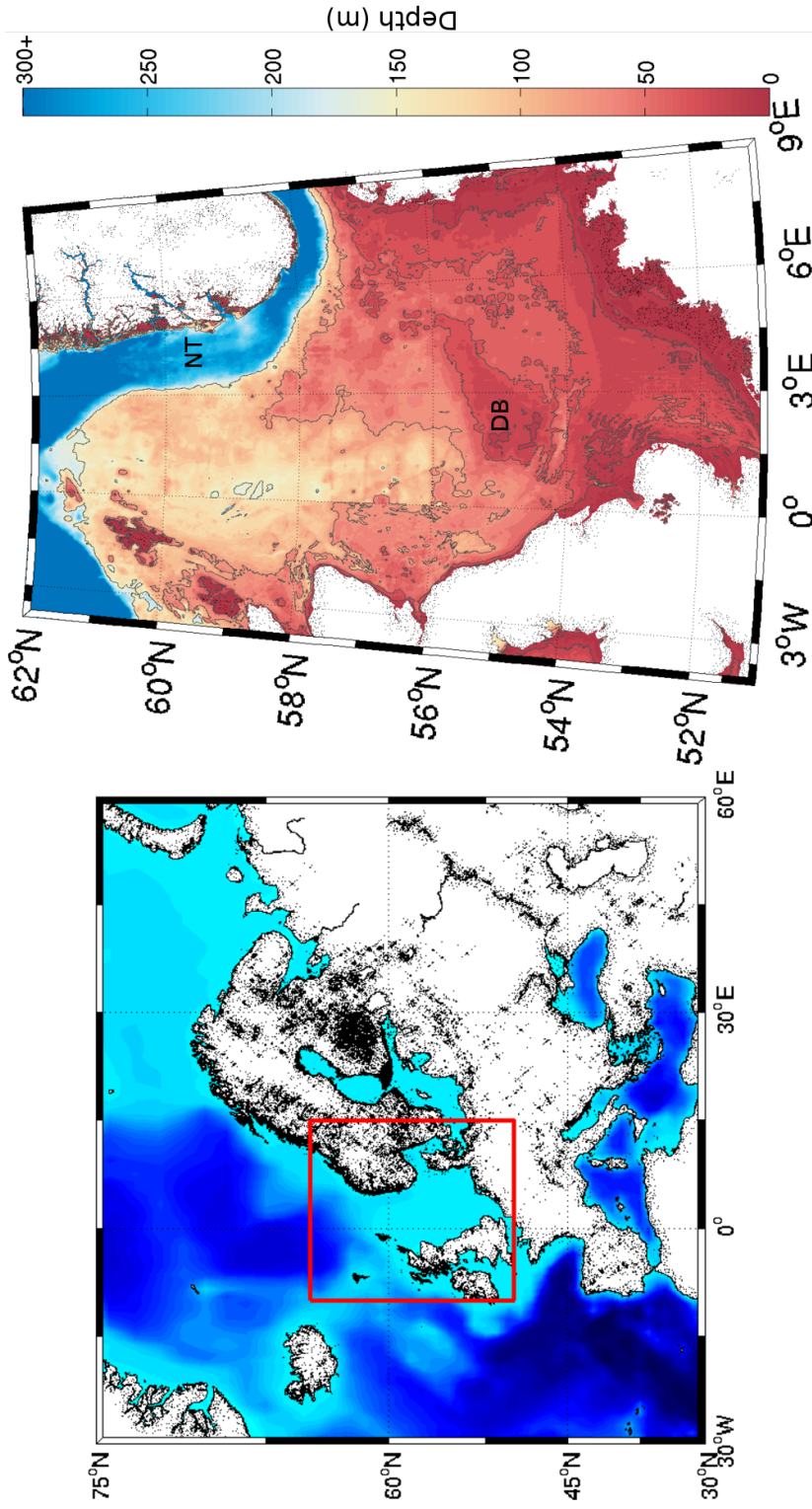


Figure 1.5: Bathymetry of the North Sea and surrounding area. Depth contours have been added for the 20, 40, 80 and 160 m isobaths. A more detailed figure is provided in Ch. 4. Locations of Dogger Bank (DB) and the Norwegian Trench (NT) are also indicated.

in off-shore waters (Otto et al., 1990; Sharples et al., 2006). The area located just north of Dogger Bank, referred to as the central North Sea, will be the focus of Chapters 4 & 5. A more detailed description and maps of the North Sea system are provided in Chapter 4.

Fluctuations in large scale circulation affect exchange along the North Atlantic boundary leading to changes in nutrient loading in the offshore waters of the North Sea (Lenhart et al., 1995; Vermaat et al., 2008). Additionally, nutrient loading in the North Sea is strongly coupled to riverine loading, atmospheric deposition, terrestrial runoff and land use.

Greenwood et al. (2010) reported low summer DO recorded by a mooring in the central North Sea. Although already described in coastal regions as caused by eutrophication (Justić et al., 2003; Keeling et al., 2010; Rabalais et al., 2009; Vaquer-Sunyer and Duarte, 2008; Zhang et al., 2009a), hypoxia had never been reported in offshore waters of the North Sea. Greenwood et al. (2010) highlighted the importance of continuous production and stratification in regulating hypoxia throughout the summer based on observations from moorings placed at two sites in the North Sea. In the shallower of the two sites, resuspension of organic matter from storm events was also put forward as a potential mechanism enhancing oxygen drawdown (Greenwood et al., 2010; Van Raaphorst et al., 1998). Testing these hypotheses is one of the goals of the thesis.

The work contained herein, as part of a project between the University of East Anglia (UEA) and the Centre for Environment, Fisheries and Aquaculture Science (Cefas), aimed to investigate the spatial and temporal distribution of North Sea summer oxygen depletion. The second remit of the project originally entitled "Understanding and predicting the development of low oxygen regions in the southern North Sea - an interdisciplinary PhD study" was to begin developing Seaglider capabilities at the UEA and Cefas. The use of a Seaglider in this project would demonstrate the ability of Autonomous Underwater Vehicles (AUVs) as persistent monitoring platforms in the North Sea and investigate, using high resolution observations, the occurrence of seasonal oxygen depletion in the North Sea.

### 1.2.2 *The Ross Sea*

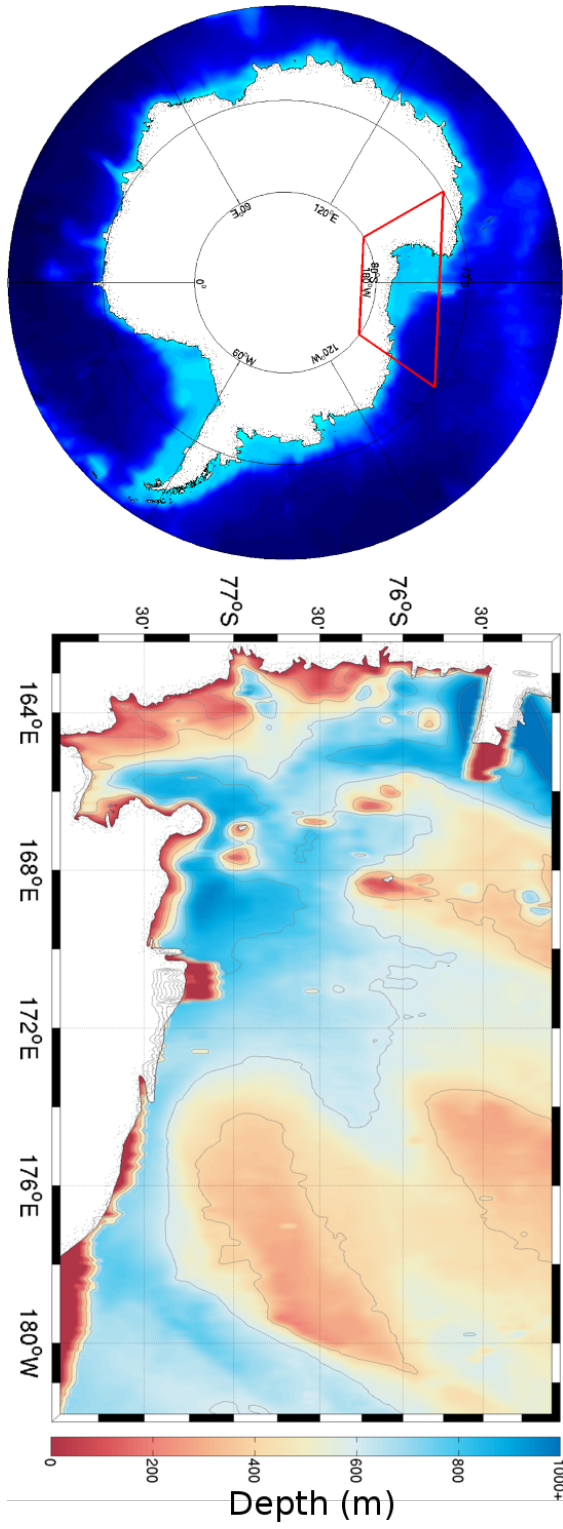
The Ross Sea is a shelf sea located south of the Pacific Ocean, straddling the International Date Line, forming an indentation into the continent of Antarctica. The western edge of the shelf is composed of a series of trenches ranging from 700 to 900 m deep and shallower (350 m) meridional banks (the Crary, Pennell and Ross Banks). Ross Island is located near the western edge and separates the Ross polynya from McMurdo Sound. A polynya is an area of open water in a region of high ice cover. Most polynyas are winter features, but large polynyas at high latitudes can last for several consecutive years (Arrigo and van Dijken, 2003).

The Ross polynya is a latent heat polynya (formed by katabatic winds and currents rather than upwelling) and as such is a site of dense water formation. Katabatic winds blow off the Ross Ice Shelf advecting existing sea ice northward and causing new ice formation (Arrigo and van Dijken, 2003). This leads to the formation of high-salinity shelf-water and Antarctic bottom water, both of which contribute to the global thermohaline circulation (Buffoni et al., 2002; Stössel et al., 2002).

Polynyas are highly productive regions; in particular, the Ross Sea shelf is one of the most productive regions of the Southern Ocean. Polynyas, by remaining open, offer a longer growing period (Mundy and Barber, 2001). In addition, they are generally much more productive than surrounding waters (Arrigo and van Dijken, 2003). The high proportion of new production makes polynyas very important CO<sub>2</sub> sinks although exact budgets remain poorly constrained (Arrigo and van Dijken, 2004; Arrigo et al., 1998; Sedwick et al., 2011; Smith and Comiso, 2008). A further description of the Ross Sea and its productivity can be found in Chapter 6.

Due to the inherent difficulties in sampling such remote areas, our understanding and estimates of deep water formation, stratification and primary production are limited in the Ross polynya. The Glider Observed Variations in the Ross Sea (GOVARS) project aimed in part to determine the spatial and temporal relation of physical drivers

Figure 1.6: Bathymetry of the Ross Sea and surrounding area. Depth contours have been added for the 200, 400, 600, 800 and 1000 m isobaths. A more detailed figure is provided in Ch. 6.



(ice cover, vertical mixing, intrusions of Modified Circumpolar Deep Water (MCDW)) and phytoplankton communities. The project aimed to obtain high-resolution observations from Seagliders early in the season, before sea ice permitted ship access, to observe the initiation of the spring bloom and the physical constraints on phytoplankton distribution and productivity.

As very little is known about the stratification and production, the two main drivers of oxygen cycling, during the early austral summer, this experiment allowed novel *in situ* observations of DO dynamics in the Ross polynya. Using the Ross Sea as a study site would provide a highly contrasting polar environment to the North Sea site potentially experiencing similar decreases in oxygen concentration. Whereas the emphasis in the North Sea is on tides and winds in shallow areas regulating stratification, we hypothesise that such processes may play a lesser role in Ross polynya oxygen cycling.

### 1.2.3 *Seagliders for ocean monitoring*

Global changes in climate and dominant climate modes have a strong impact on seasonal oxygen depletion (Justić et al., 2003; Keeling et al., 2010; Pena et al., 2010; Rabalais et al., 2009; Zhang et al., 2009b). To alleviate potential issues which could lead to negative impacts on economically and environmentally valuable shelf sea systems, it is important to understand which mechanisms drive oxygen dynamics in shelf seas and to have baseline observations from which to detect changes. In particular, understanding how processes interact on a range of scales enables better predictions of oxygen fluctuations in highly dynamic and heterogeneous environments (Pena et al., 2010).

Essentially, we need a better grasp of how the main drivers (stratification and production) can sometimes cause seasonal oxygen depletion. The past decades have seen a tremendous increase in observations on a variety of scales. Satellite imagery provides large scale synoptic views of a system, ship-based surveys provide ground truthing and are able to investigate particular areas of interest while moorings provide continuous long-term and high-resolution observa-

tions of specific features of interest. The development of large-scale observation systems, notably Argo, has provided a cross-scale view of many of these features with the use of autonomous floats. These observations then feed into numerical modelling schemes and have successfully revealed new aspects of the global functioning of the marine ecosystem (Eriksen, 1997; Howe et al., 2007; Rudnick et al., 2004; Wunsch, 2010). Today, the bottleneck in our understanding and modelling of biogeochemical processes is our lack of understanding of the finer scale interactions between physical processes and biogeochemical responses. Wunsch (2010) described this problem as “having no prospect of a single universal observation system”.

In particular, DO concentrations are difficult to measure. *In situ* observations are dependent on skilled technicians performing labour intensive titrations and remote sensing of DO is still in its infancy. It is in this context that autonomous floats have shown tremendous potential, notably with mapping of OMZ (Stramma et al., 2008). Despite recent advances and the increasing number of DO sensors on floats, this method is still unable to resolve the patchiness of biological features, particularly in high-latitude systems where small Rossby radii and weak stratification increase the heterogeneity of a system (Frajka-Williams et al., 2009; Perry et al., 2008; Sackmann et al., 2008). Over the last couple of decades, AUVs have become a powerful tool in the investigation of biological, chemical and physical oceanography (Eriksen et al., 2001; Howe et al., 2007; Rudnick et al., 2004). They provide the temporal resolution of moorings coupled to the mobility of ships, although not as rapid; their endurance allows spatially and temporally dense observations throughout an entire season even in remote or extreme environments. Not only do they complement existing technologies, particularly synoptic observation systems such as satellite or floats, they open up new avenues of investigation through their specific capabilities (Howe et al., 2007; Rudnick et al., 2004). For AUVs to benefit from the same success other long term monitoring platforms have had (moorings, Argo), it is critical to understand their limits in both monitoring and process studies.

The Seaglider, an AUV developed at the University of Washington (UW) (Eriksen et al., 2001), is one of the three main buoyancy-driven gliders available for oceanographic research (Rudnick et al., 2004). The use of Seagliders in oceanographic research and how best to process Seaglider data will be discussed in Chapter 2. There are numerous issues linked to calibration, sensor drift, and reliability associated with glider-borne sensors that must be considered in order to make best use of glider data. Calibration of Seaglider data, issues relating to survey design and the suitability of Seagliders for specific missions will be discussed in their respective chapters (Ch. 5 & 6). We also provide an overview of several Seaglider deployments by the University of East Anglia where Seagliders were pushed to the limit of their abilities (Ch. 3). Comparison of missions in extreme conditions at the limits of their depth range (70 to 1000 m) and battery life shows a need for tailored survey design and flight parameters in order to maximise mission duration, control over the Seaglider and most efficient scientific sampling.

### 1.3 RATIONALE

Although much is already known about the processes contributing to oxygen depletion in marine waters, where, when and how these processes interact to cause oxygen depletion events in dynamic shelf sea environments remains poorly understood. One element is the absence of historical observation programmes focusing on oxygen depletion where it manifests itself as a seasonal feature; due to its sporadic nature it often remains overlooked. As a consequence, we also have very little grasp as to where it may appear. Coastal regions suffering from eutrophication and OMZ are thoroughly studied due to their economic importance and global impacts respectively, but descriptions of hypoxia in off-shore shelf sea waters remain limited to extreme cases such as the Baltic Sea or the Gulf of Mexico. A study on a range of spatial and temporal scales would illustrate the links between fine-scale mechanisms (sediment resuspension, turbulence along the thermocline) to large-scale events and climate trends. This

understanding would then serve to refine our predictions of low oxygen events and aid in the management of these ecologically and economically important environments.

The thesis contains three parts, the first of which describes the use of Seagliders as a tool for hydrographic surveys, with a particular focus on obtaining high quality DO observations, and reviews the use of Seagliders in various deployments (Queste et al., 2012). The second examines the spatial and historical occurrence of seasonal oxygen depletion using historical data across the North Sea and a traditional ship-based survey of the North Sea (Queste et al., 2013) before investigating the source of the oxygen draw-down and mechanisms regulating the injection of oxygen into the BML using high-resolution Seaglider observations. This section of the thesis aims identify potential regions of low dissolved oxygen during the summer months in the central North Sea, a region previously considered normoxic during the summer months. The historical data is then used to investigate if a trend in summer bottom water oxygen saturation over the past century exists. Finally, high resolution observations from a Seaglider and model output are used to quantify the balance of oxygen supply and demand within the bottom mixed layer. The third part describes a Seaglider survey of the Ross polynya and the link between DO and biological production to draw parallels between the two different shelf sea ecosystems and highlight the processes regulating seasonal oxygen depletion. The experiment in the North Sea aimed to investigate the physical and biological controls on the spring bloom and influence on pelagic oxygen concentrations. It was hypothesised that sinking organic matter produced during the spring bloom would be rapidly remineralised during the water column also leading to a decrease in pelagic oxygen saturation. It was also suspected that this environment would present greater spatial heterogeneity due to the complex ice-related processes. The thesis ends with a summary of the research herein and recommendations for future developments.

## Part II

### SEAGLIDERS

---

Chapter 3 contained herein has been provided as published in the Institute of Electrical and Electronics Engineers (IEEE) AUV 2012 Conference Proceedings.

*Queste, B.Y., Heywood, K.J., Kaiser, J., Lee, G.A., Matthews, A.J., Schmidtko, S., Walker-Brown, C., and Woodward, S.W. (2012) Deployments in extreme conditions: Pushing the boundaries of Seaglider capabilities. IEEE AUV 2012.*

---

All work described in Ch. 2 was performed by Bastien Queste with the exception of the development of the MATLAB toolbox which was a collaborative effort with Sunke Schmidtko.

Involvement of Bastien Queste in the missions described in Ch. 3 is detailed on the following page.

	Mission Planning	Deployment	Recovery	Basestation maintenance	Web platform maintenance
Scotland trials	Collaborative	Collaborative	Collaborative	Queste	N/A
GOPINA	Others	Others	Others	Queste	Collaborative
North Sea	Queste, depending on predefined IBTS cruise track.	Queste	Queste	Queste	Queste
Tropical DISCO	Others	Others	Others	Queste	Queste
GENTOO	Collaborative	Collaborative	Collaborative	Queste	Collaborative

	Piloting	Glider repairs	Sample collection	Data calibration	Data analysis
Scotland trials	Collaborative	N/A	N/A	N/A	Collaborative
GOPINA	Collaborative	N/A	Others	Collaborative	Others
North Sea	Others	N/A	Collaborative	Queste	Queste
Tropical DISGO	Collaborative	N/A	Others	Others	Others
GENTOO	Collaborative	Collaborative	Collaborative	Collaborative	Collaborative



## SEAGLIDERS AS TOOLS FOR OCEANOGRAPHIC RESEARCH

---

### 2.1 THE INSTRUMENT

The Seaglider, originally designed by the University of Washington and licensed for commercial distribution to Kongsberg, is a buoyancy-driven AUV. Until recently, Seagliders were licensed to iRobot for commercial distribution and all work completed for this thesis was done while Seagliders were sold and supported by iRobot. It is designed to be able to travel long distances for prolonged periods of time collecting observational data from an on-board sensor package (Davis et al., 2003; Eriksen et al., 2001; IRobot, 2012). The iRobot 1KA Seagliders used in Chapters 5 and 6 were equipped with a Seabird CT sail, an Aanderaa 4330 optode with a fast response foil and WetLabs triplet ECO pucks. The latter measured Chlorophyll *a* at 470/695 nm (ex/em), Coloured Dissolved Organic Matter (CDOM) 370/460 nm and red backscatter at 650 nm for the North Sea mission. In the Ross Sea, the CDOM was replaced by blue backscatter (470 nm).

Each Seaglider is approximately 3 m in length accounting for the antenna and weighs approximately 54 kg for the lighter models (Davis et al., 2003; Eriksen et al., 2001; IRobot, 2012). The vehicle is able to achieve such high autonomy and endurance through its method of propulsion (Davis et al., 2003; Eriksen et al., 2001). Unlike conventional underwater vehicles, the Seaglider has no external moving parts. It glides through the water by altering its buoyancy, just as floats do, through the use of an external bladder. The variable buoyancy device in Fig. 2.2 functions by transferring oil in and out of the main body and into (or out of) the external bladder. To dive, it decreases its volume while maintaining the same mass by deflating the bladder. To surface, it inflates the bladder again, reducing the glider's



Figure 2.1: Four Seagliders in their handling cradles being prepared for a trial launch in Puget Sound, WA USA. The Seagliders are pointing nose down, with the red aerial extending towards the sky. The rudder is visible just below the antenna and the wings further below extending to either side. On the top side of the Seagliders, in between both wings is the Seabird CT sail.

density to slightly below surrounding water density. The forward motion is achieved by pitching the glider forward and back by displacing the asymmetrically-weighted internal 24 V battery and changing the centre of gravity; the combination of the vertical motion and the angle of the wings alongside the glider provide the necessary lift to move the glider forward. Similarly, the glider is able to change its direction by rolling the asymmetrically weighted internal battery thereby tilting the glider (Davis et al., 2003; Eriksen et al., 2001). By optimising the glider's flight and sampling, the glider can potentially remain at sea for a year. However, using a realistic sampling regime for the purposes of targeted experiments, a duration of 4 months is the norm limited by sensor batteries. It is able to cover up to  $25 \text{ km day}^{-1}$  at speeds of  $20 \text{ to } 30 \text{ cm s}^{-1}$  over ground (Queste et al., 2012).

Upon surfacing (Fig. 2.3), the glider downloads to its internal computer from a central server, the "basestation", a set of flight and sampling parameters, including waypoints, and uploads data collected during the past dive before diving again. Relay of scientific data

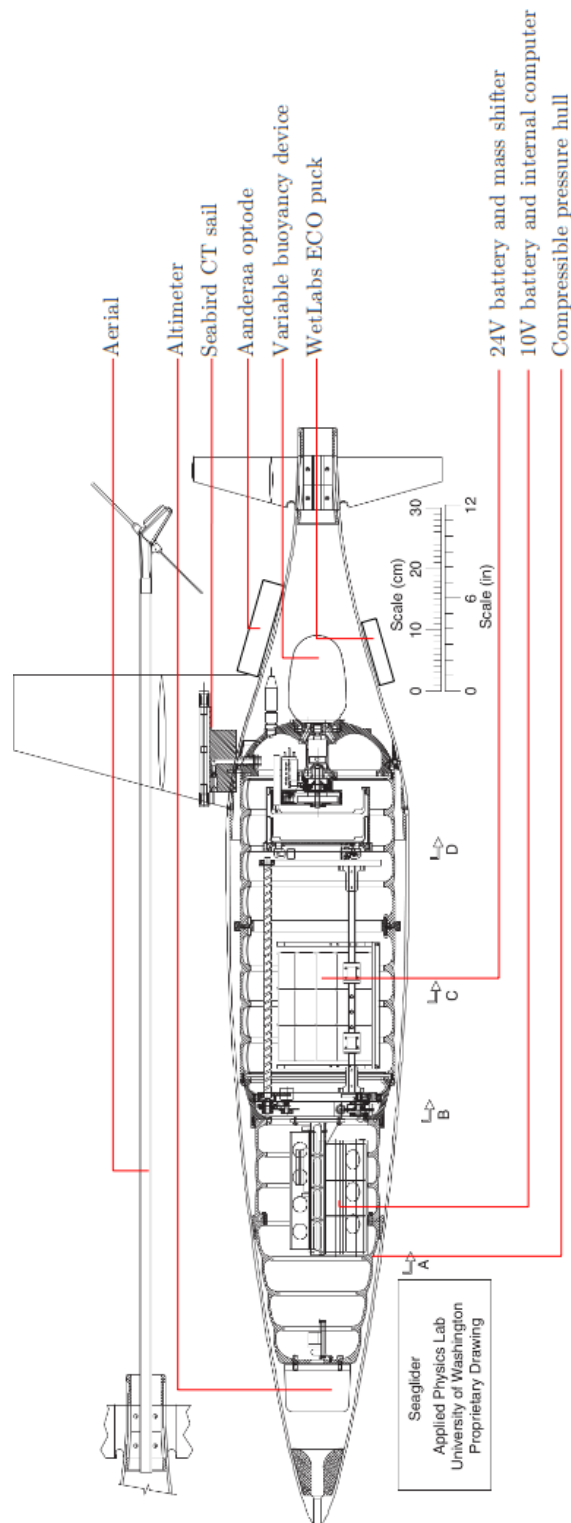


Figure 2.2: Schematic side view of a Seaglider with the wing shape provided above for reference and position of the sensors. The antenna mast is shown separately above the fairing and pressure hull. Figure and caption adapted from Eriksen et al. (2001).

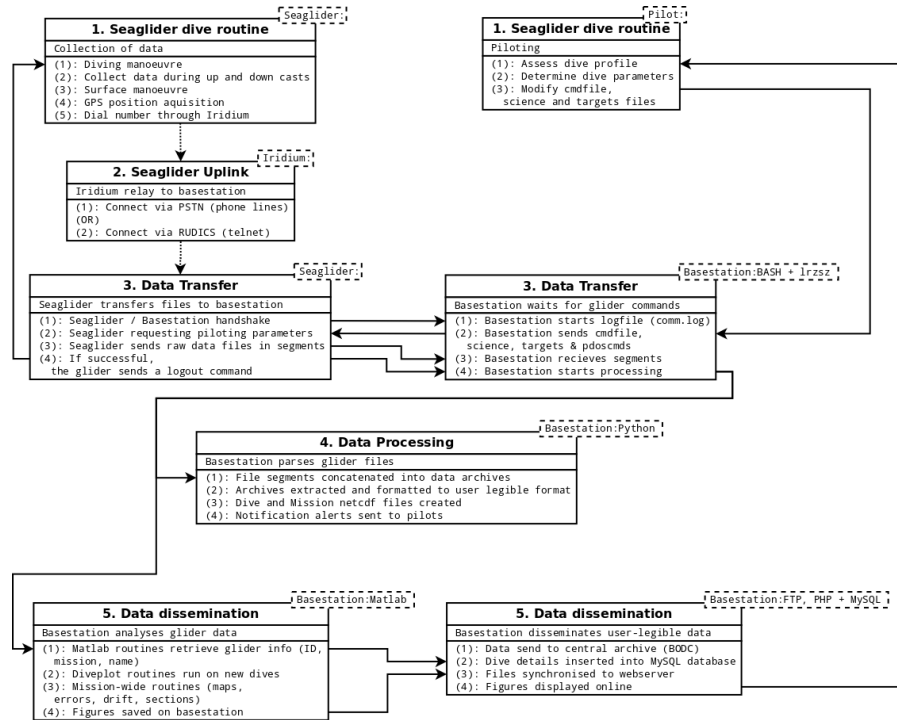


Figure 2.3: UEA Seaglider system structure. The Seaglider data are processed in near real-time and feeds back to the pilots for adjustment of piloting and sampling commands. New orders are then downloaded by the glider for the following dive. Processing is automated on a central server hosted at the UEA, the basestation, and data are disseminated to national data centres for operational purposes and are displayed online for public outreach.

after the end of every dive not only ensures recovery of data if the instrument is lost but also allows for adaptive sampling. The pilots may modify the sampling regime or choose to redirect the instrument to areas of greater interest.

This permits a very different approach to sampling than what is generally possible with other observational platforms. Autonomous underwater gliders bridge the gap between the three main means of obtaining *in situ* oceanographic observations: moorings, Argo floats and ships (Rudnick and Cole, 2011; Rudnick et al., 2004). Gliders obtain spatial coverage and vertical resolution not possible with moorings, at the expense of longevity. Although this is moderated by sensor issues (e.g. sensor drift) and collisions with vessels which often shorten the life span of moorings. In contrast to ship based surveys, gliders do not have the necessary speed to provide a synoptic view of a region's characteristics over larger distances (Davis et al., 2003; Rudnick and Cole, 2011), they do not sample at as high a resolution (0.2 Hz for a Seaglider versus the conventional 24 Hz of a ship-borne CTD) nor are they able to carry such a large and diverse sensor payload. They do however run at a greatly reduced cost and are able to maintain a presence for much longer than ships (Rudnick et al., 2004). This allows gliders to compensate by providing repeat sections of an area as well as sampling continuously, thus observing small scale features that may be missed by discrete ship profiles. In practicality, autonomous underwater gliders most resemble Argo floats, with the added benefits of being able to direct them and a much greater sampling resolution, both spatially and temporally. They are also similar to towed undulating vehicles, with a greatly reduced travel speed but longer endurance.

As all tools, they have some limitations, notably environmental constraints such as their limited density range making them unsuitable for regions with low salinity surface layers or very large vertical temperature gradients (approximately  $10 \text{ kg m}^{-3}$ , IRobot, 2012). They are also constrained by current speeds and are prone to getting "trapped" in eddies or carried away by strong currents. Beyond these basic physical limitations, we must also identify the spatial and temporal scales

which gliders are able to resolve. In order to observe physical and biological processes which change rapidly (scale of days to weeks and/or tens of kilometres), it is necessary to either obtain synoptic views of a system, or follow a feature in a Lagrangian manner (Rudnick et al., 2004). Floats move in such a manner however gliders, while gaining the advantage of being controllable, lose this Lagrangian property unless specifically directed to follow modelled currents or drifters. At the same time, they are unable to obtain a synoptic view of mesoscale features. When diving to maximum depth, a full glider dive/surface cycle (Fig. 2.4) has a period of 5 hr and an amplitude of 1000 m for a horizontal distance of 3 to 4 km. Shallow dives where the glider has to fight strong currents such as those in the North Sea mission (Ch. 5) had a period of 15 min and reached a depth of 70 m with horizontal travel of 150 m relative to the water. In the Ross Sea, shallow dives to 400 m lasted 2 hr while deeper dives to 700 m typically lasted 4 hr, travelling 1 and 2 km in the horizontal respectively. As mesoscale biological features (i. e. 10 km) change on time scales of days, it is not possible to treat glider observations as a synoptic view of a system (Rudnick and Cole, 2011). Consequently, it becomes impossible to determine whether observed changes are temporal or spatial.

This issue can be lessened by running multi-glider missions or different platforms (i. e. ships, satellites, moorings, floats) simultaneously. Having another set of observations, whether discrete (i. e. floats, moorings, other gliders) or synoptic (i. e. satellites), or using several gliders simultaneously allows for comparison between different regions and provides a context for the observations. This indicates whether changes extend to the entire survey region and are temporally dependent or whether these are spatially-dependent “localised” changes (Howe et al., 2007; Nicholson et al., 2008; Queste et al., 2012; Rudnick and Cole, 2011).

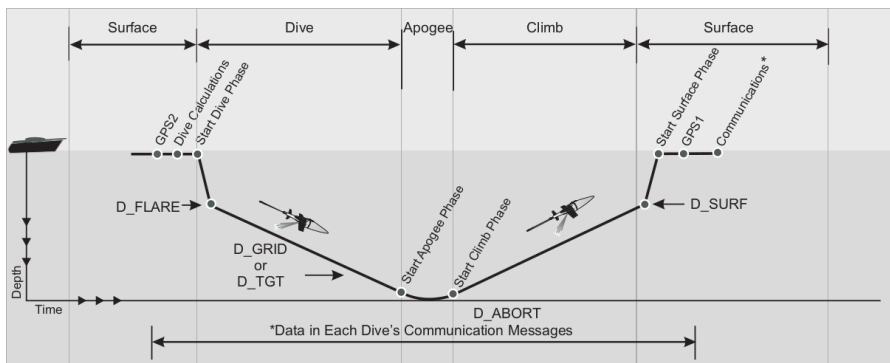


Figure 2.4: Canonical Seaglider dive. Figure taken from IRobot (2012).

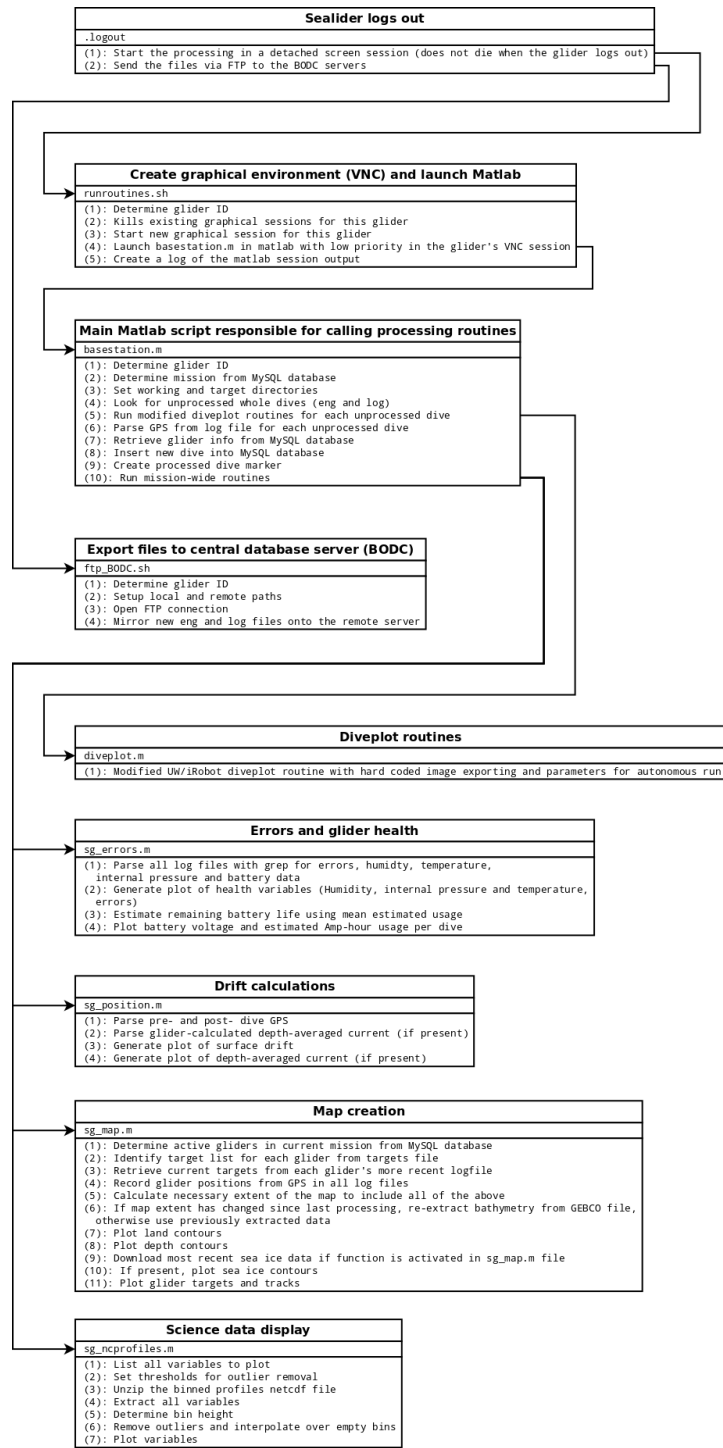


Figure 2.5: Detail of the basestation data processing routines and data dissemination methods.

## 2.2 DATA CORRECTION METHOD

### 2.2.1 *Influence of platform characteristics on data quality*

The glider's motion and battery limitations complicate correction of the data: as the gliders are never static during sampling, corrections are required for flow speed and sensor lag when passing through strong gradients. Greater battery capacity would allow the use of pumped sensors and higher sampling frequencies, thereby simplifying measurement of lags and necessary corrections. Three measured parameters are greatly affected by these issues; both the temperature and oxygen sensors have a slow response time and conductivity is altered by the thermal mass of the cell.

Both the oxygen optode and the thermal probe have significant response times which lead to hysteresis at the oxycline and thermocline. The thermal probe lag is the time required for the probe to equilibrate to the surrounding water temperature (Bishop, 2008; Fofonoff et al., 1974; Garau et al., 2011); this has been determined by the UW (0.6 s) and appears to be constant (i. e. not a function of flow speed or temperature) within the range of temperatures commonly sampled during a glider mission.

The oxygen optode's lag relates to the sensor design. The sensor measures the fluorescence decay of a luminophoric platinum-porphyrin matrix after excitation by a blue light. The fluorescence behaviour is directly related to the oxygen saturation within the matrix (Aanderaa Data Instruments, 2009). The sensor's lag is caused by the delay during which the matrix equilibrates with the surrounding environment as oxygen diffuses through the porous matrix (Tengberg et al., 2010; Tengberg and Hovdenes, 2013; Uchida et al., 2008). The Aanderaa 4330 optode is available with two different foil options. The first and original foil is provided with a teflon coating making the sensor more stable, particularly when subjected to high solar radiation. The second foil is similar, but comes without the protective teflon coating. This makes the sensor susceptible to high light (> 15 000 lux) but

greatly decreases the equilibration time (Tengberg et al., 2010; Tengberg and Hovdenes, 2013; Uchida et al., 2008).

The conductivity cell obtains measurement very rapidly (order of milliseconds) but the temperature of the water flowing through the cell is altered by the thermal mass of the sensor housing when moving through temperature gradients (Garau et al., 2011). This leads to significant biases when crossing thermoclines.

For static sensors (i. e. moorings), changes in measured parameters are slower than the sensor's lag, thereby masking this effect. For other mobile platforms (i. e. towed undulators and ship-borne CTDs), the same issues apply but the much higher sampling frequency simplifies the correction as the sampling interval is orders of magnitude smaller than the Sensor Lag ( $\tau$ ) (Fofonoff et al., 1974). For gliders, the sampling frequency and  $\tau$  are of the same order of magnitude making it difficult to properly determine the sensor's response to changes in the environment and therefore isolate and remove the signal aliasing. Unlike floats, however, sampling is frequent enough to allow some reconstruction of the original signal. For platforms such as Seagliders, a trade-off is made between battery life and sensor ability. By using a pumped CT sensor it would be possible to reduce data aliasing due to poor glider flight and sensor lag, however the battery drain of such a sensor would greatly reduce the endurance of a glider.

For longer missions, sensor drift is also a significant issue due to biofouling and sensor aging, particularly for the oxygen optode and the WetLabs puck. Furthermore, the Seaglider runs a single thread processor for both the flight control and all of the scientific sampling. This means the glider is only able to perform one action at a time. This causes a discrepancy between the timestamp recorded for a round of sensor sampling and the actual time the sensors were sampled. This leads to derived properties being calculated using asynchronous samples (i. e. salinity, density, DO).

As Seagliders remain a relatively new tool, no internationally accepted data quality control procedures exist as of yet. All of the Seaglider data used was processed using a Matlab toolbox developed at the UEA. The toolbox mimics the initial UW/iRobot data file parsing

before reprocessing the data to account for these issues. The code and relevant documentation is currently being maintained on a private repository (<http://bitbucket.org/bastienqueste/uea-seaglider-toolbox>); access to the code is possible by contacting the author. The methods used to correct the data described in Ch. 5 and 6 are described in this chapter.

### 2.2.2 *Timestamps*

The Seaglider samples at a frequency set in the science command file (Fig. 2.3). This includes the interval between guidance & control processing, compass, altimeter and science sensor sampling. A timestamp is created when the glider begins sampling and this value is set for all sensors. As the Seaglider runs a single-thread processor, it is unable to sample all sensors simultaneously. Therefore an error arises between the actual sampling time and the timestamp equal to the cumulative sampling duration of the previous sensors. This is illustrated in Fig. 3.5 of Ch. 3. This is critical when calculating salinity along temperature gradients as the conductivity is no longer related to the measured temperature.

To minimise this issue, the glider records the order in which the sensors are sampled and the total duration each sensor is powered over the course of a dive. The toolbox extracts this information from the dive metadata and calculates the mean sampling time for each sensor. A new time vector specific to each sensor is created and the timestamp correction applied to each. The toolbox does not currently account for variable sampling regimes throughout the water column. This was not of concern for either the North Sea or Ross Sea missions as all sensors were running at maximum frequency throughout the water column (5 s interval).

### 2.2.3 *Data flagging and binning*

Raw data are initially filtered by removing data outside of plausible limits for temperature and conductivity. Data is also flagged based on the glider's behaviour. A basic glide model is computed based on a smoothed vertical velocity estimate, pitch and hydrodynamic parameters estimated through a series of regressions comparing observed vertical velocity and a steady flight model. Data points where the glider's speed through water was outside of set limits ( $3$  to  $100 \text{ cm s}^{-1}$ ) are flagged as the flow through the CT sail (flushing speed) is considered to be suboptimal for sampling. Finally, erroneous outlying values and electrical noise are flagged by using a running median filter. For each value, the median of values within a  $2 \text{ m}$  range is calculated and compared to the value observed. In cases of large discrepancies, the flagged data point is removed and replaced by the median value. Using a running median filter in this situation preserves the gradient of clines in the ocean. Additionally, this range is smaller than the range used when binning data in Ch. 5 and 6 and therefore does not cause aliasing of the data or loss of resolution. Unlike larger scale studies, it was not possible to bin data over a larger vertical range as we wished to preserve vertically small scale features (i. e. a few metres) such as the DCM observed in Ch. 5. Flagged data points are not used when calculating  $\tau$  and were discarded for all processing in Ch. 5 and 6.

### 2.2.4 *Sensor lag correction*

In this section, we describe the method used by the UEA toolbox to calculate and apply the  $\tau$  correction. The UW/iRobot code originally used a first order lag correction (as per Scarlet, 1975) with a  $\tau$  of  $0.6 \text{ s}$  for temperature, a velocity dependent  $\tau$  for conductivity and applied no  $\tau$  correction for the Aanderaa optode. Assuming the response of a sensor is adequately described as

$$\frac{dT_{\text{obs}}}{dt} = \frac{1}{\tau}(T_{\text{real}} - T_{\text{obs}}), \quad (2.1)$$

where  $t$  is time and  $T$  is temperature.  $T_{\text{real}}$  &  $T_{\text{obs}}$  are real and observed temperature respectively. Then this equation can be solved for the true temperature

$$T_{\text{real}} = T_{\text{obs}} + \tau \frac{dT_{\text{obs}}}{dt}. \quad (2.2)$$

The same scheme is used in the toolbox for correction of temperature and DO data. Additionally, as the sensor records discrete measurements and due to the presence of electrical noise, Fofonoff et al. (1974) recommend smoothing the estimates of  $\frac{dT_{\text{obs}}}{dt}$ . This was performed using a least squared linear regression using 3 and 5 data points for temperature and oxygen respectively. At the time of writing, the UEA toolbox no longer uses the least squared linear regression and instead uses a 5 and 11 point lowpass filter for temperature and oxygen respectively.

Although the manufacturers provide estimates of a sensor's response time, it is preferable to determine this value for each mission due to differences between sensors and sensor aging. Biofouling may also may slow response. In particular, the fast response foil on the optode is devoid of the usual protective layer and may be more prone to aging although the exact mechanisms are unknown (Tengberg et al., 2010; Tengberg and Hovdenes, 2013; Uchida et al., 2008).

Due to the significantly smaller  $\tau$  for temperature relative to the sampling interval, it was not possible to determine  $\tau$  accurately.

Calculation of the oxygen  $\tau$  is detailed in Sec. 2.2.6. The oxygen optode's  $\tau$  is temperature dependent and corresponds to the time necessary for DO to diffuse into (or out of) the sensing foil and equilibrate with the surrounding water.

For the correction of conductivity data, the UEA toolbox uses the correction scheme described by Morison et al. (1994) and adapted to AUVs by Garau et al. (2011). This scheme relies on estimating the conductivity that would have been observed had the temperature not been affected by the sensor's thermal mass. The slope and offset of the amplitude of the error ( $\alpha$ ) and the time constant ( $\tau$ ) were estimated through trial and error. Difference between up and down casts along the thermocline were compared visually and the  $\alpha$  and  $\tau$  slopes and

offsets modified until an adequate fit was found. Up and following downcasts were used for the Ross Sea as thermoclines were located nearer to the surface than glider apogee and therefore these sections of the profile were closer in space and time and provided a better comparison. For the North Sea mission, downcasts were compared to the following upcast instead for the same reason as time spent communicating at the surface greatly increased the separation of up and following down casts.  $\alpha$  and  $\tau$  are also dependent on flow speed through the CT cell. Detailed equations can be found in Morison et al. (1994).

#### 2.2.5 *Temperature, Conductivity and Chlorophyll a sensor calibration*

After corrections of timestamps, removal of flagged data and  $\tau$  corrections, the data are compared to any calibration data available and the sensors recalibrated. For both glider deployments described in this thesis, only a single CTD cast was available for calibration. For both temperature and salinity, an offset was applied to obtain the same mean value as the CTD cast; procedures and details are available in the relevant chapters (Ch. 5 and 6).

The WetLabs ECO puck is provided with coefficients to calculate chlorophyll a concentration. These coefficients are not sufficient for accurate determination of chlorophyll a concentration due to the natural variability of the fluorescence to concentration ratio *in situ*. This is dependent on surrounding light levels, phytoplankton species and acclimatisation to light regime, the water's inherent optical properties and fouling on the sensor. For this reason, the glider's fluorometer is calibrated against lab-determined chlorophyll a concentrations from samples collected *in situ*.

First, the sensor's dark count is calculated. This corresponds to the measured counts by the sensor in the absence of chlorophyll a. The entirety of a mission's fluorometer readings are plotted in a histogram and a dark count value is selected based on the shape of the plot. In most cases, the count values show an exponential distribution above the dark count level with sensor noise below the dark count

level. Once the dark count level has been identified, the fluorometer counts minus the dark count is linearly regressed against reference chlorophyll a concentrations at corresponding depths to determine the scale factor. Finally, chlorophyll a concentrations are recalculated as per Eq. 2.3.

$$[\text{Chl a}] = \text{scaleFactor} \times (\text{fluoCounts} - \text{darkCounts}). \quad (2.3)$$

### 2.2.6 Dissolved Oxygen

In this section we first describe the method for calculating DO concentration. We then discuss the determination of optode  $\tau$  and the calibration procedure for the Aanderaa 4330 optode. As the Aanderaa optode measures oxygen saturation as opposed to actual concentration, further corrections are required.

As described in the user manual (Aanderaa Data Instruments, 2009), the optode emits blue light which excites the platinum-porphyrin luminophore. Relaxation of the luminophore occurs either through fluorescence or by energy transfer to dioxygen molecules. More energy is quenched under higher DO concentrations. The quenching causes lower fluorescence intensity but also to a shorter fluorescence half time (Aanderaa Data Instruments, 2009; Tengberg et al., 2006). This is directly related to the amount of oxygen present as described by the Stern-Volner equation

$$[\text{O}_2] = \frac{1}{K_{SV}} \left\{ \frac{\tau_0}{\tau} - 1 \right\}, \quad (2.4)$$

where  $\tau$  and  $\tau_0$  indicate decay time and decay time in the absence of dioxygen, and  $K_{SV}$  is the quenching efficiency (Aanderaa Data Instruments, 2009).

The phase angle difference between fluoresced red light from the foil and reference red light emitted from a diode is calculated to account for electronic fluctuations within the instrument. This phase angle is then temperature compensated and linearised to determine the oxygen saturation within the foil (Aanderaa Data Instruments, 2009). The reason raw output from the sensor cannot be used is because the relation between oxygen saturation and oxygen concentra-

tion is both temperature and salinity dependent. Values output by the sensor assume a constant salinity which is set within the sensor (generally 0 PSU unless specified otherwise by the user).

The UEA glider toolbox uses the phase difference (TPhase) described above for calculating DO concentration. The procedure described in the Aanderaa manual is followed to obtain oxygen saturation within the foil. The phase difference is temperature compensated to obtain a calibrated phase (CalPhase) using a linear equation (Eq. 2.5), and then linearised using 28 foil specific coefficients to obtain oxygen saturation. Phase coefficients 2 and 3 in Eq. 2.5 are null following the manufacturer’s calibration as they use a simple two-point calibration. We will return to this equation further in the text when describing the UEA toolbox calibration method when comparing Seaglider oxygen optode data to *in situ* calibration data.

Unlike in the Aanderaa protocol, concentration is calculated from this saturation value using the Benson and Krause Jr. (1984) equation for oxygen solubility. Although García and Gordon (1992) have provided new coefficients from a combined fit of two empirical formulae, Benson and Krause Jr. (1984) remain more accurate in seawater.

$$\begin{aligned} \text{CalPhase} = & \text{PhaseCoef}_0 + \text{PhaseCoef}_1 \times \text{TPhase} \\ & + \text{PhaseCoef}_2 \times \text{TPhase}^2 + \text{PhaseCoef}_3 \times \text{TPhase}^3. \end{aligned} \quad (2.5)$$

Then, a pressure correction, as per Uchida et al. (2008), is applied to the DO concentration data (Eq. 2.6).

$$[\text{O}_2]_{\text{corr}} = [\text{O}_2]_{\text{obs}} \times \left( 1.0 + \frac{0.032 \times \text{pressure}}{1000.0} \right). \quad (2.6)$$

Investigations into the oxygen sensor lag were originally performed by Tengberg et al. (2010) and Tengberg and Hovdenes (2013) with Aanderaa but failed to define  $\tau$  precisely enough for applications of DO studies on gliders. At the time this work was done, the toolbox used a heuristic approach to determining a  $\tau$  value for the optode. An ideal  $\tau$  was estimated based on the shape and differences between both casts using an automated method. For each dive in the mission, the down and up DO profile were calculated with a range of  $\tau$  values. For each dive, a “best fit  $\tau$ ” was selected based on the area between

the up and down curves when plotted against density. The median of all  $\tau$  values collected for each dive was then used to correct DO for the entire mission. The difference between the curves was calculated when plotted against density as opposed to pressure as this reduced the difference between casts caused by internal waves.

Hahn (2013) performed extensive work on determining  $\tau$  and its temperature dependence for various Aanderaa optodes. He determined the  $\tau$  of 34 different optodes (both Aanderaa 4330 and 3830 models) and identified a time constant of  $\tau = 14.8 \pm 3.9$  s at  $20^\circ\text{C}$  with a temperature dependence of  $-0.40$  s  $\text{K}^{-1}$ .

These coefficients were only made available in time for analysis of the Seaglider data in Ch. 5. Data presented in Ch. 6 were processed using the heuristic method described previously. Interestingly, the coefficients proposed by Hahn (2013) were significantly lower than those determined heuristically for the gliders in the Ross Sea and provided poor correction of the thermal lag; this is likely related to the temperature difference between both regions. The  $\tau$  value determined heuristically for the North Sea was in agreement with the coefficients suggested by Hahn (2013).

We now discuss the procedure for *in situ* calibration of Seaglider data. The need for calibration stems from the fact that the sensing foils age very rapidly over the first 100 000 samples. Afterwards they remain stable when kept in the dark and dry, although they remain prone to bleaching in strong light ( $< -0.025\%$  drift per 100 000 samples; Hahn, 2013; Tengberg and Hovdenes, 2013). Aanderaa now only sell foils that have gone through a burn-in period. The implication is that the phase coefficients provided by iRobot and Aanderaa were no longer applicable at the time and this could be observed as reduced signal amplitude in the glider data compared to calibration casts (Figs. 5.4, 6.2 & 6.3).

Glider oxygen data were compared against oxygen data from a ship CTD cast performed in proximity and simultaneously to a glider dive for both missions. Calibration of DO data was performed in phase space. The accepted method is to calibrate Aanderaa optodes in temperature-phase space (Hahn, 2013). However as only one ref-

erence cast was available for titration for each mission, it was not possible to estimate the influence of temperature. As temperature generally remained consistent during both glider deployments (Ch. 5 and 6), we assume the impact on calibration to be negligible.

The principle of the calibration relies on the assumption that two optodes with the same foil would measure the same calibrated phase (CalPhase). To calibrate Seaglider DO data, the UEA toolbox calculates the calibrated phase that the glider should have observed from the reference oxygen measurements (in this case, calibrated ship CTD profiles) if  $\text{PhaseCoef}_0$  and  $\text{PhaseCoef}_1$  of Eq. 2.5 were accurate for that deployment. This is done by back-calculating through the oxygen concentration calculation steps detailed previously by removing the pressure correction, then calculating saturation. The foil coefficients from the Seaglider's optode are then used to obtain a pseudo-CalPhase from the oxygen saturation obtained from the CTD cast. Both the glider TPhase data and the reference pseudo-CalPhase data are gridded along potential density in  $0.01 \text{ kg m}^{-3}$  intervals. A linear regression is then performed to determine  $\text{PhaseCoef}_0$  and  $\text{PhaseCoef}_1$  of Eq. 2.5 between the Seaglider's TPhase values and reference pseudo-CalPhase values. The new  $\text{PhaseCoef}_0$  and  $\text{PhaseCoef}_1$  are then used to calculate a calibrated phase that is accurate for waters within that temperature range. Finally, DO concentrations are recalculated as per the method described above to obtain a calibrated DO profile.

DEPLOYMENTS IN EXTREME CONDITIONS:  
PUSHING THE BOUNDARIES OF SEAGLIDER  
CAPABILITIES (*PUBLISHED*)

---

3.1 INTRODUCTION

The past 30 years have seen a tremendous advance in the fields of biological, chemical and physical oceanography. The advent of satellite oceanography combined with improved ship-based capabilities and numerical modelling have provided new insight into the global functioning of the marine ecosystem. This global view allowed us to identify major global issues and led us to further develop ocean models to study and predict interactions between different systems. Today, our knowledge of these issues is limited by a lack of understanding of the finer scale processes. To further refine our understanding and the accuracy of our models we must resolve the meso- and submesoscale features we cannot observe by satellite and how different temporal and spatial scales relate to each other.

This understanding is currently hindered by the disparity of our observations. Carl Wunsch distilled this issue into “having no prospect of a single universal observation system” (Wunsch, 2010). Satellites are largely constrained to surface observations, Lagrangian platforms such as floats and drifters provide excellent coverage but lack the necessary resolution to identify meso- and submesoscale features, and mooring or ship based surveys provide the necessary resolution but lack both the spatial and temporal coverage.

More recently, there has been great interest and exponential development in the field of long-range and high endurance gliders. Gliders are autonomous underwater vehicles able to bridge the gap between the different scales of observation and create a synthetic view of a system’s functioning. Their mobility allows them to act as virtual

moorings or to survey transects up to several thousand kilometres in length, their high endurance allows them to gather observations over the span of seasons, and their modular sensor packages give them the ability to record biological, chemical and physical parameters at very high resolution while providing the information to the user in near real time.

Gliders have repeatedly demonstrated their capabilities in process studies; despite this, their use in persistent observatories is only just beginning (Alkire et al., 2012; Asper et al., 2011; Briggs et al., 2011; Frajka-Williams et al., 2009; Nicholson et al., 2008; Perry et al., 2008; Rudnick et al., 2004; Sackmann et al., 2008). This is likely due to the remaining uncertainty around the technology. Gliders are a relatively new technology and their limits and abilities are not yet well defined. Gliders need to prove to the scientific community that they are suited to persistent deployments and monitoring observatories by running at low cost without compromising the science.

### 3.2 DEPLOYMENTS

In this paper, we aim to highlight the strengths and weaknesses of glider platforms by synthesising the issues faced during a series of deployments where gliders were pushed to the limit of their current abilities. The issues encountered were often specific to Seagliders, but many of the same principles apply to other glider-type AUVs. We then review how best to approach Seaglider data and provide information on a toolbox currently in development to aid in the processing of Seaglider data.

In order to fully understand the requirements for prolonged deployments we must identify the troubles which commonly affect deployments. By becoming aware of how and when mission-compromising issues arise, we are able to define strategies which either eliminate or reduce the risk and plan for contingencies.

Although less significant during short deployments, gradually occurring problems have an increasing effect as the duration of a glider's deployment increases. When not properly accounted for, changes such

Table 3.1: Commonly occurring issues during Seaglider deployments

	<b>Unforeseen / Rapid</b>	<b>Planned / Eventual</b>	<b>Constant / Gradual</b>
<b>Mechanical</b>	Equipment failures, breaks and leaks	Battery drain	Sensor drift, wear and tear
<b>Logistical</b>	Human error, incorrect calibrations and ballasting	Staff absences, system upgrades	Human error
<b>Environmental</b>	Collisions, fishing, theft and wildlife encounters	Poor weather, drop of GPS/satellite signal	Biofouling, varying density ranges

Table 3.2: Summary table of UEA Seaglider deployments. Median ( $\tilde{x}$ ) and mean ( $\bar{x}$ ) values included for several post-mission statistics. Estimated communication cost per dive includes pre-mission testing of Seagliders. \* See Asper et al. (Asper et al., 2011) for more details on the GOVARS mission

Deployment	Glider	No. of Dives	Duration (days)	Max Depth (m)	Max $\sigma$ difference ( $\text{kg m}^{-1}$ )	$\bar{x}$ AmphHrs per dive ( $10 / 24 \text{ V}$ )	$\bar{x}$ call tries	$\bar{x}$ dive & surface time (min)	$\bar{x}$ horz. & vert. speed ( $\text{cm s}^{-1}$ )	Comm. cost per dive (USD)
Scotland Trials	502	34	2	130	1.4	0.112 / 0.298	1.5	28 / 15	35 / 14	N/A
	507	18	1	134	1.4	0.180 / 0.391	1.5	27 / 10	31 / 14	N/A
	510	38	2	108	1.4	0.080 / 0.177	1.6	30 / 10	36 / 12	N/A
GOPINA	510	1611	113	1023	2.6	0.055 / 0.092	2.0	99 / 13	29 / 12	2.98 P
North Sea I & II	510	23	1	70	1.1	0.034 / 0.047	2.3	12 / 13	37 / 18	19.73 P
	510	158	4	70	2.8	0.039 / 0.049	2.8	15 / 16	32 / 15	9.31 P
Tropical DISGO	537	738	131	1019	6.2	0.101 / 0.142	2.7	242 / 14	25 / 14	4.51 R
GENTOO	522	694	80	1016	1.9	0.137 / 0.113	3.7	177 / 22	35 / 15	2.29 R
GOVARS*	502	701	59	764	0.5	0.098 / 0.143	1.7	107 / 15	34 / 13	3.64 P

as sensor drift or biofouling may compromise the quality of the results more than the loss of a glider. Table 3.1 covers the most common issues affecting glider deployments. Logistical issues can generally be avoided with sufficient forward planning, however they deserve mention as their likelihood increases with duration and complexity of a mission such as in rotations of multiple gliders required for persistent observatories. Environmental issues can generally not be anticipated and require constant monitoring (Automatic Identification System (AIS) services, weather predictions, etc.). Mechanical failures are different in that they have a higher chance of occurring early on in a mission; this provides the opportunity to correct them rapidly. Leaks and faulty equipment can generally be identified immediately, limiting the impact on data collection if proper contingencies are in place. Most deployments therefore tend to be limited by long-term mechanical issues (eg. battery drain) as it is expected gliders and sensors will be sufficiently robust that wear and tear or sensor drift will not compromise the glider's ability to function before it needs to be replaced.

Here we describe the issues encountered during 8 glider deployments by the University of East Anglia (Table 3.2). Some of these missions were very short (on the order of days) and have little in common with persistent deployments but the occurrence of issues during these missions highlights their likelihood in even longer deployments. The deployment of a UEA Seaglider in the Ross Sea (Fig. 3.1) as part of the GOVARS project will not be discussed as it was previously described by Asper et al. (Asper et al., 2011)).

### 3.2.1 *Seagliders*

All of our deployments used iRobot Seaglider model 1KA units for our ocean observations. Seagliders are autonomous underwater vehicles designed by the University of Washington (Eriksen et al., 2001) and recently licensed to iRobot for commercialisation. They have a depth range of 50 to 1000 m and can perform missions of several months travelling thousands of kilometres. The record for the longest Sea-

glider deployment is held by Charlie Eriksen, of the University of Washington, with over 5500 km over 292 days unaided by ocean currents (University of Washington, 2012). Seagliders, unlike other AUVs, have no external moving parts. They rely solely on the variable buoyancy device and internal battery pack for motion. By modifying their density, and shifting the battery pack to regulate pitch and roll, they generate lift and forward momentum with the fixed external wings. Their sensor package is fully modular. The Seagliders described in this paper carried an onboard SeaBird CT sail, an Aanderaa 4330F oxygen optode and a Wetlabs Triplet EcoPuck. Seagliders in recent deployments (2011 onwards) were also equipped with a Wildlife Instrument Finmount SPOT-100 tag used as an ARGOS transmitter for emergency location.

The UEA Seagliders use a combination of RUDICS and PSTN communications for piloting and data transfers. The basestation is mirrored every 6 hours and runs on an uninterruptible power supply. The UEA webserver containing Seaglider health status, piloting and science information for pilots and the public is kept on a different server to minimise the risk of compromising the basestation itself. The basestation runs the standard iRobot basestation software versions, complemented by a series of Python and MATLAB scripts developed in-house to render the Seaglider data. This is then displayed on a PHP based web platform using a Google Maps API to display geographic information. Maps and scientific data for all deployments described below are available on the the UEA Seaglider webpage (<http://ueaglider.uea.ac.uk>).

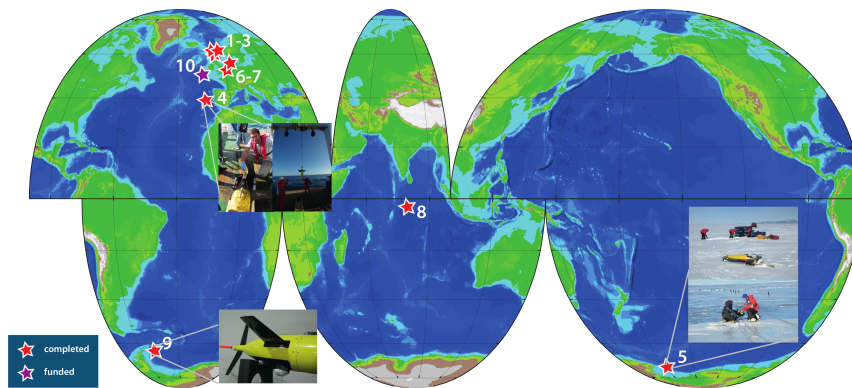


Figure 3.1: UEA Seaglider deployments and collaborations. 1-3: Scotland Trials. 4: GOPINA. 5: GOVARS, a collaboration with the Virginia Institute of Marine Science and the University of Washington (Asper et al., 2011). 6-7: North Sea. 8: Tropical DISGO. 9: GENTOO, also involving iRobot and the California Institute of Technology. 10: OSMOSIS (scheduled autumn 2012).

### 3.2.2 *Scotland Trials*

In March 2010, three Seagliders were deployed in Loch Linnhe, Scotland, to practise piloting and optimising the instruments. We performed a series of short deployments to test how the piloting team could control the Seagliders. On March 22nd we deployed and recovered one Seaglider, simply to test its buoyancy, communication channels, and deployment and recovery techniques. On the following day, we deployed and recovered SG507 and SG510 successfully. Finally, on March 24th we took all three Seagliders to the Lynn of Morvern to undertake an overnight trial. We selected a location commonly used by SAMS to test their AUVs. The location offers waters deeper than 100 m and little in the way of ship traffic. A single transit route was used regularly to link a local quarry to the mouth of the sea loch. We selected our survey location to be on the opposite side of the sea loch.

During the night, contact was lost with SG507. SG502 and SG510 were safely recovered. All available data were reviewed and it was concluded that SG507 had a collision with a ship heading to the quarry. AIS data available on the internet showed the passage of the Wilson Malm near the Seaglider's last known communication within a twelve minute period. A recovery party was sent after SG507, searching from its last known location using an acoustic transponder. A systematic acoustic survey of the area was undertaken using tidal estimates to determine possible locations of the glider. The combination of strong winds and agitated seas severely hampered the search. The search was continued to no avail in further regions and scanning the beaches around Loch Linnhe.

Despite regular monitoring of ship AIS, collision with the ship was not anticipated. The glider was diving nearly half an hour for every 10 minutes at the surface. Several scenarios were suggested, the most likely being that the glider's antenna, a particularly fragile component, was damaged. Alternatively, it is possible that the Seaglider's wings or hull were damaged. We suspect the latter is unlikely as the force required to crack the hull is very large. It is probable the bow

wave created by the ship push the glider out of the way, limiting the force of the collision.

### 3.2.3 *GOPINA - Iberian upwelling*

The GOPINA project (Glider observations of productivity in the North Atlantic) aimed to observe productivity in the Iberian Upwelling region. One Seaglider was deployed during the summer of 2010. The glider was deployed from the *Mytilus* off the coast of Vigo on June 1<sup>st</sup> 2010 where it performed 17 repetitions of a zonal 50 km transect across the shelf edge. GOPINA was a pilot study involving SG510 aiming to improve our understanding of the mechanisms driving production in the Iberian upwelling region by observing the physical, chemical and biological processes off the coast of Spain on scales which are not easily observed by moorings or ships. Here gliders offered an opportunity to observe the water masses in close proximity to the shelf edge during the entire summer season. The primary challenges with this mission were the sharply changing bathymetry along the shelf edge, biofouling, sensor drift, battery life and marine traffic.

The issue of controlling the glider depth was a trade off between simplicity and battery life. Onboard bathymetry was not used due to poorly known bathymetry at the sharp shelf edge and the desire to observe the processes as close as possible to the shelf edge. The two remaining options were frequent changes to the target depth in the command file or the use of the onboard altimeter. The safety of the glider was considered to be the primary goal and the risk of human error too great to rely solely on changing the target depth parameters therefore the onboard altimeter was switched on for the duration of the on-shelf observations. To preserve battery life, the altimeter was switched off beyond the shelf.

The second component of this deployment involved chasing a satellite-observed eddy filament using the glider. This involved crossing four large shipping lanes. The strategy employed was to minimise time spent at the surface despite risking navigational inaccuracies due to



Figure 3.2: A thick algal mat covering the Seaglider upon recovery. Growth on the Aanderaa optode may also have contributed to the sensor drift.

the reduced number of GPS fixes and the meridional currents. The glider was flown without surfacing for 10 consecutive dives thereby avoiding the shipping lanes.

The glider was recovered after 147.8 / 88.7 AmpHrs had been consumed out of total of 150 / 100 AmpHrs from the independent 24 and 10 V batteries respectively. The final battery voltages were 19.6 and 9.7 V respectively, still above the "safe limits" of 19.0 and 7.9 V. The end of the mission was precipitated by a hardware issue. Due to the partitioning of the memory card, the number of file entries was limited to 4096. When the glider had completed 1358 dives, each dive creating 3 files, and including operating system files, the maximum number of entries was reached. Neither creation or deletion of data were possible any more as they involved the creation of temporary files. Editing of existing files (i. e. changing flight and sampling parameters) were still possible but no further scientific data could be recorded. iRobot has since then implemented measures that eliminate this problem.

Over the duration of the mission, the Seaglider's flight became less stable (occasional stalling and asymmetrical dive pattern) and drift of the oxygen sensor output was observed. The first was eventually linked to biofouling covering the entirety of the Seaglider (Fig. 3.2). Sensor drift of the oxygen optode was observed across the duration of the mission (Fig 3.3). The drawback of the 4330F optode, compared to the standard 4330 optode, is that it is not protected from bleaching by excessive light with an optical isolation layer. Light intensities higher than 15000 lux may cause erroneous readings and prolonged exposure to light will accelerate bleaching of the foil. The advantage is quicker equilibration of the gas permeable sensing foil and therefore a faster response time when observing fluctuations in dissolved oxygen concentrations. Seaglider proximity to the CAIBEX repeat transect stations allowed for progressive cross-calibration to first identify this drift and to determine that it was not an environment change in dissolved oxygen, and secondly correct this drift in the data.

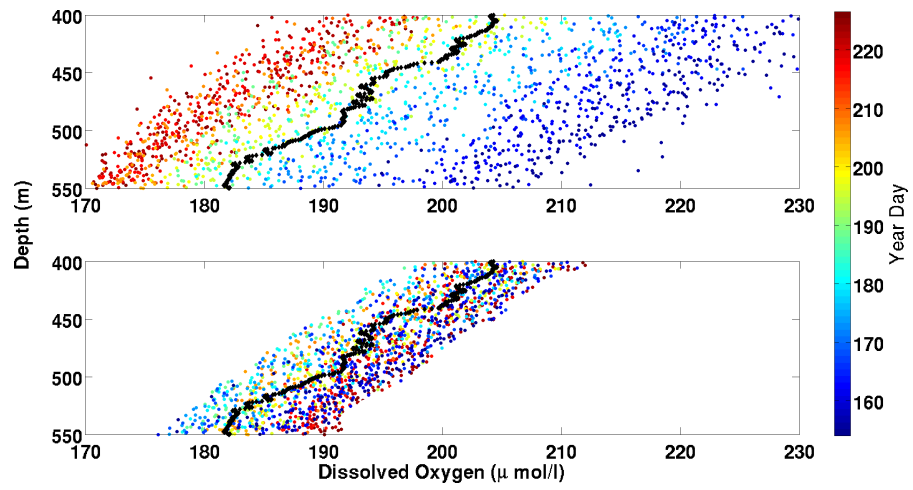


Figure 3.3: Pre (top) and post (bottom) sensor drift correction output of the Aanderaa 4330F. A net time-dependent shift is visible indicating gradual sensor drift throughout the mission. The black line represents mean values. Sensors were calibrated against Winkler titrations performed at repeated CAIBEX transect stations.

### 3.2.4 North Sea Hypoxia

The North Sea mission involved two sequential deployments of SG510 in the central North Sea. This mission aimed at investigating the evolution of mesoscale and submesoscale oxygen processes below the thermocline in the shallow North Sea. The challenge of this region is its relatively shallow depth and the difficulty the glider would have fighting the tidal currents. iRobot recommends a minimum depth of 50 m for the glider to be able to function properly. During this mission, the Seaglider was operating in waters of 70 m depth. The North Sea also suffers from very intense use by shipping and hydrocarbon industry.

To maximise the glider's ability to counter the tidal currents, the glider was sent on very steep fast dives. The result was that dives lasted an average of 14.6 minutes diving and 15.9 minutes at the surface (Table 3.2). In such a shallow environment, it is very difficult for the glider to make any headway or be easily controlled. The glider spends half of its time drifting, following dominant winds and surface currents. When it begins a dive, the bottom and top 10 m are used for adjusting pitch and roll and the glider makes no significant headway. Nevertheless, the glider was able to maintain its position, acting as a "virtual mooring", when currents were against the glider's direction. When currents pushed the glider in its desired direction, it was able to cover long distance rapidly. However, obtaining regular spatial coverage or following a clear transect line, to avoid oil platform exclusion zones for example, was very difficult. These steep, fast dives require large changes in buoyancy which drain the 24 V battery rapidly. To limit this issue, iRobot now make available an enhanced buoyancy engine, specifically designed to increase efficiency in shallow waters. This boost pump does not function at depth (below 120 m), but is both quicker and more efficient in shallow waters.

As a consequence of the faster diving speeds to counter currents, there was a need for fast sensor sampling. As the glider travelled at vertical velocities of  $0.17 \text{ m s}^{-1}$ , it was necessary to sample at the maximum rate (0.2 Hz) to properly resolve the features we wished

to observe. The combination of very large buoyancy changes to drive the glider's motion and maximum sampling rate led to a large energy consumption, despite the presence of the enhanced buoyancy engine. Typical consumption rates were of the order of 0.039 AmpHrs and 0.049 AmpHrs per dive of the 10 and 24 V batteries respectively.

The second deployment was terminated prematurely due to an error in the formatting of the memory card. Unlike the Vigo mission where an unusually large number of dives were performed, here the memory card had been incorrectly formatted thereby limiting the possible number of files to 512. The glider was placed in "virtual mooring" mode and recovered at the earliest convenience. As no further science could be recorded, there was no reason to leave the glider in a vulnerable position around oil and gas platforms or ships.

### 3.2.5 *Tropical DISGO - Indian Ocean*

A Seaglider was deployed from September 14th 2011 to January 23rd 2012 in the Indian Ocean where it performed 10 repeats of a meridional transect between 3°S to 4°S along 78°50'E. The Seaglider was deployed and recovered from R/V Roger Revelle from Scripps Institution of Oceanography, San Diego. This deployment was a component of the CINDY2011/DYNAMO project. The main objective was to investigate the atmospheric and oceanic mechanisms which trigger the Madden-Julian Oscillation (the principal mode of tropical climate variability in the Indian Ocean). The mission had two main objectives: to obtain a detailed view of the diurnal cycles in the vertical structure of the surface layers and to measure the structure of oceanic equatorial waves implicated in the generation of some Madden-Julian Oscillation events.

During deployment the main concern was battery life and balancing a long (4 month) deployment against getting sufficient data. The main issue that affected this, and could have been avoided, was that the glider was very badly trimmed for the density profile in the tropics. The Seaglider had to cope with a very strong pycnocline and very large density difference between the surface and 1000 m (Table 3.2).

It took over a month to fully trim the Seaglider's flight to an efficient level. To maximise battery life, the Seaglider's flight was adjusted for minimal necessary buoyancy and shallowest glide angle achievable. One unanticipated consequence of pushing the Seaglider's flight to the stalling limit was that this meant the flow past the conductivity sensor on the climb phase was too slow to produce accurate conductivity data.

Having pushed the glider's flight to its limit in order to maximise the 24 V battery life, the 10 V was now depleting faster. In order to regulate the consumption of the 10 V battery, changes had to be made to the sensor sampling regime. As the mission mainly aimed to obtain temperature and conductivity data, the Aanderaa optode and the Wetlabs puck were activated for a few dives every week to track longer term variations whereas the CT sail recorded continuously. To further reduce consumption, the Wetlabs optical sensor sampled once every 15 seconds at most. The optode sampled every 5 seconds in the upper water column (0 - 100 m), 15 seconds in mid water (100 - 300 m) and was switched off at depth. The CT sail recorded every 5 seconds between 0 and 300 m, and every 15 seconds below 300 m. By limiting the data recorded, battery consumption from communications and sensor sampling were both reduced, bringing the consumption rate of the 10 V battery to a manageable level.

### 3.2.6 GENTOO - Weddell Sea

We deployed three Seagliders in the western Weddell Sea, along the Antarctic Peninsula, in collaboration with the California Institute of Technology and iRobot. The mission investigated the physical and biological processes associated with the Antarctic Slope Current. The UEA glider (SG522) was deployed on January 23rd 2012 to survey the shelf edge. Iridium communication was lost with the glider on February 14th 2012. Continuous tag signals were obtained until April 14th; following this date, fixes became irregular, often several days apart. Following a 58 day absence of communications, the Seaglider entered recovery due to low 10 V battery voltage. The battery lasted enough

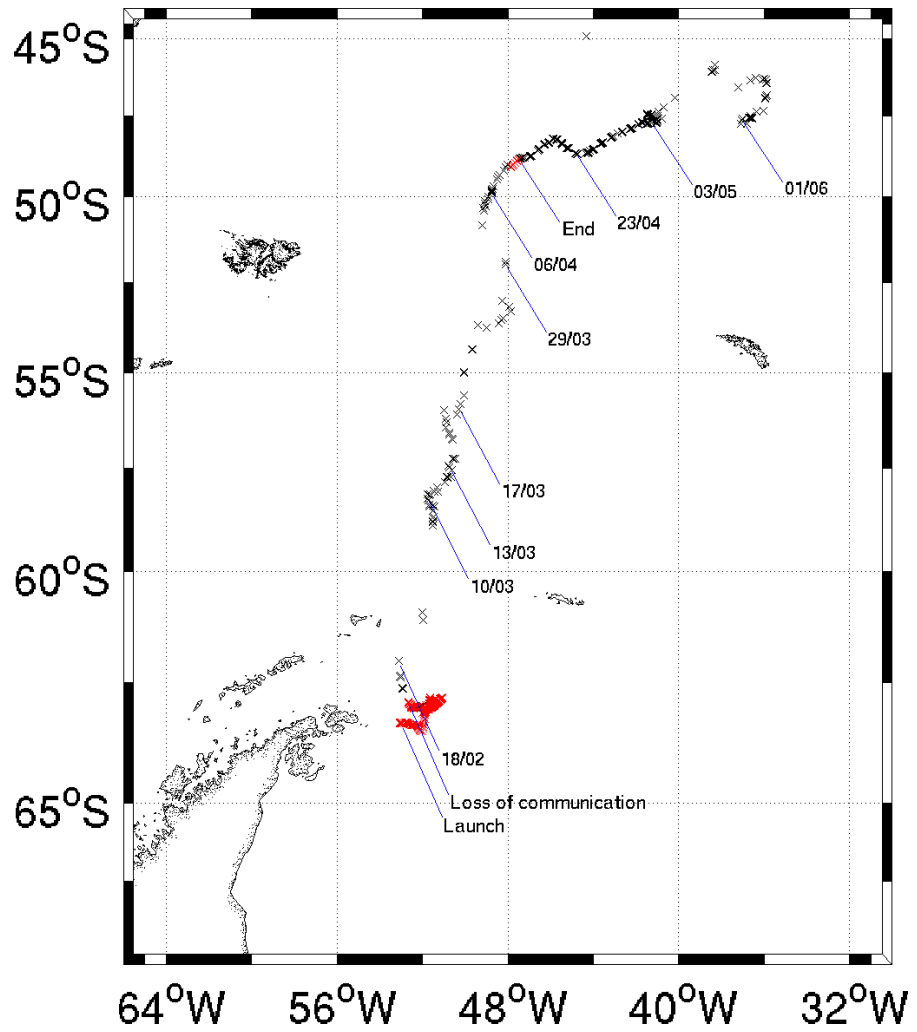


Figure 3.4: Map of Seaglider GPS positions (red) and ARGOS positions (black) with significant dates during the GENTOO mission.

for the transfer of 8 dives before dropping below the threshold necessary to power the Tattletale 8 processor. ARGOS communications continued during this period and a recovery mission was initiated. The SPOT tag ceased transmitting before the recovery ship reached the glider's location.

It was later concluded the glider's disappearance was due to a series of conflicting commands which led to the Seaglider diving continuously without attempting to communicate with the basestation. It continued on its original northward heading, crossing the Weddell Sea, the Antarctic Circumpolar Current and entering the Argentine Basin (Fig. 3.4). Despite not being piloted, the Seaglider was able to cross an area of very rapid currents and continue north by nearly  $15^\circ$ .

Although the ARGOS tag provided satellite fixes once the Seaglider stopped communicating, their use in the recovery was limited. Location fixes were usually only available 4 hours after the satellite obtained the fix. The tag was programmed to transmit only 150 times per day starting at 0:00 GMT to conserve battery life. This meant that once the glider went into recovery, all its transmissions were done during hours of darkness. The tag also did not supply fixes continuously during the mission. The cause of this is unknown but is most likely due to the effects of sea state, salt creep, and the position of the tag on the antenna. It is also possible the glider may have been in a satellite "black spot".

### 3.3 DEALING WITH DATA

Due to the relatively recent commercialisation of Seagliders and commercial decisions from the manufacturer, there are very few tools for the correction and calibration of Seaglider data. Most commercial CTD packages come with an intricate software suite which corrects for various sensor and thermal lags, applies corrections, smooths and despikes the data and provides a binned final product. iRobot provides a set of MATLAB scripts to its customers that do basic checks of glider flight and science sensor functionality but leaves it to

the customer to develop in-depth data analysis tools specific to their research and publishing needs.

To this end, we are in the process of developing a toolbox to add in the processing, both operationally and post-mission, of Seaglider data. We apply a new corrections scheme for scientific data sampled by Seagliders. The Seaglider has a single thread Tattletail 8 processor as sole CPU. Thus all guidance and control as well as scientific operations have to be handled successively. Since the guidance and control takes priority over scientific sampling, significant delays may occur between timestamping and scientific sampling. Furthermore, with increasing sensor payloads, there is a tendency to increase the number of parameters being sampled with additional sensors. Each sensor has an average wake-up and response time of one to three seconds. Cumulatively, these add up to differences of up to 12 seconds between the first and last sensor records. Since all sensor samples from a single round of measurements are associated to a single timestamp, there is a systematic bias in the data. As the timestamp is the first element to be recorded, data are sampled deeper than the timestamp on the downcast and shallower on the upcast. The depth anomaly created is of the order of 2 m with a vertical speeds of  $15 \text{ cm s}^{-1}$ , thus the difference between the up and down casts can reach 4 m or more for last triggered sensor.

This lag is not accounted for in either the Seaglider software or the data processing packages provided. The developers have suggested shifting the up and down profiles by 20 cm and assuming constant vertical speeds on the up and down casts. A formal correction is complicated by irregular sampling patterns. The sensor sampling is fully configurable with sensors sampling at different frequencies, the guidance and control routines also activate at a different frequency. To further complicate matters, this is not even regular on a single dive as frequencies may be programmed to be depth dependent. The correction we currently apply analyses each sample to determine which sensors operated and in which order, using information provided by iRobot, and uses a sensor and mission specific look-up table to correct for the average delay for each sensor (Fig. 3.5). We are confident that

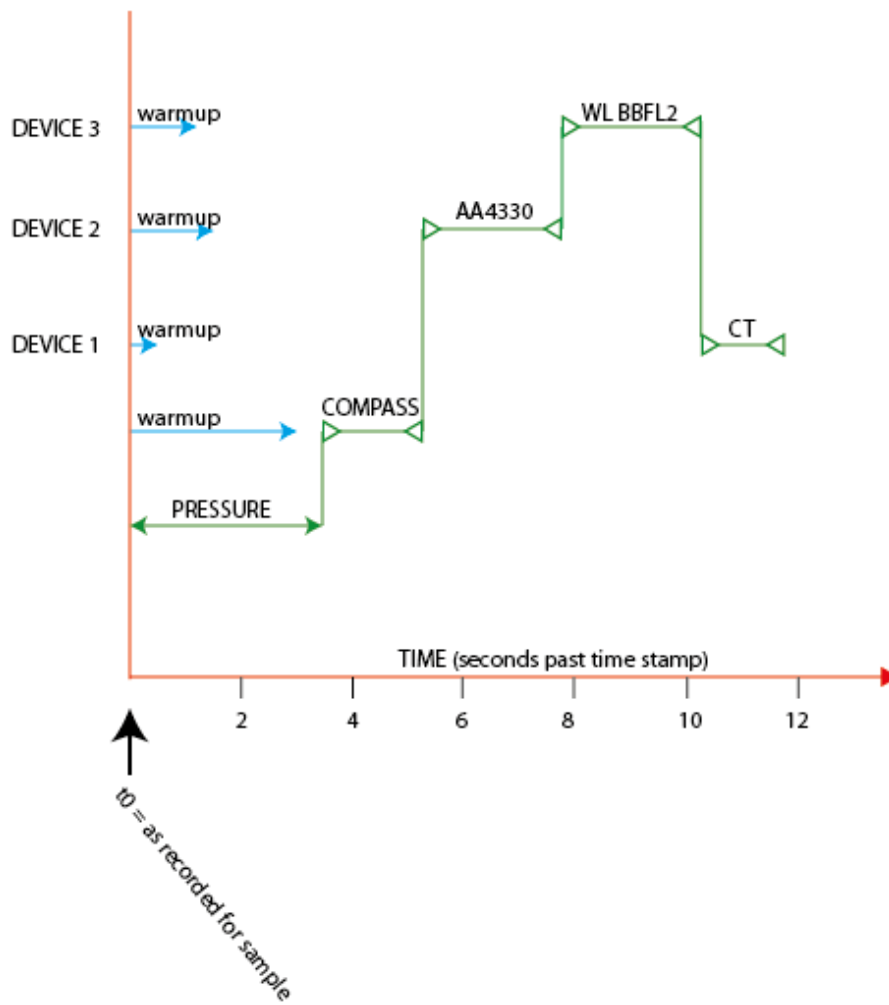


Figure 3.5: Successive sampling of devices with associated timelags and warm-up delays for a standard sensor payload on the Seaglider 1KA.

we address the associated sampling bias to a degree that is sufficient for errors to be smaller than measurement noise in pressure. After addressing this sampling bias, we apply further quality control procedures as recommended by the EGO initiative (part of the GROOM European design study), as well as time and thermal lag corrections as described by Garau et al. (Garau et al., 2011).

### 3.4 SUMMARY

Seagliders remain a fairly new technology. International collaboration between glider groups has become critical to ensure we develop the necessary understanding of glider strengths and weaknesses to push their capabilities beyond what is currently possible. Every new deployment provides a new set of experiences and problems. The next deployment the University of East Anglia will be involved in is a year-long multi-glider deployment, involving three rotations to ensure continuous coverage of the Porcupine Abyssal Plain. This project, dubbed OSMOSIS (Ocean Surface Mixing, Ocean Sub-mesoscale Interaction Study) will monitor upper ocean processes during a full seasonal cycle from September 2012 to September 2013. Full details are available on <http://ueaglider.uea.ac.uk>.

### Part III

#### THE CENTRAL NORTH SEA

---

Chapter 4 contained herein has been provided as published in the North Sea special Issue of Biogeochemistry.

*Queste, B.Y., Fernand, L., Jickells, T.D., and Heywood, K.J. (2012) Spatial extent and historical context of North Sea oxygen depletion in August 2010. Biogeochemistry.*

---

All work described in Ch. 4 & 5 was performed by Bastien Queste with the exception of that stated below:

Sampling of biochemical variables was done collaboratively with Cefas, specifically with the help of Rodney Forster, Veronique Creach and Katy Owen for the 2010 mission and with the help of Andy Hind for the 2011 mission. Analysis of chlorophyll *a* samples was performed by Cefas staff. Analysis of dissolved oxygen samples was performed by Queste and Hind. Calibration of the ESM 2 logger data was performed by Cefas staff. Planning of the cruise trajectory was determined by the Cefas Fisheries team to follow standard International Bottom Trawl Survey specifications. Piloting of the Seaglider was done by the UEA Seaglider group. Model calibration and development of the North Dogger GOTM-BFM case was performed by Cefas.



SPATIAL EXTENT AND HISTORICAL CONTEXT OF  
NORTH SEA OXYGEN DEPLETION IN AUGUST 2010  
(PUBLISHED)

---

#### 4.1 INTRODUCTION

Dissolved oxygen is necessary for the proper functioning of most marine ecosystems. In aquatic environments, the oxygen either diffuses from the atmosphere or is produced by photosynthesising organisms in the euphotic layer and is then transported by currents to different regions or mixed to depths where it is utilised. Low dissolved oxygen, or hypoxia, arises in situations where the rate of oxygen supply is less than the rate of consumption for a significant period. Hypoxia is defined as oxygen concentrations below 4 to 6 mg dm<sup>-3</sup> (125 to 190 µmol dm<sup>-3</sup>) by the Oslo and Paris Commission (OSPAR) in the Ecological Quality Objective (EcoQO) for the North Sea (Painting et al., 2005). This threshold was selected as it is generally considered that organisms may suffer sub-lethal, and potentially lethal, effects below this oxygen concentration (Diaz and Rosenberg, 2008; Vaquer-Sunyer and Duarte, 2008). Nevertheless, higher concentrations than considered hypoxic by OSPAR may cause harmful impacts on marine organisms (Pörtner and Knust, 2007). Hypoxia in stratified shelf seas is a complex phenomenon dependent on multiple interrelated factors. The most common mechanism is the export of large amounts of organic matter to the bottom of the water column, often originating from seasonal blooms or eutrophication, combined with a strong and stable pycnocline limiting mixing of oxygen to the BML. When the oxygen demand of habitual respiration levels combined with the additional oxygen required for remineralisation of new organic matter exceed the renewal of dissolved oxygen, hypoxia may occur. Some hydrographic factors have the potential of further enhancing this phe-

nomenon: higher upper ocean temperatures lead to increased organism respiratory demand, increased stratification and reduced oxygen solubility. Other hydrographic factors may lead to the resupply of oxygen to the BML. Disruption of the stratification by storms leads to the injection of oxygen into the BML (Rabalais et al., 2009), although this can also resuspend organic matter leading to post-event enhanced oxygen demand (Greenwood et al., 2010; Rabalais et al., 2010, 2009; Van Raaphorst et al., 1998; Weston et al., 2008). Recently, the possibility of increasing hypoxia in coastal zones across the globe has been highlighted by several authors (Conley et al., 2009a,b; Diaz and Rosenberg, 2008; Middelburg and Levin, 2009).

The review by Colijn et al. (2002) highlighted a paucity of studies assessing the impacts of low oxygen regions on organisms and ecosystems in the North Sea. Sedentary benthic and demersal organisms suffer the greatest impacts due to their inability to avoid hypoxic regions. For example, the commercially important species *Nephrops norvegicus* shows negative sub-lethal impacts in juveniles at oxygen concentrations below  $5 \text{ mg dm}^{-3}$  ( $156 \text{ } \mu\text{mol dm}^{-3}$ ). Although adults may withstand very low concentrations of dissolved oxygen, their habitual tolerance to other environmental variations (e.g. temperature) is severely decreased (Baden et al., 1990; Eriksson and Baden, 1997). Oxygen saturation also plays an important part in sediment biogeochemistry; Middelburg and Levin (2009) review the sedimentary processes which occur under hypoxic conditions.

It was previously estimated that the threshold for negative impacts of hypoxia was near the  $2 \text{ mg dm}^{-3}$  mark ( $62.5 \text{ } \mu\text{mol dm}^{-3}$ ), however the OSPAR Commission has elevated that level to  $4 \text{ mg dm}^{-3}$  ( $125.0 \text{ } \mu\text{mol dm}^{-3}$ ) in the light of studies assessing sub-lethal impacts and modelling fisheries productivity (Painting et al., 2005). The European Union Water Framework Directive for oxygen defines high water quality as greater than  $7 \text{ mg dm}^{-3}$  ( $218.6 \text{ } \mu\text{mol dm}^{-3}$ ), good as greater than  $4.7 \text{ mg dm}^{-3}$  ( $146.8 \text{ } \mu\text{mol dm}^{-3}$ ), moderate as greater than  $2 \text{ mg dm}^{-3}$  ( $62.5 \text{ } \mu\text{mol dm}^{-3}$ ) and poor below that value. The Shellfish Waters Directive sets standards using oxygen saturation. The minimum imperative standard is set at 60% saturation and the guide

value at 80% saturation (Best et al., 2007). Both the Water Framework Directive and the Shellfish Waters Directive apply only to coastal waters; offshore waters of the North Sea are covered by the OSPAR Commission. However, the potential influence of climate change trends on oxygen levels in shelf seas in the future is of concern. Weston et al. (2008) conjecture that climate change scenarios in the North Sea could see a decrease in BML dissolved oxygen due to increasing temperatures: a temperature increase of 2-3°C will decrease oxygen solubility by 0.4 mg dm<sup>-3</sup> (13 µmol dm<sup>-3</sup>) at atmospheric pressure. Climate change may also lead to earlier stratification each year and possibly an increase of surface layer productivity; it could also cause a decrease in summer storms disrupting the stratification. All these changes could increase the spatial and temporal extent of deep water low oxygen.

For bottom waters to have reduced oxygen content they must be isolated from sources of oxygen saturated water by a strong pycnocline and have weak advection; thus the residual circulation of the North Sea affects the supply of dissolved oxygen. The circulation in the North Sea results from a combination of wind-induced flow, topographically-steered currents and density-driven flow resulting in relatively narrow jets (Brown et al., 1999; Hill et al., 2008). The semi-enclosed situation of the North Sea, coupled with the various inflows lead to an anticlockwise circulation. Water enters from the Fair Isle Current, the Channel and the Skagerrak, and exits along the Norwegian Trench (Ducrotoy et al., 2000; Brown et al., 1999; Thomas et al., 2005, Figs. 4.1 & 4.2). Very little inflow from the northern boundary reaches south of the Dogger Bank; instead this water circulates north of the Dogger Bank to rejoin southern waters before exiting the North Sea through the Norwegian Trench (Thomas et al., 2005). In the Southern Bight, high salinity water entering the system through the Straits of Dover is gradually mixed with riverine discharge and eventually leaves the system via the Norwegian Trench. It is generally agreed that water in the North Sea has a residence time in the order of 0.6 to 1 year (Jickells, 1998; Otto et al., 1990; Thomas et al., 2005; Van Raaphorst et al., 1998; Vermaat et al., 2008).

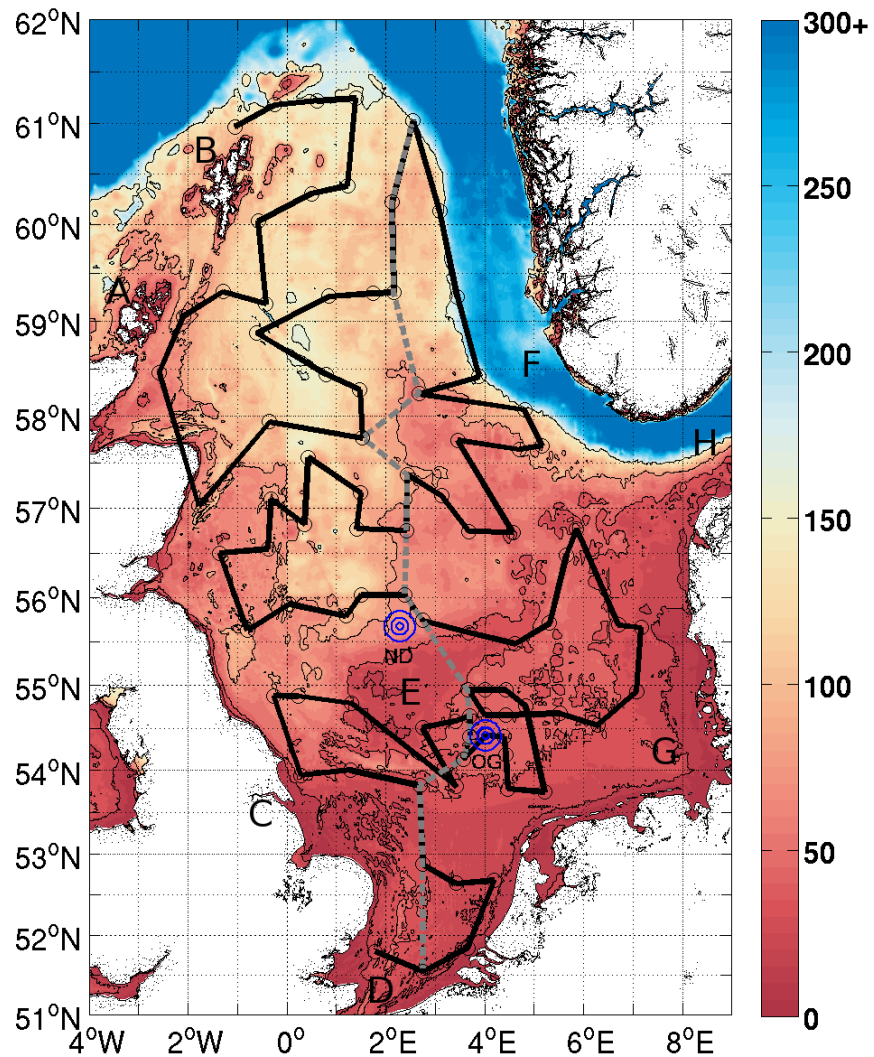


Figure 4.1: Bathymetry of the study area in metres (GEBCO, 2010). Circles mark the 88 sampling locations. The black line indicates the order of stations sampled, starting from the south and the dotted grey line the section used in Fig. 4.3. Depth contours have been added for the 20, 40, 80 and 160 m isobaths. Positions of the two SmartBuoy described by Greenwood et al. (2010) are indicated as ND for the North Dogger site and OG for the Oyster Grounds site. A & B: Shetland and Orkney Isles. C: Humber estuary. D: the Channel. E: Dogger Bank. F: Norwegian Trench. G: German Bight. H: Skagerrak

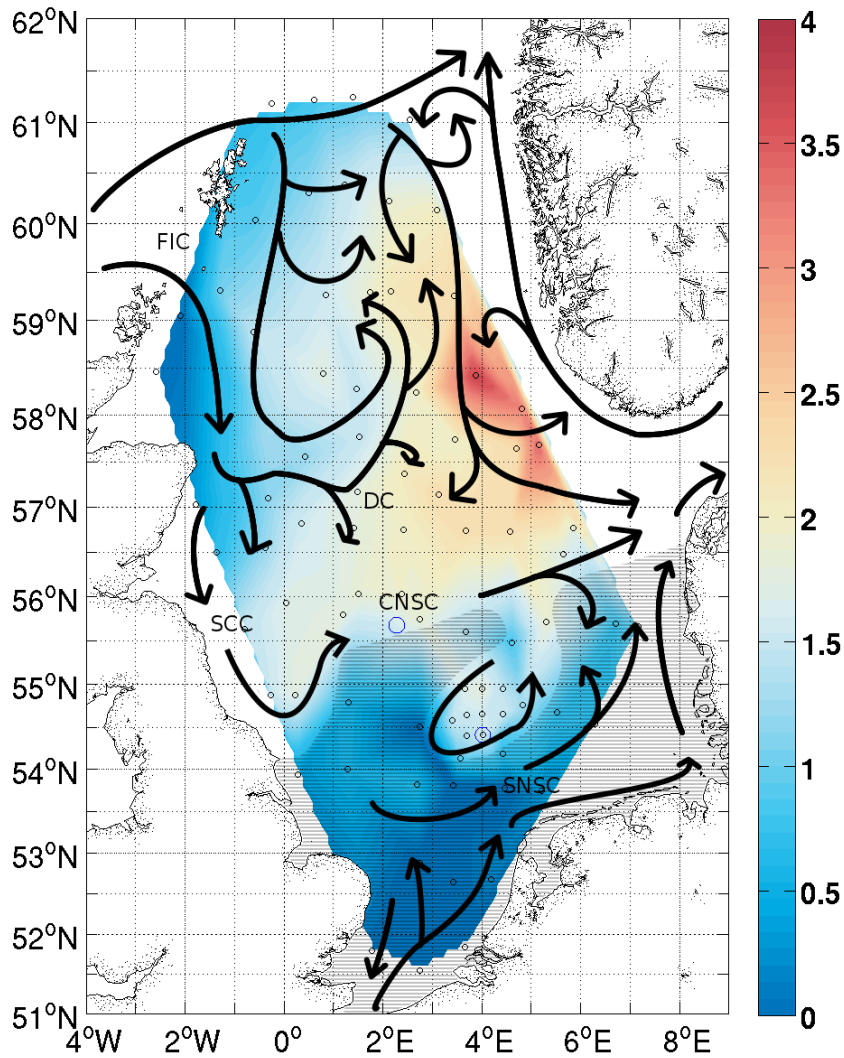


Figure 4.2: General circulation of the North Sea (adapted from Turrell et al., 1992 and Hill et al., 2008) overlaid on the density difference between the SML and BML in  $\text{kg m}^{-3}$ . FIC: Fair Isle Current, DC: Dooley Current, SCC: Scottish Coastal Current, CNSC: Central North Sea Current, SNSC: Southern North Sea Current. Hatch marks cover areas not subject to thermal stratification

The North Sea exhibits a generally vertically well mixed pattern in winter with occasional stratification in the deepest regions (Ducrotoy et al., 2000; Sharples et al., 2006). In the stratified North Sea, stratification becomes apparent from mid-April, with a thermocline at a typical depth of 30 m in the north (Ducrotoy et al., 2000; Greenwood et al., 2010; Sharples et al., 2006). South of the Flamborough-Helgoland front (see hatched area, Fig. 4.2), the shallower waters tend to remain well mixed and warmer throughout the year apart from occasional and temporary salinity stratification (Ducrotoy et al., 2000; Simpson et al., 1977; Vested et al., 1996). The region of the Oyster Grounds (Fig. 4.1) exhibits thermal stratification, albeit for a shorter period than the north (Greenwood et al., 2010), while the shallow region of the Dogger Bank shows greatly reduced stratification compared to the north (Ducrotoy et al., 2000; Vested et al., 1996). Sharples et al. (2006) showed that the main factor regulating the onset and strength of the stratification was local meteorology, particularly spring air temperatures, and that input of north-east Atlantic water played a reduced role. A correlation was also found between the North Atlantic Oscillation (NAO) and wind speeds; increased wind speeds could lead to later stratification in shallower regions or a more gradual pycnocline development (Sharples et al., 2006).

There have been recent reports of low dissolved oxygen in the North Sea. Moorings deployed at the Oyster Grounds (OG) and North Dogger (ND) sites (Fig. 4.1) during 2007 and 2008 observed summer oxygen depletion in the BML associated with strong stratification (Greenwood et al., 2010). Greenwood et al. measured gradually decreasing dissolved oxygen concentrations reaching  $203 \mu\text{mol dm}^{-3}$  (71% saturation) and  $162 \mu\text{mol dm}^{-3}$  (60% saturation) at ND and the OG at the end of the summer season prior to breakdown of the stratification in autumn. They examined the evolution of this oxygen depletion throughout the stratified season (April to October) and showed the influence of different physical and biological parameters. The importance of BML warming, accounting for 55% of the oxygen drawdown at the OG site compared with 10% at the ND site, was also demonstrated (Greenwood et al., 2010). Following Van Raa-

phorst et al. (1998), Greenwood et al. (2010) demonstrated that short-term storm events promoted sediment resuspension and subsequent oxygen consumption at the shallow (50 m) OG site. They concluded that decreasing oxygen concentrations were driven both by increasing BML temperatures and the consumption of organic matter. This organic matter originates from the spring bloom and from continuous production in the deep chlorophyll maximum (DCM) (Greenwood et al., 2010; Weston et al., 2005), with the spring bloom showing greater productivity at the ND site than the OG site. The mooring data used by Greenwood et al. (2010) document the temporal evolution of the relatively low oxygen conditions but not their spatial extent. Hence, the aims of this study are firstly to place the recent evidence of seasonally low oxygen at two sites in the North Sea in a spatial context based on a major survey of oxygen concentrations in the summer of 2010; secondly to assess the evolution of summer oxygen depletion in the North Sea over the past century using historical data obtained from the International Council for the Exploration of the Sea's (ICES) database.

## 4.2 MATERIALS AND METHODS

### 4.2.1 *Sample collection and analysis*

#### 4.2.1.1 *Sampling*

RV CEFAS Endeavour cruise CEnd13/10 (Lowestoft, UK, 7th of August to 8th of September 2010) took place approximately 2 months before the end of the stratification period north of Dogger Bank and near the end of the stratified period in the OG (Greenwood et al., 2010). A total of 88 CTD casts were performed during the first 25 days. Water was collected at every CTD station from the surface, the bottom and at the mid-depth chlorophyll maximum (when present) for sensor calibration (Fig. 4.1). Sample collection was performed with 10 dm<sup>3</sup> Niskin bottles mounted on a FSI Integrated CTD rosette (Falmouth Scientific Inc., USA) with an additional Seapoint MOB op-

tical sensor for determination of suspended load, a Seapoint fluorometer and a LICOR photosynthetically active radiation (PAR) sensor. An ESM2 minilogger with an Aanderaa oxygen optode was also attached.

Weather was consistent with low wind speeds and an absence of storms during this period. Six hourly 10 m windspeeds and 2 m temperatures were obtained from the European Centre for Medium-Range Weather Forecasts (ECMWF) ERA-Interim data for the central North Sea in August 2010. Mean 10 m windspeed was  $7.4 \text{ m s}^{-1}$  with a standard deviation of 3.0 and reached a maximum of  $15.7 \text{ m s}^{-1}$  on the final day of sampling. Mean 2 m temperature was  $15.37^\circ\text{C}$  with a standard deviation of 0.38. These data suggest that the survey may be considered as a synoptic survey of the conditions in late summer.

#### 4.2.1.2 *Oxygen titrations*

The rate of oxygen change in the water column was too low to allow accurate direct measurements of rates of oxygen consumption in incubated samples, although such rates are available from long term in situ data (e.g. Greenwood et al., 2010). Hence the goal here was to reliably map the distribution of low oxygen regions revealed by the results from the moored sampling. Oxygen sample collection and preservation was performed following the Williams and Jenkinson (1982) method to calibrate the CTD optode. Quintuplicate water samples were collected into 125 ml glass bottles through a silicone hose before any other samples were collected for other analyses. Bottles were slowly filled from the bottom three times to overflowing to ensure the elimination of bubbles. Samples were fixed with 1 ml of manganous sulphate ( $450 \text{ g MnSO}_4 \cdot 4\text{H}_2\text{O dm}^{-3}$ ) followed by 1 ml of alkaline iodide solution ( $320 \text{ g NaOH} \ \& \ 600 \text{ g NaI dm}^{-3}$ ). Titration was performed using a Sensoren Instrumente Systeme dissolved oxygen analyser (SIS, Germany) with a photometric endpoint following Williams and Jenkinson (1982) with the iodine being liberated with  $5 \text{ mol dm}^{-3}$  sulphuric acid. A total of 10 calibration standards were made using a 0.1N potassium iodate solution ( $3.567 \text{ g KIO}_3 \text{ dm}^{-3}$ ).  $\text{KIO}_3$  was oven dried for 2 hours at  $110^\circ\text{C}$  before weighing.

#### 4.2.2 *Historical data*

The North Sea is a particularly well-studied area thanks to its economic and strategic importance to Europe. Historical data in the ICES database date as far back as the early 20th century. We have investigated CTD and bottle data from this database for evidence of temporal changes in deepwater oxygen in the North Sea. Only records containing oxygen concentration, pressure, temperature and salinity measurements were used. Data were sorted to retain only measurements from June to September in the bottom third of the water column and binned into ICES grid squares in accordance with Berx and Hughes (2009), to produce data at a scale appropriate to many of the features of the North Sea system. In total, 332015 oxygen values were obtained for the Greater North Sea dating from 1900 to 2010. Of these, 155340 were from months potentially showing summer oxygen depletion (June to September). The number of data points in bottom waters was further reduced with 75 000 measurements below 45 dbar. Although the majority of observations are located in the German Bight, the North-East Atlantic boundary and the Skagerrak outflow regions, sufficient data points remain in the central North Sea. In this paper, we loosely define the central North Sea as the offshore region situated between 56 and 58°N. Data obtained during the August 2010 survey were not included in this historical analysis and are thus independent.

To identify potential trends or regime changes in the region of interest, data were further filtered to retain only areas deeper than 45 dbar and in grid squares north of 56°N. This effectively limits the analysis to the BML of the stratified North Sea, with the exception of the unstratified Pentland Firth. An 11-year running mean of summer temperature, oxygen concentration and oxygen saturation was used to ensure sufficient data points were present in each bin.

In order to map spatial change, the original data selection criterion was used; measurements from the bottom third of the water column from the entire North Sea were kept, hence allowing analysis of trends in the generally mixed southern North Sea. Grid squares containing

fewer than 5 data points for each period considered were discarded. Mean fields were calculated for 1900-1990 and 1990-2010 time periods to show changes in oxygen saturation. The year 1990 was selected as the boundary due to the results of the timeseries analysis discussed later.

The reliability of oxygen concentration values from the ICES database cannot be determined. Although current methods for the determination of oxygen concentrations in seawater are relatively accurate (0.1%; Williams and Jenkinson, 1982), Carritt and Carpenter (1966) found errors near  $22 \mu\text{mol dm}^{-3}$  (of the order of 10%) in historical datasets. For this analysis, the data have been treated as reliable despite our inability to verify this.

## 4.3 RESULTS AND DISCUSSION

### 4.3.1 *Hydrography of the North Sea in August 2010*

#### 4.3.1.1 *Temperature, salinity and stratification*

The mapped CTD results reflected contrasting patterns in surface and bottom temperatures (Fig. 4.3). Surface temperatures (Fig. 4.3b) gradually increased from  $13^{\circ}\text{C}$  in the north-west to  $19^{\circ}\text{C}$  in the German Bight, with slightly higher temperatures than surrounding areas above the shallower Dogger Bank. Bottom temperatures (Fig. 4.3a) remained low (circa  $8^{\circ}\text{C}$ ) in the stratified areas (e.g. north of Dogger Bank).

In shelf seas, stratification is dependent on vertical temperature and salinity gradients, tidal mixing and depth (Simpson et al., 1977). Away from the influence of fresh water inputs (e.g. in the central North Sea) the difference in temperature between the SML and BML provides a proxy for stratification. We observed a very strong temperature-driven stratification ( $10^{\circ}\text{C}$  difference between the SML and the BML) in the central North Sea (Fig. 4.2h) with a maximum density difference of  $2 \text{ kg m}^{-3}$  between the BML and SML (Fig. 4.2). South of this stratified region, the water column was well mixed. In the off-

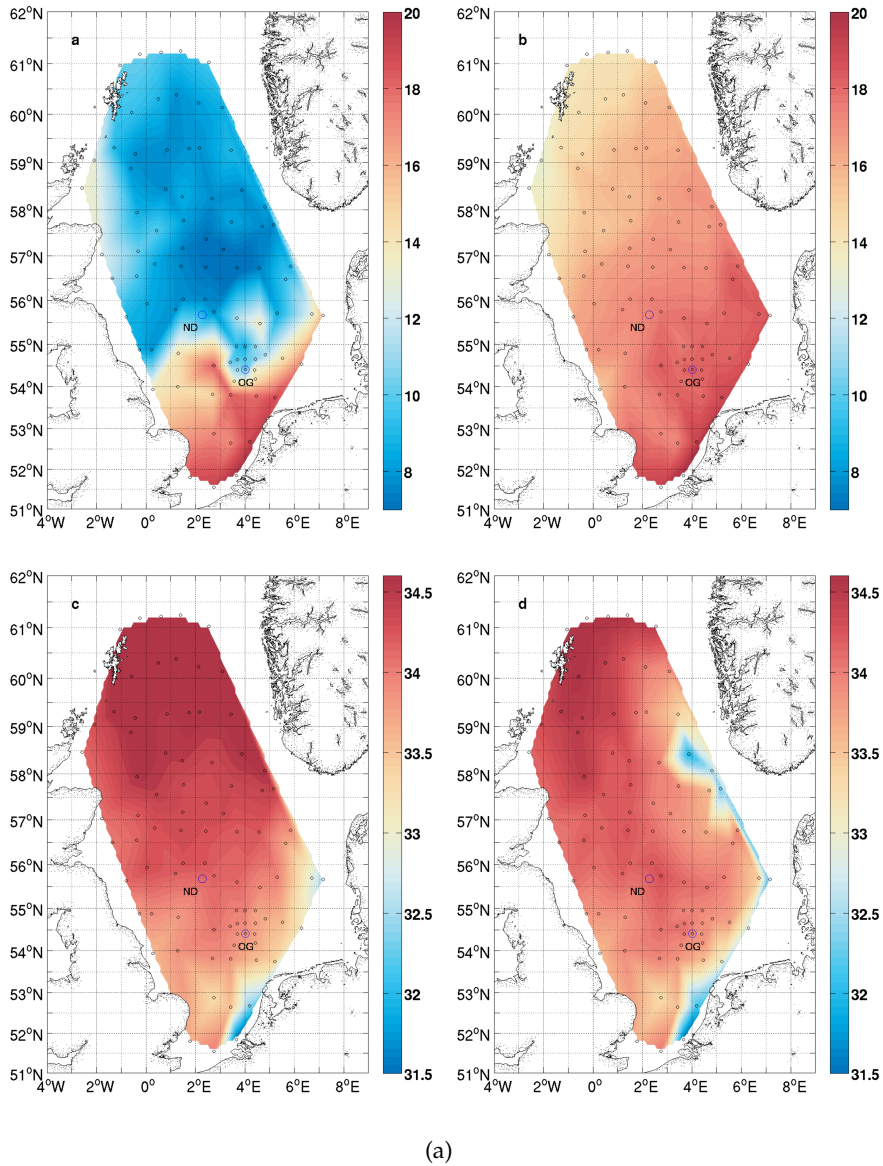
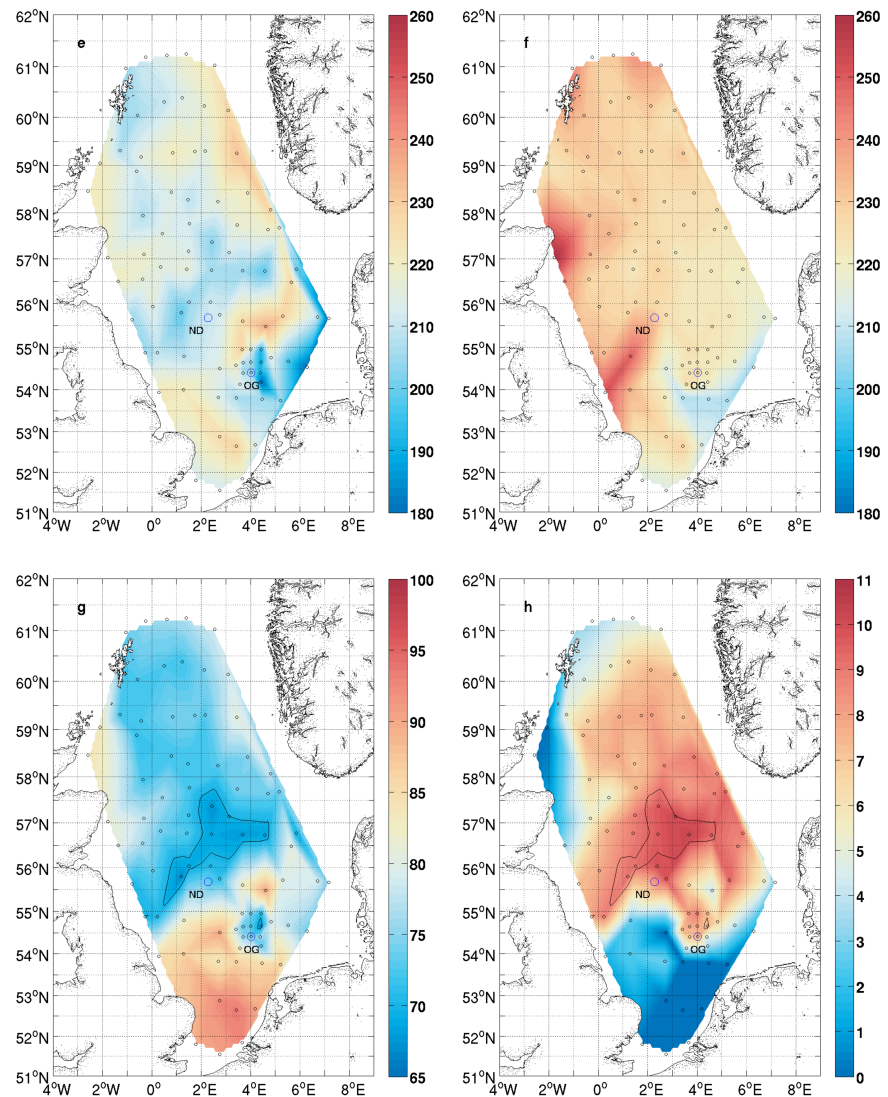


Figure 4.3: Results from surface and bottom waters sampled during all CTD casts from the shallowest 3m and the deepest 3m of the water column. (a) Deepest and (b) shallowest temperature ( $^{\circ}\text{C}$ ). (c) Deepest and (d) shallowest salinity.



(b)

Figure 4.2: **cont.** Results from surface and bottom waters sampled during all CTD casts from the shallowest 3m and the deepest 3m of the water column. (e) Deepest and (f) shallowest oxygen concentration ( $\mu\text{mol dm}^{-3}$ ). (g) Deepest oxygen saturation (%) and (h) temperature difference between surface and bottom mixed layers ( $^{\circ}\text{C}$ ). The 70% saturation contour line is included to highlight the similarity in spatial extent

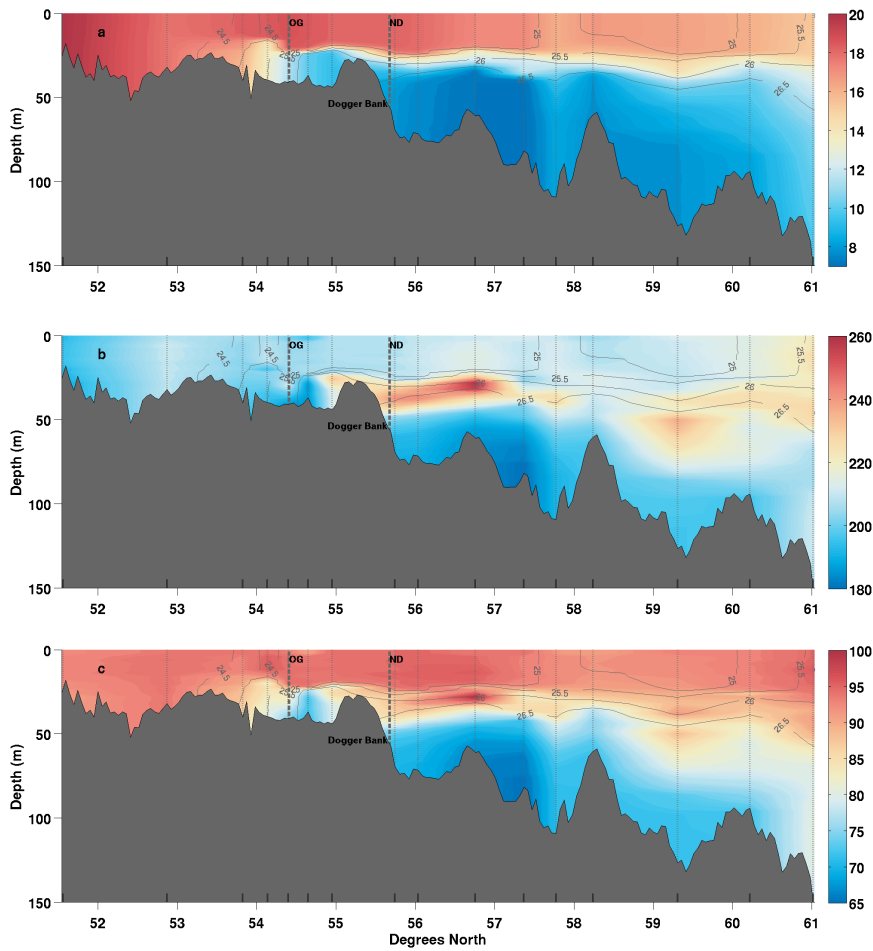


Figure 4.3: North-south section of selected parameters: (a) potential temperature ( $^{\circ}\text{C}$ ), (b) oxygen concentration ( $\mu\text{mol dm}^{-3}$ ) and (c) oxygen saturation profiles (%). Section position is indicated by the grey dotted line in Fig. 1. Station positions are indicated by dotted lines in this section and by circles in Fig. 1. Density contours are depicted for reference. Stations nearest to the ND and OG sites are indicated as well as the position of the Dogger Bank

shore northern North Sea, stratification weakened to a  $1.5 \text{ kg m}^{-3}$  difference between both layers ( $7^\circ\text{C}$  temperature difference between the BML and SML) as bottom waters warmed (Fig. 4.2). The most strongly stratified region was the Skagerrak outflow near the southern tip of the Norwegian trench ( $3 \text{ kg m}^{-3}$  difference between SML and BML waters, Fig. 4.2) due to the fresher surface water. Both the southern North Sea and the Scottish coast as far south as the Forth estuary were well mixed with stratification reducing gradually to a generally mixed water column as depth decreases (Figs. 4.2 & 4.2h).

A North-South section of water column temperatures (Fig. 4.3a) shows that a strong thermocline separating uniformly mixed layers was present north of  $54^\circ\text{N}$ . At  $54^\circ\text{N}$ , the thermocline was at a depth of approximately 25 m, gradually reducing in sharpness and deepening to 40 m north of  $54^\circ\text{N}$  (Fig. 4.3a). Shifts in the depth of the thermocline were observed above rises in bathymetry. In the OG basin, the shallower areas on both sides exhibited a less stratified water column with similar properties to the OG SML. The cold BML of the OG basin remained effectively isolated by the topography and relatively weak tides. One notable feature was that the water in the BML north of the ND site was 1 to  $2^\circ\text{C}$  cooler than BML waters further north (Figs. 4.3a & 4.3a). In the north-south section (Fig. 4.3a), this cooler water mass was located between  $56$  and  $58^\circ\text{N}$ . The lowest oxygen concentration was associated with this cooler water around  $57^\circ\text{N}$  (Fig. 4.3b) and was bounded to the south and north by a rise of the seafloor. These banks effectively isolated this area from meridional transport.

The salinity distribution (Figs. 4.3c & d) was consistent with previous observations (Bozec et al., 2005) of fresh surface water input from the Skagerrak as well as coastal fluvial outflow from rivers draining through the Netherlands, the German Bight and the UK. A tongue of more saline water was observed coming from the Atlantic, following the central North Sea currents and reaching the Dogger Bank region. Bottom water salinities exhibited a much more uniform pattern with a gradual north to south decrease due to the northern inflow of high salinity Atlantic water and fresher water discharges into the southern region (Fig. 4.3c) following currents illustrated in Fig. 4.2.

#### 4.3.1.2 *Dissolved oxygen*

Surface oxygen concentrations were highest off the Humber estuary (Fig. 4.1) and the Scottish coast, reaching  $250 \mu\text{mol dm}^{-3}$  (Fig. 4.2f). Two regions demonstrated subsaturation concentrations of oxygen with  $220 \mu\text{mol dm}^{-3}$  (85% saturation) and  $205 \mu\text{mol dm}^{-3}$  (87% saturation) for the Fair Isle current between the Orkney and Shetland Isles and the German Bight respectively. The rest of the North Sea surface water was at saturation concentration (circa  $230 \mu\text{mol dm}^{-3}$  depending on temperature).

A very different pattern was observed in bottom waters (Figs. 4.2e & g). Shallow waters not subject to stratification because of tidal mixing (i. e. the southern North Sea; Simpson et al., 1977) were saturated throughout the entire water column (around  $210 \mu\text{mol dm}^{-3}$ ). Similar results were observed on the eastern Dogger Bank ( $230 \mu\text{mol dm}^{-3}$ ). Due to the absence of stations on the Dogger Bank, the interpolation was not able to accurately depict this area but we may assume that the shallow bank showed the same saturated water column as the eastern tip. Although coastal waters off the north-east tip of Scotland were not stratified, bottom water oxygen saturation remained lower than surface waters at approximately 80% (approx.  $220 \mu\text{mol dm}^{-3}$ ). The region west of the Norwegian Trench showed a similar saturation level, with a slightly greater concentration of  $230 \mu\text{mol dm}^{-3}$ . The region just west of the coast of Denmark, extending to the OG, had the lowest bottom water dissolved oxygen concentrations (as low as  $180 \mu\text{mol dm}^{-3}$ ). This equated to about 80% saturation west of Denmark and 70% saturation in the OG. The major mass of oxygen depleted water (65% saturation, Fig. 4.2g) was located in the central North Sea, spanning from the south-east of Scotland towards the southern tip of Norway but stopping where the stratification increased due to the Skagerrak outflow (located between  $56$  and  $58^\circ\text{N}$ ). Despite having low oxygen saturation, this region did not exhibit a particularly low oxygen concentration ( $200 \mu\text{mol dm}^{-3}$ ) due to the lower water temperatures causing increased solubility.

The North-South section of oxygen concentrations (Fig. 4.3b) showed them to be highest at the thermocline. This further suggests that the DCM is a region of enhanced primary productivity (Weston et al., 2005). The two locations showing highest oxygen concentrations ( $250$  and  $260 \mu\text{mol dm}^{-3}$ ), and therefore showing greatest evidence of enhanced primary production, were mid-water at the OG and around  $57^\circ\text{N}$  away from the coasts (Fig. 4.3b). Fig. 4.3c shows super-saturated (above 100%) mid-depth layers in both these areas where the SML exhibited uniformly saturated (approx. 100%) surface waters. The lowest oxygen saturation (65%) was situated in the area of coldest waters; minimum oxygen saturation was found at the seabed with oxygen saturation increasing vertically. The OG region had 75% saturation at the bed. The BML (north of the Dogger Bank) can be considered as separated meridionally into three regions defined by the banks at  $55.5$ ,  $57$  and  $58.5^\circ\text{N}$  (Fig. 4.3). It is likely that little flow occurs meridionally between these three regions at depth due to the topographic features separating them (Figs. 4.2 & 4.3c), thus these regions are isolated vertically by stratification and meridionally by the banks.

#### 4.3.2 *Historical records of oxygen concentrations in the North Sea*

Fig. 4.4 displays a 5-yearly 11-year running mean of summer temperature, oxygen concentration and oxygen saturation of the BML in the stratified North Sea. An 11-year running mean was used to ensure sufficient data points were present in each bin to eliminate sampling biases. Points are shown every 5 years to demonstrate the variability in sample size, standard error and standard deviation. These three time-series show no clear trends in oxygen concentration, oxygen saturation or temperature in bottom waters of the stratified North Sea up to 1990. After 1990 the data indicate increased temperatures and decreased oxygen concentrations and saturations. The change in solubility between  $7^\circ\text{C}$  and  $8.5^\circ\text{C}$  only accounts for approximately  $10 \mu\text{mol dm}^{-3}$  of the observed  $30 \mu\text{mol dm}^{-3}$  decrease in dissolved oxygen concentration. A decrease in oxygen saturation of this magnitude implies that the decrease in dissolved oxygen concentration is

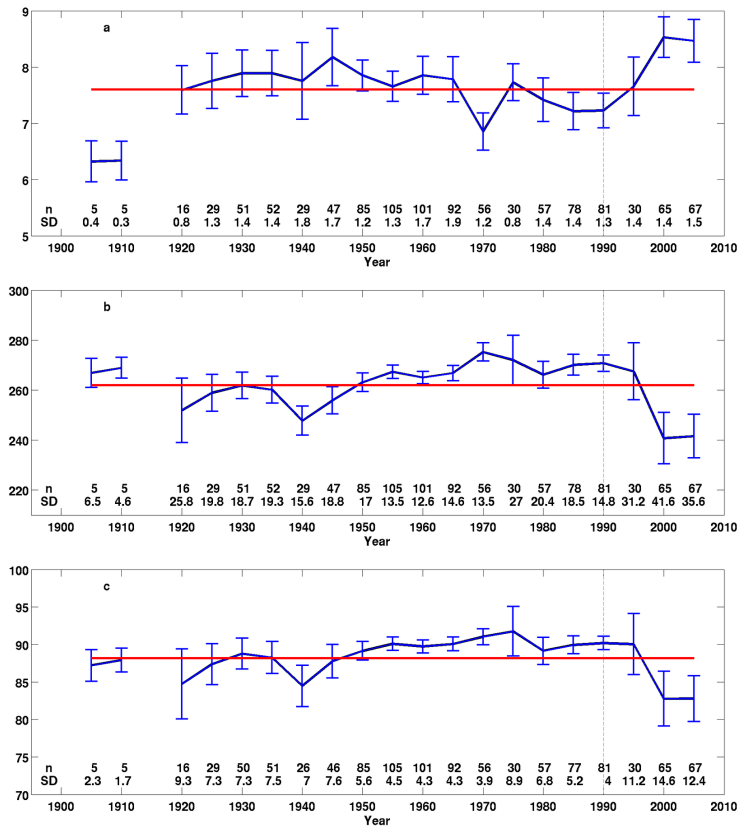


Figure 4.4: 5-yearly values of an 11-year running mean of (a) summer BML temperature ( $^{\circ}\text{C}$ ), (b) oxygen concentration ( $\mu\text{mol dm}^{-3}$ ) and (c) oxygen saturation (%) in the stratified central North Sea, subdivided into ICES grid squares (Fig. 6). Only data from the months of June to September below 30 m, in regions deeper than 45m and in grid squares north of  $56^{\circ}\text{N}$  with over 5 data points were retained for analysis (total of 16250 measurements). Error bar length is equal to two standard errors. The horizontal line indicates the overall mean of the time-series. Standard deviation and number of grid squares retained are indicated below each data point

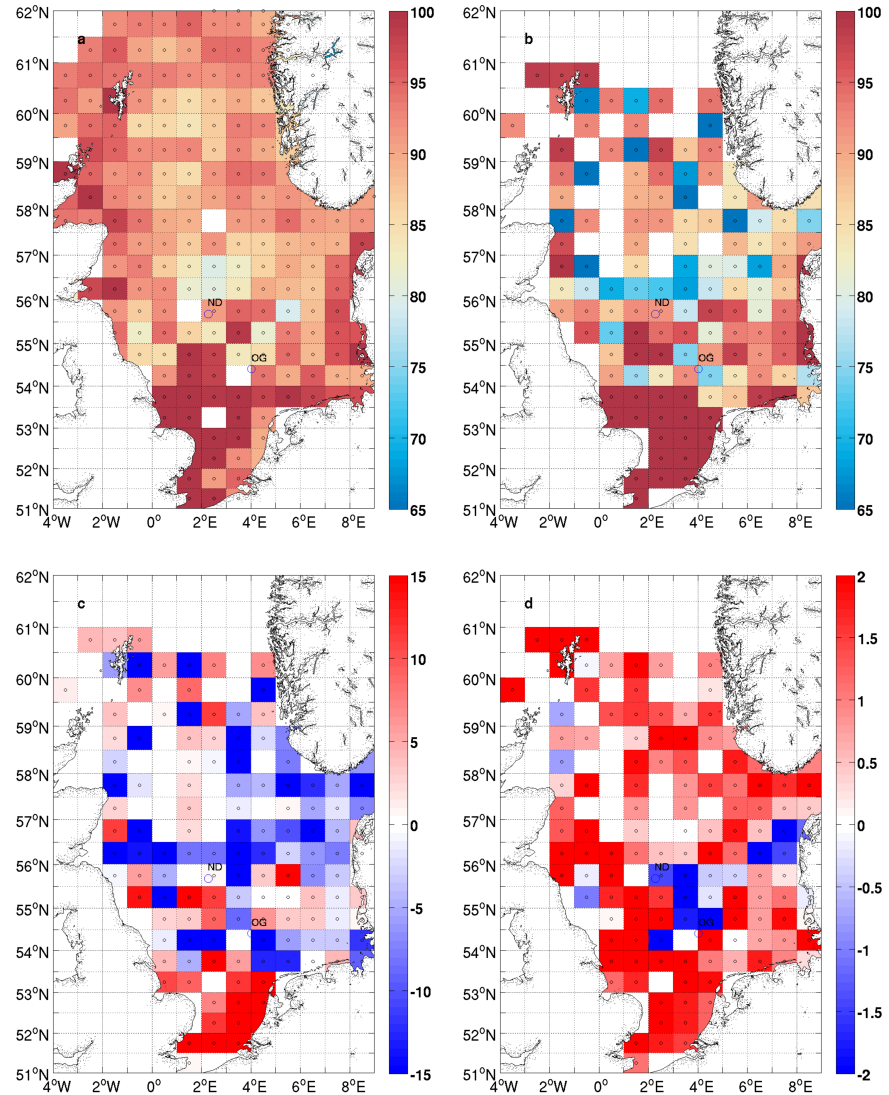


Figure 4.5: Mean summer bottom oxygen saturation values (%) from (a) 1900 to 1990 (10425 data points over 199 grid squares) and (b) 1990 to 2010 (21057 over 133 grid squares). Change in bottom oxygen saturation (c) and temperature (d) between the first and the second periods

not due to a temperature-driven decrease in solubility alone but also to an increase in oxygen utilisation.

The year 1990 was selected as the boundary because of the 1.5°C increase in temperature (Fig. 4.4a) and the doubling of the variability in oxygen saturations (Fig. 4.4c). Mean fields were calculated for 1900-1990 and 1990-2010 time periods to show changes in oxygen saturation.

ICES data used in this study (Fig. 4.4 & 4.5) show that prior to 1990, oxygen saturation in bottom waters of the northern North Sea (north of 58°N) was typically 85 - 95%, with elevated oxygen saturations (100%) in the coastal regions of the United Kingdom, the Netherlands, Germany and Denmark (Fig. 4.5a). Lowest values were observed just north of the ND site and at the OG with oxygen saturations of around 80%. Post-1990, low oxygen saturations of 70% are clearly visible both at the OG and north of the Dogger Bank (Fig. 4.5b). A few isolated ICES squares also show low oxygen saturations in the northern North Sea. This suggests a decreased average oxygen concentration post-1990.

Fig. 4.5c suggests a decrease in oxygen saturation in the central and eastern North Sea after 1990, and increased oxygen saturation in Channel waters, the German Bight and the United Kingdom coastal waters. The regions showing this increasing oxygen saturation signal were well mixed throughout the summer months. Regions with the greatest temperature difference between the BML and SML in August 2010 are the same as those with the lowest oxygen saturation in the 1990 to 2010 data (Fig. 4.2h & 4.5b).

A general increase in bottom water temperatures is visible across the greater North Sea (Fig. 4.5d). This 2°C increase is uniform across the majority of the North Sea. The German Bight bottom temperatures increase by only 1°C. Two regions show a decrease in bottom water temperatures: the Dogger Bank, specifically between the ND and OG sites, and the north-west coast of Denmark.

#### 4.3.3 *Drivers of oxygen depletion in the central North Sea*

Diaz (2001) summarises key findings from similar studies of low oxygen in other areas. Shelf seas such as the North Sea function differently to upwelling regions and resemble areas such as the Gulf of Mexico and the Baltic Sea more closely. However, Foden et al. (2011) found no evidence of undesirable disturbance in English and Welsh waters due to nutrient enrichment. This sets the central North Sea apart from regions such as the Baltic.

In this study, both increases and decreases of oxygen saturation were visible in bottom waters of different regions across the North Sea after 1990. Data from the early 20th century show much less oxygen depletion than data from after 1990, however the geographic pattern of low and high dissolved oxygen remains similar. This indicates that the North Sea summer oxygen depletion around the ND and OG sites is not a recent phenomenon but its intensity has been greatly affected in recent years. The most likely causes of this decreased oxygen saturation are warming, altered nutrient loads (either increased concentrations or shifts in N:P:Si ratios) and changes in wind speeds governed by the NAO (Sharples et al., 2006). Greenwood et al. (2010) suggest that increasing thermal stratification, temperatures and biomass input lead to oxygen depletion at both the ND and OG sites. This is consistent with both the ICES historical data and results from the August 2010 survey.

BML temperatures increased over the past century (Berx and Hughes, 2009; Meyer et al., 2011; Ting et al., 2009). This would result in an expected reduction in oxygen concentration. However, the observed reduction of oxygen concentration cannot be explained simply by changes in oxygen solubility due to rising temperatures. Regions of oxygen super-saturation pre-1990 exhibited elevated values post-1990, whilst regions showing sub-saturation oxygen concentrations pre-1990 had even lower values after 1990. Increase in bottom water temperatures (Fig. 4.5d) affects oxygen saturation in two ways. Firstly, bacterial and planktonic activity rates are increased by small amounts of warming, leading to higher respiration rates (Beaugrand

et al., 2008). Secondly, temperature influences oxygen solubility and stratification; cold waters will be less saturated for a given oxygen concentration, whilst warmer waters will show higher saturation values. In the central North Sea, stratification is necessary for the occurrence of oxygen depletion (defined as the decrease of oxygen saturation) at depth, whereas a mixed water column may promote saturation. Also, assuming the same initial oxygen concentration, increased temperatures intensify the change in oxygen saturation. In regions with a mixed water column during the summer months, increased primary production would lead to increased super-saturation during blooms. Summer stratified regions also show increased productivity. This greater load of organic matter, however, is remineralised at a greater rate in the bottom layer, away from primary production, leading to further oxygen depletion. Increased nutrient loading in the North Sea would affect planktonic community structure and primary productivity and may contribute to the observed oxygen distribution (Jickells, 1998), although other factors also influence the distribution and long-term changes in phytoplankton community in this region (Eppley, 1972; McQuatters-Gollop et al., 2007; Reid et al., 1990).

Results from the August 2010 survey show the same oxygen saturation distribution as the ICES data and highlight two areas showing summer oxygen depletion: the OG and the central North Sea. Although absolute concentrations do not reach levels requiring management action under the EU Water Framework Directive at ND ( $200 \mu\text{mol dm}^{-3}$ ), dissolved oxygen concentrations of  $180 \mu\text{mol dm}^{-3}$  ( $5.76 \text{ mg dm}^{-3}$ ) in the OG are close to the Water Framework Directive threshold between good and moderate ecological status and therefore the OSPAR boundary between problem and non-problem area ( $4$  to  $6 \text{ mg dm}^{-3}$ ). Both regions are subject to stratification. They were the most strongly stratified regions of the North Sea in 2010 outside the fresh water inflow from the Skagerrak (Fig. 4.3d), emphasising the importance of the sequestration in the BML.

Greenwood et al. (2010) highlighted the importance of warming waters decreasing oxygen solubility and calculated that 10% of the observed consumption could potentially be attributed to increasing

temperatures during the stratified season at the ND site. The difference in oxygen concentration at saturation, assuming constant pressure and salinity, at temperatures at the start and end of the stratified season provides a value for the maximum oxygen consumption attributable to warming (Greenwood et al., 2010). The bottom mixed layer reaches a minimum of approximately 7°C before the stratification is established (Greenwood et al., 2010). Warming of the BML during summer 2010 to its observed temperature of 8°C (Fig. 4.3) and consequent decrease in oxygen solubility would only account for approximately 7  $\mu\text{mol dm}^{-3}$  of the 90  $\mu\text{mol dm}^{-3}$  apparent oxygen utilisation (AOU) for the region. The AOU is the difference between oxygen concentration at saturation and the observed concentration. This value is similar to the 10% attributable to warming found by Greenwood et al. (2010) but was recorded in August when temperatures would still increase before the end of the stratified season. Consequently, we may assume that the remaining decrease in dissolved oxygen occurred as a result of oxygen consumption fuelled by organic matter from the spring bloom and the DCM. This is consistent with observations of a persistent DCM (Weston et al., 2005) in this region and agrees with the evidence (Figs. 4.3b & c) of higher dissolved oxygen concentration and super-saturation originating from DCM production. As the spring bloom occurs in April (Sharples et al., 2006), it was over by the time of the August survey reported here; nevertheless it remains a large source of organic matter for the BML (Davies and Payne, 1984).

We suggest that the ND oxygen depletion is regulated by two opposing factors while the water column remains stratified. The continual primary production in the DCM increases dissolved oxygen concentration at the thermocline, however the presence of a strong pycnocline prevents the injection of this oxygen into the BML. Oxygen consumption in the BML could be linked to the remineralisation of surface-derived organic matter produced during the spring bloom and in the DCM (Greenwood et al., 2010; Weston et al., 2005).

The bathymetry of the surrounding area, in particular large banks, contributes to isolating this water mass from advective processes; to

the south is Dogger Bank and to the north is the Great Fisher Bank located south-west of the Norwegian Trench (Fig. 4.1). The stratification prevents injection of oxygen from the surface, while these two banks prevent meridional advection of well mixed water from the south or oxygen-rich water from the north. Possible mechanisms of oxygen replenishment in this situation are limited to the disruption of stratification during storms (Greenwood et al., 2010), most commonly at the start of winter, or the advection of more oxygenated water from the east or west (Fig. 4.2).

The characteristics of the circulation in this area may exacerbate oxygen depletion in ND. Both the Dooley Current (DC) and the Scottish Coastal Current (SCC) reach this region (Fig. 4.2). The SCC mostly continues along the south of Dogger Bank. The DC reduces in intensity as it enters the central North Sea (Dooley, 1974). Otto et al. (1990) identified ND as an area with little advection and variable, weak wind-driven currents. This slow circulation isolates the deep water mass, provides more time for the remineralisation of organic matter relative to oxygen resupply and may promote settling of organic matter. Although currents in ND seem insufficient to replenish oxygen to saturated levels, it is likely that they inhibit further oxygen depletion by advecting a small yet continuous supply of water with a higher dissolved oxygen concentration to counter balance the consumption.

Relatively low ( $180 \mu\text{mol dm}^{-3}$  or 70%) dissolved oxygen concentrations are also observed at the OG site (Fig. 4.3). It is likely that the same mechanisms lead to the depletion of oxygen in the BML of the OG as in ND. The presence of the Dogger Bank limits advection from the north and west to the OG while increasing tides and the topography lead to the formation of thermal fronts to the south and east (Fig. 4.2). These features prolong residence times of water in the OG (Van Raaphorst et al., 1998; Weston et al., 2008). When combined with the presence of a DCM (Weston et al., 2008), this leads to a downward export of organic matter. Although the stratification period is shorter and the DCM is weaker than at the ND site (Greenwood et al., 2010; Weston et al., 2008), the AOU was similar to that observed at the ND site. AOU at the OG site does, however, represent a greater por-

tion of the dissolved oxygen as ND had  $210 \mu\text{mol dm}^{-3}$  compared to  $180 \mu\text{mol dm}^{-3}$ . It should be noted that the OG site is shallower than ND by nearly 40 metres and therefore has a much smaller BML volume so the oxygen consumption per unit volume of water will be higher for a similar vertical organic carbon flux; the shallow depth also facilitates resuspension of bottom sediment by storms, causing further remineralisation of organic carbon (Greenwood et al., 2010; Van Raaphorst et al., 1998).

In contrast to the ND site, Greenwood et al. (2010) found a much greater importance of warming in accounting for the oxygen depletion observed at the OG site. Winter temperatures at the OG site are similar to ND, with a bottom temperature of approximately  $7^\circ\text{C}$  (Greenwood et al., 2010). During the August 2010 cruise, bottom temperatures at the OG site reached  $10^\circ\text{C}$ ; the  $3^\circ\text{C}$  difference equates to approximately  $20 \mu\text{mol dm}^{-3}$  corresponding to approximately 25% of the 70 to  $90 \mu\text{mol dm}^{-3}$  apparent oxygen utilisation. The 25% attributed to warming in summer 2010 is half of the observed 55% AOU in 2007 (Greenwood et al., 2010). This discrepancy is due to the difference in bottom water temperatures. During summer 2007, the BML at the OG site was  $3^\circ\text{C}$  warmer than in 2010. This may be due to the storm event reported by Greenwood et al. (2010). A sufficiently strong storm weakens the stratification, facilitating injection of warm surface water into the BML.

One of the main difficulties in surveys of regions as large as the North Sea is differentiating between spatial and temporal variations. Variability in the BML can be caused by storms; these may cause a break down of the pycnocline and cause mixing of both surface and bottom layers (Van Raaphorst et al., 1998; Vermaat et al., 2008). Air temperature and wind speeds varied minimally during August 2010 and no storms of a sufficient strength to cause such events were observed during the survey period. Synopticity of the survey could also be compromised by natural gradual changes in temperature and oxygen concentration. Greenwood et al. (2010) observed a daily increase of  $6.4 \times 10^{-3} \text{ }^\circ\text{C}$  at ND and  $7.25 \times 10^{-3} \text{ }^\circ\text{C}$  at the OG sites. Assuming that temperatures increased at the same rate in Au-

gust 2010, the temperature difference between the beginning and end of the survey would have been  $0.16^{\circ}\text{C}$  at ND and  $1.81^{\circ}\text{C}$  at the OG. The consequence of this temperature increase would be a decrease in oxygen solubility of  $1\ \mu\text{mol dm}^{-3}$  at ND and  $12\ \mu\text{mol dm}^{-3}$  at the OG. Similarly, biological oxygen consumption rates in 2007 were  $0.38\ \mu\text{mol dm}^{-3}\ \text{day}^{-1}$  in ND and  $0.34\ \mu\text{mol dm}^{-3}\ \text{day}^{-1}$  at the OG (Greenwood et al., 2010). Over the 25 days of the August 2010 observations, biological oxygen consumption would have amounted to  $10\ \mu\text{mol dm}^{-3}$  at both ND and the OG based on these estimates. This represents only about 10% of the observed change and so we can assume that temporal variations were minimal, and that the observed differences were due primarily to different environmental conditions in the ND region. As the OG site was sampled on day 5 of the survey, the observed temperature and apparent oxygen utilisation would have been higher by  $0.3^{\circ}\text{C}$  and  $3.5\ \mu\text{mol dm}^{-3}$  when ND was sampled on day 9.

To fully assess the extent of oxygen depletion in the North Sea in the summer of 2010, we must estimate depletion until the breakdown of the stratification. Stratification sets in around the 3rd week of April (+/- 1 week; Sharples et al., 2006) with little variability, whereas the end of the stratified period is determined by the occurrence of winds sufficiently strong to break down the stratification. This stratification typically breaks down in September and October for the OG and ND sites respectively. Overall oxygen depletion rates in 2007 were  $0.43\ \mu\text{mol dm}^{-3}\ \text{day}^{-1}$  at ND and  $0.75\ \mu\text{mol dm}^{-3}\ \text{day}^{-1}$  at the OG (Greenwood et al., 2010). Based on these rates, oxygen concentrations would be  $25.5\ \mu\text{mol dm}^{-3}$  lower on the 15th of September at the OG and on the 15th of October at ND. With this decrease, oxygen concentration would be  $154.5\ \mu\text{mol dm}^{-3}$  at the OG and  $174.5\ \mu\text{mol dm}^{-3}$  at ND at the end of the stratification period. At these concentrations, both sites would classify as “good” under the Water Framework Directive. A hypothetical decrease of a further  $10\ \mu\text{mol dm}^{-3}$ , potentially caused by increased stratification or greater export of organic matter, would lead the OG to being classified as “moderate”.

It is particularly difficult to assess the evolution of oxygen saturation at depth due to the sparsity of data available in the North Sea. A few regions have been regularly sampled and provide near continuous data while other regions contain solely opportunistic or point measurements. Nevertheless, the results of the hydrographic survey of the North Sea performed in August 2010 are consistent with the recent and historical observations of dissolved oxygen during the summer stratified period. The August 2010 observations build upon observations from the ICES database and results of Greenwood et al. (2010) to elucidate the mechanisms that constrain the location of this deoxygenation. Greenwood et al. (2010) began quantifying the oxygen depletion in the central North Sea, but more studies are required to clarify the drivers behind this phenomenon.

## DRIVERS OF SUMMER OXYGEN DEPLETION IN THE CENTRAL NORTH SEA

---

### 5.1 INTRODUCTION

Both an investigation into historical data contained in the International Council for the Exploration of the Sea (ICES) database and a systematic hydrographic survey of the North Sea in August 2010 revealed repeated incidents of seasonal oxygen depletion in offshore waters in the North Sea (Ch. 4, Queste et al., 2013). A survey in 2011 was performed to further investigate the mechanisms causing this seasonal oxygen depletion by deploying a Seaglider in the region that exhibited highest oxygen depletion in August 2010.

The August 2010 survey (Ch. 4) recorded bottom waters with oxygen saturations below 70% at both the ND and OG sites (circa 200 and 180  $\mu\text{mol dm}^{-3}$  respectively, Fig. 5.1). The analysis of data contained in the ICES database also revealed a similar distribution of low DO in the BML during the summer months with two areas located approximately 2 degrees north of Dogger Bank and another at the OG site. Queste et al. (2013) suggested that the same mechanisms likely led to the depletion of oxygen in the BML of the OG as that at the ND site. Replenishment of oxygenated waters through advective processes is limited by the hydrography of the regions. The region identified as ND in Ch. 4 is an area away from the frontal regions with little advection and variable, weak wind-driven currents (Otto et al., 1990). This slow circulation limits horizontal supply of DO while also both increasing residence time of waters in the region and promoting settling of organic matter due to slower currents. At the same time, weak winds and strong stratification promote a long stratified season and keeps the BML isolated from air-sea exchanges. The OG site also suffers from weak inflow of oxygenated waters as

tides and topography lead to the formation of thermal fronts to the south and east (Van Raaphorst et al., 1998; Weston et al., 2008). At the same time, production occurring at the DCM, particularly at the ND site, leads to a continuous downward export of organic matter (Fernand et al., 2013; Thomas et al., 2004; Weston et al., 2008). This organic matter, when remineralised, leads to the consumption of DO in the BML. At both the OG and ND sites, it has been suggested that mixing events may cause resuspension of bottom sediment. Transfer of this organically rich sediment into the water column could cause rapid increases in pelagic DO consumption (Greenwood et al., 2010; Van Raaphorst et al., 1998).

The 2010 survey data and the ICES historical data showed the distribution of seasonal oxygen depletion in the central North Sea (Fig. 5.1). It was possible to infer the broad-scale features which permit this seasonal oxygen depletion from the distribution of low DO concentrations. Regions of high stratification with reduced advection promote a longer and stronger separation of the BML from sources of DO replenishment (air-sea exchange and advection of oxygenated waters). This is, however, insufficient to cause oxygen depletion on its own. The BML is never fully isolated from sources of elevated DO. The SML constantly provides a supply of oxygenated water into the BML through diffusion and vertical mixing. The decrease in BML DO is dependent on the ratio of oxygen consumption to oxygen supply. It is this balance of consumption and supply which ultimately determines the intensity and duration of the oxygen depletion. It is necessary to identify the sources of organic matter which lead to the consumption of DO in the BML and the amount of DO supply through the pycnocline on a finer scale to be able to accurately predict potential seasonal oxygen consumption under future climate scenarios.

The deployment of a Seaglider aimed to provide high resolution observations of physical and biochemical processes in the BML on the scale of days to identify the importance of mixing on the supply of DO and the relative importance of the different sources of organic matter. Notably, it has been suggested the DCM provides up to 60% of the annual production in the North Sea (Fernand et al., 2013). A frac-

tion of this organic matter is rapidly exported to the BML (Fernand et al., 2013; Weston et al., 2005, 2008). This study aimed to determine whether the DO consumption in the BML was directly linked to pelagic consumption of sinking organic matter or if it was dominated by consumption of organic matter resuspended from a thin superficial benthic layer. This has critical importance in how the timing and strength of stratification influences seasonal oxygen depletion. If consumption is dominated by DCM sinking organic matter, a longer and stronger stratification will promote DCM production and hence low BML DO, however if it is dominated by benthic or resuspension processes, an increase in storms which break down the stratification and cause mixing down to the sediment will lead to strong decreases in BML DO as suggested by Greenwood et al. (2010); Van Raaphorst et al. (1998).

In order to investigate the relative importance of each mechanism, the Seaglider observations are complemented with a 1 dimensional coupled model of the North Sea, the General Ocean Turbulence Model (GOTM) - Biogeochemical Flux Model (BFM). The model runs an idealised case based on the Seaglider deployment area and provides further insight into the mechanisms regulating the balance of oxygen consumption and supply in the central North Sea (Lenhart et al., 2010; van der Molen et al., 2012). A fuller description of the model data is provided in Sec. 5.2.2. The model data will fill the gaps in understanding due to the short glider timeseries. At the same time, the high resolution data from the Seaglider can highlight shortcomings of the 1-D model by observing features not resolved in the model which are suspected to contribute significantly to the consumption of DO in the BML of the central North Sea.

Fig. 5.1 (*bottom right*) shows mean August oxygen saturation values at the bottom of the water column obtained from a forecast of the 3-D implementation of the General Estuarine Ocean Model (GETM)-BFM (van der Molen et al., 2012). Although the presence of a low oxygen tongue extending from the Skagerrak dominates the signal, the familiar features of both ND and OG are clearly visible. The difference in magnitude of the low oxygen signal extending from the

Skagerrak between the ICES data (*bottom left*) and GETM results (*bottom right*) can be partially attributed to different means of collecting data but is mostly determined by the representation of Baltic waters in the model. The western end of the Baltic Sea was contained within the model domain for this run with an open boundary forced by temperature and salinity climatologies along 16°E. Climatological forcing may have not been representative of the state observed in 2010 and 2011. Alternatively, processes modelled within the western Baltic Sea and Skagerrak may be overestimating freshwater outflow into the North Sea; in particular, the influence of run-off into the Skagerrak and Kattegat may be mis-represented.

This chapter attempts to identify the magnitude of DO supply through the pycnocline as the primary source of DO. It then goes on to look at the three primary sources of DO consumption in the BML: sinking matter from the DCM, benthic consumption and resuspension of organic matter using a combination of Seaglider observations, model outputs and past studies.

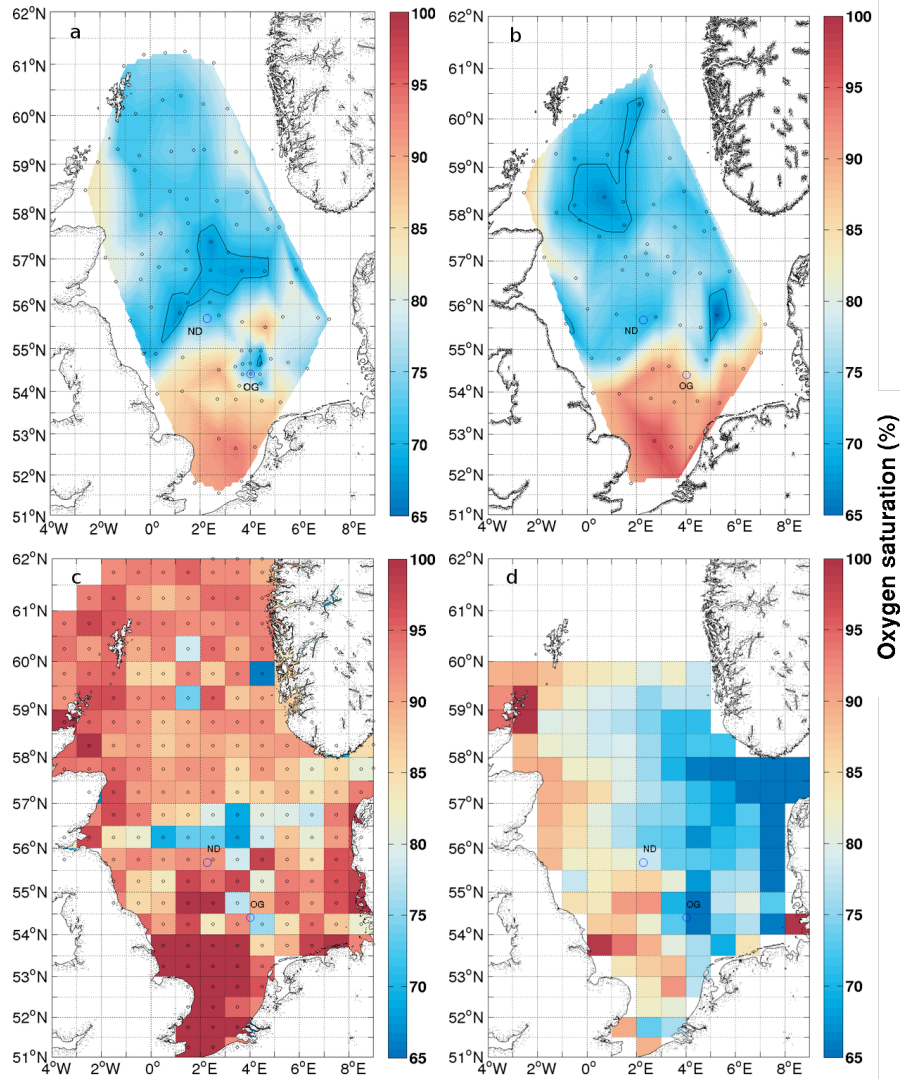


Figure 5.1: BML oxygen saturation (%) and with the 70% saturation contour during the August 2010 (a) and August 2011 surveys (b), mean summer bottom oxygen saturation values (%) from 1900 to 2010 from the ICES database (c) and mean summer bottom oxygen saturation values (%) from 1958 to 2008 from the GETM-ERSEM model output using ERA interim reanalysis data (d).

## 5.2 METHODS

### 5.2.1 *Survey*

The North Sea is a relatively shallow (15 - 200 m) shelf sea situated between the British Isles and north-western continental Europe. The North Sea gradually deepens from South to North with the exception of the shallow Dogger Bank (Fig. 5.2). Dogger Bank effectively separates the North Sea into two regions of different physical, chemical and biological properties (Lenhart et al., 1997; Otto et al., 1990). Along the eastern edge of the North Sea, the Norwegian Trench allows export of Skagerrak waters along the 300 m deep trough (Fig. 5.2). Water properties in the northern half of the North Sea are largely dominated by North Atlantic inflow. In their study of carbon dynamics, Thomas et al. (2005) attempt to determine the water budget of the North Sea; estimates place the North Atlantic as the source for 90% of the input ( $9\,000\text{ km}^3\cdot\text{yr}^{-1}$  via the Pentland Firth and Fair Isle,  $42\,000\text{ km}^3\cdot\text{yr}^{-1}$  via the Shetlands), followed by slightly over 8% for the English Channel ( $4\,900\text{ km}^3\cdot\text{yr}^{-1}$ ), the final 2% are divided between Baltic waters ( $500\text{ km}^3\cdot\text{yr}^{-1}$ ) and riverine flow ( $200\text{ km}^3\cdot\text{yr}^{-1}$ ). Dispersion simulations and measurements of radioactive isotopes have indicated residence times of 3-5 years for the North Sea (Lenhart et al., 1995). Water entering the North Sea from the northern boundary follow a generally anticlockwise circulation, following the Scottish coast south before turning east and crossing the North Sea just north of Dogger Bank (Brown et al., 1999; Hill et al., 2008; Turrell et al., 1992). The strength of this anticlockwise circulation is strongly correlated with the North Atlantic Oscillation Index (NAOI). Positive NAOI correlate to strong anticlockwise circulation while negative NAOI correlate to greatly reduced anticlockwise circulation in the northern North Sea (Lenhart et al., 2004, 1995; Rodwell et al., 1999). The northern half of the North Sea is seasonally stratified through surface heating and this stratification breaks down completely in winter (Ducrottoy et al., 2000; Greenwood et al., 2010; Sharples et al., 2006). Despite representing only 2% of inflow into the North Sea, Baltic waters can

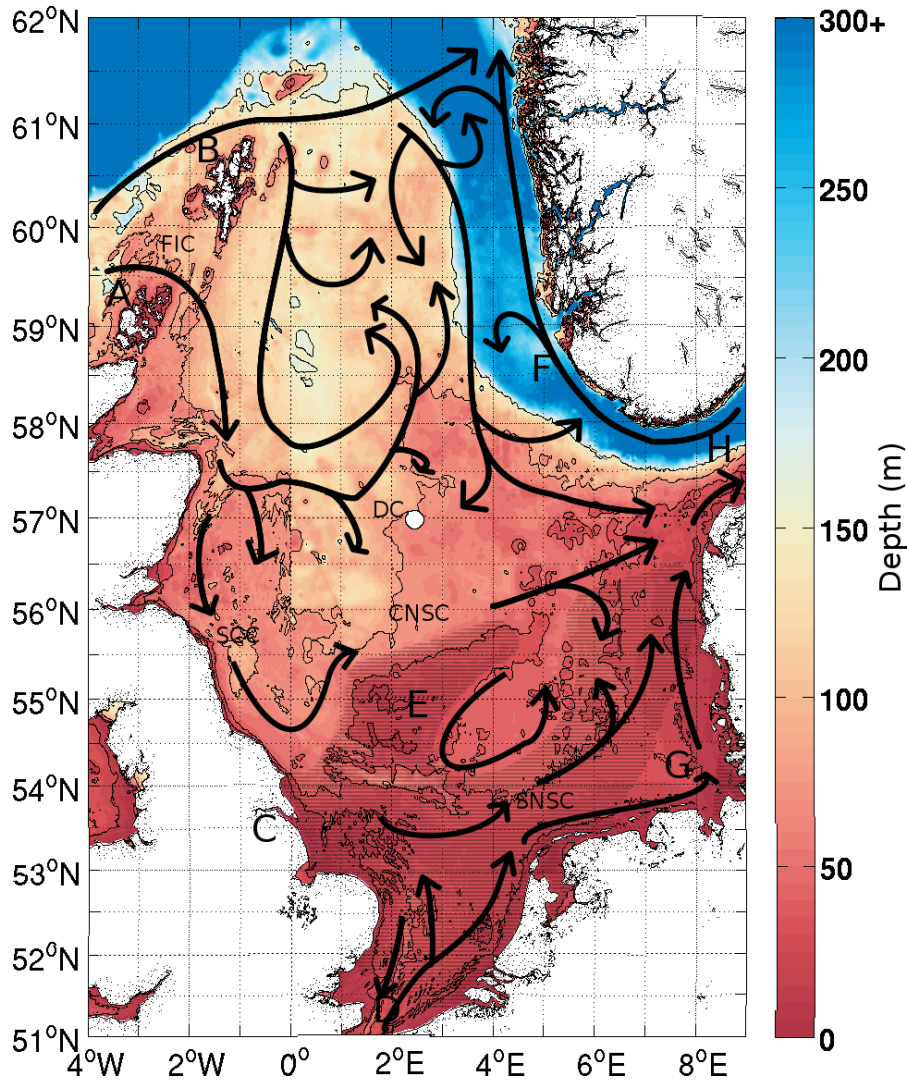


Figure 5.2: Bathymetry of the study area in metres (GEBCO, 2010). Depth contours have been added for the 20, 40, 80 and 160 m isobaths. The region where the glider was deployed in indicated by the large white dot at approximately 57° N 2°30' E. Major land marks are indicated as A & B: Shetland and Orkney Isles. C: Humber estuary. D: the Channel. E: Dogger Bank. F: Norwegian Trench. G: German Bight. H: Skagerrak. The general circulation of the North Sea (adapted from Turrell et al., 1992 and Hill et al., 2008) is overlaid as arrows for FIC: Fair Isle Current, DC: Dooley Current, SCC: Scottish Coastal Current, CNSC: Central North Sea Current, SNSC: Southern North Sea Current. Hatch marks cover areas not subject to thermal stratification in summer.

play a disproportionate role in defining the biochemical properties of the central North Sea as under specific conditions of circulations or surface wind stress, the fresh water run-off issuing from the Baltic, Kattegat and Skagerrak can be advected into the central North Sea (Otto et al., 1990). This not only affects stratification by increasing the salinity difference between SML and BML but also supplementary nutrients to the SML.

A Seaglider from the University of East Anglia, SG510, was deployed at  $56^{\circ}41.96' \text{ N}$ ,  $2^{\circ}26.37' \text{ E}$  on the 19th of August 2011. Seagliders, manufactured by iRobot, are buoyancy-driven AUVs which move through the water in a sawtooth pattern between the surface and the bottom, to a depth of 1000 m. They sample every 5 seconds using an on-board biochemical sensor suite (Seabird unpumped CT sails, Wetlabs Triplet EcoPucks and Aanderaa 4330 optode) to observe physical, chemical and biological processes. Here, SG510, sampled along a 32 km northward transect during a 3 day period (158 dives). This averages a full dive (up and down cast) every 32 min down to ca. 65 m depth. A full description of the instrument is included in Chapter 2.

The Seaglider mission was cut short after 3 and half days due to an instrument failure. The Seaglider, at the time of the survey, ran a legacy version of the PicoDOS operating system which was incompatible with the current FAT32 filesystem format. All data were stored on a standard FAT partition and suffered from a file number restriction. To remedy this issue, the boot record had to be manually edited by the manufacturer to permit a greater number of files. The memory card in SG510 had not had this restriction removed. After 158 dives, the Seaglider was no longer able to record data and deleting files remotely required the creation of a temporary file on the Seaglider. At this point, the mission was terminated.

During the ship survey, a smaller CTD package, a CEFAS ESM2 mini-logger, was attached to the ship's CTD. This instrument has an Aanderaa 4330F DO sensor. All ship data presented here were collected with the ESM2 logger. Water sample collection was performed using the same methodology as described in Sec. 4.2.1.1. ESM2 DO data were calibrated against Winkler titrations. Due to poor analysis, the

calibration from Winkler titrations is not accurate. Replicates showed wildly varying results: mean standard deviation between triplicates was  $7.86 \mu\text{mol dm}^{-3}$  (mean concentration was  $217.05 \mu\text{mol dm}^{-3}$ ). Fig. 5.3 shows the relation between CalPhase and TCPhase from the Cefas Endeavour's oxygen optode calibration coefficients (dotted black line). The red dots on Fig. 5.3 show poor Winkler titrations. The blue line is the regression performed using the set of "good" Winkler titrations to obtain calibrated coefficients (see Sec. 2.2.6). Only 21 sets of replicates have a standard deviation under  $4.47 \mu\text{mol dm}^{-3}$  ( $0.1 \text{ ml l}^{-1}$ ), these were the data points used for the regression. It is thought the strong differences between replicates were linked to inadequate experimental handling; further work during the cruise showed samples were not being mixed sufficiently prior to incubation. No relation between standard deviation and chlorophyll a fluorescence was found.

The Seaglider is provided calibrated, but the oxygen sensor in particular is prone to drift. It was desirable to calibrate the Seaglider oxygen data against *in situ* measurement but not critical due to the recent refurbishment (19<sup>th</sup> of April 2010). As the glider was recovered prematurely, it was not possible to perform a full depth calibration cast and no Winkler data were available for calibration. Similarly, the Wetlabs calibration provided during refurbishment was used instead. This leaves us with an instrument that is internally consistent with good instrument performance and high precision, but uncertain accuracy. Despite these limitations, the Seaglider data does allow short term variability to be assessed with the data as discussed below.

Seaglider temperature, salinity, oxygen and optical data correction was done as described in Ch. 2. Seaglider up-cast data were then averaged into 45 min by 1 dbar bins to provide regularly gridded data. This averaged one and a half dives, or three casts, in the horizontal, with no bin containing less than 2 different casts. Bins were not constrained to complete dives and many dives are split across bins. Fig 5.4 shows Seaglider data pre-correction (red) and post-correction (blue). Notice the greatly improved depiction of the pycnocline in variables requiring calculation from temperature and salinity data.

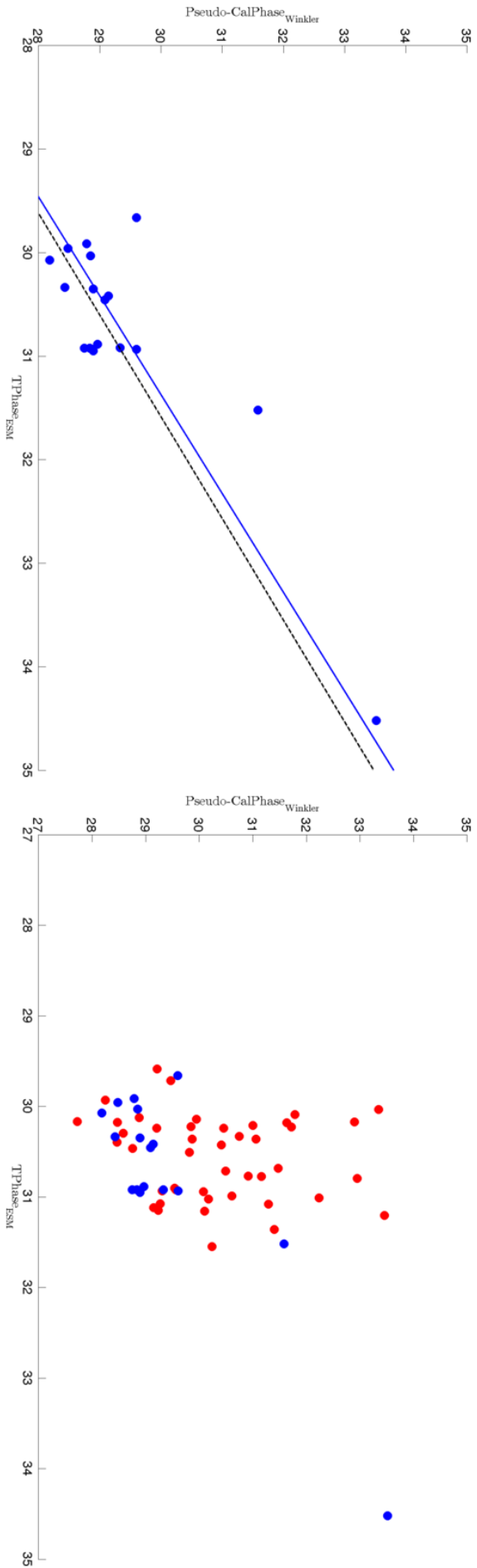


Figure 5.3: Linear regression of TCPPhase from the CEFAS Endeavour’s oxygen optode and corresponding median Winkler titration triplicate pseudo-CalPhase back-calculated using the optodes’s foil coefficients (*blue line*) and manufacturer’s calibration (*dotted black line*). Due to poor experimental handling, many sets of replicates had high standard deviations. Blue dots indicate the 21 sets of replicates used in the linear regression (standard deviation less than  $0.1 \text{ ml l}^{-1} / 4.47 \text{ } \mu\text{mol dm}^{-3}$ ). Phase coefficient 0 =  $-2.856$ , phase coefficient 1 =  $1.0472$ .  $R^2 = 0.87$ .

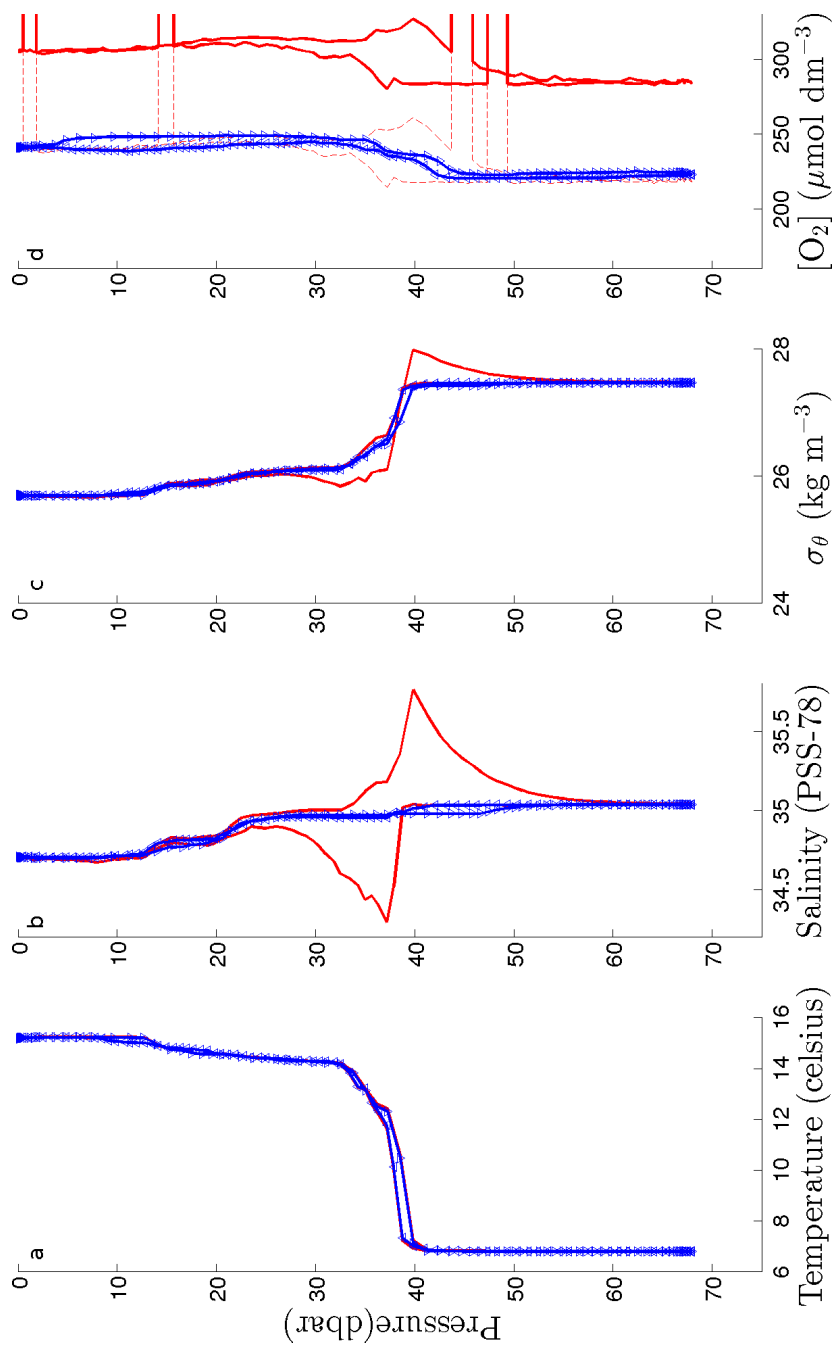


Figure 5.4: Temperature (a), salinity (b), potential density (c) and DO profiles (d) of the final dive for SG510. Glider observations as output by the iRobot processing are in red. Glider observations after calibration by the UEA toolbox are in blue. The dotted red line is iRobot processed DO offset for ease of comparison with calibrated data. The greatest difference between the iRobot processed data and the UEA toolbox data is located near the thermocline. The UEA toolbox provides additional corrections for thermal lag and inertia of sensors as well as corrects offsets in timestamps for each sensor providing synchronous temperature, conductivity and oxygen optode phase measurements for calculation of seawater properties.

### 5.2.2 GOTM-BFM

GOTM is a one-dimensional water-column model which resolves the main thermo- and hydrodynamic vertical mixing processes but omits all horizontal processes (Fig. 5.5; Burchard et al., 1999). This limitation is believed to have a negligible impact on the scale of days in the area of interest due to the suspected low flow in the region (Otto et al., 1990) and greatly simplifies the modelling and understanding of the vertical processes involved in representing the injection of high DO waters into the BML. GOTM is forced by irradiance and temperature data obtained from European Centre for Medium-Range Weather Forecasts (ECMWF) ERA Interim reanalysis data (van der Molen et al., 2012).

The biochemical model used in this chapter is an extended version of BFM which follows on from the original European Regional Seas Ecosystem Model (ERSEM) (Ruardij et al., 1997; van der Molen et al., 2012). BFM is being developed cooperatively by CEFAS and the Royal Netherlands Institute for Sea Research and was originally developed for integration into a 3-dimensional model (GETM), which includes both BFM and GOTM (van der Molen et al., 2012). The model is a biomass-based collection of biogeochemical equations describing pelagic and benthic carbon, macronutrient and oxygen cycling. Carbon, macronutrients and oxygen are represented as physical and biological reservoirs: benthic and pelagic containers, each divided into biological functional groups: phytoplankton, zooplankton, decomposers, benthic and pelagic bacteria (Fig. 5.5); Baretta et al., 1995; Ruardij et al., 1997; Vichi et al., 2007, 2004). GOTM and BFM are coupled to provide a mathematical representation of physical and biochemical interactions throughout the water column and benthos.

For this study, a forecast run was performed with identical forcing and similar initial conditions as the ND case described in van der Molen et al. (2012). Model time-step was increased to 10 min and run over 40 vertical levels representing a water column of 75 m at the location of 56°59'N 20°27'E from 1958 to 2098. The first 10 years of

output were discarded to allow the model to spin-up. After 8 years, the pelagic variables had stabilised.

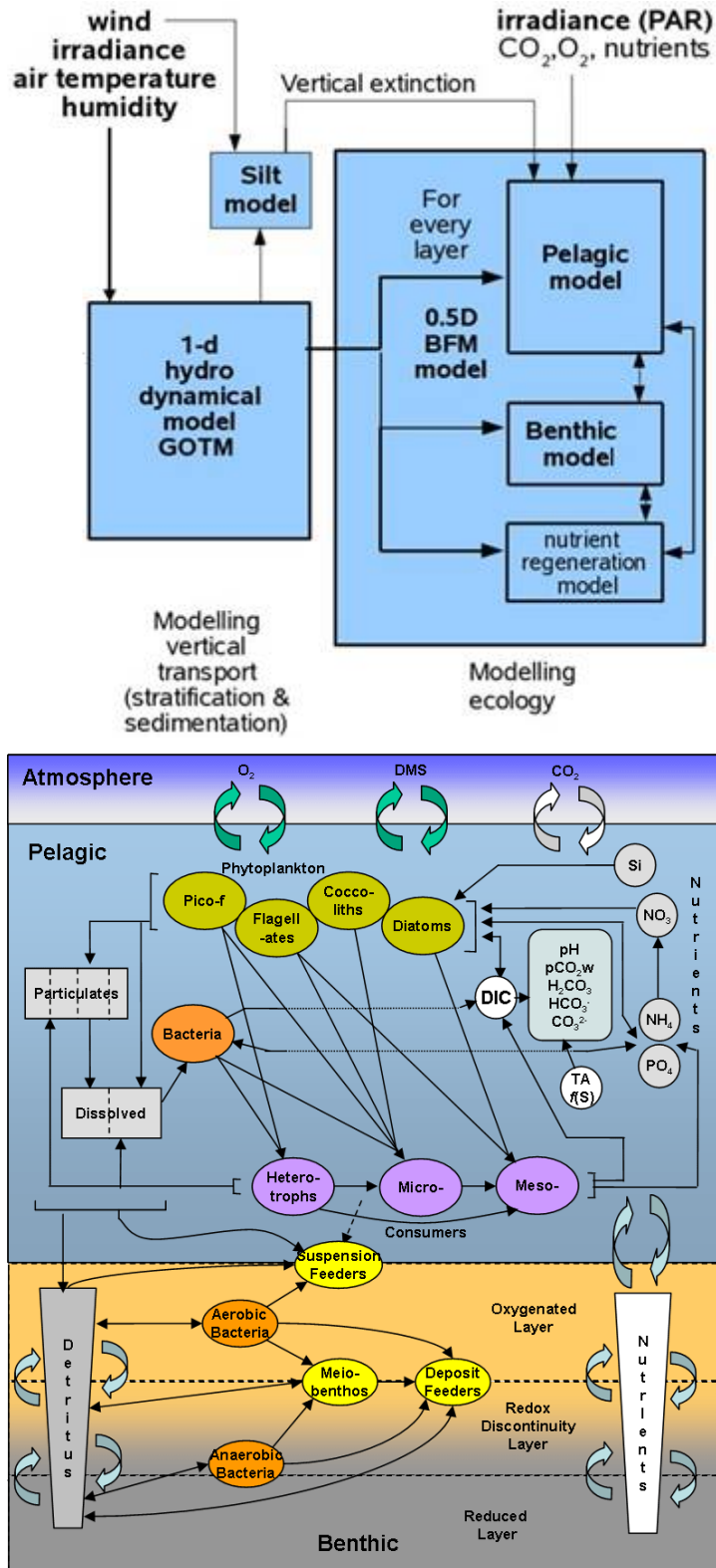


Figure 5.5: Schematic representation of forcing and feedback between GOTM and ERSEM (top) and schematic of the interactions between containers and functional groups within ERSEM (bottom).

## 5.3 RESULTS AND DISCUSSION

### 5.3.1 *Supply of oxygenated water*

#### 5.3.1.1 *Horizontal transport*

To observe vertical processes in the water column, ideally the glider would sample the same vertical section throughout the mission. This requires no horizontal displacement of the glider relative to the water. During survey planning, it was expected that horizontal gradients would be minimal in this region as they had been in August 2010 and therefore any horizontal displacement would have negligible impact on changing observed watermass properties. However, August 2011 was very different in terms of circulation and hydrographic characteristics. Fig. 5.6 shows MODIS Aqua sea surface temperature and chlorophyll *a* concentration across the North Sea and around the deployment area over the 3 day Seaglider deployment. The figure reveals a surprising amount of horizontal variability across the Seaglider transect in surface waters. It appears the glider was deployed in a frontal region with waters issuing from Skagerrak outflow and continental coastal waters encroaching into the central North Sea. This is further revealed in Fig. 5.7 where the Seaglider observed a dramatic freshening of the SML at the end of the survey ( $-0.3$  PSU). This change was not reflected in the BML, where the glider observed a weak but opposing trend. In the BML, the Seaglider observed a  $-0.1^{\circ}\text{C}$  change in temperature and  $+0.03$  PSU change in salinity ( $+0.035 \text{ kg m}^{-3}$  change in density), likely due to increasing Atlantic water influence. As the Seaglider was in a frontal region, it is possible that many of the features observed during this deployment are not representative of the wider northern North Sea and are, instead, due to frontal processes.

The front observed by the Seaglider did not extend to the bottom of the water column. During the survey, the Seaglider observed no bottom fronts which have been reported several times in the region (Brown et al., 1999; Fernand et al., 2006, 2013; Hill et al., 2008; Weston

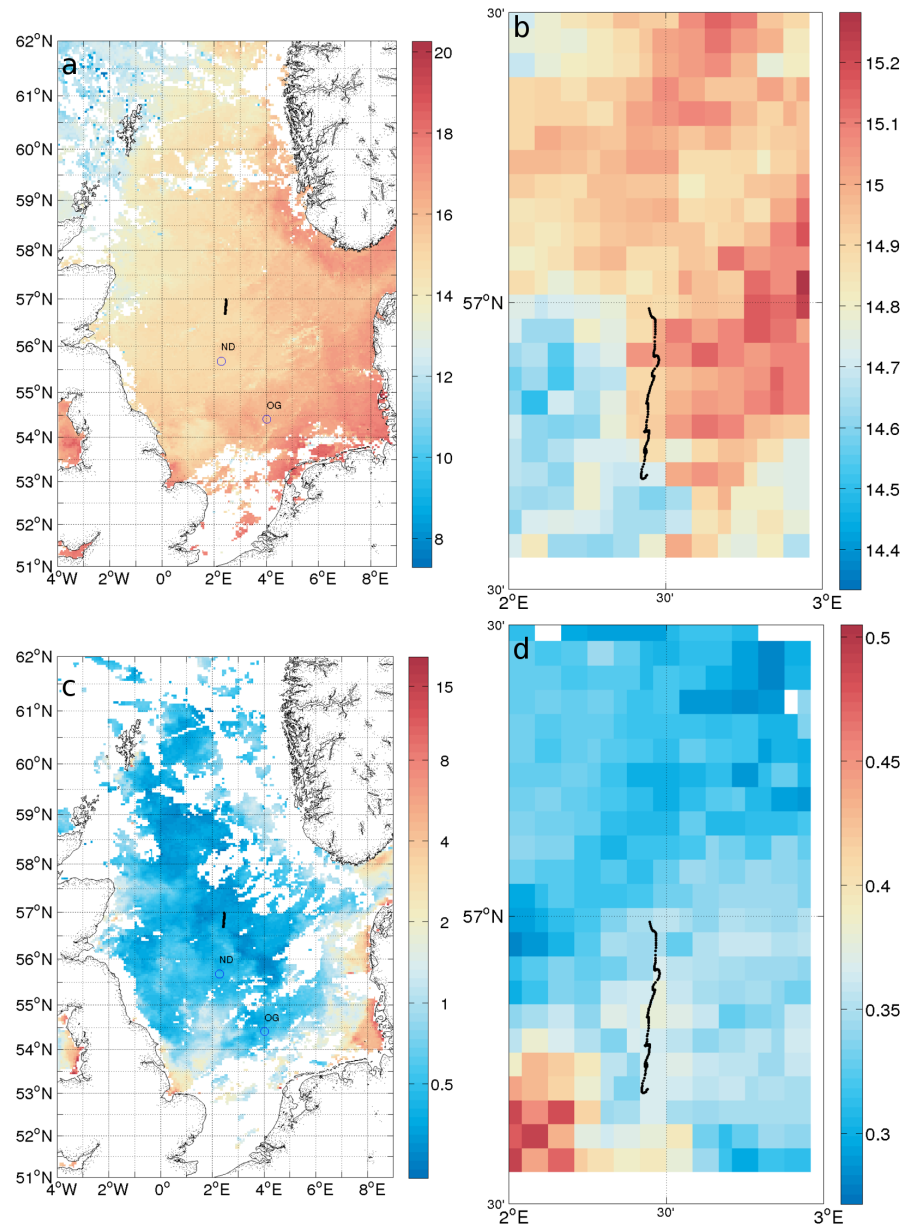


Figure 5.6: 3-day composite of MODIS Aqua daytime sea surface temperature at  $11 \mu\text{m}$  ( $^{\circ}\text{C}$ , a and b) and chlorophyll a concentration ( $\text{mg m}^{-3}$ , c and d) across the entire North Sea (*left*) and around the Seaglider deployment area (*right*) from the 20<sup>th</sup> to 22<sup>nd</sup> of August 2011. The colour scale for the North Sea map of chlorophyll a is logarithmic to highlight chlorophyll a distribution in the central North Sea where concentrations are low. Northward Seaglider track is indicated by the black line.

et al., 2005). These strong seasonal features line denser pools of BML water and exhibit fast narrow jets above ( $> 0.2 \text{ m s}^{-1}$ ; (Brown et al., 1999)). In particular, they are considered to exacerbate seasonal oxygen depletion within the OG (Van Raaphorst et al., 1998). Not only do the frontal structures isolate the denser waters creating “temporary depocentres” or “retention areas” (Hill et al., 2008), the enhanced flow along the thermocline encourages further productivity. In this study, the glider was located further north than regions reported by Weston et al. (2005) and Fernand et al. (2013) where the sharp bathymetric gradient of the northern face of Dogger Bank encourages the formation of bottom fronts. Little information is available in the literature pertaining to the occurrence of bottom fronts in the region where the Seaglider was launched. This region exhibits a more uniform topography with only shallow localised basins; strong bathymetric gradients are located along the Norwegian Trench and Dogger Bank. The lack of bottom fronts in data from the glider lends credibility to the assumption that Seaglider observes little horizontal advection in the BML.

Despite this, care must be taken as horizontal gradients in water properties make it difficult to distinguish changes as a function of time as spatial variations dominate temporal trends at this scale. Although we observe changes as a function of time, they cannot be interpreted as being wholly due to changes in a single body of water but rather may reflect gradients around the survey region. Determine rates of DO consumption within the BML would likely not be strongly impacted by aliasing due to advection, however investigating the evolution of the DCM would be difficult as changes of this magnitude in physicochemical properties of the SML will likely be represented at the same scale if not finer in the biology (Powell, 1995). It is still also possible to investigate rapid vertical transport mechanisms of oxygenated water, sediment and chlorophyll *a*. Observed rapid vertical processes may be easier to identify and interpret over gradual changes in the properties of the mixed layers which could either be attributed to natural horizontal gradients or gradual changes over time.

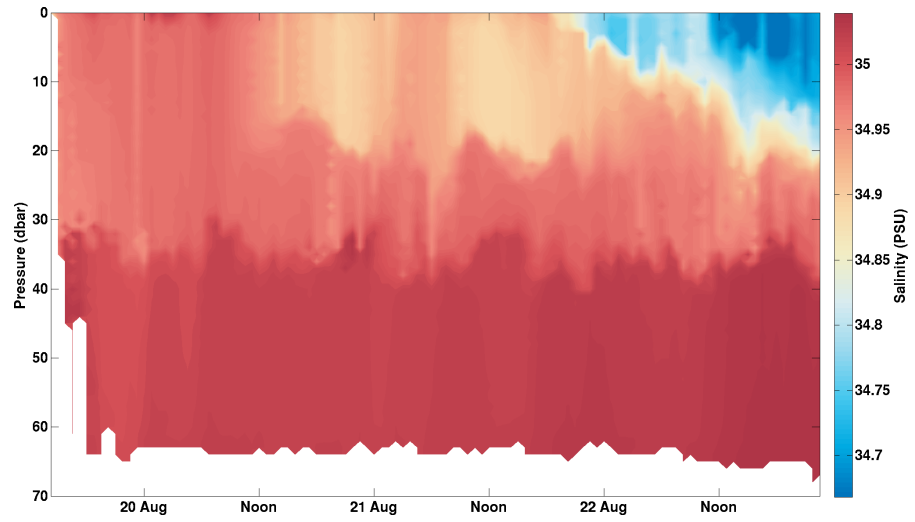


Figure 5.7: Seaglider section of salinity (PSU) sampled along the transect.

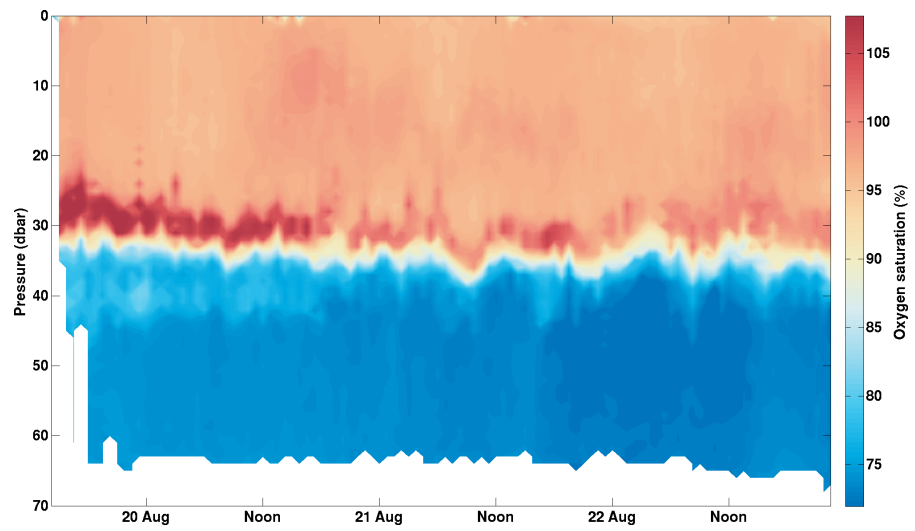


Figure 5.8: Seaglider section of DO saturation (%) sampled along the transect.

These observations do however point to a greater influence of advective processes than previously thought and assumed in Chapter 4. Interestingly, oxygen saturation shows a decreasing trend as Atlantic water influence increases which is an opposite trend to 2010 (Fig. 5.1). In 2010, the low oxygen (< 70% saturation) region was located along 57°N with the North Atlantic boundary showing high BML oxygen saturations (75% saturation). In 2011, this trend was reversed with sub-70% saturations north of 58°N and BML saturations between 70% and 75% in the ND region. Two regions of low BML DO saturation were present: the northern North Sea and the eastern reach of the Central North Sea Current (Fig. 5.1). The Seaglider was not deployed in the region of strongest BML oxygen depletion. Even so, the glider did observe significant oxygen depletion (Fig. 5.8). The SML was consistently near saturation, while the BML decreased from 75% to 72.5% with a sharp increase back to 75% in the final 12 hours of the survey. Supersaturated water was present just above the pycnocline (105%) throughout the survey although this highest supersaturation was recorded by the glider either during the first day or along the first third of the transect. This pattern of supersaturation near the thermocline is typical of production at a DCM and is consistent with Seaglider observations of chlorophyll *a* (Fig. 5.9). The intensity of the supersaturated thin layer follows the intensity of the DCM observed by the glider. Additionally, influence of DCM production was observed directly below the thermocline. Less oxygen depleted water (83%) was observed in the 10 m directly below the peak in DCM chlorophyll *a* concentration relative to the more depleted BML water.

Lenhart et al. (2004) investigated the influence of the North Atlantic Oscillation (NAO) on production across the North Sea. They found that the NAO had a very strong impact on the physical environment and ecosystem of the North Sea. Notably, years with high NAOI had dramatically different circulation in the northern North Sea and saw changes of more than one order of magnitude in volume transport at Fair Isles and along the northern boundary of the North Sea compared to years with low NAOI. Strongest counter clockwise circulation occurred in 1994, a year of high NAOI (1.8), also leading to in-

creased inflow and outflow along the northern boundary and strong flow of surface Baltic waters into the North Sea. In 1996, a low NAOI year (-2.3), Lenhart et al. (2004) could find no evidence of the usual counter clockwise circulation pattern. In low NAOI years, mean Sea Surface Temperature (SST) decreases, while general wind direction changes from S-W to S-E and exchange along the northern boundary of the North Sea decreases (Dippner, 1997; Lenhart et al., 2004). Fettweis et al. (2012) also report strong variations in suspended particulate matter between low and high NAOI years which is linked to light and nutrient availability for primary production and organic matter in the water column (McQuatters-Gollop et al., 2007), both of which impact pelagic respiration. The 2010 survey in Chapter 5 was during a very low NAOI year ( $NAOI_{July2010} = +0.06$ ,  $NAOI_{Aug2010} = -2.01$ ,  $NAOI_{Sept2010} = -2.38$ ) whereas the 2011 survey was performed during a transition to a very high NAOI year ( $NAOI_{July2011} = -3.39$ ,  $NAOI_{Aug2011} = -0.18$ ,  $NAOI_{Sept2011} = +2.97$ ) (Osborn, 2011). This is the likely cause of the observed difference in distribution in summer oxygen depletion in the North Sea between 2010 and 2011.

Due to the high variability of horizontal transport processes, both interannually and across the North Sea, it is not possible to rule out advection as a significant regulator of seasonal oxygen depletion. Horizontal transport processes likely affect seasonal oxygen depletion by influencing BML and SML temperatures thereby affecting stratification and by potentially supplying labile organic matter to the BML. Models of North Sea circulation are improving rapidly and beginning to include wider areas (i.e. the North Atlantic) and are becoming more able to model the effects of the NAO in the North Sea (Lenhart et al., 2010). Skogen and Moll (2005) state that improvements in physical modelling of the North Sea will result in improved modelling of phytoplankton and nutrient distributions across the North Sea and will reduce the differences observed such as the one in the GETM results (Fig. 5.1).

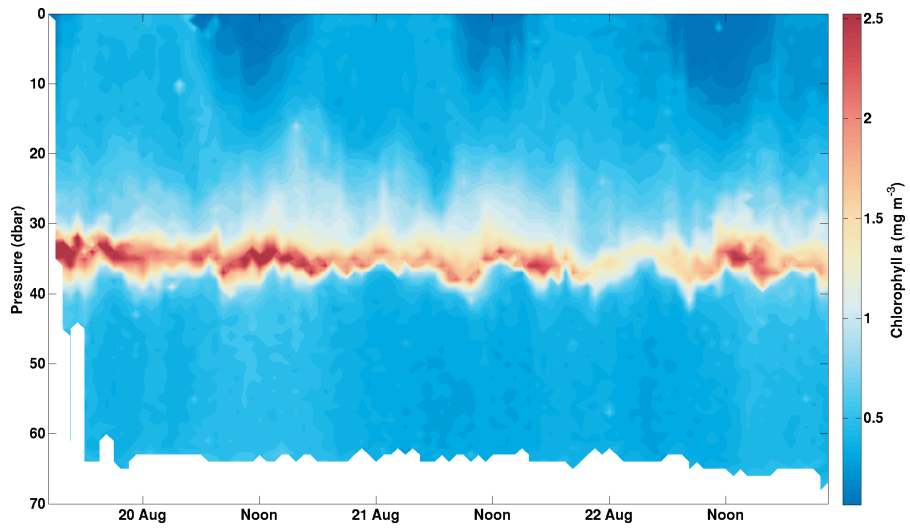


Figure 5.9: Seaglider section of chlorophyll a concentration ( $\text{mg m}^{-3}$ ) sampled along the transect.

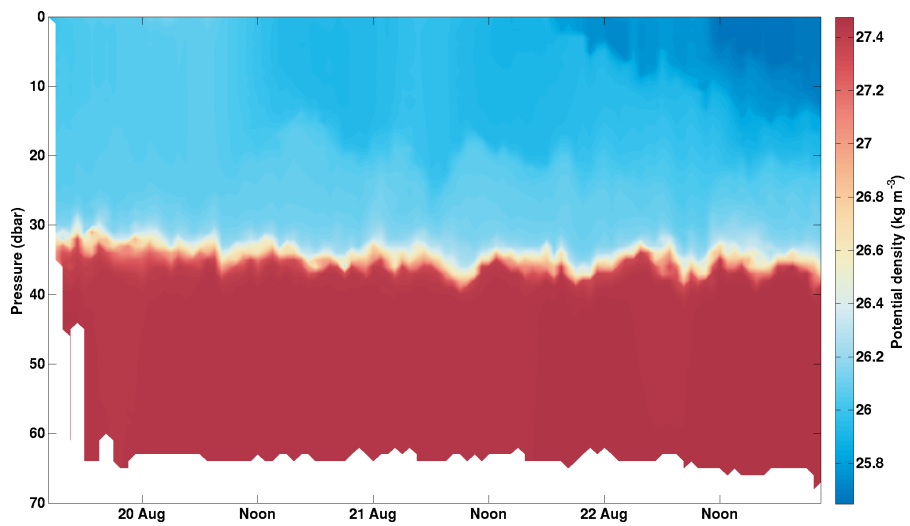


Figure 5.10: Seaglider section of potential density ( $\text{kg m}^{-3}$ ) sampled along the transect.

### 5.3.1.2 *Mixing*

Aside from horizontal transport of oxygenated water, vertical mixing is assumed to be the largest potential source of oxygen input into the BML. Despite not directly measuring turbulence flow, the Seaglider can still provide some insight into the extent of mixing across the pycnocline. Seaglider observations reveal a highly stratified water column with a strong pycnocline spanning approximately 3 m with a density difference of  $1.5 - 2 \text{ kg m}^{-3}$  (Fig. 5.10). During the first two days of the deployment, the density difference is dominated by the temperature difference ( $8^\circ\text{C}$ , Fig. 5.11). During the final day of deployment, the intrusion of continental or Baltic water observed in the SML (Fig. 5.7) creates a salinity gradient that was not present before and leads to an increase in density difference between the SML and BML of  $0.5 \text{ kg m}^{-3}$ .

Evidence of mixing can be found in changing properties of the BML. Temperature, salinity, chlorophyll *a* and oxygen are all potential tracers that can be used to assess mixing across the pycnocline on such short time scales (Fig. 5.12). Binned data from 45 dbar and below (the BML, excluding the 5 m below the thermocline) were plotted against time and coloured by pressure. This shows a vertical gradient in all four properties observed. Temperature and chlorophyll *a* were highest near the thermocline while salinity and DO increased with depth. All four properties show large fluctuations affecting the entire BML which are difficult to interpret and attribute to vertical mixing as it is possible horizontal variability and proximity to the front play a role in changing BML properties. Alongside, the extent of the vertical gradient for each property is shown by the black vertical lines. This illustrates changes in vertical gradients; a small value indicates a homogenous BML while a large value indicates a strong vertical gradient in the BML. The temperature data in Fig. 5.12 show small-scale changes in vertical gradients of the order of a few hours or hundreds of metres. The gradient between the top and bottom of the BML increases alongside BML-wide temperature increases. This indicates

warming of BML water from above caused by cross-thermocline injection of SML water.

Neither salinity, chlorophyll *a* or oxygen concentration worked as a suitable tracer. In the case of salinity, the salinity difference between the SML and BML is too small. Although the data show a similar signal, it is much more difficult to identify due to the background noise. This noise is in part caused by sensor accuracy, but also inaccuracies caused by the Seaglider data processing. Accurate correction of the salinity data requires correct identification of thermal lag parameters and flow speed through the cell to match temperature and conductivity measurements (Ch. 2). As the glider observes a very rapid and strong change in temperature between the SML and BML, any inaccuracies in the determination of the conductivity cell's hydrodynamic properties are reflected very strongly in the salinity data. Due to the nature of the fluorescence sensor, and the distribution of phytoplankton in the SML, the data are naturally very spiky. This background noise makes it difficult to identify clear intrusions into the BML. Finally, DO data show little evidence of vertical mixing. The sensor precision is low and data are also severely affected by issues in post-processing on this scale. Most importantly, as shown in Fig. 5.8, there is evidence of production occurring just below the thermocline. It is likely that the euphotic depth extends to below the thermocline allowing some production to occur in the top of the BML. This creates a vertical gradient in DO unrelated to vertical mixing processes.

We now try to explain these mixing events evident in the temperature data. Fig. 5.13 shows wind and tidal velocities along with sea surface temperature and salinity. There is no obvious correlation between small mixing events identified in Fig. 5.12 and tidal velocities. The majority of mixing events tend to occur during periods of peak wind velocities, but the duration of mixing events does not seem to match the time scale of wind velocity changes; additionally, two mixing events are visible in periods of low wind velocities. Mixing events do not seem to correlate with bathymetry in the region either (Fig. 5.13).

These mixing events are short scale (a few hours or a couple kilometres) processes which the Seaglider is able to reveal through its

very high resolution observation. These events could be linked to internal waves propagating through the North Sea. Weston et al. (2005) highlighted the importance of internal waves propagating northwards from the shallow Dogger Bank on the ND site located further south. Also, as the glider is travelling along a front (Fig. 5.6), it is also possible that these mixing features are linked to the presence of the front.

Observations of hydrography in the region have shown evidence of both horizontal and vertical processes having significant impact on BML properties. This points to potentially elevated rates of DO supply to the BML. Horizontal processes were not resolved by the GOTM-BFM model, yet Fig. 5.14 shows similar findings. Fig. 5.14 shows model results treated in the same manner as Seaglider observations in Fig. 5.12. Evidence of fluctuations in model temperature gradients in the BML is similar to Seaglider observations in terms of intensity although not as rapid. However, model mixing events seem closely correlated to ECMWF re-analysis wind velocities. As these mixing events are also visible in the model, it is likely they are not caused by bathymetric features, internal wave propagation or frontal processes. Both chlorophyll *a* and DO also show variations in vertical gradients in the BML. These will be discussed further in the following section.

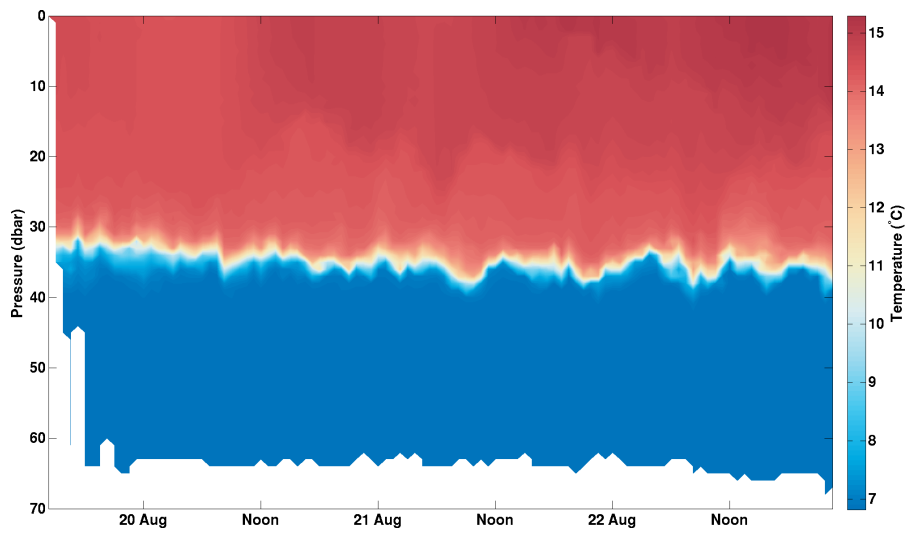


Figure 5.11: Seaglider section of temperature ( $^{\circ}\text{C}$ ) sampled along the transect.

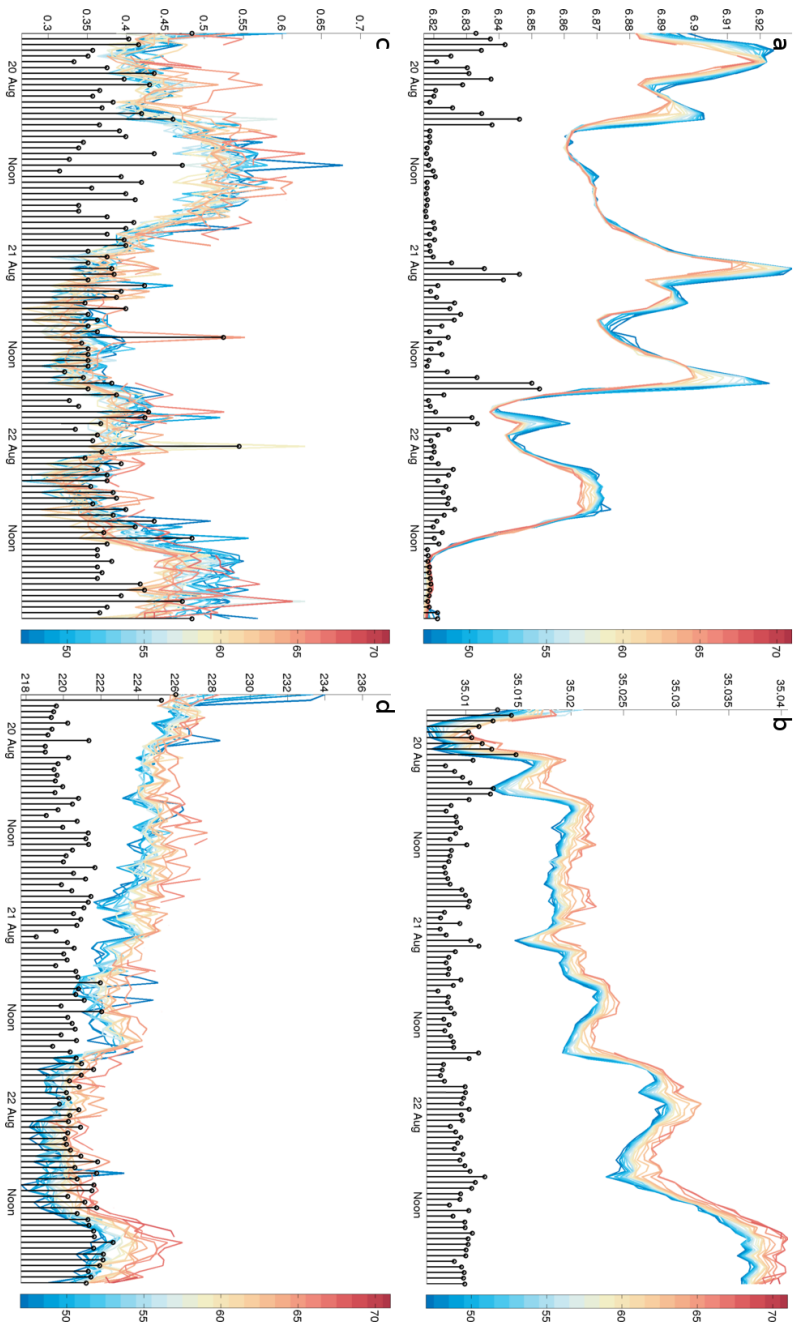


Figure 5.12: Seaglider temperature ( $^{\circ}\text{C}$ , a), salinity (PSU, b), chlorophyll a ( $\text{mg m}^{-3}$ , c) and DO concentration ( $\mu\text{mol dm}^{-1}$ , d) along isobars at 1 dbar intervals from 45 dbar to 71 dbar, coloured by pressure. Black vertical lines indicate the difference between minimum and maximum values at each time step. Binned data from the BML (45 dbar and below) are plotted against time and coloured by pressure. This highlights a vertical gradient in all four properties observed. Temperature and chlorophyll a were highest near the thermocline while salinity and DO increased with depth. Alongside, the extent of the vertical gradient for each property is shown by the black vertical lines. This illustrates changes in vertical gradients; a small value indicates a homogenous BML while a large value indicates a strong vertical gradient in the BML. We can clearly see events where the temperature gradient increases in the BML, showing injection of warmer surface water across the thermocline.

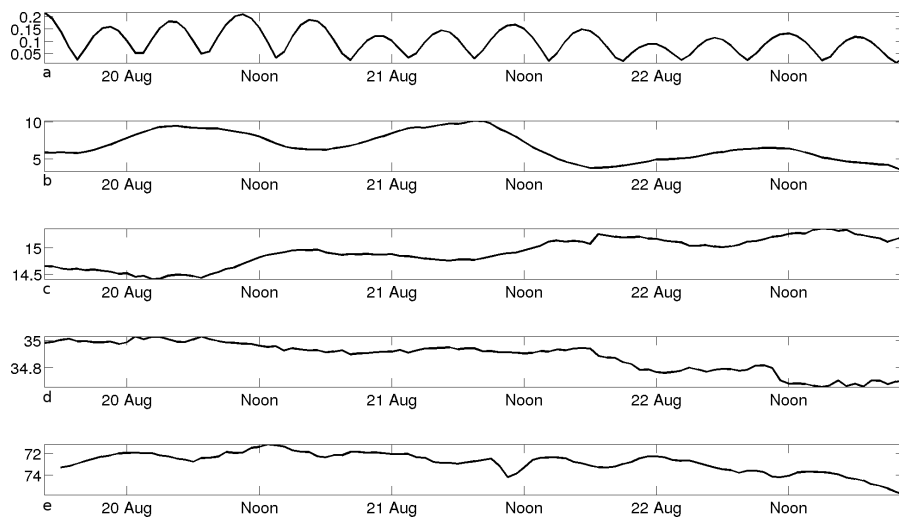


Figure 5.13: Tidal velocities ( $\text{m s}^{-1}$ , a), 10 m wind speed ( $\text{m s}^{-1}$ , b), sea surface temperature ( $^{\circ}\text{C}$ , c) and sea surface salinity (PSU, d) and depth (m, e) at the Seaglider's location during the survey. Tidal data was obtained from the TMD tide toolbox and OTIS European Shelf Model (Egbert et al., 2010). Wind data was obtained from ECMWF ERA-Interim reanalysis data. Bathymetry was gathered by the Seaglider's on-board acoustic altimeter.

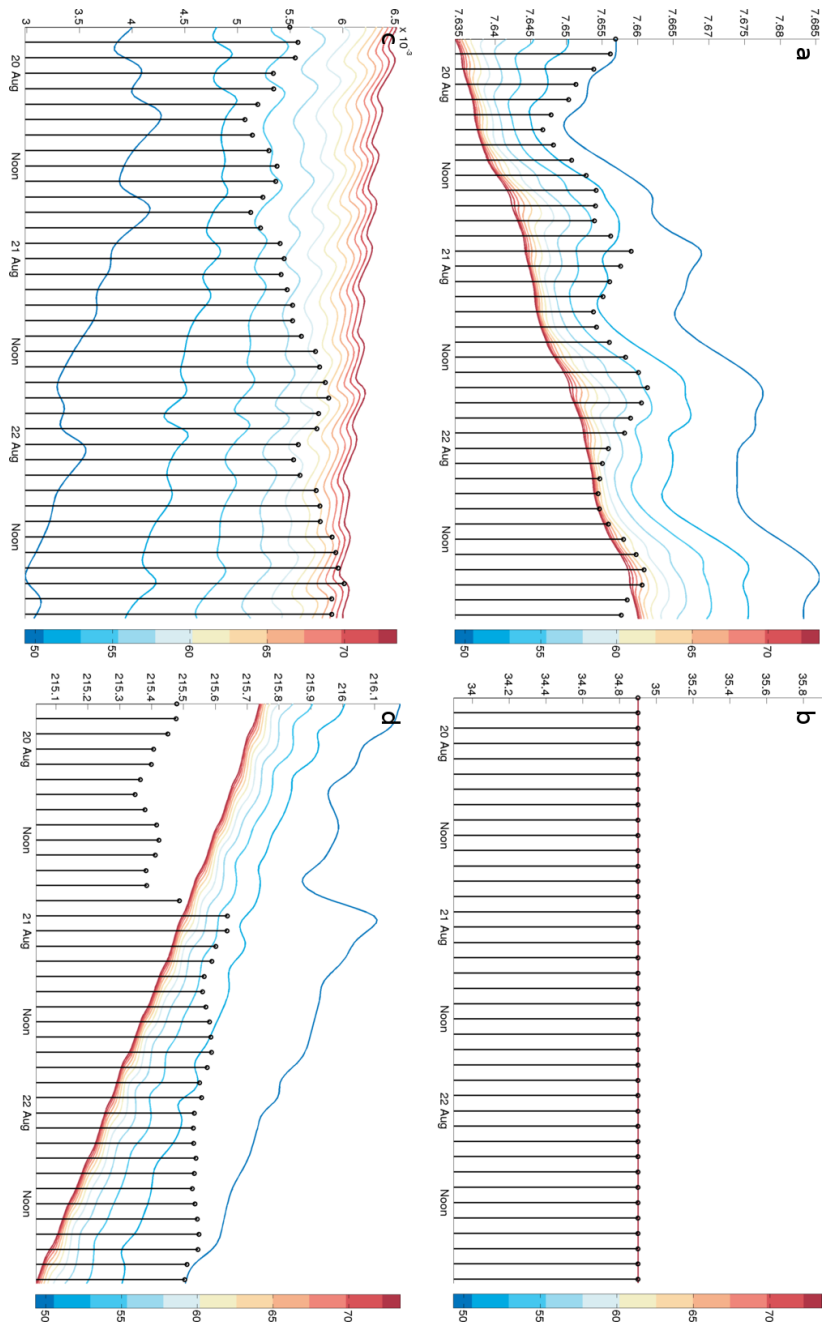


Figure 5.14: GOTM-BFM temperature ( $^{\circ}\text{C}$ , a), salinity (PSU, b), chlorophyll a ( $\text{mg m}^{-3}$ , c) and DO concentration ( $\mu\text{mol dm}^{-1}$ , d) along isobars at 1 dbar intervals from 48 dbar to 76 dbar, coloured by pressure. Black vertical lines indicate the difference between minimum and maximum values at each time step. Binned data from the BML (45 dbar and below) are plotted against time and coloured by pressure. This highlights a vertical gradient in all four properties observed. Temperature and DO were highest near the thermocline while chlorophyll a increased with depth. Salinity shows constant values as the model represented the BML with no salinity gradients. Alongside, the extent of the vertical gradient for each property is shown by the black vertical lines. This illustrates changes in vertical gradients; a small value indicates a homogeneous BML while a large value indicates a strong vertical gradient in the BML.

### 5.3.2 Sources of oxygen consumption

#### 5.3.2.1 Deep chlorophyll maximum export

The North Sea is a highly productive region. Primary production estimates for the North Sea range from 40 to 300 gC m<sup>2</sup> yr<sup>-1</sup> depending on area and technique (modelling vs. empirical), with maxima in the central North Sea area (north of Dogger Bank). A transect by Weston et al. (2005) north of Dogger Bank showed whole water column-integrated primary production values of 167, 370 and 270 gC m<sup>2</sup> yr<sup>-1</sup> for areas classified as Dogger Bank, the front (located along the northern edge of Dogger Bank) and the stratified area (the ND site) respectively.

More recently, the importance of the DCM has been reviewed. DCM contribution to total primary production for the stratified North Sea during the summer months has been estimated at between 58% and 60% (Fernand et al., 2013; Weston et al., 2005). Values for new production range from 37% to 66% produced at the DCM for the whole water column (Fernand et al., 2013; Weston et al., 2005). As the DCM relies on small scale mixing across the pycnocline to provide nutrients, it is necessarily located very near to the pycnocline. Consequently, any mixing will inject highly labile organic matter into the BML. Furthermore, sinking of organic matter produced at the DCM is exported to the BML immediately, therefore any remineralisation of organic matter occurs in the BML. This means that the near totality of new production from the DCM is consumed within the BML.

The Seaglider observed DCM chlorophyll a concentrations of 2 to 3 mg m<sup>-3</sup> in 2011 (Fig. 5.9). These values are similar to those found by Fernand et al. (2013) but lower than concentrations observed by Weston et al. (2005) (ca. 5 - 10 mg m<sup>-3</sup>). This is likely explained by the systematic variation in DCM chlorophyll a concentrations across the North Sea. The site considered here is located further north and is not subject to as much mixing from waves propagating northward from Dogger Bank which fuel the DCM in the ND region (Ducrotoy et al., 2000; Weston et al., 2005). Chlorophyll a concentrations at

the DCM fluctuate on a near diurnal cycle (Fig. 5.9). This may be linked to either fluctuations in light availability, or a diurnal change in wind velocities. Increased wind velocities could lead to an increase in chlorophyll *a* fluorescence a few hours later by encouraging nutrient supply to the DCM. Chlorophyll *a* concentration fluctuations are likely not an artefact of non-photochemical quenching as periods of high DCM chlorophyll *a* concentrations are present when surface chlorophyll *a* fluorescence is affected by high light intensity. Quenching is clearly visible in the top 10 m every day after noon. Without a longer high-resolution time series, it is not possible to confirm whether fluctuations of chlorophyll *a* concentrations at the BML are due to increased light availability or wind-induced nutrient supply. Interestingly, this fluctuation in DCM chlorophyll *a* is likely to lead to a bias in estimates of production at the DCM. Past observations have relied on traditional CTD and towed undulator surveys which tend to mostly be performed during daylight hours.

We now investigate the export of DCM organic matter to the BML. Figs. 5.9 & 5.12 show a similar pattern for BML chlorophyll *a* concentration and DCM chlorophyll *a* concentrations. We do observe a delay between peaks in DCM chlorophyll and BML chlorophyll; BML chlorophyll *a* concentrations peak a few hours later. As we have already observed a delay between peaks in wind velocities and DCM chlorophyll *a* concentrations, we can assume that wind-driven mixing is not responsible for injecting these large amount of organic matter into the BML. Neither is this export correlated to tidal velocities or changes in BML salinity, thus ruling out the influence of horizontal transport processes or tidal mixing on export of DCM organic matter to the BML. It seems likely that the wind drives production at the DCM but export mechanisms are driven by biological processes. We observe a daily increase in BML chlorophyll *a* concentrations of  $0.15 \text{ mg m}^{-3}$ . With an approximate BML height of 38 m, this amounts to  $5.7 \text{ mg m}^{-2} \text{ day}^{-1}$  of chlorophyll *a* export to the BML. Using a POC:chlorophyll *a* ratio of 50:1 (Sathyendranath et al., 2009; Weston et al., 2004), this amounts to approximately  $0.285 \text{ g C m}^{-2} \text{ day}^{-1}$  export to the BML. If all this organic matter is remineralised in the

BML, this would equal  $33.58 \text{ mmol DO m}^{-2} \text{ day}^{-1}$  (Nixon, 1982). If all this organic matter were remineralised within the BML, this could potentially lead to the consumption of  $123.7 \text{ } \mu\text{mol dm}^{-3}$  if we assume a BML height of 38 m over a 140 day stratified period ( $0.884 \text{ } \mu\text{mol dm}^{-3} \text{ day}^{-1}$ ). No POC:chlorophyll a ratio could be obtained from North Sea DCM phytoplankton communities in this region. It is likely the ratio is in fact lower as phytoplankton at the DCM are adapted to strong light limitation. Additionally, the sensor does not take into account organic matter which does not fluoresce such as faecal pellets, phytoplankton and bacteria which will augment the carbon flux and oxygen consumption.

#### 5.3.2.2 *Benthic respiration*

As the North Sea is a shallow region, vertical transport from the SML and BML to the benthic layer is fairly rapid. Van Raaphorst et al. (1998) report that 17 to 45% of primary production is remineralised in the sediments although the bulk of this occurs in the Skagerrak and Norwegian Channel area (50 to 70%) due to transport processes. Tidal currents resuspend and transport this organic matter to temporary depocentres. This makes estimating benthic respiration across the North Sea difficult due to the consequent spatial heterogeneity. Van Raaphorst et al. (1998) report a number of studies which demonstrate that particulate matter from the East Anglian plume and the southern North Sea may settle in the OG, and possibly other locations along the Dogger Bank. Van Raaphorst et al. (1998) maintain that the near totality of primary production is mineralised in the first six months of transport before being recycled and later exported; this is in agreement with Middelburg and Levin (2009), Bozec et al. (2005) and Thomas et al. (2005, 2004).

Neubacher (2009) observed nutrient and oxygen dynamics at the benthic-pelagic interface at the ND site. DO uptake by the sediment was determined to be approximately  $250 \text{ } \mu\text{mol m}^{-2} \text{ hr}^{-1}$  with variations linked to organic matter export to the benthic layer. Assuming a uniformly mixed BML with a height of 38 m, this amounts to a decline in oxygen concentration of  $1.58 \text{ } \mu\text{mol dm}^{-3} \text{ day}^{-1}$  consumed

throughout the BML. During this survey, the Seaglider would begin its ascent 5 m from the bottom preventing any observation of a possible benthic fluff layer or hyperbenthic oxygen gradients. Instead, we investigated benthic-pelagic DO exchange in the model. The GOTM-BFM model provided values of 50 - 75  $\mu\text{mol m}^{-2} \text{hr}^{-1}$ , or 0.32 - 0.47  $\mu\text{mol dm}^{-3} \text{day}^{-1}$ , for the same region in August 2011.

### 5.3.2.3 *Resuspension of organic matter*

Another driver of oxygen consumption in the BML is resuspension of organic matter. Background benthic DO consumption is limited by oxygen penetration depth and Red-Ox levels (Neubacher, 2009). When benthic organic matter is resuspended into an oxygenated water column, bioavailable surface area is greatly increased and oxygen is readily available. Three particular causes have been identified in the literature as providing enough turbulent energy to the seafloor to resuspend organic matter, these being: tidal resuspension, large wind mixing events and trawling (Couceiro et al., 2013; Greenwood et al., 2010; Jago et al., 2002, 2006; Thompson et al., 2011; van der Molen et al., 2012; Van Raaphorst et al., 1998). Current speeds and storm events sufficient to cause resuspension have been recorded at both the OG and ND sites (de Jonge et al., 1996; Greenwood et al., 2010; Kröncke and Knust, 1995; Weston et al., 2008). The influence of trawling has only recently been investigated but has been shown to potentially lead to a small (0.5%) decrease in BML DO (van der Molen et al., 2012).

Seaglider observations of optical backscatter at 650 nm in the BML can potentially be used to consider the influence of such resuspension events. Observations showed a general trend similar to that of chlorophyll *a* concentrations (Fig. 5.15). Higher frequency noise is also visible and seems to occur, at least superficially, on the same timescales as fluctuations in tidal velocities. Attempts at running a fast Fourier transform analysis to BML backscatter were unsuccessful at highlighting a signal around this frequency (Fig. 5.16); if anything, a signal at twice the frequency can be seen. This is likely due to the short deployment; a longer time series would help isolate the signal

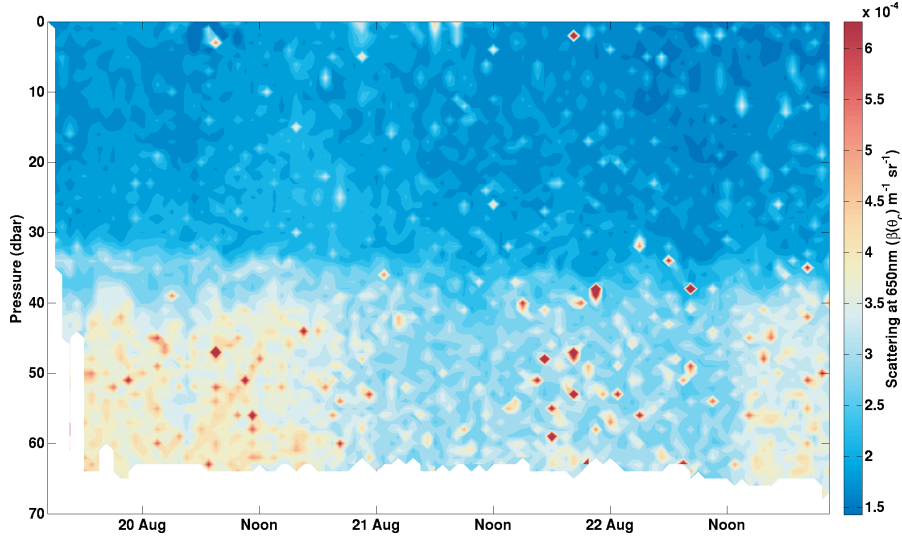


Figure 5.15: Seaglider section of scattering at 650 nm ( $\beta(\theta_c) \text{ m}^{-1} \text{ sr}^{-1}$ ) sampled along the transect.

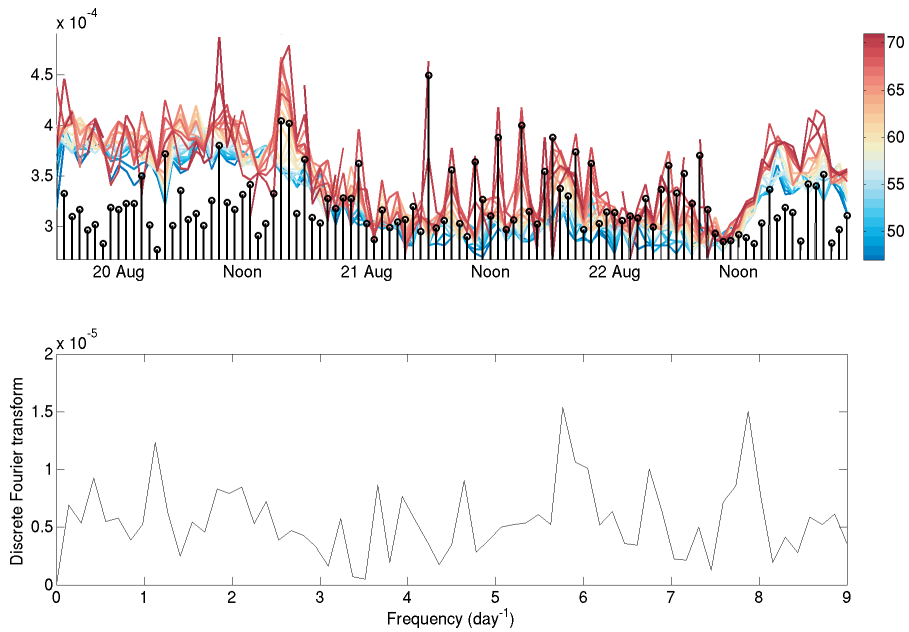


Figure 5.16: Seaglider scattering at 650 nm ( $\beta(\theta_c) \text{ m}^{-1} \text{ sr}^{-1}$ , *top*) along isobars at 1 dbar intervals from 45 dbar to 71 dbar, coloured by pressure. Black vertical lines indicate the difference between minimum and maximum values at each time step. Discrete Fourier transform of the anomaly of the difference between the maximum and minimum values in the BML (*bottom*). This can identify dominating frequencies in the mixing events. Peaks indicate periodic mixing events at that frequency. There is no evident periodicity in the signal.

from background noise. In particular, the distance from the seafloor likely hinders the glider from observing fluctuations in the near bottom fluff layer. Nevertheless, there is a clear gradient present with elevated concentrations nearer the seabed showing that bottom stress does resuspend some organic matter. Lack of ground-truthing prevents estimation of organic matter percentage from optical backscatter and impact on BML DO from this suspended matter. No short-term wind events were strong enough to erode the stratification and resuspend sediment during the period of observation as such mixing would also be evident in density and temperature observations (Fig. 5.11).

Work by Couceiro et al. (2013) investigated the percentage of each month when both benthic fluff layers and actual sediment were resuspended at the OG site using ship surveys and moorings. Resuspension of fluff was recorded during less than 1% of August (compared to 100% for January) and actual bed sediment resuspension was not observed in August (compared to 100% in January). These data cannot be used for the glider site where sediment are coarser, tidal velocities are higher and the site is four times deeper (Ducrottoy et al., 2000; Otto et al., 1990). However, they highlight that wind mixing is a significant driver of resuspension and that it is governed by a strong seasonal cycle. As the glider site is deeper and sediment coarser, we can assume wind mixing will have a reduced effect on bed resuspension in that region, with the possible exception of extreme wind events as described in Greenwood et al. (2010). Lenhart et al. (2004, 1995) recorded evidence of extreme wind events causing mixing in the previous version of the ERSEM model but no such wind events were observed during the Seaglider deployment.

This leaves tidally induced turbulence as the dominant driver of organic matter resuspension. The GOTM-BFM model provides some insight into the processes leading to resuspension of benthic organic matter. Fig. 5.14 *bottom left* shows a clear tidal signal in chlorophyll *a* concentration. Pulses of elevated chlorophyll *a* concentrations are seen along the deepest isobaths with decreasing concentrations in shallower waters; interestingly the model shows more tidal resuspen-

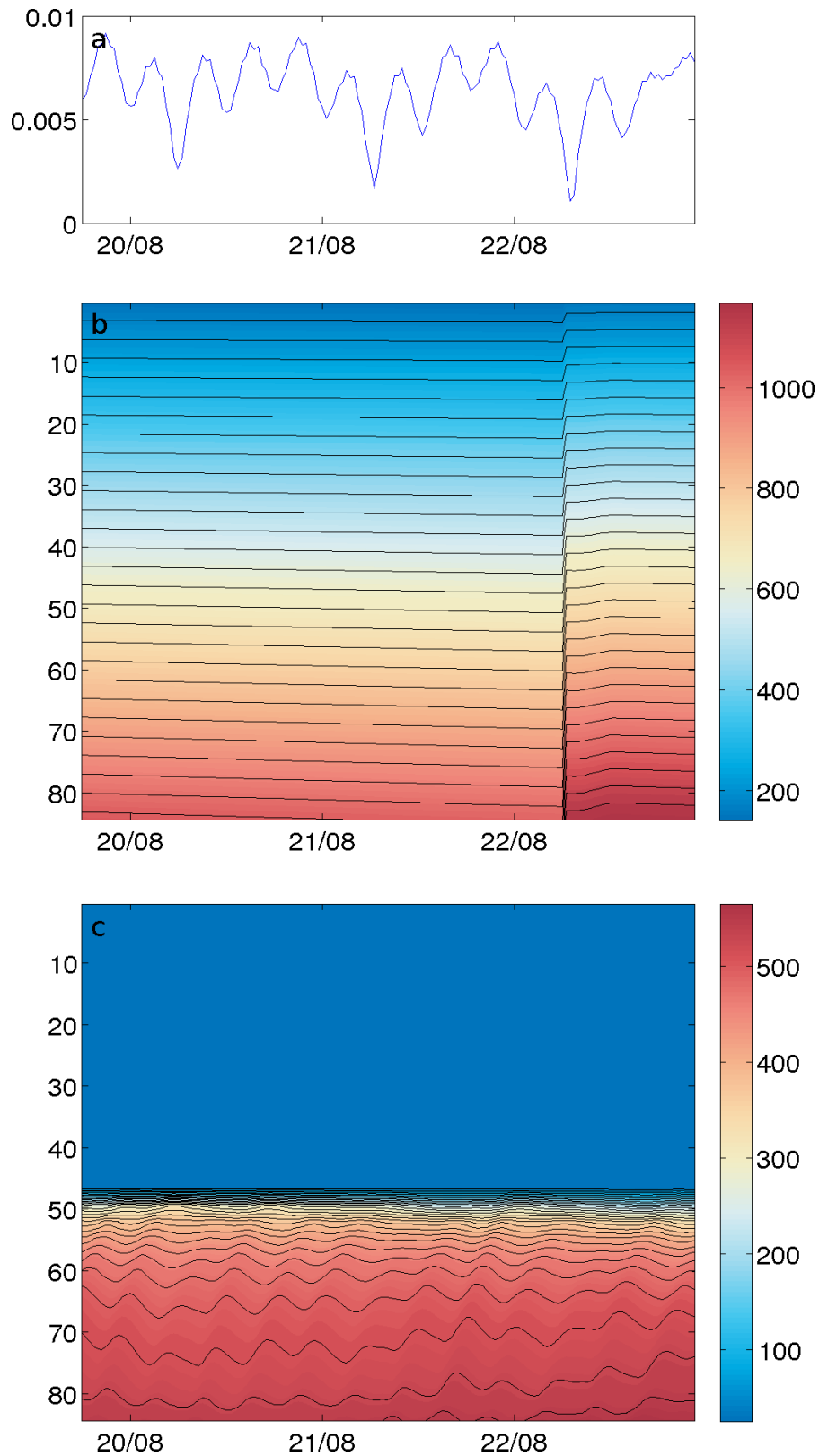


Figure 5.17: GOTM-BFM output relevant to resuspension of organic matter from the benthic layer. Bottom friction velocity ( $\text{m s}^{-1}$ , a), suspended sediment ( $\text{mg m}^{-3}$ , b) and particulate organic carbon ( $\text{mg C m}^{-3}$ , c) during model runs simulating the glider deployment period.

sion of chlorophyll *a* than it does downward mixing of chlorophyll *a* originating from the DCM. The same is demonstrated in Fig. 5.17 where we observe a tidal signal in pelagic particulate organic carbon which follows the bottom shear stress signal. Interestingly, the suspended sediment portion of the model does not seem to be representative of conditions at the ND site; this has already been identified as one limitation of the model (Lenhart et al., 2010; van der Molen et al., 2012). The model does not resolve the larger scale downward mixing events of chlorophyll *a* but does demonstrate sufficient tidal energy at the seafloor to cause resuspension of organic matter. Due to the lack of groundtruthing for glider observations and issues with the model it is not possible to estimate the oxygen drawdown resulting from resuspension of organic matter. However it does highlight the greater importance of tidally-induced bottom turbulence in resuspending sediment compared to wind mixing in the central and northern North Sea.

### 5.3.3 *Conclusion*

Limitations in the survey reduced the amount of information that could be obtained. The lack of usable calibrations combined with the premature end of the glider survey prevent actual quantification of the oxygen draw-down originating from the various sources of organic matter. Despite this, several conclusions can be drawn from the observations particularly when taken in conjunction with results from the GOTM-BFM model. This study aimed to observe the balance of DO supply and remineralisation. Observations showed a much greater heterogeneity and influence of advective processes in the central North Sea than previously thought. Significant shifts in water properties were observed occurring on the scale of a few kilometres. Alongside, fluctuations in BML chlorophyll *a* concentrations and suspended load were observed occurring on a variety of time scales. Tidal flow and wind velocities regulated cross pycnocline mixing, resuspension from the sea floor and production at the DCM. The latter was also affected by the diurnal cycle of irradiance.

Greenwood et al. (2010) recorded oxygen depletion rates in 2007 of  $0.43 \mu\text{mol dm}^{-3} \text{ day}^{-1}$  at ND and  $0.75 \mu\text{mol dm}^{-3} \text{ day}^{-1}$  at the OG. We observed export of organic matter from the DCM with the potential of consuming  $0.884 \mu\text{mol dm}^{-3} \text{ day}^{-1}$ , and the study by Neubacher (2009) found rates of  $1.58 \mu\text{mol dm}^{-3} \text{ day}^{-1}$  for sediment-water oxygen flux in incubation experiments. This highlights two particular aspects of the mechanisms governing seasonal oxygen depletion in the North Sea. The first is that consumption along the sea-floor plays a predominant role in the consumption of BML oxygen. This supports the idea that depocentres, such as the OG, are particularly prone to seasonal oxygen depletion. Advected organic matter will add to the consumption budget, increasing the ratio of consumption to supply whilst the reduced water flow which promotes this deposition also promotes stronger stratification. The second is that supply and consumption of organic matter are tightly coupled. Net oxygen depletion is significantly smaller than gross oxygen consumption. Net oxygen consumption is the total observed change in dissolved oxygen while gross oxygen consumption is the total oxygen used when remineralising organic matter. This indicates oxygen supply rates are also elevated despite the strong stratification. Physical processes (vertical mixing and advection) likely play a strong role, but we also observed a sub-DCM elevated oxygen signature, indicating the presence of a photosynthesising phytoplankton community in the BML. It is possible that in the summer, when DCM chlorophyll *a* concentrations are low, sufficient light penetrates to the BML to encourage production. This feature has yet to be investigated. A longer glider deployment would provide more confidence in these estimates to the temporal variability of biological processes and would also allow investigation of this BML production.

This study has shown the potential of new AUVs in regions such as the North Sea. This deployment lasted approximately 5% of its potential duration. Over a period of only three days, it was able to identify small scale mixing mechanisms which would not be identifiable with traditional oceanographic methods. A Seaglider deployed performing repeat transects in and out of known depocentres could provide

critical high resolution observations of subsurface primary production and organic matter transport in regions of both low and high biomass accumulation. A longer survey would also increase the likelihood of observing larger mixing events (i.e. storm events) and the impact these have on resuspension of organic matter and subsequent oxygen drawdown. The physical and biological high resolution observations obtained by a Seaglider are critical to improving models such as GOTM-BFM. There remain limitations to such models, many processes are simplified and do not resolve finer processes due to lack of understanding and observations, particularly feedback and subsurface processes. van der Molen et al. (2012) highlight that GETM-BFM's modelling of advective processes and particulate organic carbon (burial, degradation, resuspension) requires further knowledge to adequately represent these processes. These are gaps that season-long glider deployments could fill. These models could then, in turn, fill the gaps left by the Seaglider to provide a comprehensive view of the processes occurring in these highly dynamic and heterogeneous environments. As it is now well established that the central North Sea undergoes seasonal oxygen depletion, it is critical to increase the presence of persistent observation systems to improve GETM-BFM in order to provide useful policy advice about future development in the North Sea.

## Part IV

### THE WESTERN ROSS SEA POLYNYA

---

Chapter 6 contained herein was funded through an Antarctic Science bursary. Antarctic Science Ltd is a charitable company, registered in the UK (Charity Number 1090581), whose role is to promote Antarctic science nationally and internationally. The GOVARS project was funded by the US National Science Foundation's Office of Polar Programs (NSF-ANT-0838980)

---

All work described in Ch. 6 was performed by Bastien Queste with the exception of that stated below:

Seaglider deployment was done collaboratively with Walker Smith, Craig Lee, Mike Dinniman and Vernon Asper. Piloting of the Seagliders was done by Craig Lee and Jason Gobat of the University of Washington. Collection and analysis of all calibration samples was done by scientists and staff of the RVIB Nathaniel B. Palmer.



## HYDROGRAPHY OF THE WESTERN ROSS POLYNYA

---

### 6.1 INTRODUCTION

The Ross Sea is the most productive sea in the Antarctic, partly due to the polynyas present there, and may prove to be a significant CO<sub>2</sub> sink (Arrigo et al., 1998; Smith et al., 2000). The Ross polynya is a latent heat polynya created by the northward displacement of sea ice by strong katabatic winds coming off the Ross ice shelf and intrusions of warmer modified circumpolar deep water (MCDW) onto the shelf. New ice is formed in the open polynya leading to the downwelling of dense brine (Orsi and Wiederwohl, 2009).

The timing of phytoplankton blooms in Ross Sea waters is strongly dictated by physical factors (ice retreat, solar irradiance and wind mixing). Arrigo et al. (1998) and Arrigo and van Dijken (2004) reported that the opening of the polynya is dependent on the ice cover compactness and thickness, which is regulated by winter air temperatures, rather than by katabatic winds. Once the polynya is open, the katabatic winds regulate the onset of the bloom by controlling water column stratification. Strong winds occurring early in the season delay the bloom by advecting phytoplankton standing stocks and reducing water column stability (Arrigo and van Dijken, 2004; Arrigo et al., 1998).

The general consensus is that as the polynya expands, an initial short *Phaeocystis antarctica* bloom occurs, followed immediately by diatom growth (Arrigo et al., 1999; Smith et al., 2000). However, more recent observations have found high variability in this phenology (Arrigo and van Dijken, 2004; Peloquin and Smith, 2007; Smith et al., 2006). As the *Phaeocystis* and diatom blooms have little spatial or temporal overlap, it has been suggested that their occurrence is depend-

ent upon environmental conditions rather than successional dynamics (Arrigo et al., 2000).

Surveys by Smith et al. (2011a,b) looking at chlorophyll dynamics found that a combination of physical (advection, wind mixing) and biochemical (nutrient limitation, zooplankton and aggregate sinking) factors regulate fluctuations on short time scales and small spatial scales. This results in strong biological patchiness in the Ross Sea (Hales and Takahashi, 2004; Smith et al., 2006).

It is unclear what mechanisms limit and terminate the initial phytoplankton bloom. During spring, it is likely that light is the main factor limiting phytoplankton growth during the primary bloom (Smith et al., 2000, 2011b). The termination of the primary bloom and the limiting factor of subsequent blooms is likely another mechanism. Sedwick and DiTullio (1997) hypothesise that iron limitation inhibits *P. antarctica* growth, thereby promoting diatom growth which require relatively less iron. Smith et al. (2011b) suggest that mixing events may contribute to the termination of the initial bloom, at least in certain locations, by reducing standing stock vertical stability in the euphotic zone. It is likely that the combination of both mechanisms triggers the end of the primary bloom while the change in iron availability alters phytoplankton community composition for the rest of the season.

Intrusions of MCDW onto the shelf have been linked to the supply of iron to the SML through episodic vertical mixing (Dinniman et al., 2011; Sedwick et al., 2011) possibly enhancing *P. antarctica* growth. Another source of iron may be linked to ice melt, however the majority of sea ice is advected away rather than melting in place and therefore likely only plays a limited role (Arrigo and van Dijken, 2004).

Several estimates of primary productivity in the Ross Sea have been made, identifying it as the most productive region of the Southern Ocean; rates exceeding  $2 \text{ g C m}^{-2} \text{ d}^{-1}$  or  $200 \text{ g C m}^{-2} \text{ yr}^{-1}$  (with a growing season of approximately 120 days) are commonly cited (Arrigo et al., 2000, 1999; Arrigo and van Dijken, 2004; Smith and Gordon, 1997; Smith et al., 2006).

Strong interannual variability of both standing stocks and productivity has been recorded in the Ross Sea. It has been shown by satellite

observations (Arrigo and van Dijken, 2004; Peloquin and Smith, 2007), ship-board surveys (Peloquin and Smith, 2007; Smith et al., 2011a,b, 2006) and modelling studies (Reddy and Arrigo, 2006; Smith and Comiso, 2008) that interannual variations in ice-melt and opening of the polynya along with wind mixing impact standing stocks, productivity and community composition. A general trend of increasing water column stability, consistent with predictions of climate models of the Southern Ocean (Boyd et al., 2008), would encourage stronger phytoplankton blooms in the long-term future.

Productivity and standing stocks of phytoplankton have been estimated via satellite observations but satellites prove unable to accurately estimate chlorophyll *a* concentrations. This is mainly due to the high ice and cloud cover, and the smaller scale of physical forcing as a function of the smaller Rossby radius at these latitudes. Ship surveys have aimed to understand the temporal and spatial variations of productivity and biomass but found doing so difficult as the polynya cannot be monitored continuously by ship due to the persistent ice presence and prohibitive costs. As variability in production and standing stocks is very closely tied to physical and chemical drivers, it is critical that we resolve the physical, chemical and biological features at these smaller scales if we are to understand the controls on productivity in this highly productive region and how these might change in the future.

This study aims to investigate the potential of AUVs for monitoring early season bloom dynamics in the polynya where conventional platforms (i. e. ships and moorings) struggle to provide data due to ice presence. In particular, observations presented here were focused on determining the spatial and temporal variability of phytoplankton blooms and the physical drivers which lead to the documented heterogeneity. By deploying Seagliders (Eriksen et al., 2001), we aimed to observe intrusions of MCDW and the distribution of chlorophyll *a* across the banks and along the troughs of the western Ross Sea. In particular, it was anticipated that the very high resolution temporal and spatial data provided by gliders would resolve features

that could not be observed any other way and had never been documented this early during the bloom season.

## 6.2 METHODS

### 6.2.1 *Sampling*

From November 2010 to February 2011, two Seagliders (see Ch. 2; Eriksen et al., 2001) were deployed in the Ross Sea polynya by the Virginia Institute of Marine Science (VIMS), the UEA and the UW.

Seaglider 502 (SG502) was initially launched into McMurdo polynya on the 22<sup>nd</sup> of November 2010 and crossed over into the Ross polynya on the 14<sup>th</sup> of December 2010 (Fig. 6.1). It performed a repeat zonal transect between 172 and 180° E at 76°30' S with a total of 702 dives. SG502 first surveyed McMurdo Sound before crossing beneath an ice bridge in the lee of Ross Island. SG502 then crossed the Central Basin and the Ross Bank before turning around at the eastern edge of Ross Bank and returning to the Central Basin (Fig. 6.1).

Seaglider 503 (SG503) was launched on the 29<sup>th</sup> of November 2010 directly into the Ross polynya, but suffered an instrument failure on the Wetlabs puck after 3 days. This prevented collection of chlorophyll *a* fluorescence or optical backscatter data, but did not affect collection of temperature, salinity and DO data. It surveyed a meridional bowtie track twice between 76° S and 77° S, crossing SG502's track, with a total of 923 dives. SG502 and SG503 were recovered on the 20<sup>th</sup> and 30<sup>th</sup> of January respectively. SG503 first repeated the crossing of the Ross Bank before turning back and starting the bowtie survey pattern. The southern half of the bowtie pattern was above the 400 m isobath of the western end of Ross Bank. The northern half of the bowtie pattern surveyed the trough between the Pennell and Ross Banks (Fig. 6.1).

The survey was designed to capture spatial variability across the polynya with SG502. Simultaneously, the bowtie pattern surveyed by SG503 aimed to increase repeat passages over the same area to constrain temporal variability. It also aimed to obtain observations along

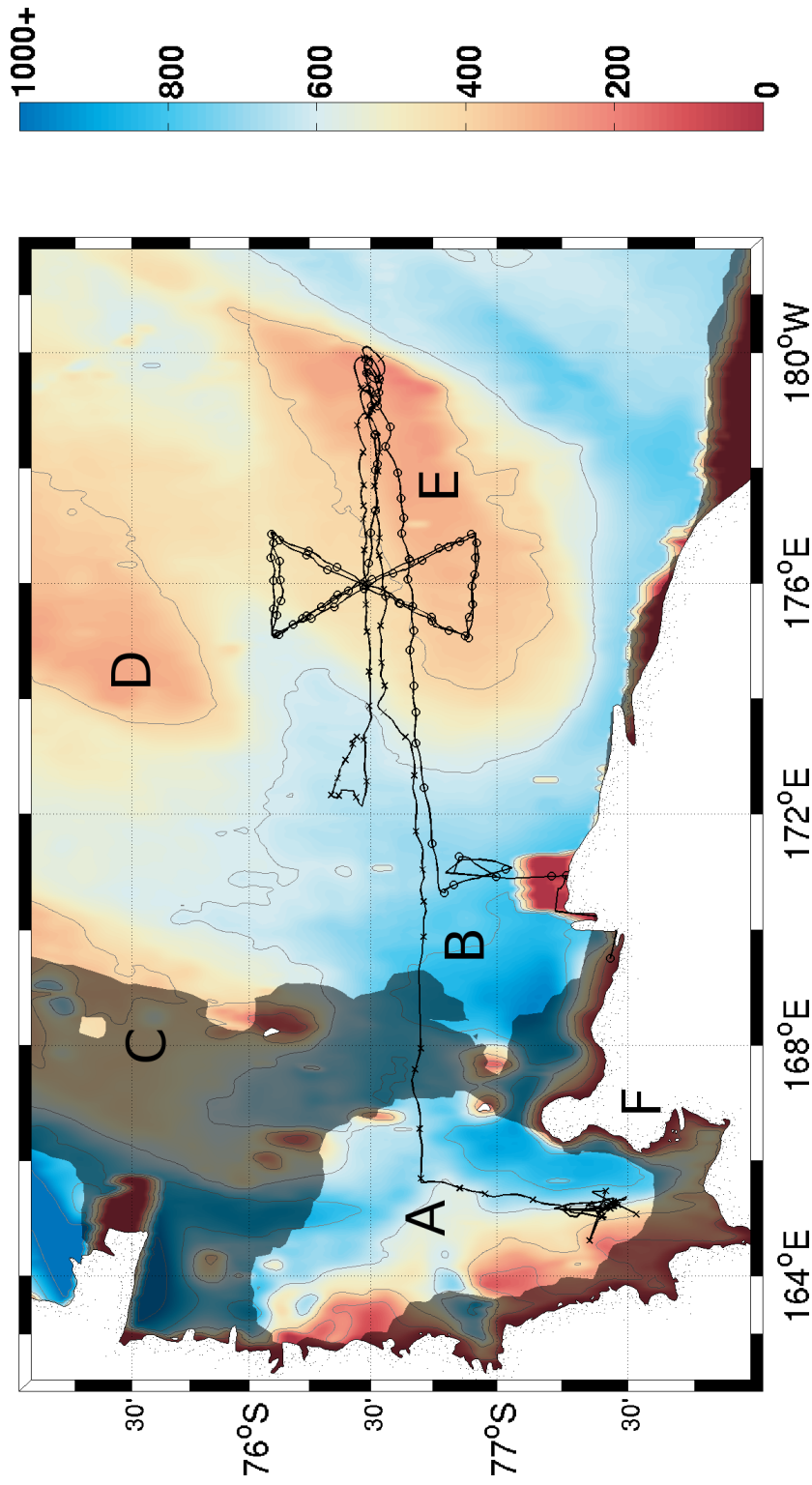


Figure 6.1: Seaglider survey locations. Crosses show every tenth dive by SG502, circles show every tenth dive by SG503. Dark shading corresponds to the 50% ice cover contour on the day SG502 crossed beneath the ice bridge (December 14th 2010) and entered Ross polynya. Contours correspond to bathymetry in metres (GEBCO, 2010). Contours are located at 200 m intervals down to 1000 m. A. McMurdo Sound, B. Central Basin, C. Crary Bank, D. Pennell Bank, E. Ross Bank, F. Ross Island.

the edge of Ross Bank and in the channel between the Ross and Pen-  
nell banks to investigate intrusions of MCDW onto the shelf.

## 6.2.2 Data Processing

### 6.2.2.1 Calibration

Both gliders were calibrated against a single CTD cast each from the R/V Palmer during recovery (Figs. 6.2 & 6.3). Launch procedures did not permit an additional cast and no moorings were available for cross calibration during the survey. Temperature, salinity, DO, and chlorophyll a data from gliders were calibrated against the data acquired by the ship's CTD. To verify the validity of the glider data calibration, temperature, salinity, DO and chlorophyll a data from the two closest profiles in both space and time from SG502 and SG503 were compared.

We now discuss the calibration of each data set in turn. Comparison between the glider and ship data is presented in Figs. 6.2 and 6.3.

**TEMPERATURE** Temperature data for both Seagliders were very similar to the ship's temperature data. A  $\tau$  correction was applied as described in Chapter 2. The UW/iRobot default value of 0.6 s was used for the temperature lag correction for both SG502 and SG503. Offsets of  $8.3 \times 10^{-3} \text{ }^\circ\text{C}$  and  $3.1 \times 10^{-3} \text{ }^\circ\text{C}$  were applied to SG502 and SG503's temperature data respectively. These offsets were determined by taking the mean difference between the calibration and corresponding glider profiles; after calibration, mean difference between the calibration and the glider profiles was zero. Root Mean Square (RMS) difference to the calibration profile was  $7.5 \times 10^{-2} \text{ }^\circ\text{C}$  for SG502. RMS difference to the calibration profile was  $7.8 \times 10^{-2} \text{ }^\circ\text{C}$  for SG503. RMS differences remain relatively high due to different isotherm depths.

**SALINITY** As the thermal mass of the CT sail affects the water flowing through to the conductivity cell, salinity was calculated using observed conductivity and estimated temperature within the cell following Morison et al. (1994) and Garau et al. (2011), as described in Chapter 2. Neither glider salinity nor conductivity matched the calibration profiles. Offsets of  $1.5 \times 10^{-1} \text{ mS cm}^{-1}$  and  $-1.8 \times 10^{-1} \text{ mS cm}^{-1}$

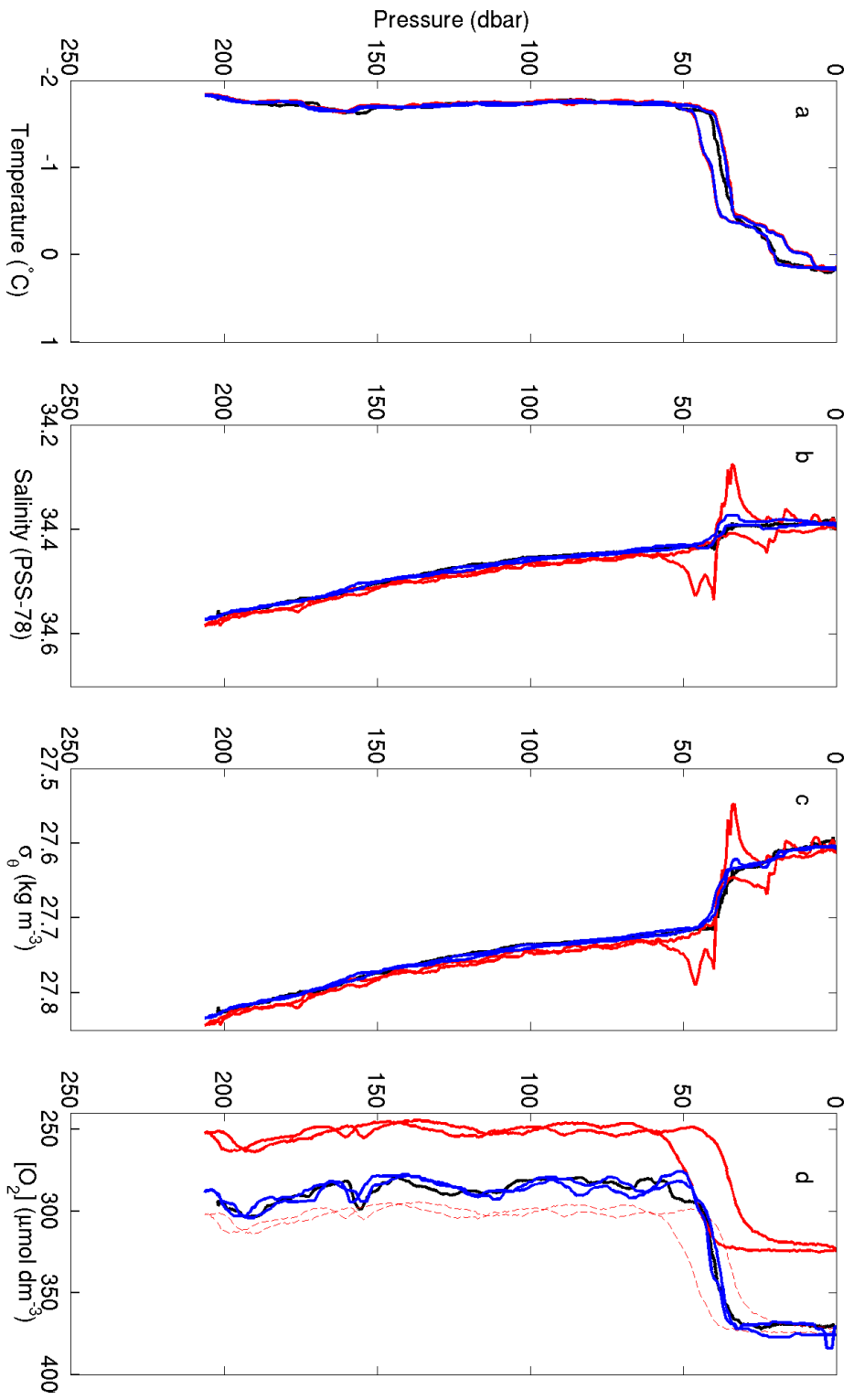


Figure 6.2: Calibration of temperature, salinity, potential density and DO profiles (*a to d*) for SG502. Ship calibration casts are in black. Glider observations as output by the iRobot processing are in red. Glider observations after calibration by the UEA toolbox are in blue. The dotted red line is iRobot processed DO offset by  $50 \mu\text{mol dm}^{-3}$  for ease of comparison with calibrated data to highlight reduced signal amplitude.

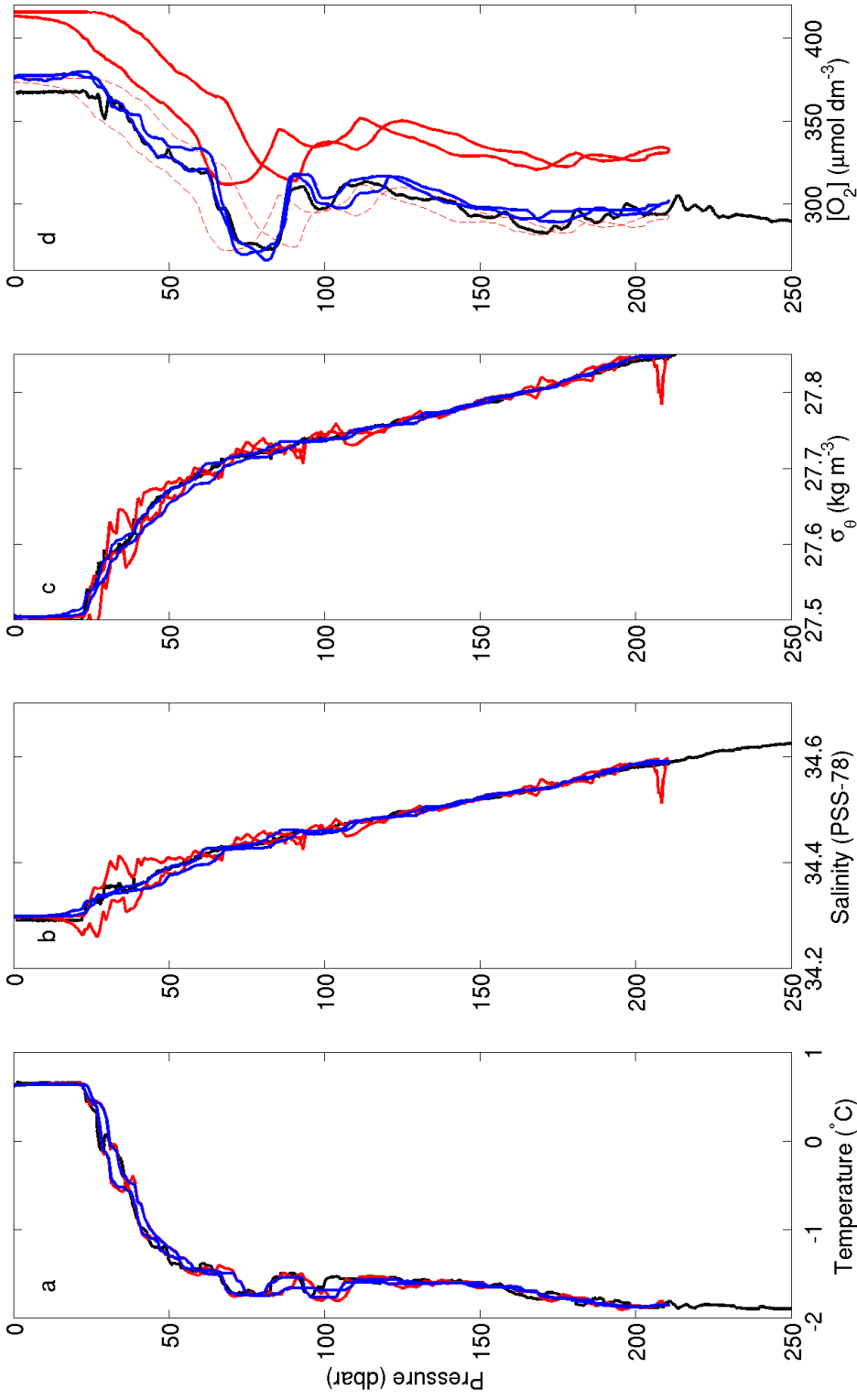


Figure 6.3: Calibration of temperature, salinity, potential density and DO profiles (*a to d*) for SG503. Ship calibration casts are in black. Glider observations as output by the iRobot processing are in red. Glider observations after calibration by the UEA toolbox are in blue. The dotted red line is iRobot processed DO offset by  $-40 \mu\text{mol dm}^{-3}$  for ease of comparison with calibrated data to highlight reduced signal amplitude.

were applied to conductivity measurements for SG502 and SG503 respectively. Again, these were calculated by taking the mean difference between calibration and glider profile data. Corrected salinity for SG502 had a RMS difference of  $5.3 \times 10^{-3}$  PSU with the ship's calibration profile. Corrected salinity for SG503 had a RMS difference of  $6.7 \times 10^{-3}$  PSU with the ship's calibration profile.

**DISSOLVED OXYGEN** The ship's DO profile was back-calculated to a pseudo calibrated phase (pseudo-CalPhase; see Ch. 2) using the Seaglider's foil coefficients as described in Chapter 2. A linear regression was then performed on the Seaglider's observed TCPhase against the pseudo-CalPhase to obtain the best fit phase coefficients (Figs. 6.4 & 6.5). The new phase coefficients were used for calculating the Seaglider DO concentrations using the Benson and Krause Jr. (1984) combined fit solubility constants.

The alternative approach of using directly measured oxygen concentrations was not used because Winkler titrations were performed on-board the R/V Palmer during recovery but the results were not usable for calibration. Differences between replicates were very large and therefore all numbers were discarded. The R/V Palmer's CTD sensor package was equipped with a Seabird SBE43 sensor. These sensors are less prone to drift or damage from UV than the Seagliders' optodes and therefore are more stable between deployments. After enquiry with ship's technical staff, it was determined that the calibration of the ship-board sensor was recent and so data from the ship's DO probe were the best available data for calibration. Due to the lack of validation from titrations, we cannot fully trust the absolute accuracy of the DO measurements, however the relative accuracy throughout the mission should be sufficient for the purposes of this work.

$\tau$  for both SG502 and SG503 were determined heuristically as described in Ch. 2. The "best fit"  $\tau$  value determined for SG502's optode with fast response foil was 38 s. The "best fit"  $\tau$  value determined for SG502's optode with fast response foil was 55 s. The estimated  $\tau$  value using coefficients suggested by Hahn (2013) was of the order

of 22 s. It is likely that the coefficients suggested by Hahn (2013) are not applicable at near freezing temperatures thereby explaining the significant difference.

**CHLOROPHYLL  $a$**  As SG503's optical puck failed after 3 days, no validation is possible through comparison of both gliders. Satellite ocean colour data are also insufficient to perform any validation of SG502's data due to the small scale of biological features and extensive sea and cloud cover (Fig. 6.18). SG502's optical data were therefore calibrated as described in Chapter 2 (Fig. 6.8). The dark count value was calculated by determining the lowest measured value by the sensor after removing outliers due to electrical noise; a value of 49 counts was obtained (Fig. 6.6). The glider's fluorometer counts were linearly regressed against the collected chlorophyll  $a$  fluorometry samples from the ship to determine the scale factor ( $7.4517 \times 10^{-3}$ ,  $R^2 = 0.878$ ; Fig. 6.7). Mean difference between the ship's chlorophyll samples and the glider's calibrated chlorophyll  $a$  concentration data was  $0.06 \text{ mg dm}^{-3}$ ; RMS difference was  $0.39 \text{ mg dm}^{-3}$ . Finally, these calibration coefficients were used to calculate chlorophyll values for the entire mission.

**DRIFT** As no calibration data were available from the deployment, it was not possible to accurately determine whether any sensor drift occurred during the Ross Sea mission. We make the assumption that the temperature probe did not suffer from drift as it has not yet been observed in any deployments that the author is aware of. Drift is a significant issue with the DO optode, however this drift mainly occurs under UV exposure or through repeated drying/humidifying cycles (Hahn, 2013). To identify potential drift in the optodes, DO data were binned by temperature, salinity and time ( $0.03^\circ\text{C}$ ,  $0.005 \text{ PSU}$  and 1 day bins). Simply observing oxygen along isopycnals and looking for a long term trend was not a viable option as deep isopycnal depths shoaled into the photic zone when approaching Ross Bank. By identifying watermasses by their Potential Temperature - Salinity ( $\theta - S$ ) properties, it was possible to clearly identify the dense

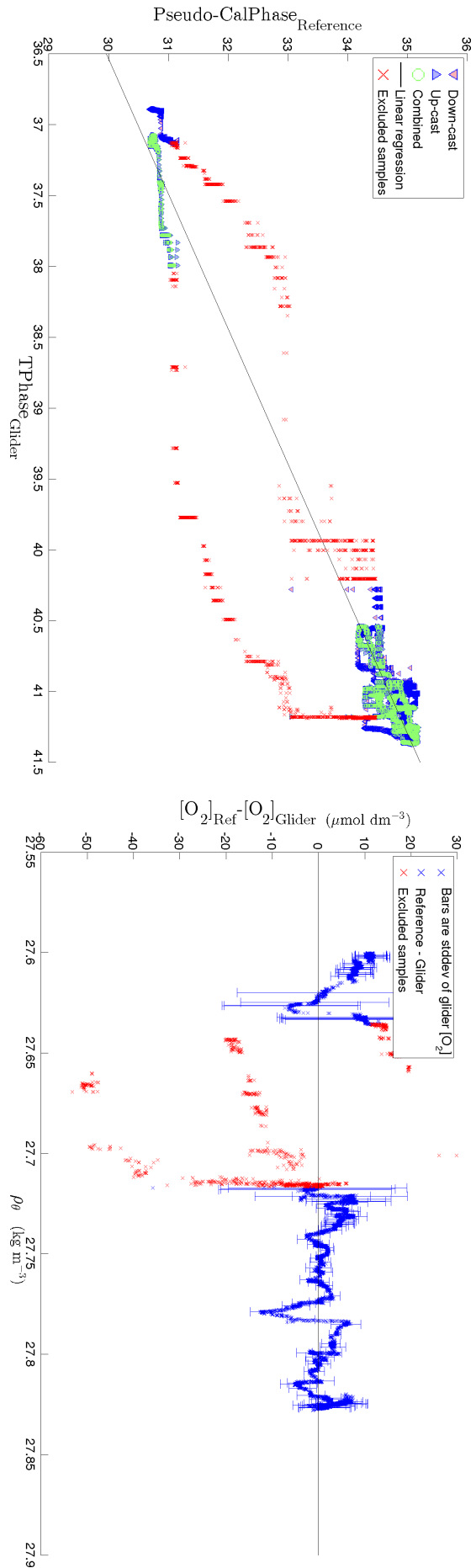


Figure 6.4: *Left:* Linear regression of TCPPHase from SG502's dive 701 and corresponding pseudo-CalPhase from the ship's CTD oxygen backcalculated using SG502's optode's foil coefficients. *Right:* Difference between the ship's calibration DO profile and recalculated glider DO profile with respect to potential density.

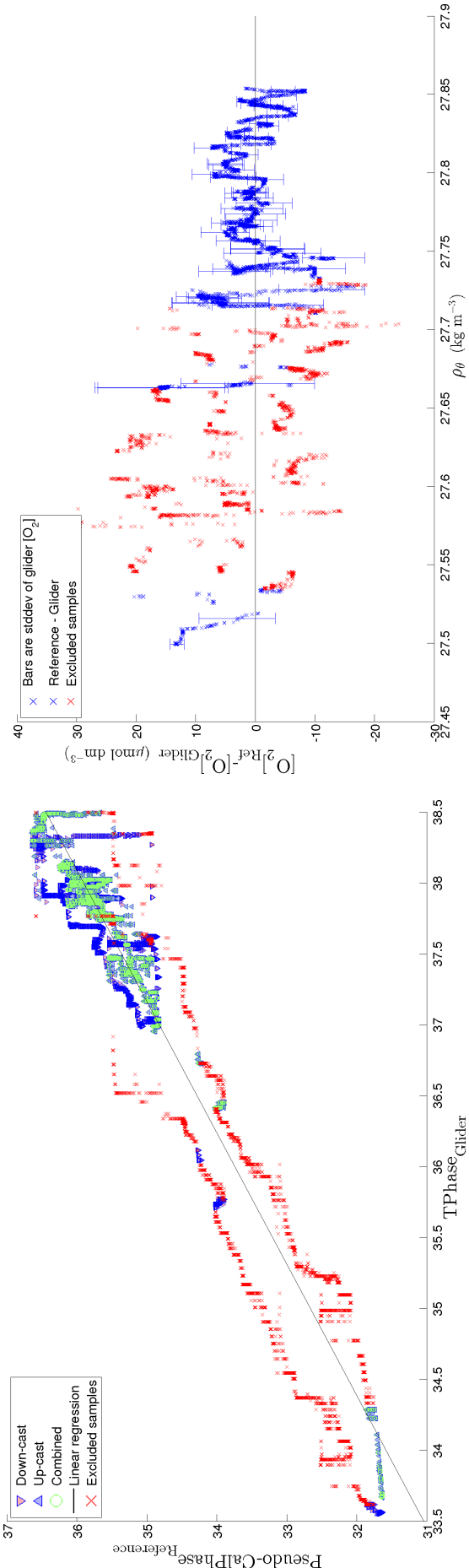


Figure 6.5: *Left*: Linear regression of TCPhase from SG503's dive 919 and corresponding pseudo-CalPhase from the ship's CTD oxygen backcalculated using SG503's optode's foil coefficients. *Right*: Difference between the ship's calibration DO profile and recalculated glider DO profile with respect to potential density.

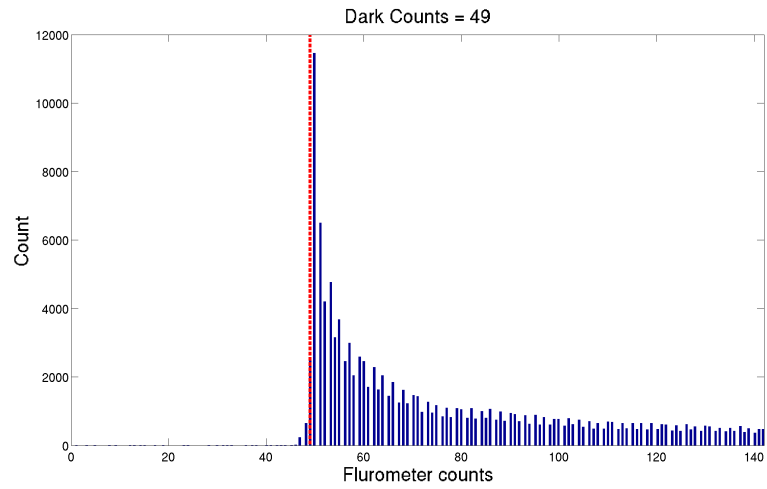


Figure 6.6: Histogram of WetLabs ECO puck fluorometer counts. The vertical red line indicates the determined dark count value for the sensor.

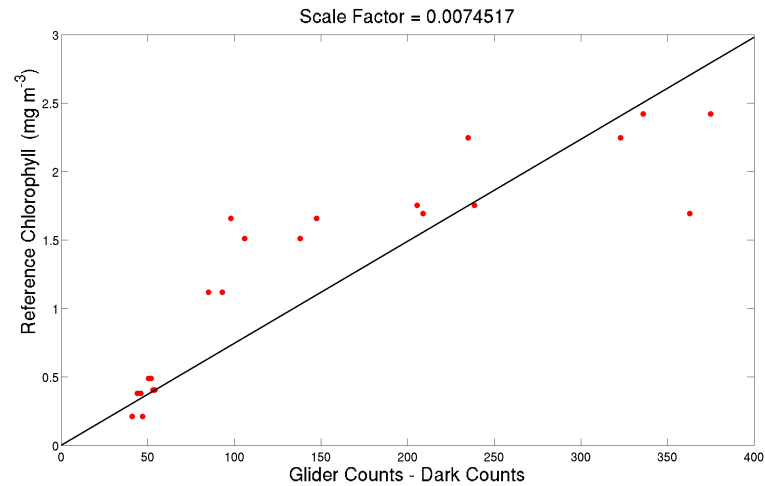


Figure 6.7: Regression of the glider's fluorometer counts after dark count compensation against bottle chlorophyll *a* concentrations from the R/V Palmer vessel during recovery after dive 701. Scale factor =  $7.4517 \times 10^{-3}$ ,  $R^2 = 0.878$ .

stable watermasses. The trend in DO was calculated for each  $\theta - S$  bin (Fig. 6.9). The fresher and warmer watermasses show declining DO for both SG502 and SG503. A watermass showing increasing DO is also visible for SG502. The most saline and coldest water in the region however is the most stable (Orsi and Wiederwohl, 2009). The optode on SG503 showed minimal drift during the mission ( $-0.1 \mu\text{mol dm}^{-3} \text{ day}^{-1}$ ), however SG502 observed a much stronger drift ( $-0.55 \mu\text{mol dm}^{-3} \text{ day}^{-1}$ ). The difference is possibly due to the presence of a protective foil on SG503. A linearly increasing offset equal to the drift identified was applied to the DO data for both SG502 and SG503. This method relies on the assumption that the deepest watermass identified was minimally affected by bacterial respiration.

#### 6.2.2.2 Validation

The distance between both gliders was calculated throughout the mission (Fig. 6.10) to identify when the gliders were in closest proximity. SG502 and SG503 were separated by only 6.8 km on the 25<sup>th</sup> of December with dives beginning 44 min apart. If observations from both gliders were similar, this would reinforce our confidence in the calibration performed with the ship data. The profiles show very different temperature, salinity and DO signals above 250 m depth (Figs. 6.11 to 6.13). Below 250 m, both gliders show a similar signal for DO and temperature. To further investigate the difference above 250 m, temperature, salinity and DO profiles plotted against pressure and against density from near the centre of the bowtie were compared. This area was selected as this region had the most glider passages. Despite minor differences when comparing the two nearest profiles, gliders showed similar ranges and variability across multiple profiles. Very strong variability was present within the top 200 m, highlighting the small scale of features in the upper water column. We therefore conclude that the Seaglider data are sufficiently similar to attribute confidence to the ship based calibration of the Seaglider data.

### 6.2.2.3 *Data gridding*

All figures in subsequent sections use gridded Seaglider observations rather than individual variably spaced data points as described below. Erroneous outlying data points were first flagged and discarded for the analysis as described in Ch. 2. Data were then gridded onto 3 hr by 3 db bins; this insured no bins contained less than 5 data points. Only bins at either end of the dives (surface and bottom values) occasionally contained less than 5 values. The mean value for each bin was used. This bin size was used as it included sufficient observations to accurately flag anomalous values from each bin whilst still being sufficiently small to preserve small scale features.

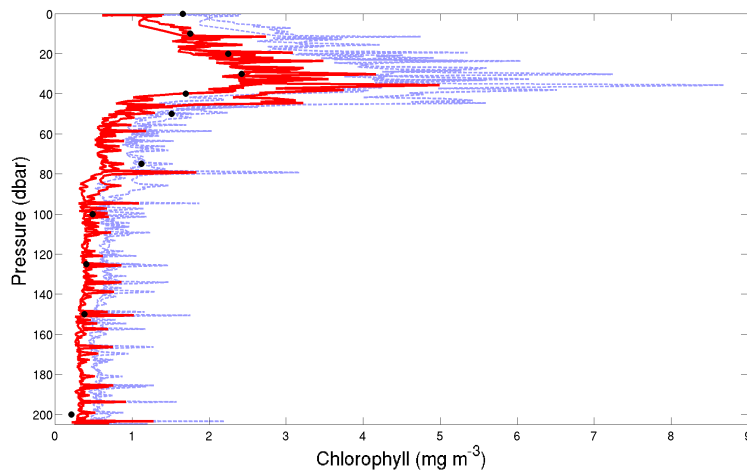


Figure 6.8: Comparison of bottle chlorophyll *a* concentrations from the R/V Palmer vessel during recovery after dive 701 (*black dots*) against the WetLabs ECO puck manufacturer calibration (*dotted line, blue*) and calibrated data (*solid line, red*). Mean difference =  $0.06 \text{ mg dm}^{-3}$ ; RMS difference =  $0.39 \text{ mg dm}^{-3}$ .

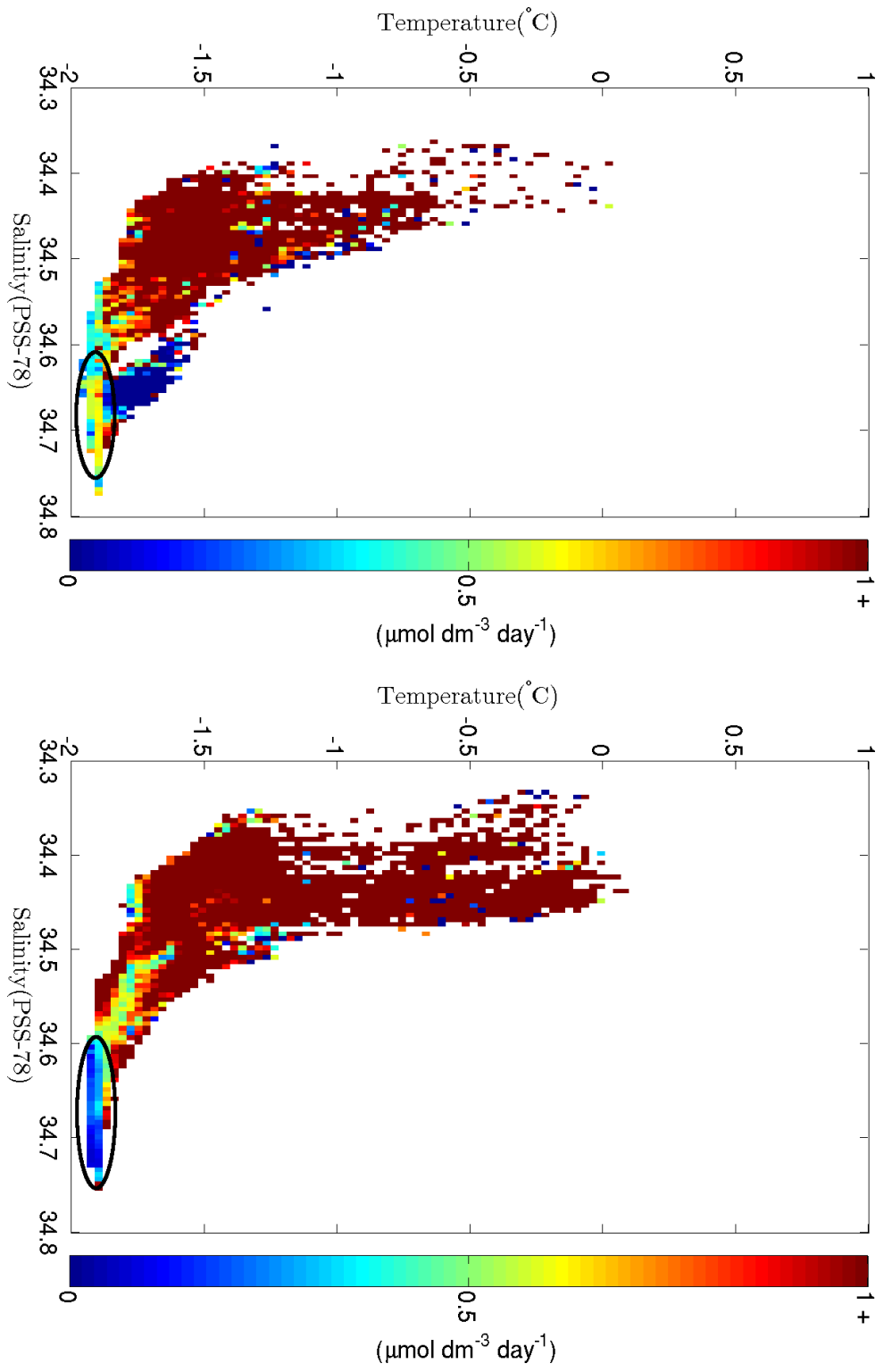


Figure 6.9: Decrease in DO concentrations per day ( $\mu\text{mol dm}^{-3} \text{ day}^{-1}$ ) for each potential temperature - salinity bin for SG502 (*left*) and SG503 (*right*). The most saline and coldest watermass is used as reference and the change in DO is assumed to be a linear drift affecting the optodes. This watermass identified by the black circle.

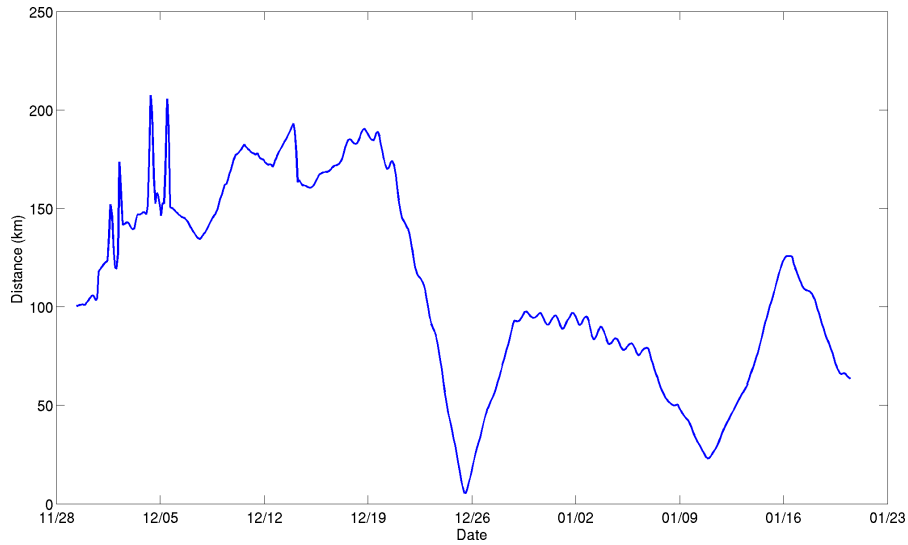


Figure 6.10: Horizontal distance between SG502 and SG503 during the mission. The gliders passed within 6.8 km of each other on the 25-Dec-2010. Those profiles are used to validate the calibration performed based on the R/V Palmer observations.

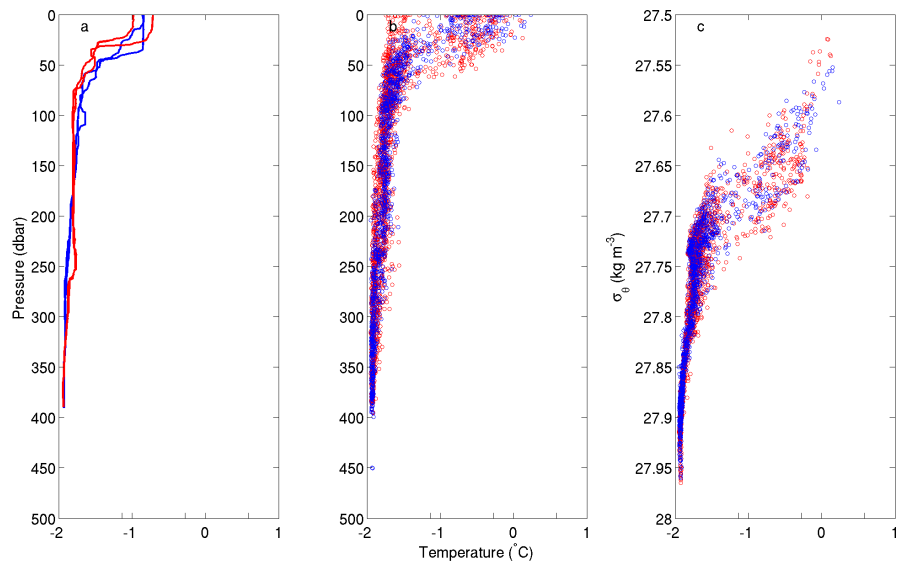


Figure 6.11: *a.* Temperature as observed by SG502 (*blue*) and SG503 (*red*) for their nearest profile in space and time as identified in Fig. 6.10 located 6.8 km apart on the 25-Dec-2010. *b.* All temperature measurements from SG502 (*blue*) and SG503 (*red*) against pressure around the centre of the bowtie pattern. This area was delimited as a box between 174 to 178° E and 76° 15' to 76° 45' S. *c.* Same as centre, but against potential density.

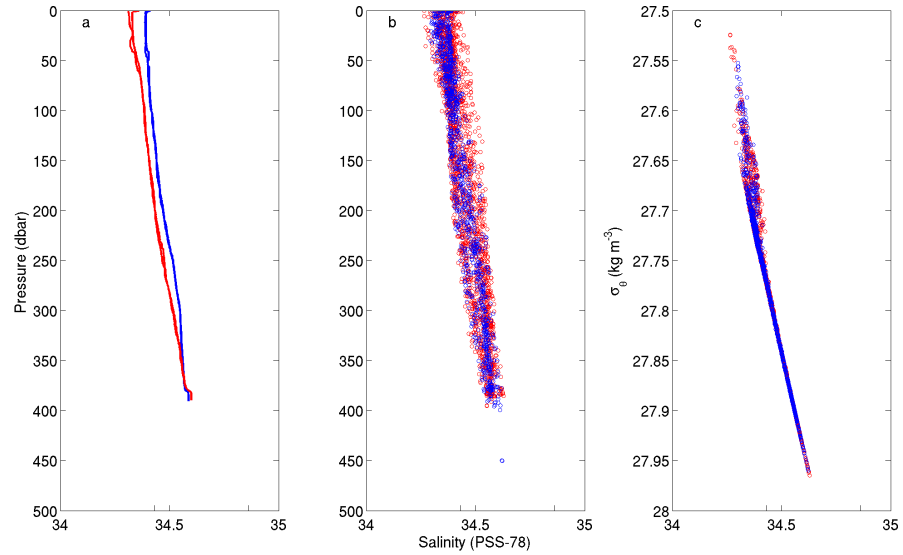


Figure 6.12: *a.* Salinity as observed by SG502 (*blue*) and SG503 (*red*) for their nearest profile in space and time as identified in Fig. 6.10 located 6.8 km apart on the 25-Dec-2010. *b.* All salinity measurements from SG502 (*blue*) and SG503 (*red*) against pressure around the centre of the bowtie pattern. This area was delimited as a box between  $174$  to  $178^\circ$  E and  $76^\circ 15'$  to  $76^\circ 45'$  S. *c.* Same as centre, but against potential density.

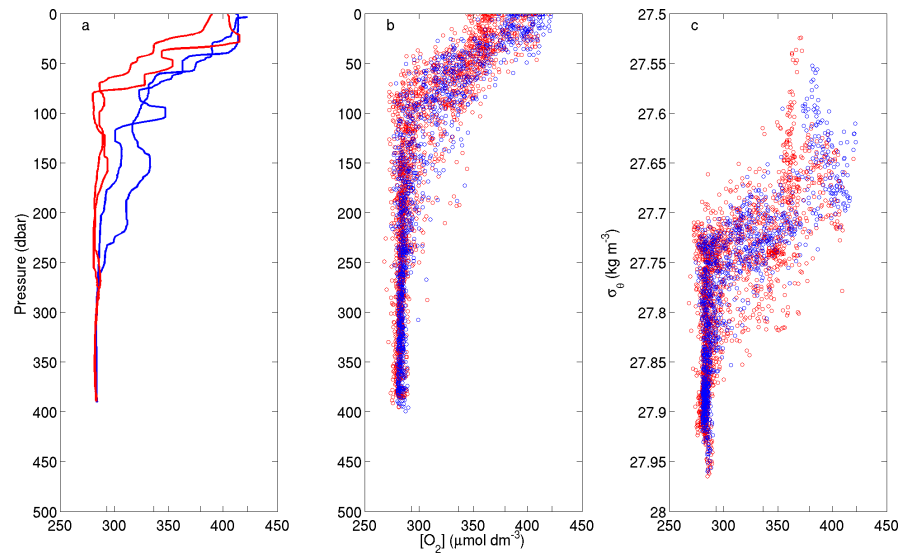


Figure 6.13: *a.* DO as observed by SG502 (*blue*) and SG503 (*red*) for their nearest profile in space and time as identified in Fig. 6.10 located 6.8 km apart on the 25-Dec-2010. *b.* All DO measurements from SG502 (*blue*) and SG503 (*red*) against pressure around the centre of the bowtie pattern. This area was delimited as a box between  $174$  to  $178^\circ$  E and  $76^\circ 15'$  to  $76^\circ 45'$  S. *c.* Same as centre, but against potential density.

### 6.3 RESULTS AND DISCUSSION

#### 6.3.1 *Hydrography of the Ross Sea polynya*

The Seagliders were launched early in the season when ice cover was still extensive in the Ross Sea (Fig. 6.14). The gliders were thus able to observe the gradual opening of the polynya, the onset of stratification and phytoplankton blooms in the Ross polynya. Sea ice covered the large majority of the western Ross Sea until the second week of December 2010 at which point only an ice bridge extending in the lee of Ross Island remained. This ice bridge eventually disappeared by the last week of January. Fig. 6.14 shows percentage sea ice cover at the beginning and end of the mission recorded by Special Sensor Microwave Imager / Sounder, as well as mean sea ice cover during the entire deployment. The position of the ice bridge in the lee of Ross Island is clearly visible.

SG502 observed little vertical structure in density profiles in McMurdo Sound during the last week of November (Fig. 6.15b). Seaglider observations show weak stratification with no clear pycnocline or mixed layers until the second week of December. Both gliders observed the gradual deepening of the  $27.8 \text{ kg m}^{-3}$  isopycnal from the 8<sup>th</sup> of December onwards (dotted line, Fig. 6.15). As the isopycnals generally followed bathymetric contours in regions of 500 m or less, it is likely this difference is due to the position of SG503 in a shallower region. This difference could also be attributed to the greater wind velocities above SG503's position during this period (Fig. 6.15, *a*). Subsequently, wind speeds are estimated to have stayed consistent over both gliders. Another elevated wind speed episode ( $> 10 \text{ m s}^{-1}$ ) occurred mid-January but had no visible impact on water column density structure (Fig. 6.15). In deeper regions of the polynya, a stronger vertical density gradient was present with a uniform SML above the  $27.65 \text{ kg m}^{-3}$  isopycnal. Small scale changes in isopycnal depths were visible at scales of up to 20 km or 1 day. Isopycnal depths observed by SG502 and SG503 were decoupled showing a clear spatial dependence, particularly over Ross Bank.

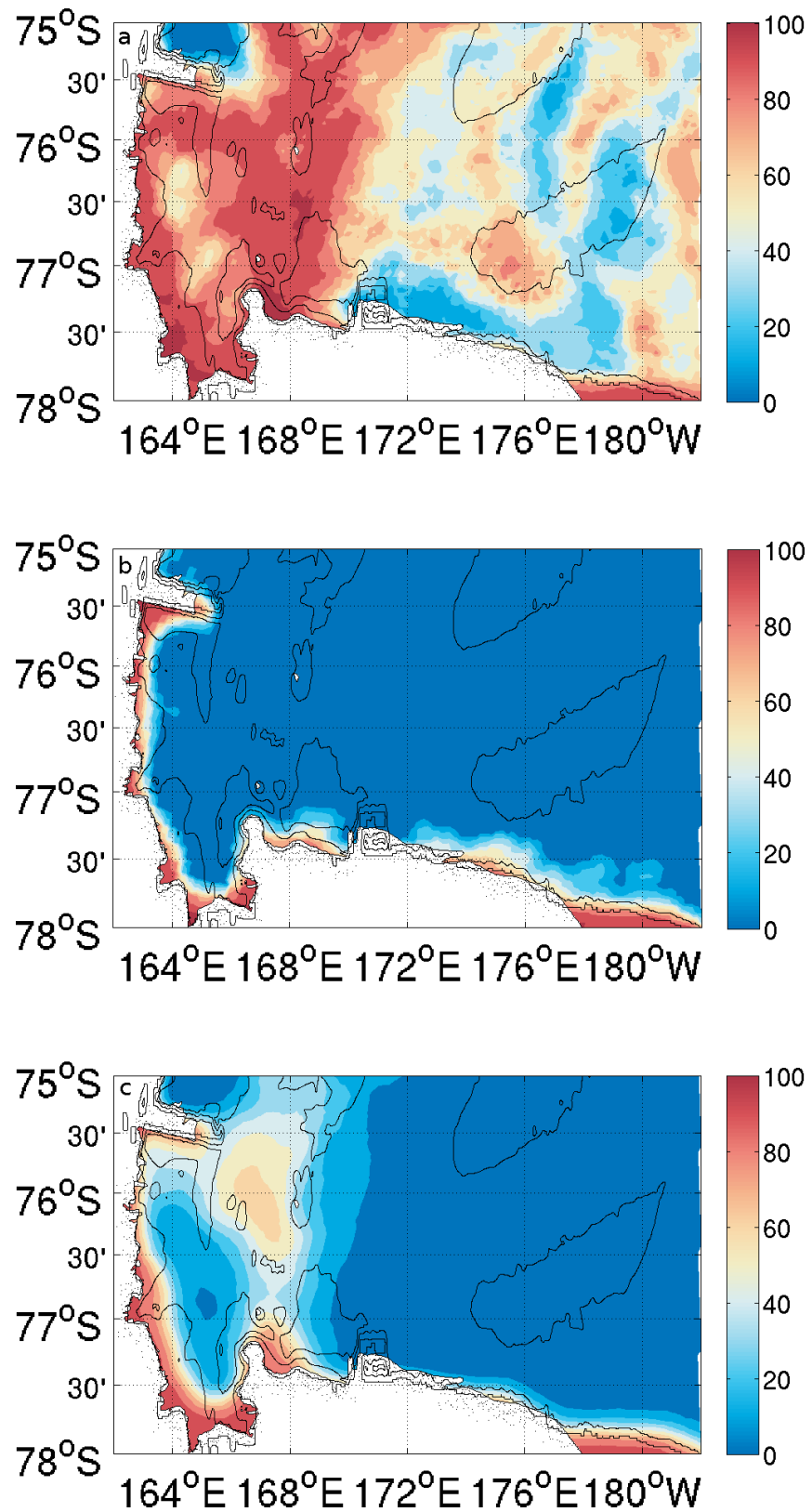


Figure 6.14: Special Sensor Microwave Imager / Sounder percentage sea ice cover data for either end of the mission, the 25<sup>th</sup> of November 2010 (a) and 30<sup>th</sup> of January 2011 (b). Mean sea ice cover during the deployment period (c). 0, 400 and 1000 m contours are in black (GEBCO, 2010).

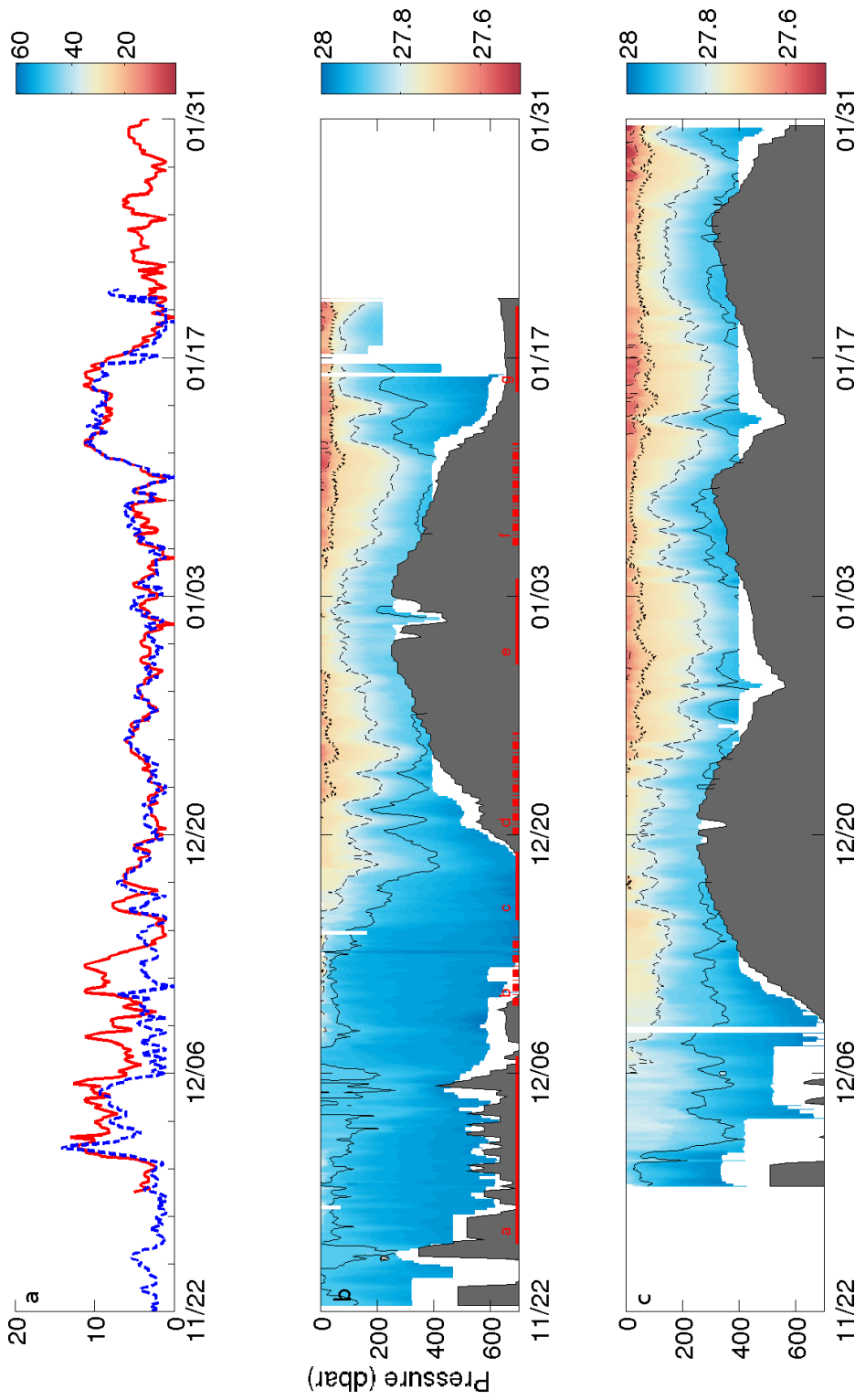


Figure 6.15: 10 m windspeeds from ERA Interim reanalysis data (*a*) over each glider's position ( $\text{m s}^{-1}$ ; SG502: blue, SG503: red) and Seaglider density sections ( $\text{kg m}^{-3}$ ) from SG502 (*b*) and SG503 (*c*). Density contours are shown at  $0.1 \text{ kg m}^{-3}$  intervals from  $27.9 \text{ kg m}^{-3}$  (solid line) to  $27.6 \text{ kg m}^{-3}$  (dash-dot line). GEBCO\_08 bathymetry is indicated by the grey shaded area (GEBCO, 2010). Alternating solid and dashed red bars at the bottom of section *b* delimit the regions labelled a to g and described in Fig. 6.22.

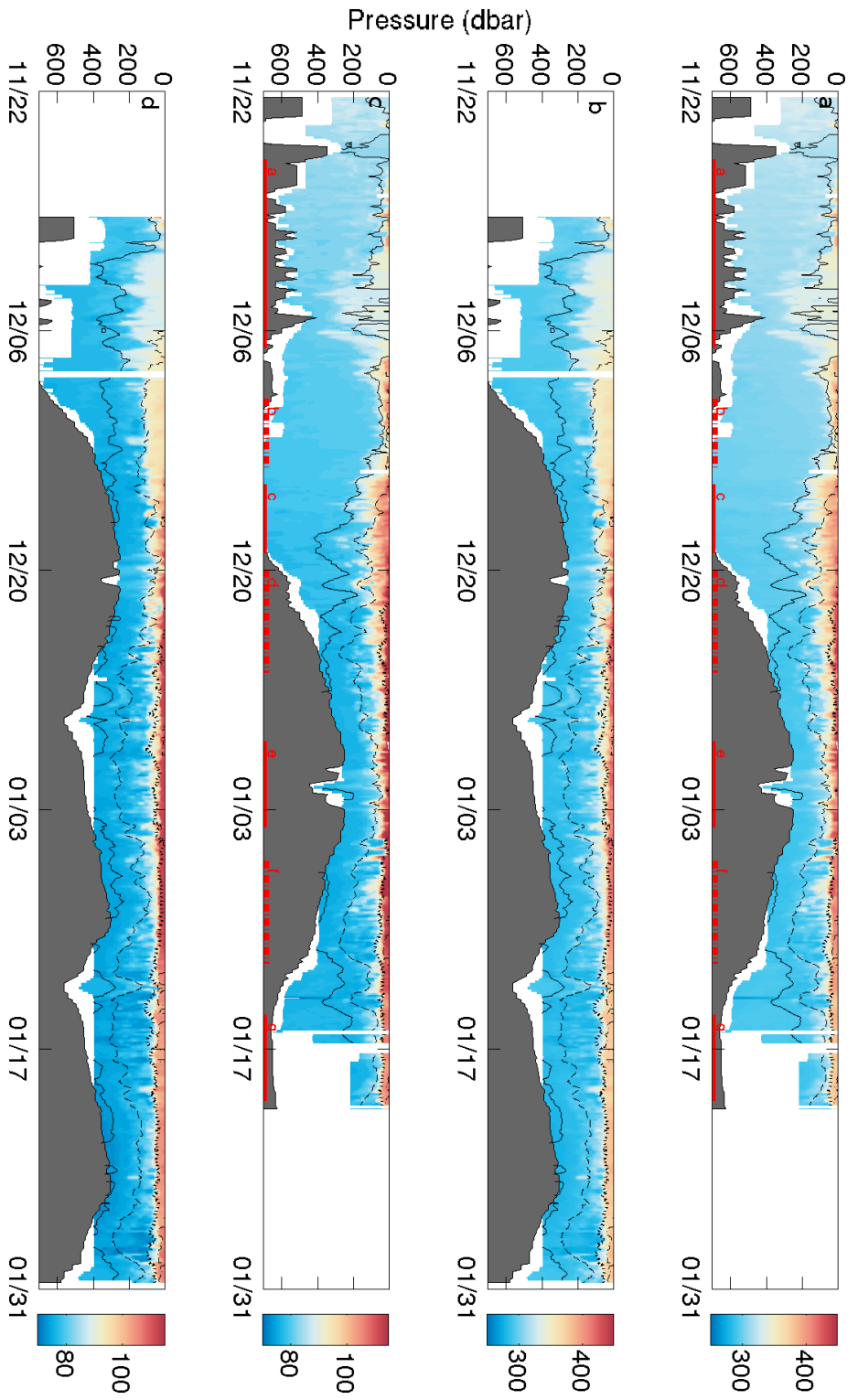


Figure 6.16: DO sections ( $\mu\text{mol dm}^{-3}$ ) from SG502 (a) and SG503 (b) and oxygen saturation (%) sections from SG502 (c) and SG503 (d). Density contours are shown at  $0.1 \text{ kg m}^{-3}$  intervals from  $27.9 \text{ kg m}^{-3}$  (solid line) to  $27.6 \text{ kg m}^{-3}$  (dash-dot line). GEBCO\_08 bathymetry is indicated by the grey shaded area (GEBCO, 2010). Alternating solid and dashed red bars at the bottom of graphs a and c delimit the regions labelled a to g and described in Fig. 6.22.

By late December, a clear SML was visible in the data down to 50 m at both gliders' positions. Below this surface layer, density increased gradually and showed no distinct mixed layers. A difference of  $0.2 \text{ kg m}^{-3}$  was present between the surface and the thermocline. Below, density increased by  $0.3 \text{ kg m}^{-3}$  between the thermocline and the bottom.

Therefore, it seems the onset of the stratification is dependent on wind mixing, ice melt and irradiation with, in this particular deployment, elevated wind speeds delaying the onset of the stratification. However spatial differences are visible in the depth of isopycnals and strength of the stratification between the shallower Ross Bank and deeper Central Basin. This indicates that bathymetry induced mixing processes regulate the depth of isopycnals and the strength of the stratification. The likely consequence of isopycnals following bathymetry is strong advective processes and fronts leading to a strong physical and chemical heterogeneity in the western Ross Sea polynya.

### 6.3.2 *Location and timing of phytoplankton bloom and production*

SG502 observed vertically uniform DO, with concentrations slightly below saturation, in McMurdo Sound (90%, Fig. 6.16). The passage under the ice bridge revealed more structure in the DO profile with concentrations  $15 \mu\text{mol dm}^{-3}$  higher between 0 and 300 m than below. Both Seagliders however observed a very different regime in the Ross Polynya. A supersaturated surface layer was present at both SG502 and SG503's locations above the  $27.8 \text{ kg m}^{-3}$  isopycnal. Supersaturation was visible within the top 70 m for both gliders and did not follow isopycnals along the edges of Ross Bank. Highest supersaturation was observed while the gliders were surveying the bank, east of  $175^\circ\text{E}$  between the 20<sup>th</sup> of December and the 15<sup>th</sup> of January. Fluctuations in surface saturation were synchronous between both gliders (Fig. 6.19a). Finally, surface saturations decreased again during the final two weeks of the mission as the gliders surveyed the trough and great basin (west of  $175^\circ\text{E}$ ).

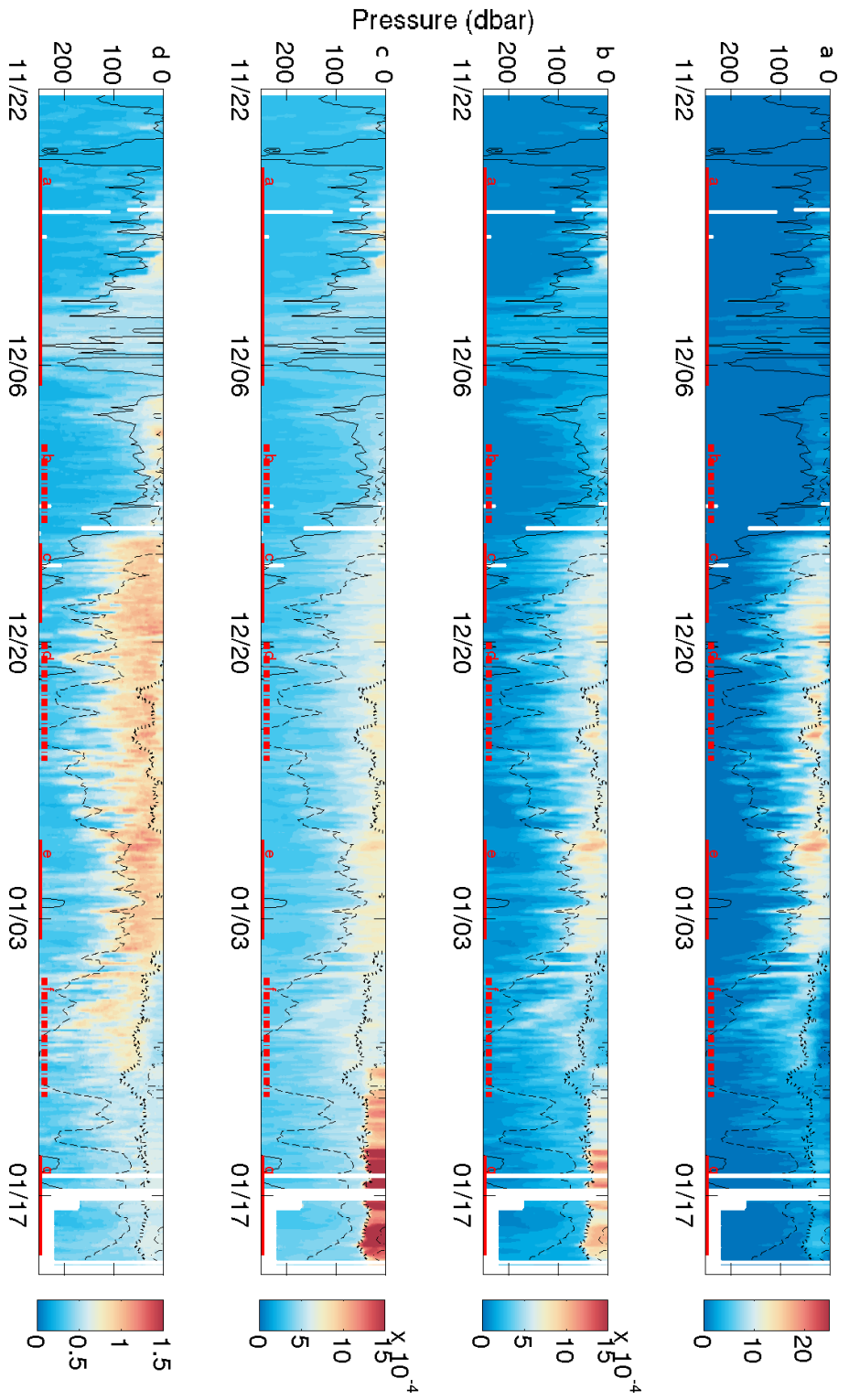


Figure 6.17: Chlorophyll *a* concentration calibrated against fluorometer samples from the R/V Palmer (*a*,  $\text{mg m}^{-3}$ ), red optical backscatter counts at 700 nm (*b*), blue optical backscatter counts at 470 nm (*c*), and red/blue optical backscatter count ratio (*d*) sections from SG502's transect. Density contours are shown at  $0.1 \text{ kg m}^{-3}$  intervals from  $27.9 \text{ kg m}^{-3}$  (*solid line*) to  $27.6 \text{ kg m}^{-3}$  (*dash-dot line*). Alternating solid and dashed red bars at the bottom of each graph delimit the regions labelled a to g and described in Fig. 6.22.

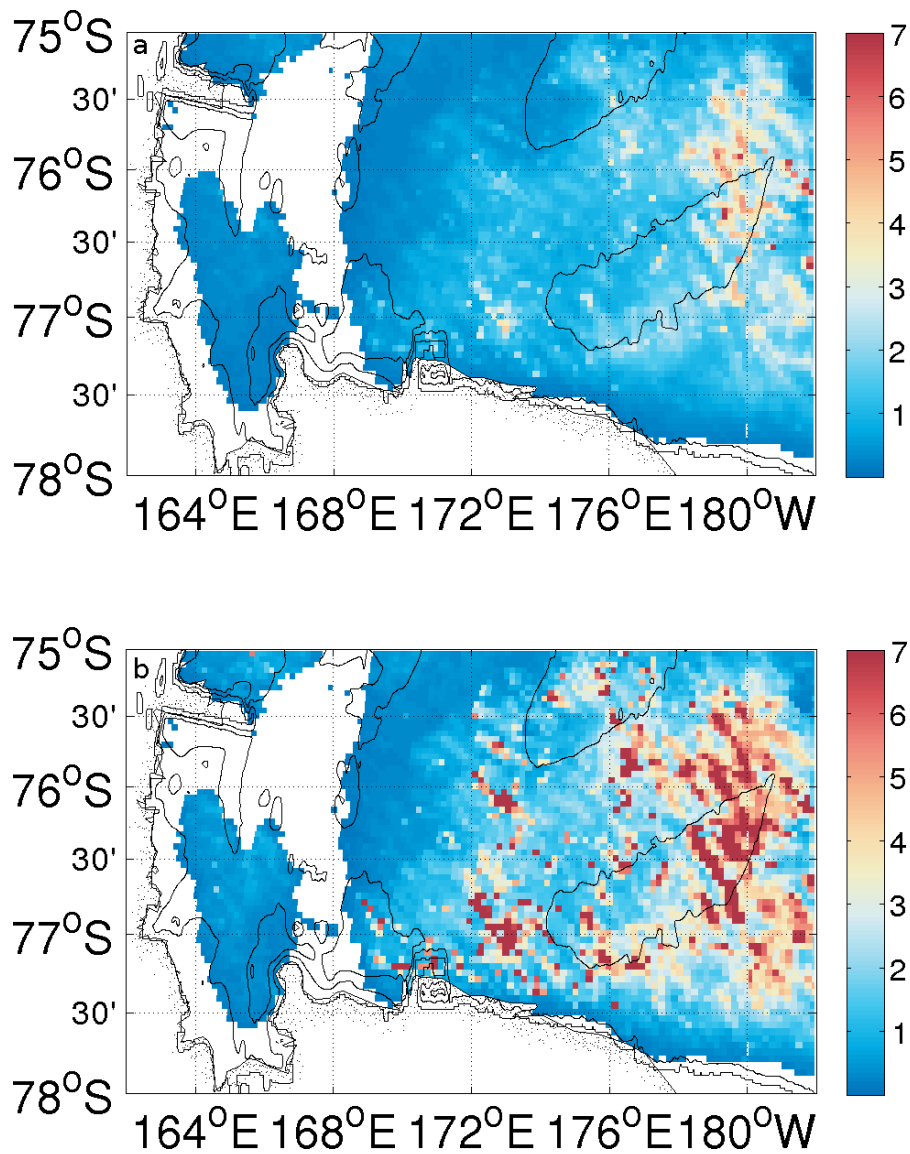


Figure 6.18: Mean (a) and maximum values (b) of a 21 day composite of MODIS ocean colour surface chlorophyll a concentrations ( $\text{mg m}^{-3}$ ) from the 14<sup>th</sup> of December to the 4<sup>th</sup> of January. This period corresponds to the SG502's observations of a large phytoplankton bloom over Ross Bank. White areas are devoid of data due to the continuous cloud and ice cover during the 21 day period.

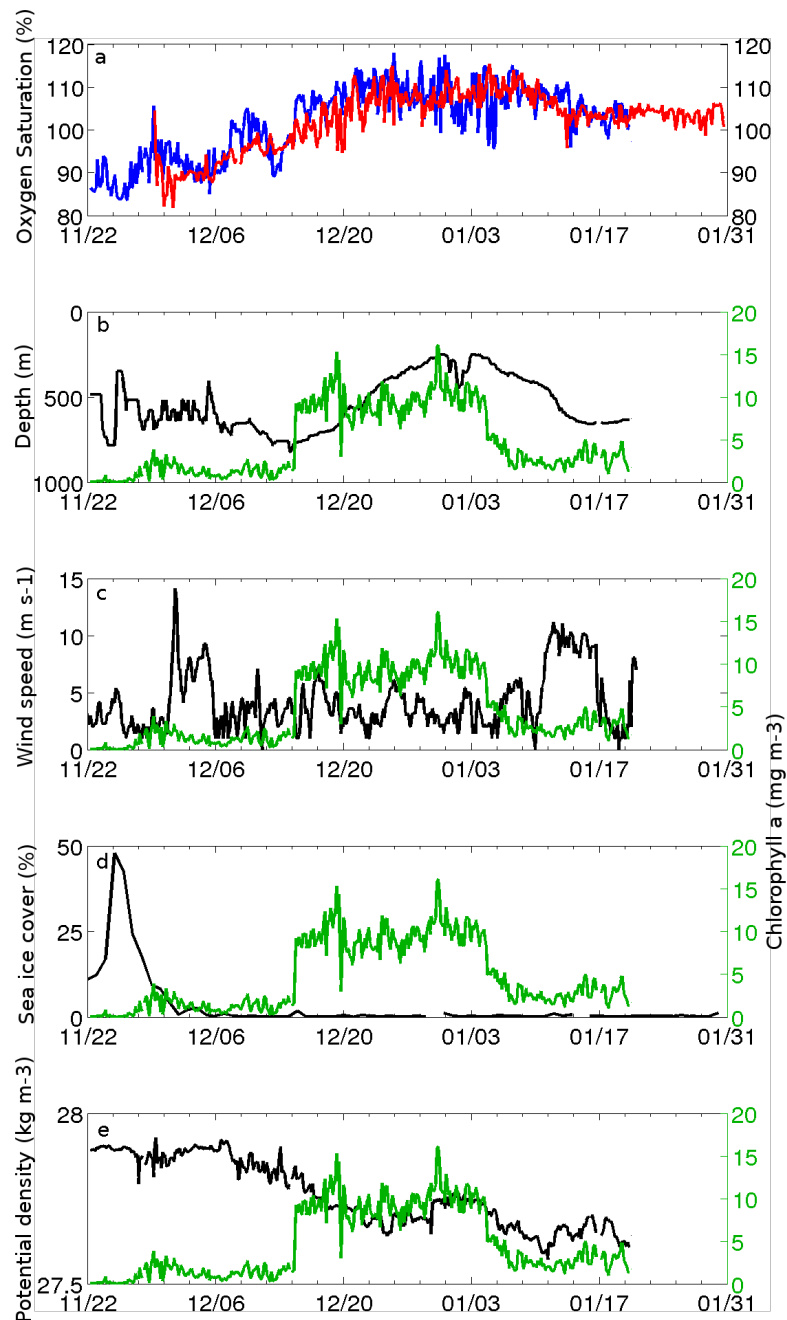


Figure 6.19: Timeseries of mean oxygen saturation (a. %) within the top 50 m of the water column for SG502 (blue) and SG503 (red). Panels b to e compare SG502 mean chlorophyll a concentration within the top 50 m of the water column ( $\text{mg m}^{-3}$ , green) with depth of the water column at SG502's position (b. m), ERA-Interim reanalysis winds at SG502's position (c.  $\text{m s}^{-1}$ ), mean sea-ice cover within the bloom region (d. %) and mean potential density of the top 50 m of the water column (e.  $\text{kg m}^{-3}$ ).

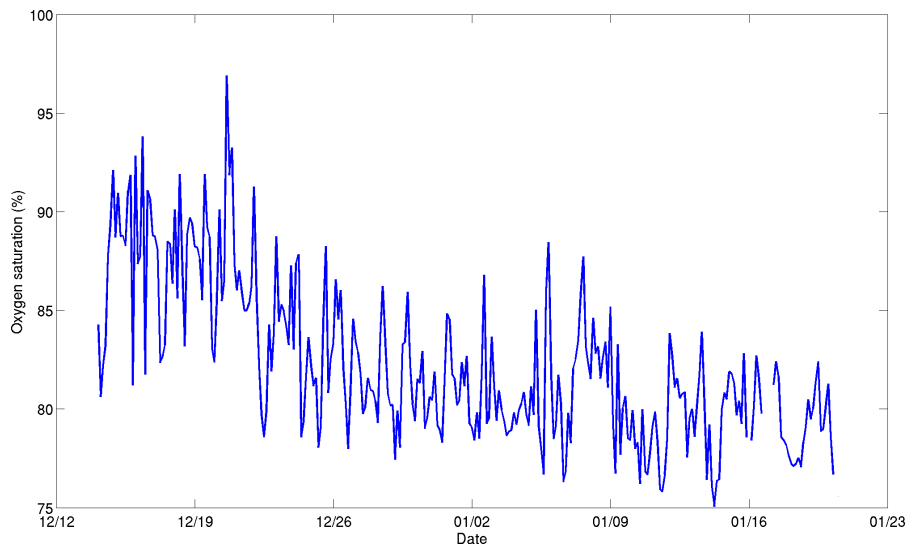


Figure 6.20: Oxygen saturation (%) between 75 dbar and 200 dbar as recorded by SG502 between the 14<sup>th</sup> of December 2010 and the end of the survey.

While supersaturation was limited to the top 70 m for most of the mission, SG502 did observe supersaturated water following isopycnals as they sank along the western edge of Ross Bank (18<sup>th</sup> of December and 10<sup>th</sup> of January; Fig. 6.16). SG503 also observed saturated waters following the  $27.8 \text{ kg m}^{-3}$  isopycnal to 300 m depth along the north edge of Ross Bank (Fig. 6.16). This is likely downward injection of supersaturated water by frontal mixing processes located along the edge of Ross Bank.

Oxygen concentrations showed a gradual change below the SML, beginning near 90% saturation east of the ice-bridge, and decreasing to 78% by the end of the mission (Fig. 6.20). East of the ice-bridge, in McMurdo Sound, pelagic oxygen saturation varied between 90 and 95%. The linear trend recorded lower oxygen saturations in the trough between the Ross and Pennell Banks (14<sup>th</sup>–28<sup>th</sup> of January). This is likely evidence of MCDW intrusions onto the shelf. Low DO is one of the signatures of MCDW (Kohut et al., 2013; Orsi and Wiederwohl, 2009), however it is likely heavily modified this far south which is why it does not show the typical temperature and salinity signal as described in section 6.3.4 (Smith & Dinniman, pers. comm.). Further discussion of the possible presence of MCDW will be presented in section 6.3.4.

The optical puck on SG503 failed three days into the mission so no data are available from this sensor. The sensor was only active in the top 250 m for SG502 (Fig. 6.17). Three different features are visible. Chlorophyll a concentrations of 2-6 mg m<sup>-3</sup> are present under the ice bridge with fluorescence detected as deep as 250 m. The largest bloom feature is observed within the Ross polynya as SG502 surveys the Ross Bank (18<sup>th</sup> of December). Chlorophyll a concentration peaks of 25 mg m<sup>-3</sup> are observed, with the majority of the bloom showing subsurface maxima of 12-18 mg m<sup>-3</sup> around 50 m depth. Observed chlorophyll a concentrations decrease rapidly after the 10<sup>th</sup> of January when SG502 crosses the western boundary of the Ross Bank and re-enters the Central Basin. Chlorophyll peaks of 10 mg m<sup>-3</sup> are detected to below 250 m, also following the 27.8 kg m<sup>-3</sup> isopycnal, at the western edge of the bank as SG502 heads westward. Chlorophyll concentrations reduce to 4-10 mg m<sup>-3</sup> until the end of the deployment within the top 70 m however a very different optical signature is observed by the two optical backscatter sensors from the main bloom event.

The plankton community below the ice bridge showed a red/blue optical backscatter count ratio of 0.6, with ratios rising to 0.8-1 in surface waters to either side of the ice bridge. The main bloom observed over the Ross Bank had a red/blue optical backscatter count ratio of 0.8-1.2. The final plankton community observed once SG502 had entered the Central Basin for the second time had a ratio of 0.6. The red/blue colour ratio can serve as an indication to the nature of the plankton community (Vaillancourt et al., 2004). However, due to the absence of ground truthing data in the region, it can only serve to distinguish between different bloom communities without any indication as to composition in this case. Studies of the phenology of the Ross Sea polynya would suggest that the main bloom observed between December and January was dominated by diatoms while the phytoplankton community in McMurdo Sound and at the end of the survey would be *Phaeocystis* dominated (Smith, pers. comm.).

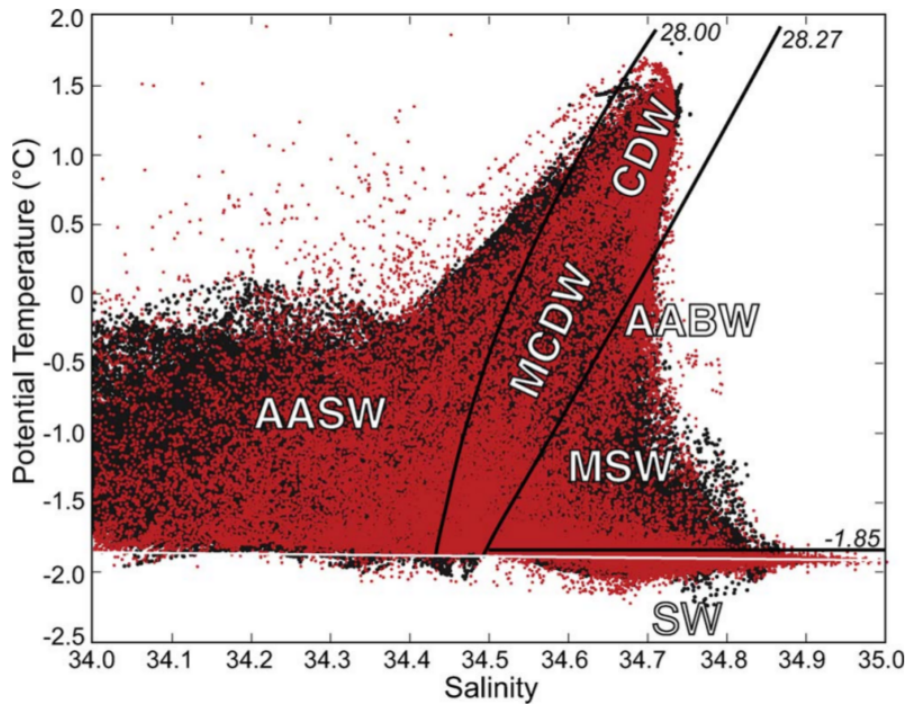


Figure 6.21:  $\theta - S$  diagram of Ross Sea climatology (*black*) and data collected by Orsi and Wiederwohl (2009) (*red*) at water depths shallower than 2000 m. Solid traces show the 28.00 and 28.27  $\text{kg m}^{-3}$  neutral density  $\gamma^{\text{N}}$  surfaces. The white horizontal line shows the surface freezing point of seawater. Major water masses are labelled: Antarctic Surface Water (AASW), Modified Circumpolar Deep Water (MCDW/CDW), Modified Shelf Water (MSW/SW), and Antarctic Bottom Water (AABW). (For interpretation of the references to colour in this figure legend, the reader is referred to the web version of the Orsi and Wiederwohl (2009) article.). Figure and caption taken from Orsi and Wiederwohl (2009).

### 6.3.3 Controls on the timing of the austral spring bloom

The exact mechanisms which regulate the timing and location of phytoplankton blooms in the Ross Sea are still relatively unknown. We were interested to see if the large bloom observed was constrained to the shallower Ross Bank and caused by physical processes linked to the bank.

As SG503 did not collect optical data, it is not possible to tell if the bloom was observed by both SG502 and SG503 at the same time or if the bloom changed significantly across the polynya. To identify if the phytoplankton bloom was specifically located over Ross Bank,

we compared observed chlorophyll *a* concentrations with bathymetric depth (Fig. 6.19b). The increase in surface chlorophyll *a* concentration observed by SG502 began just before the glider reached the bank and finished before the glider returned to the Central Basin. Also, Fig. 6.19a shows that oxygen saturation within the top 50 m as observed by both SG502 and SG503 changed in the same way over time, regardless of location. Assuming that the intensity of oxygen supersaturation within the surface layer is mainly driven by primary production, we can reasonably conclude that the phytoplankton bloom developed synchronously at both SG502 and SG503's positions.

This is further confirmed by ocean colour data from the MODIS instrument. Fig. 6.18 shows a 21-day composite of ocean colour data of the period when SG502 observed the bloom over Ross Bank (14<sup>th</sup> of December to the 4<sup>th</sup> of January). Despite gathering data over a 3 week period, a large area is devoid of data due to the extensive cloud and ice cover in the region. Satellite imagery revealed an extensive bloom of much lower concentration than that observed by the Seaglider extending into the Central Basin. A much stronger bloom was observed to the northeast of Ross Bank but was not observed by the Seagliders as the transect did not extend that far. The lower concentration observed by the satellite relative to the Seaglider is possibly due to the depth of the chlorophyll maximum observed by the glider and the inherent difficulty in treating satellite imagery in high latitudes with extensive ice and cloud cover. The satellite data indicate that the bloom was not spatially constrained, at least at the surface, to only the Ross Bank, but was also present in the Central Basin region.

Studies have suggested that blooms may be caused by or enhanced by intrusions of MCDW (Kohut et al., 2013; Peloquin and Smith, 2007; Smith et al., 2006). As this bloom was not a small localised feature but was instead widespread, beginning approximately at the same time across the polynya, we investigated the mechanisms which could have triggered the onset of the bloom. As this bloom begins across a large area including both the banks and basin (Fig. 6.18), it is not likely that its onset is regulated by advective processes such as meso-scale intrusions of MCDW. However, the more intense bloom to the

northeast of Ross Bank could be fuelled by MCDW. The onset of the first bloom in the Ross Sea polynya is often considered to be caused by increased irradiance and vertical stability in the water column due to rapid ice melt (Smith and Comiso, 2008; Smith et al., 2000). However, in this case, there was a 3 week period between melting of the surface ice in the bloom region and the onset of the bloom (Fig. 6.19d). Fig. 6.19c also compares wind velocity above SG502 and chlorophyll *a* concentrations in the top 50 m. We see a much closer relation; a week after wind speeds drop below  $5 \text{ m s}^{-1}$ , there is a dramatic increase in chlorophyll *a* concentration. This also corresponds to a rapid decrease in surface water density, although changes in isopycnal depths could also be linked to proximity to the bank and may therefore be coincidental.

Overall, these elements would tend to indicate that the factor delaying the onset of the bloom was vertical instability of the phytoplankton in the water column. Once the ice receded, sufficient nutrients and light were available for phytoplankton growth, but elevated wind speeds prevented the phytoplankton community from adapting to the light regime by maintaining instability in the upper water column. Once wind speeds decreased, surface warming accelerated enabling stratification of the surface layer. This then provided the phytoplankton community the necessary vertical stability to bloom. It appears that ice melt is not the sole control of stratification in the region; strong katabatic winds also play a strong role in controlling the onset of the stratification of the water column which provides the necessary light for phytoplankton blooms.

The bloom ended in the first week of January with strong downward mixing of chlorophyll *a* (Fig. 6.17). This coincides with the second elevated wind speed event ( $> 10 \text{ m s}^{-1}$ ) as shown in Fig. 6.19. This correlates with observations by Smith et al. (2011b) that mixing events may be the cause of bloom termination in the Ross Sea polynya.

#### 6.3.4 *Watermass properties and distribution of chlorophyll a*

As the glider observations described previously revealed high spatial and temporal variability in both the physical and biochemical properties along SG502's transect, different sections based on temperature and salinity were identified along the glider's path. SG502's transect was cut into 7 sections of similar temperature and salinity properties to investigate the relation between the presence of specific watermasses (namely MCDW) and the distribution of chlorophyll a within these watermasses (Fig. 6.22). Sections are also indicated by the red bars in Fig. 6.15 and are coloured along the glider track in Fig. 6.23. Watermasses will be named as per Orsi and Wiederwohl (2009) (Fig. 6.21).

Sections a (McMurdo Sound), b (Ice bridge) and c (Central Basin) in Fig. 6.22 show similar  $\theta - S$  properties with a strong presence of Modified Shelf Water (MSW). The region around the ice bridge also shows evidence of Antarctic Surface Water (AASW), likely originating from ice melt. Below the fresher surface layer ( $27.85 \text{ kg m}^{-3}$  isopycnal), both regions show the same  $\theta - S$  properties as section b (under the ice bridge). This indicates that the sill north of Ross Island (located under the ice bridge) likely does not inhibit exchange of MSW between McMurdo Sound and the Central Basin. We can see the clear presence of elevated chlorophyll a on either side of the ice bridge, whilst the ice covered region shows reduced concentrations (Fig. 6.22).

As the glider approached Ross Bank (region d) and the bloom began, a stratified generally fresher water column is visible with a warmer water mass appearing above the  $27.7 \text{ kg m}^{-3}$  isopycnal. Interestingly, the bulk of the chlorophyll a is located below this warmer surface layer. This contrasts very strongly with waters located on the eastern boundary of the Ross Bank (region e). Here, we observe a clear jump in  $\theta - S$  properties of the water column; waters along the eastern edge of the Ross Bank show the typical signature of MCDW, contrary to waters further west. As the glider returns west (region f), we observe the same properties as along the first passage along

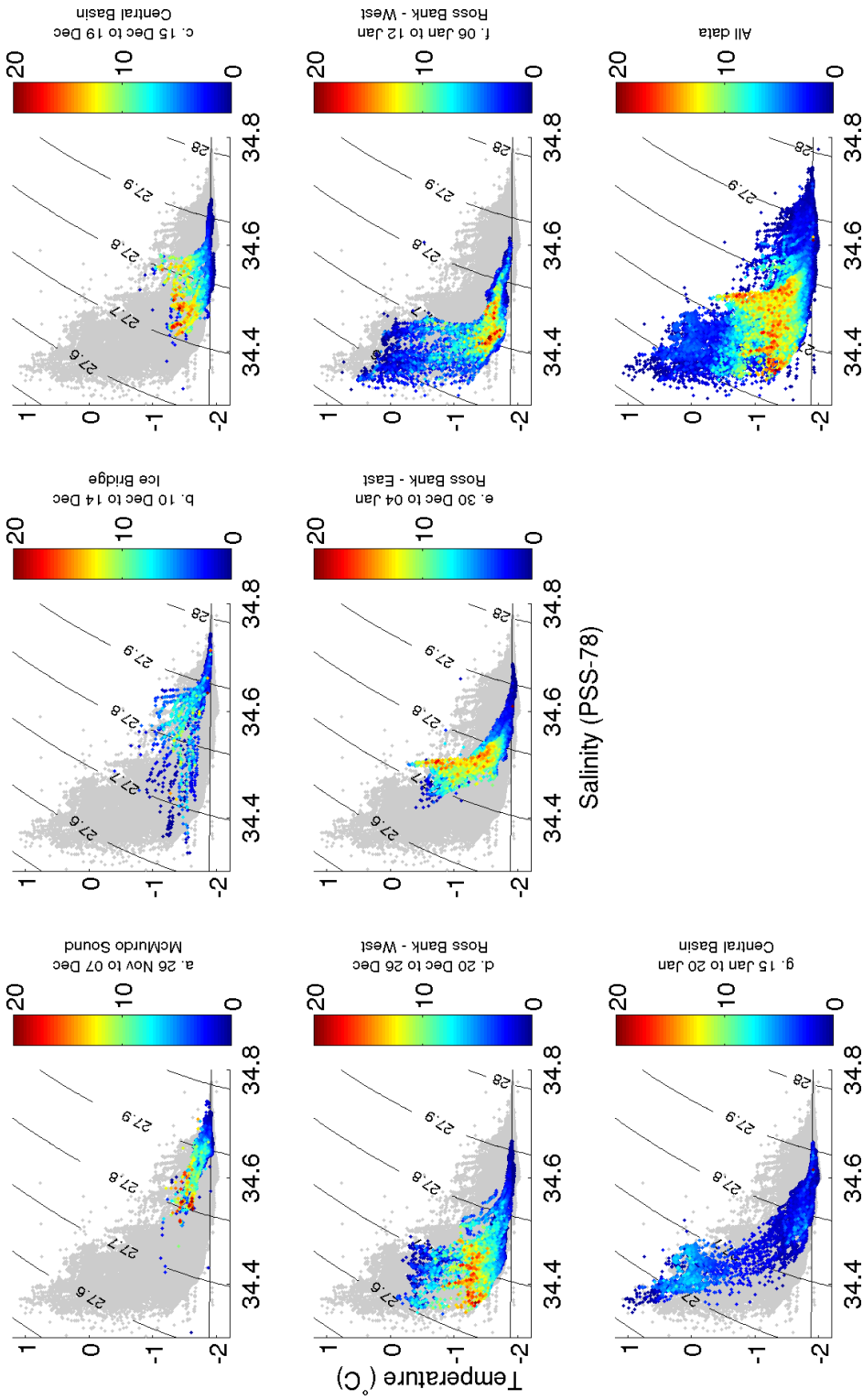


Figure 6.22:  $\theta - S$  diagrams of the 7 different sections identified from 502's observations coloured by chlorophyll a concentration ( $\text{mg m}^{-3}$ ). Each section is identified by the red bars on Figs. 6.15 to 6.17.

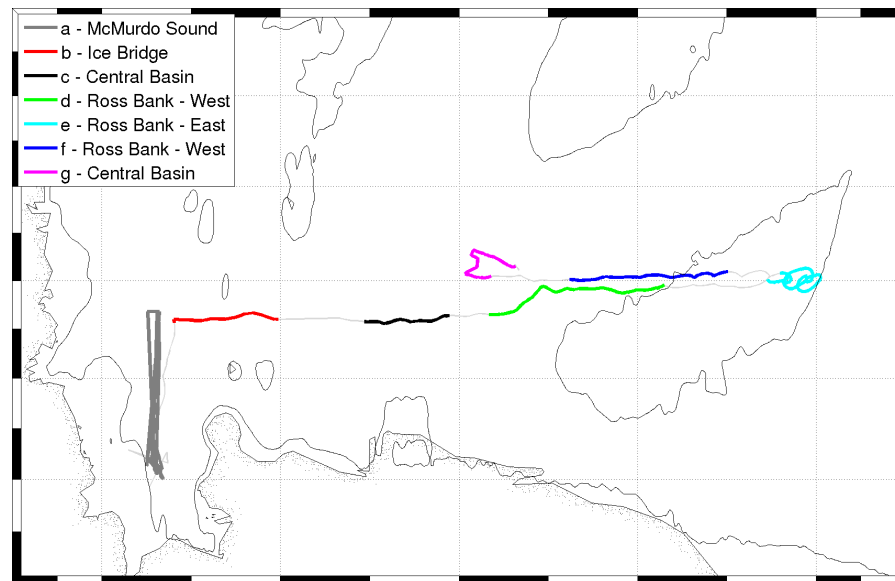


Figure 6.23: Location of the 7 different sections identified along SG502's track. 400 m isobaths are included to highlight the position of Ross Bank.

the western edge of Ross Bank. Two weeks later, surface waters had warmed noticeably, with an increase of  $0.5\text{ }^{\circ}\text{C}$ .

The western and eastern edges of Ross Bank also show a very different pattern in chlorophyll a distribution. Along the western edge, chlorophyll a is concentrated in the fresher colder sub-surface layer whilst along the eastern edge, chlorophyll a concentration is highest in the MCDW. This region is very near the elevated chlorophyll a concentrations observed by the MODIS instrument (Fig. 6.18). As this watermass is also the least dense in the region, this explains why the MODIS instrument was recording higher chlorophyll a concentrations in the region. Additionally, a gradient can be observed with lower chlorophyll a concentrations in the intermediate watermasses between the MCDW and AASW. This indicates, and is agreement with the MODIS data, that these are two distinct blooms; the larger of which is located along the North-East of Ross Bank and is likely fuelled by an intrusion of MCDW.

As the glider returns to the Central Basin (region g), observed chlorophyll a concentrations decrease and we observe the onset of a new bloom with a different plankton community based on optical backscatter ratios (Fig. 6.17). Contrastingly, during the glider's second

passage through the Central Basin, chlorophyll *a* is concentrated in the warm and fresh surface water.

### 6.3.5 *Variability within the Ross Sea polynya*

As is evident from previous descriptions, this is a very rich and complex dataset with features occurring on a range of scales. This section attempts to highlight both the horizontal and vertical variability of the Ross Sea polynya to demonstrate the complexity of estimating productivity in this region. Figs. 6.24 to 6.26 provide an indication as to the scales of variability of temperature, salinity and oxygen at different depths. These empirical variograms illustrate the variance in points separated by set distances in space and time. Black lines have been added to illustrate the increases in variability. These variograms are traditionally used in kriging to estimate influence radii when interpolating or extrapolating datasets. Although this technique provides limited statistical accuracy with such irregularly spaced data and few transect repeats it manages to capture whether features change in a uniform way across the study region or are defined by strong spatial variability. Due to the absence of chlorophyll *a* data from SG503, this method cannot be used to assess variability of chlorophyll *a* in the Ross Sea polynya.

Temperature in the top 75 m of the water column appears to be relatively homogeneous horizontally over spans of over 200 km with temporal variability dominating fluctuations in SML temperature (Fig. 6.24). SML temperature in this region is governed by solar irradiation, ice melt and surface air temperature. However, below the SML, a completely different pattern of variability is observed. Little fluctuations are observed in temperature over time, but strong spatial heterogeneity is observed in waters between 100 and 200 m depth. Intrusions of various watermasses following bathymetric contours and the presence of strong fronts is the likely cause of this high horizontal temperature variability. Below 250 m, regular striations are visible beyond the red line. These are artefacts caused by the greatly reduced num-

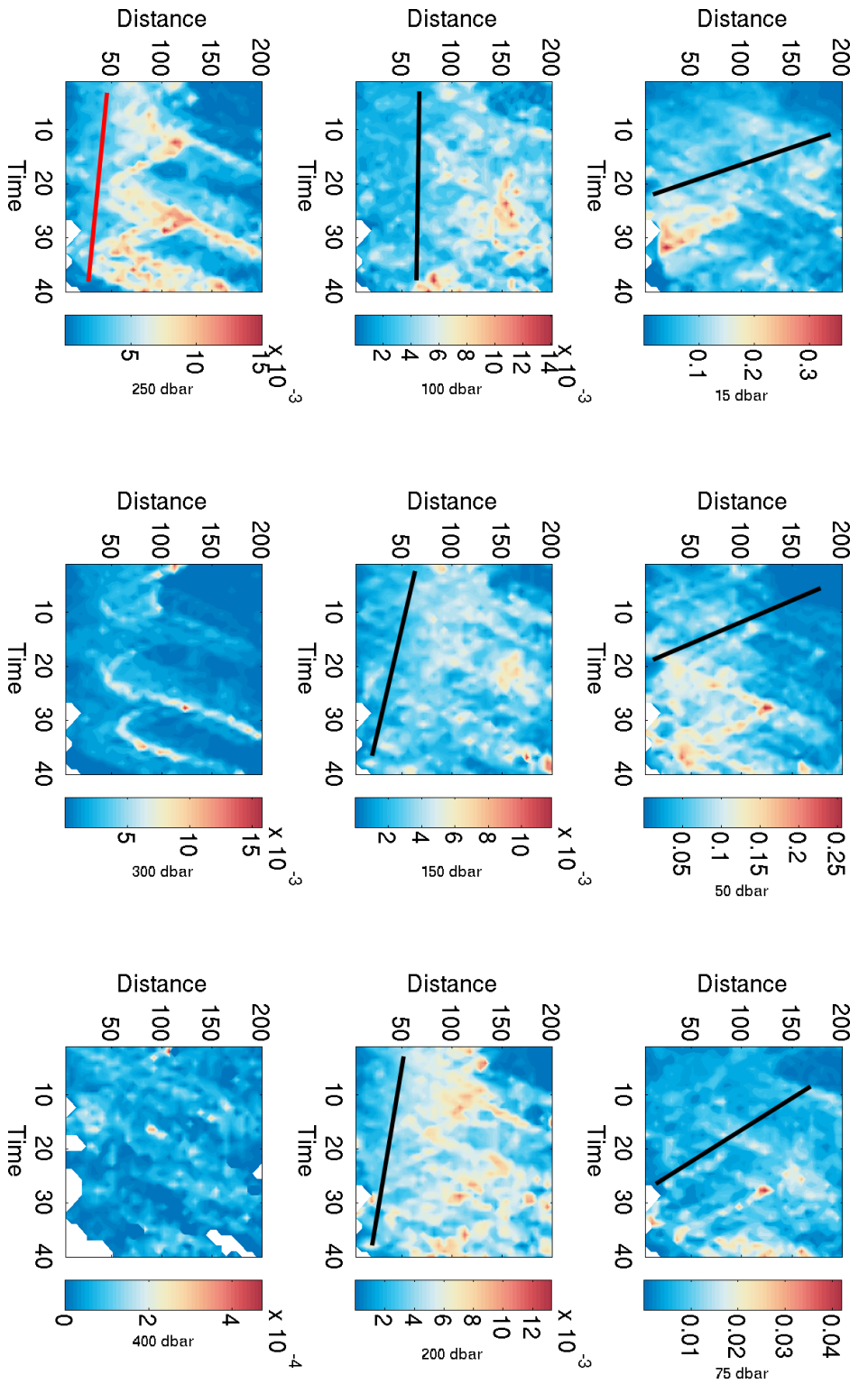


Figure 6.24: Empirical variogram of temperature ( $^{\circ}\text{C}$ ) recorded by SG502 and SG503 along different isobars (15, 50, 75, 100, 150, 200, 250, 300, 400 dbar). Due to the irregular spacing of the data and spatial sparseness, a proper statistical fit was not performed. Instead, a black line has been added to highlight the general location of the sill. This indicates the dominant spatial and temporal scales of variability. A red bar indicates poor significance of the plot due to aliasing, generally due to absence of data from one glider. Distance is in kilometres and time is in days.

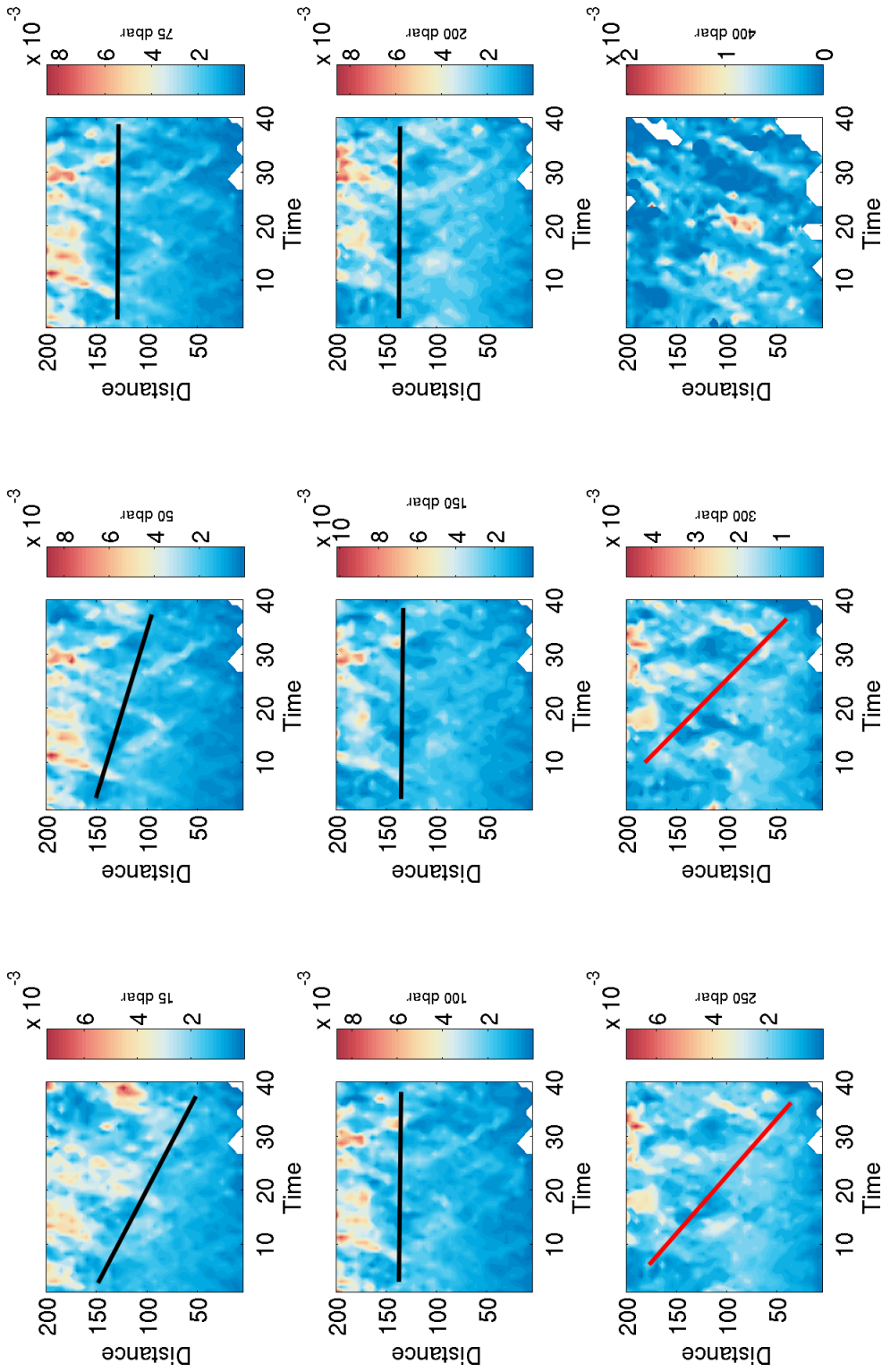


Figure 6.25: Empirical variogram of salinity (PSS-78) recorded by SG502 and SG503 along different isobars (15, 50, 100, 150, 200, 250, 300, 400 dbar). Due to the irregular spacing of the data and spatial sparseness, a proper statistical fit was not performed. Instead, a black line has been added to highlight the general location of the sill. This indicates the dominant spatial and temporal scales of variability. A red bar indicates poor significance of the plot due to aliasing, generally due to absence of data from one glider. Distance is in kilometres and time is in days.

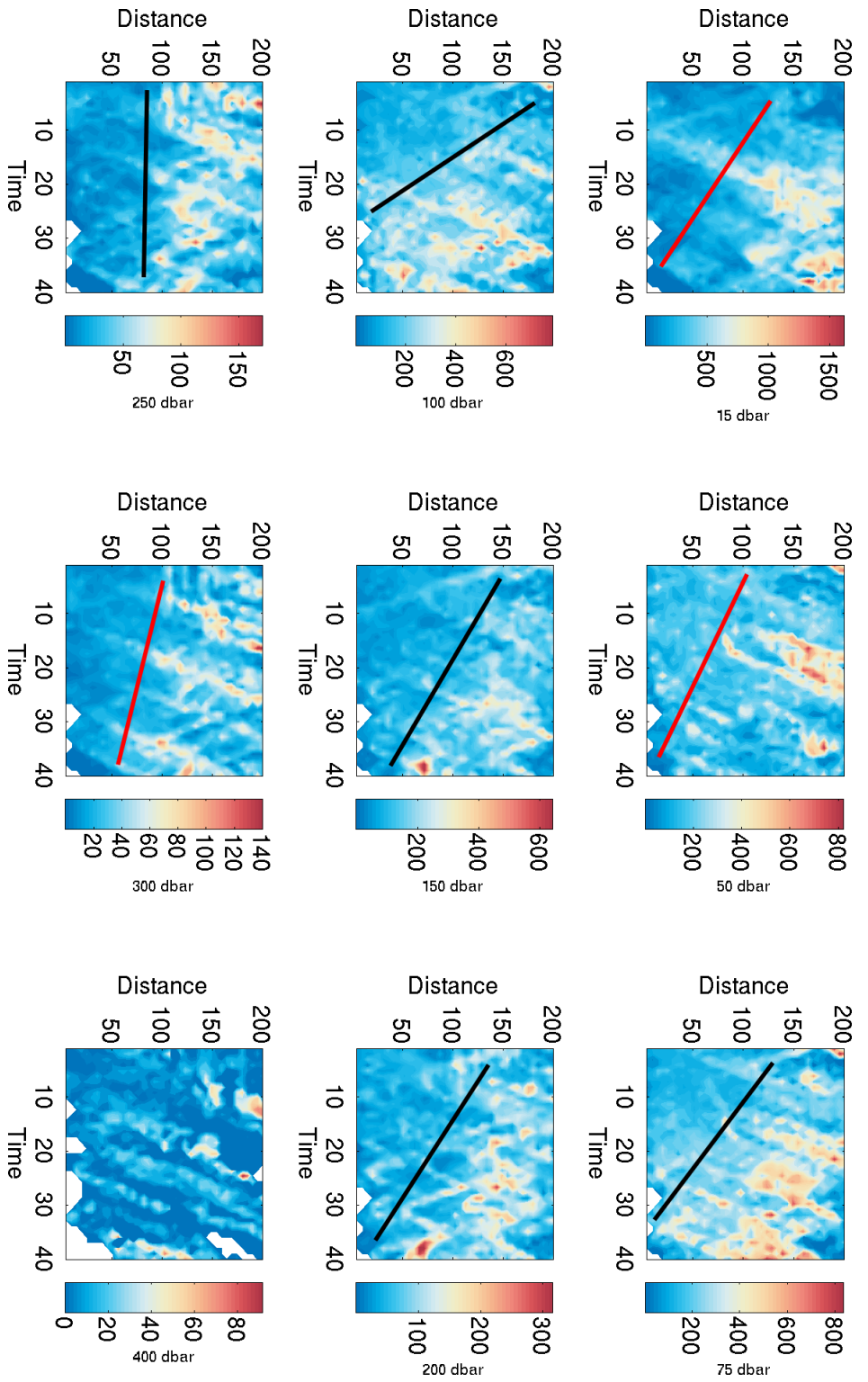


Figure 6.26: Empirical variogram of DO ( $\mu\text{mol dm}^{-3}$ ) recorded by SG502 and SG503 along different isobars (15, 50, 75, 100, 150, 200, 250, 300, 400 dbar). Due to the irregular spacing of the data and spatial sparseness, a proper statistical fit was not performed. Instead, a black line has been added to highlight the general location of the sill. This indicates the dominant spatial and temporal scales of variability. A red bar indicates poor significance of the plot due to aliasing, generally due to absence of data from one glider. Distance is in kilometres and time is in days.

ber of data points at this depth and below for one glider leading to excessive weighting of the other glider's observations.

Salinity, unlike temperature, shows a much greater spatial dependence near the surface as well as in deeper waters (Fig. 6.25). This spatial heterogeneity in the SML likely relates to the presence of ice and sea-ice processes (melt and formation) during the first half of the deployment. This spatial heterogeneity gradually decreases with depth. Interestingly, although salinity is consistent over time at depth, it is also less spatially variable than temperature. It is difficult to hypothesise why this may be the case, although it is possible that the presence of melt water dominates the variability and therefore masks the variability that could be observed in the deeper, more uniform, watermasses. It is also possible that the greater spatial heterogeneity in temperature is linked to diapycnal mixing as temperature shows a stronger vertical gradient than salinity (Figs. 6.27a & 6.28a). Downward mixing of SML water below the thermocline would show a greater signal in temperature than in salinity. It is worth noting though that the variance in salinity at each depth level is of the same order of magnitude unlike that of temperature. The spread of temperature values within the SML is much greater than that below the thermocline,

No clear signal can be identified near the surface in the DO data (Fig. 6.26). However DO seems to vary differently from both temperature and salinity in the top 200 m of the water column. Fig. 6.26 illustrates that neither temporal nor spatial variability are solely responsible for the DO distribution described in the previous sections. As salinity and temperature predominantly vary along different dimensions, it is not possible to attribute the variability in DO in the SML to biological processes. However, the DO data has a strong temporal component to its variability below the thermocline which is absent from both the temperature and salinity data. This is most pronounced along the 100 dbar isobar. Variability in DO concentrations without simultaneous changes in  $\theta - S$  properties at this depth are most likely due to biological processes. Subsurface production at the DCM or consumption of sinking organic matter will produce or con-

sume DO at depth leading to the increased variance observed in the data.

These three figures (Figs. 6.24 - 6.26) confirm that both SML temperature and salinity are affected by atmospheric processes (ice melt and formation, solar irradiation, winds and air temperature) but in different ways. Drivers of temperature change occur on a basin wide scale, likely affecting the polynya in a uniform fashion. Salinity, by contrast, seems affected by mesoscale factors, such as sea ice processes. As the bloom described in the previous sections was triggered by the stabilisation of the water column, understanding how temperature and salinity vary in the SML and therefore how the Ross Sea polynya stratifies, becomes critical in developing our capacity to model the onset of the bloom. Biological production and consumption of DO was also shown to be important in determining the distribution of DO. The effects of biological activity on DO were shown by the greater temporal variability down to 200 m. As it is unlikely the photic zone extends to that depth, it highlights the significance of organic matter export in the region and reinforces the idea that the polynya may be an important site of carbon export.

### 6.3.6 *Dissolved oxygen change within the water column*

Following the observations of DO variability below the SML, likely due to biological activity, Figs. 6.27 & 6.28 investigate the vertical distribution of DO change throughout the mission. A rate of DO change per day was estimated by linearly regressing DO concentrations against time for each depth bin; the slope of the regression was used as an estimate of  $\frac{d[O_2]}{dt}$ . Data before the 14<sup>th</sup> of December were discarded for this analysis. This cut-off date was selected as there was a step change in oxygen concentrations as SG502 crossed the ice-bridge and this led to an artificial signal in the calculation of rates.

It cannot be assumed that the observed  $\frac{d[O_2]}{dt}$  is solely due to biological activity. As the previous two sections have shown, this is a highly variable environment and a significant portion of the signal observed in the vertical distribution of  $\frac{d[O_2]}{dt}$  will be due to the Sea-

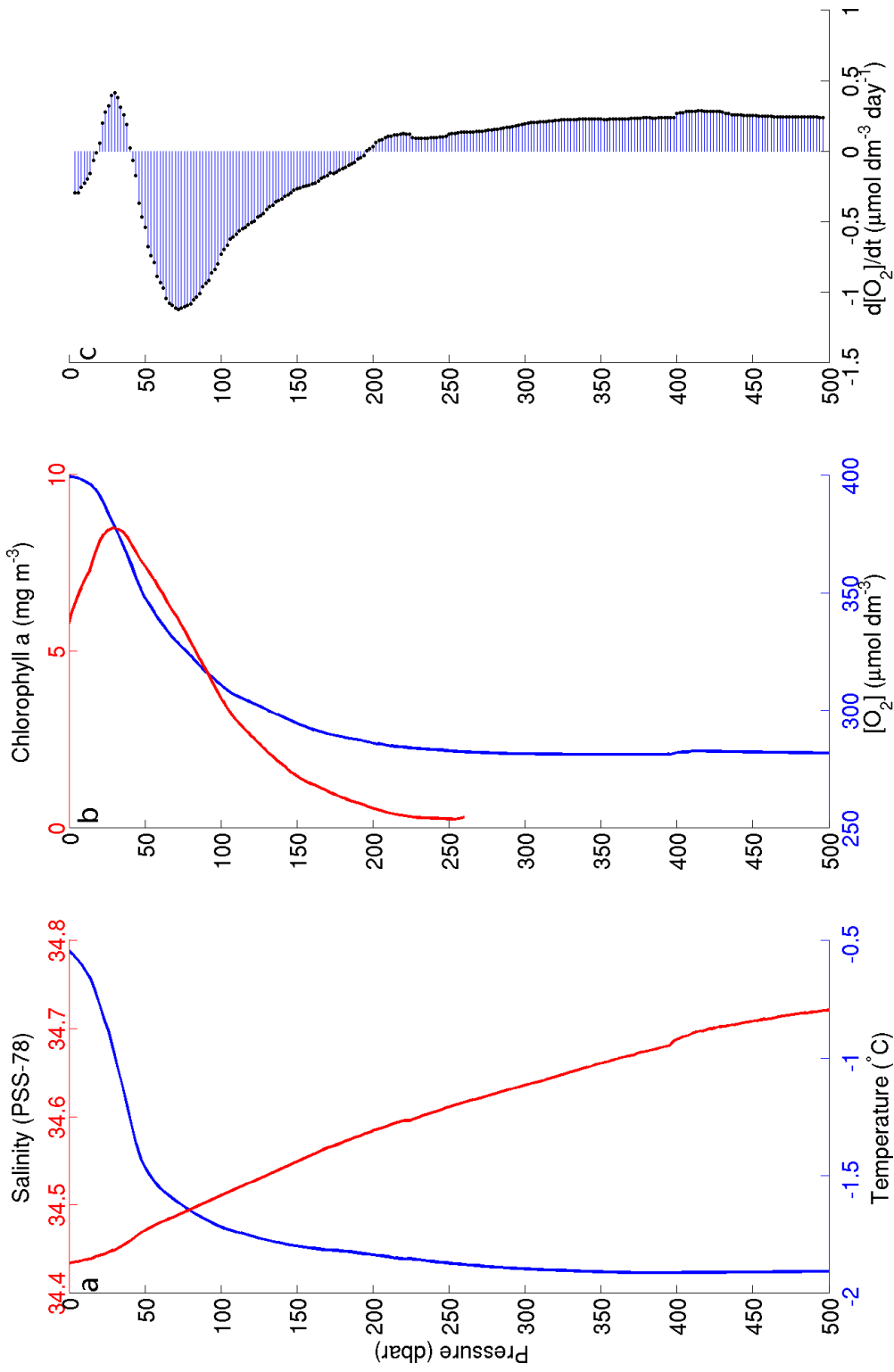


Figure 6.27: *a.* Mean temperature (°C, *blue*) and salinity (PSS-78, *red*) profiles between the 14<sup>th</sup> of December 2010 and the end of the survey. *b.* Mean DO ( $\mu\text{mol dm}^{-3}$ , *blue*) and chlorophyll *a* (PSS-78, *red*) concentrations between the 14<sup>th</sup> of December 2010 and the end of the survey. *c.* Estimated daily change in DO concentration at each depth bin ( $\mu\text{mol dm}^{-3} \text{ day}^{-1}$ ). Data as recorded by SG502 between the 14<sup>th</sup> of December 2010 and the end of the survey.

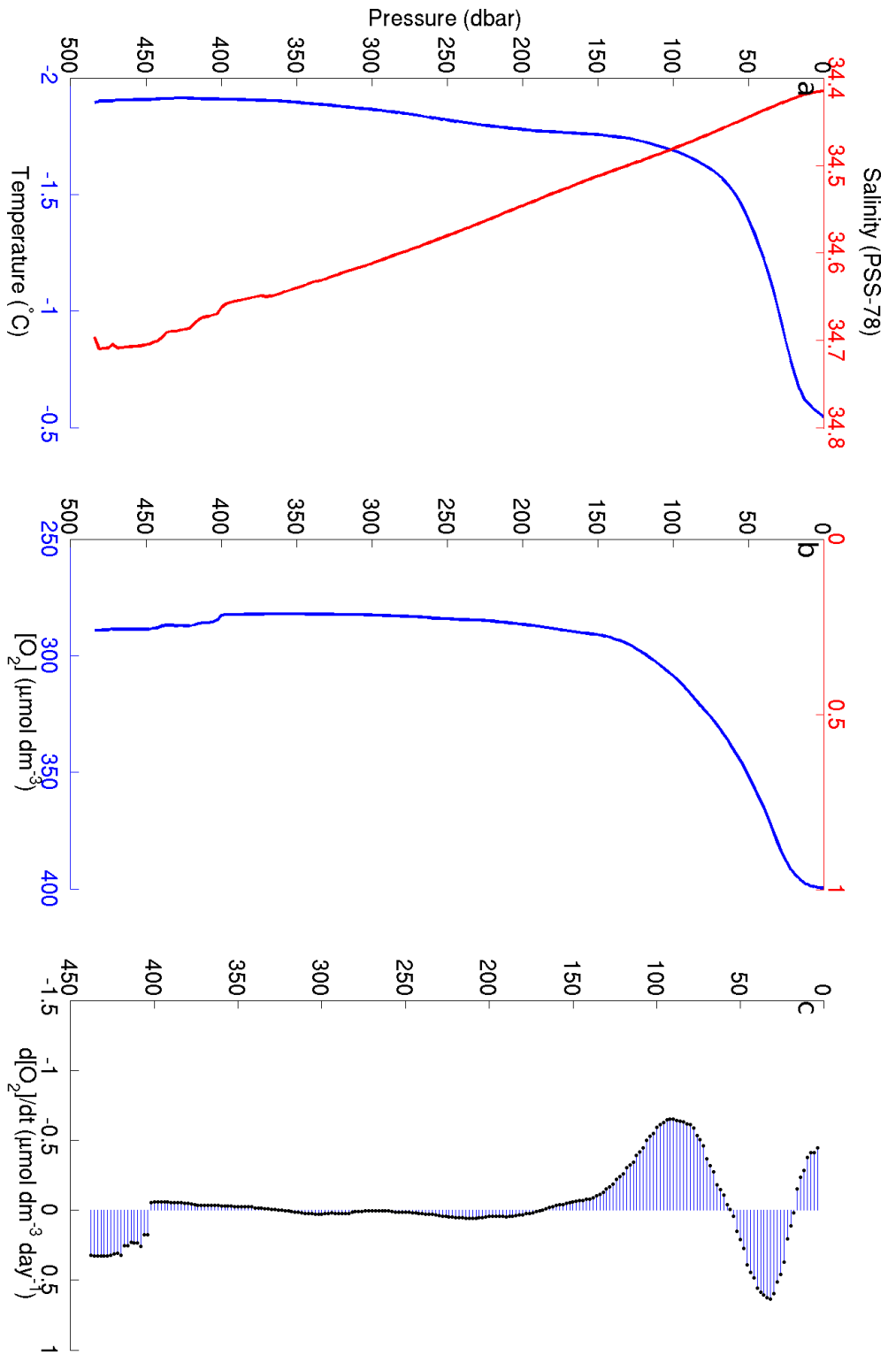


Figure 6.28: *a.* Mean temperature ( $^{\circ}\text{C}$ , *blue*) and salinity (PSS-78, *red*) profiles between the 14<sup>th</sup> of December 2010 and the end of the survey. *b.* Mean DO ( $\mu\text{mol dm}^{-3}$ , *blue*) concentrations between the 14<sup>th</sup> of December 2010 and the end of the survey. *c.* Estimated daily change in DO concentration at each depth bin ( $\mu\text{mol dm}^{-3} \text{ day}^{-1}$ ). Data as recorded by SG503 between the 14<sup>th</sup> of December 2010 and the end of the survey.

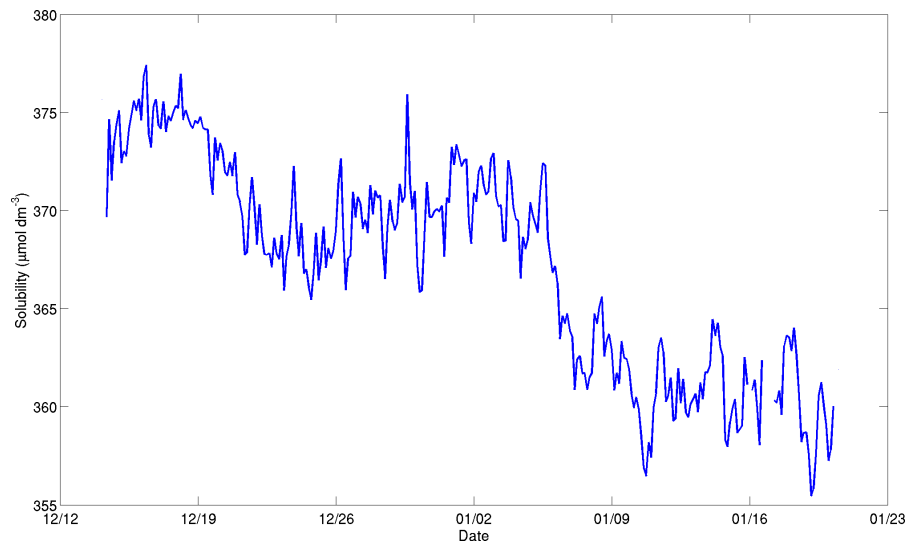


Figure 6.29: Oxygen solubility ( $\mu\text{mol dm}^{-3}$ ) of the top 20 m of the water column as recorded by SG502 between the 14<sup>th</sup> of December 2010 and the end of the survey.

glider travelling to regions of lesser or greater DO concentrations. While this implies that the differences between Figs. 6.27 & 6.28 are artefacts of the Seaglider's travel and spatial variability, it also lends credibility to the assumption that any similarities observed are likely present throughout the survey area and therefore due to biological activity. Additionally, as SG503 performed more repeats of its transect and remained in a relatively smaller area than SG502, the impact of spatial variability on the  $\frac{d[\text{O}_2]}{dt}$  signal will be less in Fig. 6.28. Additionally, errors in the determination of the sensor drift will directly affect the accuracy of these results.

The most striking feature between Figs. 6.27 & 6.28 is the difference in the DO profiles (b) and the  $\frac{d[\text{O}_2]}{dt}$  (c). Both gliders show a decrease in DO in the surface 20 m of approximately  $0.5 \mu\text{mol dm}^{-3} \text{ day}^{-1}$ . This feature is likely caused by the changing properties of the surface layer. Both Figs. 6.27a & 6.28a show a strong temperature gradient near the surface. Fig. 6.29 shows DO solubility within the top 25 m of the water column after the 14<sup>th</sup> of December. The solubility decrease of nearly  $20 \mu\text{mol dm}^{-3}$  is enough to account for the surface decrease in DO throughout the mission assuming the surface layer remained near saturation through air-sea exchanges. Below this surface layer, DO increase peaks in both SG502 and SG503's observations.

Maximum  $\frac{d[O_2]}{dt}$  also correlates with the maximum observed chlorophyll *a* concentrations (Fig. 6.27b). This illustrates primary production along the DCM, however it is not possible to relate the primary productivity of the DCM to that of the surface layer as any excess production in the surface 20 m would likely lead to rapid outgassing of DO through air-sea exchanges. Below the DCM, chlorophyll *a* concentrations decrease gradually and remain relatively high ( $2 \text{ mg m}^{-3}$ ) down to 150 m. Although it is possible that light penetrates to this depth, maintaining a population of high chlorophyll *a* concentration phytoplankton highly adapted to these low light levels, it seems more likely that this is evidence of sinking organic matter. Simultaneously, we observe a strong decrease in DO below the DCM. The consumption or decrease of DO is strongest just below the DCM and gradually decreases to what are likely background bacterial DO consumption rates and artefacts of the Seaglider's movement below 200 m. This would indicate that the majority of organic matter produced within the euphotic zone is rapidly remineralised within the water column before it reaches a depth of 200 m. In future studies, it would be desirable to perform bottle incubations in the region to better resolve the vertical variability of primary productivity and heterotrophy within the water column, as well as isolating the influence of air-sea exchanges within the surface.

With pelagic respiration in the order of  $1 \text{ } \mu\text{mol dm}^{-3} \text{ day}^{-1}$ , it is not surprising to observe pelagic oxygen saturations between 75 and 80% (Fig. 6.16). Here the low DO is enhanced by the advection of old watermasses with low DO saturation signatures and this pelagic respiration leads to a further decrease of 10-15% (Fig. 6.20). Whereas in the North Sea (Ch. 5), the water column is well mixed and saturated when it stratifies and a single season's worth of production leads to a decrease in oxygen saturation to well below the 75 to 80%; it is possible that the oxygen depletion observed in the Ross Sea is also limited due to the much greater depth of the sub-SML portion of the water column as well as the very heterogeneous distribution of watermasses indicating continuous advective processes throughout the polynya.

## 6.4 CONCLUSION

This project was the first to deploy gliders at high latitudes and demonstrated their ability to observe biogeochemical processes in such extreme environments. The gliders provided an overview of the processes occurring across the western Ross Sea polynya during the onset of the austral spring bloom. Notably, they were able to identify transitions between very heterogeneous watermasses across the shelf and difference in scales and timing between changes in seawater physical and biological properties. By providing such high resolution observations, they highlighted small scale features such as the termination of the primary bloom which would be difficult to observe using conventional methods due not only to the presence of ice, but also due to its short time-scale. The gliders also provide critical insight into the ability of satellite imagery to assess chlorophyll *a* concentrations at high latitudes in the presence of both ice and clouds. The gliders recorded much higher concentrations sub-surface than could be identified by the MODIS instrument.

The simultaneous deployment of two Seagliders also enabled a coarse estimation of the scales of temporal and spatial variability throughout the water column. Such insights are generally only available from modelling studies or on very large scales through the collection of many years of data (i. e. floats). Additionally, the gliders were able to observe rates of change in dissolved oxygen through the survey region. It is difficult to attribute these results to primary production and community respiration due to the very high variability across the study period. However, with a survey design that would alleviate the issue of disentangling spatial and temporal variability, such as by following drifters or deploying a fleet of gliders, these observations would be able to provide accurate estimates of community production and therefore carbon export within the western Ross Sea polynya.

Beyond this, the gliders have also shown potential for studying the mechanisms and processes surrounding many other critical processes relating to production in the Ross Sea polynya. Observations

from under-ice passages reveal many features on a variety of scales which were not discussed in detail in this chapter, such as step like structures in temperature and salinity, as well as increased chlorophyll a production along the ice edge. One of the limiting factors for these studies is the glider survey design. As an exploratory study, the gliders were programmed to provide observations along as wide an area as possible in the hope that SG503's butterfly pattern would provide a point of reference for comparison. However, not only did the optical sensor on SG503 fail to provide data, the scale of the butterfly pattern was much greater than the scale of physical and biological processes. A future study wishing to focus on processes and the evolution of oxygen or phytoplankton blooms and export would benefit greatly either from a fixed point of reference (i. e. a mooring, a stationary glider or a much smaller butterfly pattern), or on the other hand, a Lagrangian-like platform for gliders to follow (i. e. drifters). For this study, there were insufficient repeats of the glider transects; this prevented proper identification of timing and spatial differences in observed features. By providing a fixed or Lagrangian reference, it becomes much simpler to understand the variability. Likewise, a greater number of repeats along a transect would also provide insight into changes over time while still observing the same range of different regions. Gliders possess great potential but they are not a ship. Due to their reduced speeds, they cannot cover large expanses in the same way and still obtain a synoptic view of a region. Best use of Seaglider comes when their observations are studied in tandem with other observation platforms.

Part V

CONCLUSIONS

---



## SUMMARY AND OUTLOOK

---

### 7.1 THE NORTH SEA

The first component of this research project aimed to investigate the seasonal oxygen depletion observed by Greenwood et al. (2010). The first North Sea field campaign consisted of a ship-based systematic CTD survey of the North Sea during August 2010 to obtain a snapshot of North Sea DO concentrations (Ch. 4). Typical near-bed DO saturations in the stratified regions of the North Sea were 75-80 % while the well-mixed regions of the southern North Sea reached 90 %. Two regions of strong thermal stratification, the area between the Dooley and Central North Sea Currents and the area known as the OG, had oxygen saturations as low as 65 and 70 % ( $200$  and  $180 \mu\text{mol dm}^{-3}$ ) respectively. Oxygen saturations this low are known to cause significant impacts on fauna, including commercially important species (Baden et al., 1990; Colijn et al., 2002; Eriksson and Baden, 1997). Low DO was apparent in regions characterised by low advection, high stratification, elevated organic matter production from the spring bloom and a DCM.

Temperature, salinity and DO concentration records were extracted from the ICES database and analysed to investigate whether the low DO concentration events described by Greenwood et al. (2010) were new or reoccurring but only recently observed (Ch. 4). This provided further context for both the 2010 and 2011 field campaigns observations (Ch. 4 & 5). Results highlighted an increase in seasonal oxygen depletion and warming over the past 20 years. Two regions in the central North Sea show evidence of seasonal oxygen depletion in late summer: a site known as the OG, and the region north of the Dogger Bank. The 2010 survey results were consistent with, and reinforced,

the signal of recent depleted oxygen at key locations seen in the historical data.

In order to provide useful policy advice about future developments of seasonal oxygen depletion in the North Sea, it was necessary to determine the mechanisms underlying the consumption and supply of DO within the BML. In August 2011, a similar systematic survey of the North Sea was performed along with the deployment of a Seaglider. Due to an instrument malfunction, the Seaglider was only deployed for a total of 3 days but still acquired 318 profiles over this period. This very high resolution dataset was used to investigate the drivers of organic matter supply to the BML and downward oxygen injection across the pycnocline which regulates the intensity of the seasonal oxygen depletion. Field observations were compared to results from GOTM-BFM, a 1-D coupled physical/biogeochemical model of a ND like site. Due to the short deployment and the glider's proximity to a surface salinity front, determining the spatial and temporal components of the phenomena observed was difficult. The combination of both the glider observations and model estimates did however allow the relative quantification of supply of organic matter from different sources (DCM, benthic respiration and resuspension of accumulated organic matter). Observations of warm water injections into the BML also gave an indication as to the importance of cross-pycnocline mixing and downward supply of oxygen.

Model data and previous studies (Neubacher, 2009) showed benthic respiration played a predominant role in the depletion of BML DO. This emphasises the sensitivity of depocentres; regions of reduced current, such as that identified in August 2010 or the OG, are particularly prone to accumulation of organic matter. This accumulation leads to excessive consumption of DO in the bottom layer. The Seaglider was also able to reveal small scale diapycnal mixing. Due to the short duration of these mixing events, a few hours only, observing them without a high resolution profiling system would have been both impractical and unlikely. These observations showed large amounts of oxygenated water being mixed into the BML. Both DO consumption and supply rates were elevated. This indicates that if

either rates of supply or consumption were to change, the repercussions on BML DO would be significant and rapidly visible. The central North Sea is therefore likely a region highly sensitive to future changes in climate and requires continued observation and modeling efforts to maintain the necessary standards for current legislative obligations.

The hydrographic surveys are repeated most years, however to provide more understanding, an in depth study of the North Sea system would be required. Distribution of central North Sea oxygen depletion was reported to be highly correlated with the NAOI. Ideally, further work should also investigate northern boundary exchanges to determine whether the relation to the dominant NAO mode is from changing regimes of inflow (Atlantic versus Baltic and Channel water) or linked to local atmospheric forcing (changing wind regime over the central North Sea). Investigations into the relation of winter BML temperatures to the intensity of summer stratification would also be of great interest as the duration and strength of stratification is what limits input of DO into the BML. Finally, Seaglider deployment lasting the entire stratified season may help understand the influence of episodic events, such as mixing from storms, but would also permit the observation of season-long oxygen decline, thereby determining the relative importance of DCM and spring bloom production.

## 7.2 THE ROSS SEA

The GOVARS project, led by the Virginia Institute of Marine Science, aimed to investigate the spatial coherence of MCDW intrusions onto the Ross Sea shelf, phytoplankton blooms and influence on DO. Work for this project included the full calibration and quality control of both Seagliders (Ch. 2) and a description of bloom and oxygen dynamics in the region (Ch. 6).

This deployment offered an unprecedented opportunity to observe early season bloom dynamics. Until February, ice generally prevents ship access to the polynya; traditionally, all early season data available were collected from satellite observations or moorings. For the first

time, Seagliders were able to provide high-resolution early-season observations of the Ross Sea polynya, providing both a spatial context not obtainable with moorings and sub-surface observations which cannot be obtained from remote sensing. The two Seagliders observed highly variable watermass properties along a zonal transect from McMurdo Sound to the Ross Bank and in the trough between Ross Bank and Pennell Bank. The timing of the first and largest phytoplankton bloom observed by the Seaglider was found to likely be determined by stratification and stability of phytoplankton in the water column. Further east, it is likely that the bloom intensity, as measured by satellite ocean colour, was enhanced by probable intrusions of MCDW. SG502 only surveyed this region briefly and therefore did not permit accurate identification of MCDW in the region although  $\theta - S$  properties show some evidence of MCDW; this is also supported by Kohut et al. (2013). In particular, the analysis of data from SG502 highlighted that remote sensing observations in the region underestimate chlorophyll *a* concentrations due to the presence of a DCM which cannot be detected from the surface.

The high resolution observations from the gliders were also able to highlight the physical variability in the region, with several different watermasses identified along the zonal transect. The location of these different watermasses is determined by bathymetric features, with fronts located on either side of Ross Bank. Interestingly, chlorophyll *a* and DO concentrations were decoupled from  $\theta - S$  properties. Biological features seemed to be more temporally than spatially dependent with blooms occurring across the entire region rather than being entirely dependent on intrusions of MCDW or constrained to shallower banks.

A method to determine vertical distribution of oxygen production using Seaglider observations highlighted the importance of the DCM and the downward export of organic matter in the regulation of bottom water DO concentrations. Significant limitations were found with the method relating to the assumption that the Seaglider samples a homogeneous water mass over a period longer than required to obtain a signal. The quality of the signal directly relates to the produc-

tion rates and sensor precision. Estimates were greatly impacted by noise in part due to the small Rossby radius at high latitudes and rapid turnover of biological features in the western Ross polynya. As regions of similar water properties were smaller than the distance travelled by the glider over the time required to determine a clear trend in DO, estimates were too noisy to provide significant insight into production rates in the western Ross Sea polynya.

Since this study, Seagliders have been launched with new sensors, including an echosounder, to investigate the relationship between receding ice, plankton biomass and macrofaunal grazing. To build upon the results of the GOVARS study, the deployment of sensors traditionally only available on ships would provide critical information on the mechanisms leading to the start and collapse of the austral spring bloom. Sensors currently in development, such as nitrate and trace metal sensors, would provide valuable information on the constraints and drivers of biological production in this region and would reveal whether the regime is dominated by physical drivers (receding ice, vertical stability) or is entirely dominated by nutrient limitation.

### 7.3 PHYSICAL DRIVERS OF DISSOLVED OXYGEN VARIABILITY

The North and Ross Sea are two very different regions, not only with different physical, chemical and biological properties but also with dramatically different atmospheric forcing and cross-shelf exchange because of ice conditions and bathymetric properties. Despite these differences, the mechanisms which regulate pelagic DO concentrations remain very similar. The North Sea ship surveys showed on a basin-scale that reduced ventilation was the critical element which allowed for seasonal oxygen depletion in off-shore shelf sea waters. This strongly contrasts with coastal hypoxia driven by eutrophication where it is the excessive amount of organic matter production and then remineralisation which tips the balance towards net consumption of DO. Seaglider observations in the Ross Sea showed that phytoplankton blooms, and particularly the DCM, were linked to strong apparent oxygen production signals similarly to the central North Sea.

However, this did not translate into low oxygen at depth as both advective processes and vertical mixing maintained DO concentrations at elevated levels.

The overarching rule that determines the occurrence of DO depletion is that consumption must exceed supply. In shelf seas, where production is often elevated, there is strong potential for remineralisation of produced organic matter and consumption of DO. However, unlike in eutrophic regions, the remineralisation of accumulated organic matter is rarely sufficient to counterbalance both supply originating from primary production and mixing. For seasonal oxygen depletion to occur, consumption must be decoupled from production, generally through sinking of organic matter, and isolated from oxygenated water, generally through strong stratification.

Both of these features were observed in the North Sea, further enhanced by the accumulation of organic matter in depocentres increasing potential for oxygen depletion. In the Ross Sea however, despite the bloom being widespread and there being evidence of organic matter being exported below the photic zone, both advective and vertical mixing processes prevented significant oxygen depletion from occurring over the two months of observations. A critical element missing from both these observations is an estimation of interannual variability. The North Sea has shown significant variability, whereas this remains relatively unknown in the Ross Sea.

In future, Seaglider investigations of dissolved oxygen dynamics would benefit greatly from sensors currently in development. Specific sensor payloads would help better constrain the importance of each process implicated in seasonal oxygen depletion. Both ADCP and microstructure sensors are currently under trial for use on autonomous underwater platforms and have shown potential for measuring both advective flow and cross-pycnocline mixing to quantify supply of dissolved oxygen to isolated watermasses. Nutrient, pH and pCO<sub>2</sub> will also soon be available and will greatly increase the capability of gliders to measure flows of biogenic gases in and out of the ocean and estimate primary production. These sensors currently suffer from either slow response times or short endurance and still require fur-

ther development to be fully field-applicable. The biological aspect of seasonal oxygen dynamics is the most difficult to properly understand through glider data. Optical sensors (fluorescence and backscatter) are the only field ready sensors able to provide estimates of biomass. Several echosounder models are in development but currently focus on larger species (specifically Antarctic krill, *Euphausia superba*) but their use in estimating phyto- and zooplankton populations is difficult due to the lack of accurate models relating acoustic backscatter to biomass. Current best methods for estimating phytoplankton, zooplankton and particulate organic carbon rely on using ratios of different backscatter and fluorescence wavelengths however this method requires large number of *in situ* samples for calibration are very sensitive to environmental variation (irradiance, cloud cover). Development of a portable flow-cytometer has begun for larger low-endurance autonomous underwater vehicles however it is unlikely it will be sufficiently small or energy efficient to integrate on gliders. Through the use of these sensors, it is likely gliders will be better able to quantify the supply and demand of dissolved oxygen in regions exhibiting seasonal oxygen depletion.

#### 7.4 SEAGLIDERS AS TOOLS FOR OCEAN OBSERVATION

Autonomous underwater gliders in general are slowly becoming the instrument of choice for specific types of survey. Their ability to carry a varied sensor load makes them ideally suited to interdisciplinary studies whilst their extended battery life and autonomous nature not only allow for long missions but also access to remote or difficult study sites. Studies such as that by Nicholson et al. (2008) or Alkire et al. (2012) highlight the potential of Seagliders for oceanographic investigations. These studies required a prolonged presence at sea with the ability to imitate Lagrangian platforms in order to follow blooms; the combination of both mobility and endurance is difficult to achieve with other conventional means. This was combined with an adaptive sensor payload, where sampling frequency could be adapted for each biological, chemical and physical sensor to observe

sub-surface features as efficiently as possible. The observations from gliders were then analysed in tandem with *in situ* samples to measure production rates. The added data from *in situ* sampling, ship-borne sensors and satellite observations complemented the Seaglider data to provide a synoptic view of the survey areas and primary productivity dynamics. More recently, a year-long mission of continuously rotating pairs of gliders was run at the Porcupine Abyssal Plain site by the UEA, University of Southampton and CalTech. This study aimed to investigate small scale spatial variability (< 10 km) and vertical mixing processes. This work was not possible with the existing mooring equipment as it did not resolve the spatial variability adequately. The gliders demonstrated the ability to not only resolve the small scale spatial variability but also maintain a persistent presence at a relatively low cost.

Through the diversity of regions and properties investigated, this work provided an excellent opportunity to assess the viability and capabilities of Seagliders as tools for oceanographic observations. The different regions and features investigated within this thesis have highlighted the ability of Seagliders to observe features on a wide range of scales. The gliders demonstrated an ability to observe basin-wide features of the Ross Sea polynya, identifying the location of large watermasses, frontal regions and blooms. At the other end of the scale, the gliders were also able to resolve very short scale features (of the order of hours) when investigating injections of warm oxygenated water into the BML of the central North Sea. Such features could not have been resolved by the ship-based hydrographic surveys performed in 2010 and 2011; doing so would have required the use of a similarly high resolution instrument such as a towed undulating profiler. Gliders excelled at linking different spatial scales of observation over season-long periods; it is the combination of high resolution sampling with mobility and long-term presence which sets them apart from other conventional oceanographic observation tools.

Despite and because of this ability, the use of Seagliders still requires careful consideration during the planning stages. Their biggest deficiency is also linked to their mobility and prolonged presence

at sea. Unlike stationary equipment which track changes over time or ship based surveys and satellite observations which are able to provide a synoptic view of a region, it is not possible to tell what the glider is observing unless the survey has been specifically designed to tease out where or when changes occur. This was particularly pronounced in the Ross Sea where gliders performed a limited number of repeat transects and the optical puck failure on SG503 prevented inter-glider comparisons. In the North Sea mission, the proximity to a front and the poor resolution of satellite imagery relative to the glider transect size also meant that observed changes could not be reliably attributed to changes in time or space. This can be remedied by using multiple gliders simultaneously, repeating transects faster than the timescale of targeted features to avoid aliasing or using multiple platforms. Moorings in particular seem suited to this purpose due to their deployment durations. Another reason that complementing glider deployments with moorings is highly beneficial is the potential for cross calibration. Seagliders are suited to deployments in remote regions with difficult access (i. e. the Ross Sea) or for rapid deployments as they can provide a wealth of data for a relatively short amount of scientist field time; neither situation is suited to repeated ship-based chemical sampling to calibrate glider sensors and identify potential sensor drift. An ideal situation was the Vigo deployment (Ch. 3); SG510 followed a line of moorings allowing for cross-calibration between moorings and the Seaglider. These two issues were those that were most felt when processing and analysing the Seaglider data. Although it is neither evident nor likely that these factors would have changed the conclusions drawn from the data, both the poor calibration and spatio-temporal contextualisation do detract from the confidence that can be put into the numbers obtained. Nevertheless, although the quantitative aspect of the results could be improved with better survey design, they remain valid qualitatively.

Fig. 7.1 highlights the trade-offs involved in planning a Seaglider mission. When planning a Seaglider mission, care must be taken to understand the scientific requirements. The glider's ability to survey a region can be defined by three criteria: mission duration, sampling

resolution and the glider's ability to travel. Endurance of the glider is primarily dependent on remaining battery amperage; however the use of certain sensors can also limit glider endurance by consuming finite reagents or reaching maximum memory storage capacity. Mobility encompasses both horizontal travel and vertical density gradients. Increasing the bladder volume difference between surface and apogee increases the glider's horizontal velocity and density range. This allows the glider to more ground and survey areas of with greater density gradients. This requires additional pumping and increases the energy demand of the glider. Increasing sensor sampling resolution leads to a direct increase in energy demand. For the default sensors, this represents a minimal increase. However, continuous sampling from active sensors such as Wetlabs ECO puck, ADCP, and echosounder can reduce a Seaglider's endurance to less than a month. The various deployments discussed in the thesis have been indicated on Fig. 7.1 for context. During the North Sea deployment, the glider consumed large amounts of power to counter tidal currents and the strong density gradient while sampling at maximum frequency. The DISGO deployment (Ch. 3), on the other hand, reduced sampling frequency and mission duration in order to maintain adequate flight throughout the extreme density gradient ( $> 6 \text{ kg m}^{-3}$ ). Finally, the glider had to be recovered at the end of the GOPINA mission as it had exceeded the maximum number of files which could be stored on the memory card. The other missions were more balanced in terms energy trade-offs in order to answer the specific scientific questions of the experiment.

Seagliders remain a recent technological advance in the field of oceanography. Over the course of this doctorate, there has been a rapid increase in uptake of Seagliders and similar instruments by oceanographic and marine monitoring institutions. iRobot began commercial distribution of Seagliders in 2009 and these have now been licensed to Kongsberg. Seagliders are becoming of particular interest in both integrated monitoring systems and targeted experiments because of their unique capabilities. This work has been an important stepping stone for developing both methods and confidence in

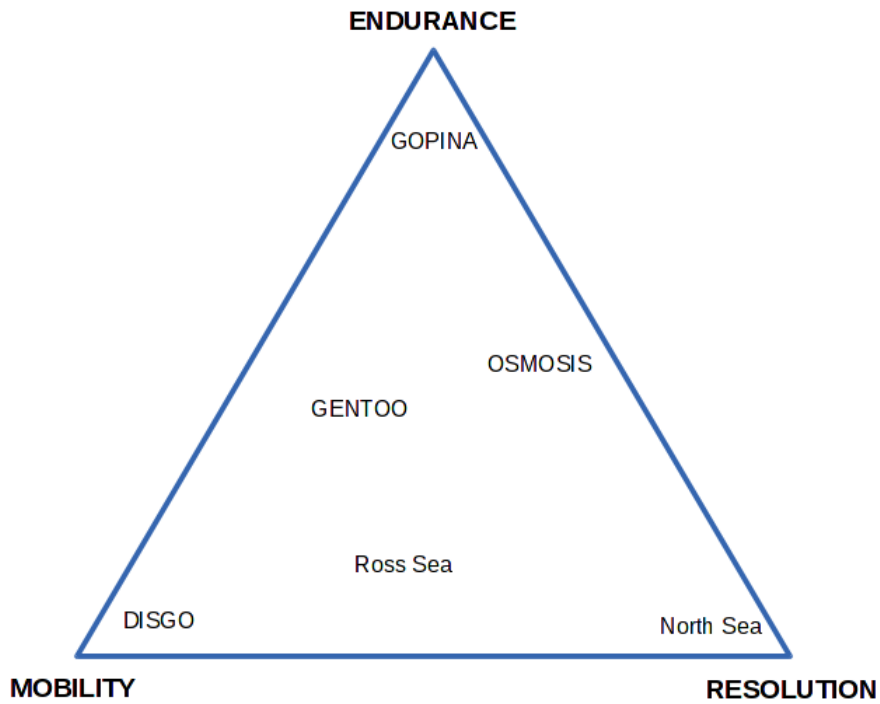


Figure 7.1: Seaglider mission trade-off triangle. When planning a Seaglider mission, the user must identify the requirements to answer the scientific question.

Seagliders as instruments for oceanographic research internationally. As we, as a community, learn to make best use of Seagliders and improve both survey design and our confidence in Seaglider observations, they will become critical tools for improving models by providing observations along multiple scales of interest. At the same time, they will be able to maintain a persistent presence to fully assess variability and provide continuous monitoring to satisfy new criteria for marine legislation.



## BIBLIOGRAPHY

---

- Aanderaa Data Instruments (2009). TD 269: Operating manual oxygen optode 4330, 4835. Technical report, Aanderaa Data Instruments, Bergen.
- Alkire, M. B., D'Asaro, E., Lee, C., Jane Perry, M., Gray, A., Cetinić, I., Briggs, N., Rehm, E., Kallin, E., Kaiser, J., and González-Posada, A. (2012). Estimates of net community production and export using high-resolution, Lagrangian measurements of O<sub>2</sub>, NO<sub>3</sub><sup>-</sup>, and POC through the evolution of a spring diatom bloom in the North Atlantic. *Deep Sea Research Part I: Oceanographic Research Papers*, 64:157–174.
- Arrigo, K. R., DiTullio, G. R., Dunbar, R. B., Robinson, D. H., VanWoert, M., Worthen, D. L., and Lizotte, M. P. (2000). Phytoplankton taxonomic variability in nutrient utilization and primary production in the Ross Sea. *Journal of Geophysical Research*, 105(C4):8827–8846.
- Arrigo, K. R., Robinson, D. H., Worthen, D. L., Dunbar, R. B., DiTullio, G. R., Van Woert, M., and Lizotte, M. P. (1999). Phytoplankton community structure and the drawdown of nutrients and CO<sub>2</sub> in the Southern Ocean. *Science*, 283(5400):365–367.
- Arrigo, K. R. and van Dijken, G. L. (2003). Phytoplankton dynamics within 37 Antarctic coastal polynya systems. *Journal of Geophysical Research*, 108(C8):3271.
- Arrigo, K. R. and van Dijken, G. L. (2004). Annual changes in sea-ice, chlorophyll a, and primary production in the Ross Sea, Antarctica. *Deep Sea Research Part II: Topical Studies in Oceanography*, 51(1-3):117–138.

- Arrigo, K. R., Weiss, A. M., and Smith, W. O. (1998). Physical forcing of phytoplankton dynamics in the southwestern Ross Sea. *Journal of Geophysical Research*, 103(C1):1007–1021.
- Asper, V. L., Smith Jr, W. O., Lee, C., Gobat, J., Heywood, K. J., Queste, B. Y., and Dinniman, M. (2011). Using gliders to study a phytoplankton bloom in the Ross Sea, Antarctica. In *OCEANS 2011*, pages 1–7.
- Baden, S. P., Pihl, L., and Rosenberg, R. (1990). Effects of oxygen depletion on the ecology, blood physiology and fishery of the Norway lobster *Nephrops norvegicus*. *Marine Ecology Progress Series*, 67:141–155.
- Baretta, J. W., Ebenhöh, W., and Ruardij, P. (1995). The European regional seas ecosystem model, a complex marine ecosystem model. *Netherlands Journal of Sea Research*, 33(3-4):233–246.
- Beaugrand, G., Edwards, M., Brander, K., Luczak, C., and Ibanez, F. (2008). Causes and projections of abrupt climate-driven ecosystem shifts in the North Atlantic. *Ecology letters*, 11(11):1157–68.
- Beaumont, N. J., Austen, M. C., Atkins, J. P., Burdon, D., Degraer, S., Dentinho, T. P., Deros, S., Holm, P., Horton, T., van Ierland, E., Marboe, A. H., Starkey, D. J., Townsend, M., and Zarzycki, T. (2007). Identification, definition and quantification of goods and services provided by marine biodiversity: implications for the ecosystem approach. *Marine pollution bulletin*, 54(3):253–65.
- Behrenfeld, M. J., O'Malley, R. T., Siegel, D. A., McClain, C. R., Sarmiento, J. L., Feldman, G. C., Milligan, A. J., Falkowski, P. G., Letelier, R. M., and Boss, E. S. (2006). Climate-driven trends in contemporary ocean productivity. *Nature*, 444(7120):752–5.
- Benson, B. B. and Krause Jr., D. (1984). The concentration and isotopic fractionation of oxygen dissolved in freshwater and seawater in equilibrium with the atmosphere. *Limnology and Oceanography*, 29:620–632.

- Berx, B. and Hughes, S. L. (2009). Climatology of surface and near-bed temperature and salinity on the north-west European continental shelf for 1971–2000. *Continental Shelf Research*, 29(19):2286–2292.
- Best, M. A., Wither, A. W., and Coates, S. (2007). Dissolved oxygen as a physico-chemical supporting element in the Water Framework Directive. *Marine pollution bulletin*, 55(1-6):53–64.
- Bishop, C. (2008). *Sensor dynamics of autonomous underwater gliders*. M.sc. thesis, Memorial University of Newfoundland.
- Boyd, P., Doney, S., Strzeppek, R., Dusenberry, J., Lindsay, K., and Fung, I. (2008). Climate-mediated changes to mixed-layer properties in the Southern Ocean: assessing the phytoplankton response. *Biogeosciences*, 5:847–864.
- Bozec, Y., Thomas, H., Elkalay, K., and de Baar, H. J. W. (2005). The continental shelf pump for CO<sub>2</sub> in the North Sea - evidence from summer observation. *Marine Chemistry*, 93(2-4):131–147.
- Briggs, N., Perry, M. J., Cetinić, I., Lee, C., D'Asaro, E., Gray, A. M., and Rehm, E. (2011). High-resolution observations of aggregate flux during a sub-polar North Atlantic spring bloom. *Deep Sea Research Part I: Oceanographic Research Papers*, 58(10):1031–1039.
- Brown, J., Hill, A. E., Fernand, L., and Horsburgh, K. J. (1999). Observations of a Seasonal Jet-like Circulation at the Central North Sea Cold Pool Margin. *Estuarine, Coastal and Shelf Science*, 48(3):343–355.
- Buffoni, G., Cappelletti, A., and Picco, P. (2002). An investigation of thermohaline circulation in Terra Nova Bay polynya. *Antarctic Science*, 14(1):83–92.
- Burchard, H., Bolding, K., and Villarreal, M. (1999). GOTM, a general ocean turbulence model: theory, implementation and test cases. *Tech. Rep. EUR 18745 EN, European Commission*.
- Caddy, J. F. (1993). Toward a comparative evaluation of human impacts on fishery ecosystems of enclosed and semi-enclosed seas. *Reviews in Fisheries Science*, 1(1):57–95.

- Carritt, D. and Carpenter, J. (1966). Comparison and evaluation of currently employed modifications of the Winkler method for determining dissolved oxygen in seawater; a NASCO report. *Journal of Marine Research*, 24:286–318.
- Colijn, F., Hesse, K.-J., Ladwig, N., and Tillmann, U. (2002). Effects of the large-scale uncontrolled fertilisation process along the continental coastal North Sea. *Hydrobiologia*, 484(1-3):133–148.
- Conkright, M. E., Antonov, J. I., Baranova, O., Boyer, T. P., Garcia, H. E., Gelfeld, R., Johnson, D., Locarnini, R. A., Murphy, P. P., O'Brien, T. D., Smolyar, I., and Stephens, C. (2002). *World Ocean Database 2001, Volume 1: Introduction*. U.S. Gov. Printing Office, Washington D.C., noaa atlas edition.
- Conley, D. J., Björck, S., Bonsdorff, E., Carstensen, J., Destouni, G., Gustafsson, B. G., Hietanen, S., Kortekaas, M., Kuosa, H., Meier, H. E. M., Müller-Karulis, B., Nordberg, K., Norkko, A., Nürnberg, G., Pitkänen, H., Rabalais, N. N., Rosenberg, R., Savchuk, O. P., Slomp, C. P., Voss, M., Wulff, F., and Zillén, L. (2009a). Hypoxia-related processes in the Baltic Sea. *Environmental science & technology*, 43(10):3412–20.
- Conley, D. J., Paerl, H., Howarth, R., Boesch, D., Seitzinger, S., Havens, K., Lancelot, C., and Likens, G. (2009b). Controlling eutrophication: nitrogen and phosphorus. *Science*, 323(5917):1014–1015.
- Couceiro, F., Fones, G. R., Thompson, C. E. L., Statham, P. J., Sivyer, D. B., Parker, R., Kelly-Gerreyn, B. A., and Amos, C. L. (2013). Impact of resuspension of cohesive sediments at the Oyster Grounds (North Sea) on nutrient exchange across the sediment-water interface. *Biogeochemistry*, 113(1-3):37–52.
- Cullen, J. J. (1982). The Deep Chlorophyll Maximum: Comparing Vertical Profiles of Chlorophyll a. *Canadian Journal of Fisheries and Aquatic Sciences*, 39(5):791–803.
- Davies, J. M. and Payne, R. (1984). Supply of organic matter to the sediment in the northern North Sea during a spring phytoplankton bloom. *Marine Biology*, 78(3):315–324.

- Davis, R. E., Eriksen, C., and Jones, C. (2003). Autonomous buoyancy-driven underwater gliders. In Griffiths, G., editor, *The Technology and Applications of Autonomous Underwater Vehicles*, pages 37–58. Taylor & Francis, London.
- de Jonge, V. N., Bakker, J. F., and Van Stralen, M. (1996). Recent changes in the contributions of river Rhine and North Sea to the eutrophication of the western Dutch Wadden Sea. *Netherlands Journal of Aquatic Ecology*, 30(1):27–39.
- Diaz, R. J. (2001). Overview of hypoxia around the world. *Journal of environmental quality*, 30(2):275–81.
- Diaz, R. J. and Rosenberg, R. (2008). Spreading dead zones and consequences for marine ecosystems. *Science*, 321(5891):926–9.
- Dinniman, M., Klinck, J. M., and Smith, W. O. (2011). A model study of Circumpolar Deep Water on the West Antarctic Peninsula and Ross Sea continental shelves. *Deep Sea Research Part II: Topical Studies in Oceanography*, 58(13-16):1508–1523.
- Dippner, J. W. (1997). SST anomalies in the north sea in relation to the North Atlantic Oscillation and the influence on the theoretical spawning time of fish. *Deutsche Hydrographische Zeitschrift*, 49(2-3):267–275.
- Dooley, H. D. (1974). Hypotheses concerning the circulation of the northern North Sea. *ICES Journal of Marine Science*, 36(1):54–61.
- Ducrotoy, J.-P., Elliott, M., and de Jonge, V. N. (2000). The North Sea. *Marine Pollution Bulletin*, 41(1-6):5–23.
- Egbert, G. D., Erofeeva, S. Y., and Ray, R. D. (2010). Assimilation of altimetry data for nonlinear shallow-water tides: Quarter-diurnal tides of the Northwest European Shelf. *Continental Shelf Research*, 30(6):668–679.
- Ekau, W., Auel, H., Pörtner, H. O., and Gilbert, D. (2010). Impacts of hypoxia on the structure and processes in the pelagic community (zooplankton, macro-invertebrates and fish). *Biogeosciences* . . . , 7:1669–1699.

- Eppley, R. (1972). Temperature and phytoplankton growth in the sea. *Fishery Bulletin*, 70(4):1063–1085.
- Eriksen, C. C. (1997). Instrumentation for physical oceanography: the last two decades and beyond. In *Proceedings of the NSF APROPOS Workshop*, Asilomar, CA.
- Eriksen, C. C., Osse, T. J., Light, R. D., Wen, T., Lehman, T. W., Sabin, P. L., Ballard, J. W., and Chiodi, A. M. (2001). Seaglider: a long-range autonomous underwater vehicle for oceanographic research. *IEEE Journal of Oceanic Engineering*, 26(4):424–436.
- Eriksson, S. P. and Baden, S. P. (1997). Behaviour and tolerance to hypoxia in juvenile Norway lobster (*Nephrops norvegicus*) of different ages. *Marine Biology*, 128(1):49–54.
- Fernand, L., Nolan, G., Raine, R., Chambers, C., Dye, S., White, M., and Brown, J. (2006). The Irish coastal current: A seasonal jet-like circulation. *Continental Shelf Research*, 26(15):1775–1793.
- Fernand, L., Weston, K., Morris, T., Greenwood, N., Brown, J., and Jickells, T. (2013). The contribution of the deep chlorophyll maximum to primary production in a seasonally stratified shelf sea, the North Sea. *Biogeochemistry*, 113(1-3):153–166.
- Fettweis, M., Monbaliu, J., Baeye, M., Nechad, B., and Van den Eynde, D. (2012). Weather and climate induced spatial variability of surface suspended particulate matter concentration in the North Sea and the English Channel. *Methods in Oceanography*, 3-4(September - December 2012):25–39.
- Foden, J., Devlin, M. J., Mills, D. K., and Malcolm, S. J. (2011). Searching for undesirable disturbance: an application of the OSPAR eutrophication assessment method to marine waters of England and Wales. *Biogeochemistry*, 106(2):157–175.
- Fofonoff, N., Hayes, S., and Millard, R. (1974). WHOI/Brown CTD microprofiler: methods of calibration and data handling. Technical Report 083, Woods Hole Oceanographic Institution, Woods Hole, Massachusetts.

- Fonselius, S. and Valderrama, J. (2003). One hundred years of hydrographic measurements in the Baltic Sea. *Journal of Sea Research*, 49(4):229–241.
- Frajka-Williams, E., Rhines, P. B., and Eriksen, C. C. (2009). Physical controls and mesoscale variability in the Labrador Sea spring phytoplankton bloom observed by Seaglider. *Deep Sea Research Part I: Oceanographic Research Papers*, 56(12):2144–2161.
- Garau, B., Ruiz, S., Zhang, W. G., Pascual, A., Heslop, E., Kerfoot, J., and Tintoré, J. (2011). Thermal Lag Correction on Slocum CTD Glider Data. *Journal of Atmospheric and Oceanic Technology*, 28(9):1065–1071.
- García, H. and Gordon, L. (1992). Oxygen solubility in seawater: Better fitting equations. *Limnology and Oceanography*, 37(6):1307–1312.
- GEBCO (2010). The GEBCO\_o8 Grid, version 20100927.
- Glud, R. (2008). Oxygen dynamics of marine sediments. *Marine Biology Research*, 4(4):243–289.
- Gray, J. S., Wu, R. S., and Or, Y. Y. (2002). Effects of hypoxia and organic enrichment on the coastal marine environment. *Marine Ecology Progress Series*, 238:249–279.
- Greenwood, N., Parker, E. R., Fernand, L., Sivyer, D. B., Weston, K., Painting, S. J., Kröger, S., Forster, R. M., Lees, H. E., Mills, D. K., and Laane, R. W. P. M. (2010). Detection of low bottom water oxygen concentrations in the North Sea; implications for monitoring and assessment of ecosystem health. *Biogeosciences*, 7(4):1357–1373.
- Hahn, J. (2013). *Oxygen Variability and Eddy-driven Meridional Oxygen Supply in the Tropical North East Atlantic Oxygen Minimum Zone*. PhD thesis, Helmholtz Centre for Ocean Research Kiel.
- Hales, B. and Takahashi, T. (2004). High-resolution biogeochemical investigation of the Ross Sea, Antarctica, during the AESOPS (U. S. JGOFS) Program. *Global Biogeochemical Cycles*, 18(3).

- Helly, J. J. and Levin, L. A. (2004). Global distribution of naturally occurring marine hypoxia on continental margins. *Deep Sea Research Part I: Oceanographic Research Papers*, 51(9):1159–1168.
- Hill, A., Brown, J., Fernand, L., Holt, J., Horsburgh, K., Proctor, R., Raine, R., and Turrell, W. (2008). Thermohaline circulation of shallow tidal seas. *Geophysical Research Letters*, 35(11):L11605.
- Hofmann, A. F., Soetaert, K., and Middelburg, J. J. (2008). Present nitrogen and carbon dynamics in the Scheldt estuary using a novel 1-D model. *Biogeosciences*, 5:981–1006.
- Howe, B. M., McGinnis, T., and Boyd, M. L. (2007). Sensor Network Infrastructure: Moorings, Mobile Platforms, and Integrated Acoustics. *2007 Symposium on Underwater Technology and Workshop on Scientific Use of Submarine Cables and Related Technologies*, pages 47–51.
- ICES (1983). Flushing times of the North Sea. *ICES Cooperative Research Report*, 123.
- IRobot (2012). Seaglider 1KA User Guide, Revision D.
- Jago, C., Jones, S., Latter, R., McCandliss, R., Hearn, M., and Howarth, M. (2002). Resuspension of benthic fluff by tidal currents in deep stratified waters, northern North Sea. *Journal of Sea Research*, 48(4):259–269.
- Jago, C., Jones, S., Sykes, P., and Rippeth, T. (2006). Temporal variation of suspended particulate matter and turbulence in a high energy, tide-stirred, coastal sea: Relative contributions of resuspension and disaggregation. *Continental Shelf Research*, 26(17-18):2019–2028.
- Jickells, T. D. (1998). Nutrient Biogeochemistry of the Coastal Zone. *Science*, 281(5374):217–222.
- Justić, D., Turner, R. E., and Rabalais, N. N. (2003). Climatic influences on riverine nitrate flux: Implications for coastal marine eutrophication and hypoxia. *Estuaries*, 26(1):1–11.
- Keeling, R. F., Körtzinger, A., and Gruber, N. (2010). Ocean Deoxygenation in a Warming World. *Annual Review of Marine Science*, 2(1):199–229.

- Kemp, W. M., Sampou, P., Caffrey, J., Mayer, M., Henriksen, K., and Boynton, W. R. (1990). Ammonium recycling versus denitrification in Chesapeake Bay sediments. *Limnology and Oceanography*, 35(7):1545–1563.
- Kemp, W. M. and Testa, J. M. (2009). Coastal hypoxia responses to remediation. *Biogeosciences*, 6:1985–3008.
- Kohut, J., Hunter, E., and Huber, B. (2013). Small-scale variability of the cross-shelf flow over the outer shelf of the Ross Sea. *Journal of Geophysical Research: Oceans*, 118(4):1863–1876.
- Kröncke, I. and Knust, R. (1995). The Dogger Bank: A special ecological region in the central North Sea. *Helgoländer Meeresuntersuchungen*, 49(1-4):335–353.
- Lefort, S., Gratton, Y., Mucci, a., Dadou, I., and Gilbert, D. (2012). Hypoxia in the Lower St. Lawrence Estuary: How physics controls spatial patterns. *Journal of Geophysical Research*, 117(C7):C07018.
- Lenhart, H.-J., Mills, D. K., Baretta-Bekker, H., van Leeuwen, S. M., van der Molen, J., Baretta, J. W., Blaas, M., Desmit, X., Kühn, W., Lacroix, G., Los, H. J., Ménesguen, A., Neves, R., Proctor, R., Ruardij, P., Skogen, M. D., Vanhoutte-Brunier, A., Villars, M. T., and Wakelin, S. L. (2010). Predicting the consequences of nutrient reduction on the eutrophication status of the North Sea. *Journal of Marine Systems*, 81(1-2):148–170.
- Lenhart, H. J., Pätsch, J., Kühn, W., Moll, A., and Pohlmann, T. (2004). Investigation on the trophic state of the North Sea for three years (1994-1996) simulated with the ecosystem model ERSEM - the role of a sharp NAOI decline. *Biogeosciences Discussions*, 1:725–754.
- Lenhart, H. J., Radach, G., Backhaus, J. O., and Pohlmann, T. (1995). Simulations of the north sea circulation, its variability, and its implementation as hydrodynamical forcing in ERSEM. *Netherlands Journal of Sea Research*, 33(3-4):271–299.

- Lenhart, H. J., Radach, G., and Ruardij, P. (1997). The effects of river input on the ecosystem dynamics in the continental coastal zone of the North Sea using ERSEM. *Journal of Sea Research*, 38(3-4):249–274.
- Martínez, M. L., Intralawan, A., Vázquez, G., Pérez-Maqueo, O., Sutton, P., and Landgrave, R. (2007). The coasts of our world: Ecological, economic and social importance. *Ecological Economics*, 63(2-3):254–272.
- McQuatters-Gollop, A., Raitzos, D. E., Edwards, M., Pradhan, Y., Mee, L. D., Lavender, S. J., and Attrill, M. J. (2007). A long-term chlorophyll data set reveals regime shift in North Sea phytoplankton biomass unconnected to nutrient trends. *Limnology and Oceanography*, 52(2):635–648.
- Mee, L. D., Friedrich, J., and Gomoiu, M. T. (2005). Restoring the Black Sea in times of uncertainty. *Oceanography*, 18(2):32–43.
- Meyer, E. M., Pohlmann, T., and Weisse, R. (2011). Thermodynamic variability and change in the North Sea (1948–2007) derived from a multidecadal hindcast. *Journal of Marine Systems*, 86(3-4):35–44.
- Middelburg, J. J. and Levin, L. A. (2009). Coastal hypoxia and sediment biogeochemistry. *Biogeosciences Discussions*, 6:1273–1293.
- Moodley, L., Middelburg, J. J., Herman, P. M. J., Soetaert, K., and de Lange, G. J. (2005). Oxygenation and organic-matter preservation in marine sediments: Direct experimental evidence from ancient organic carbon-rich deposits. *Geology*, 33(11):889–892.
- Morison, J., Andersen, R., Larson, N., D'Asaro, E., and Boyd, T. (1994). The correction for thermal-lag effects in Sea-Bird CTD data. *Journal of Atmospheric and Oceanic Technology*, 11:1151–1164.
- Mundy, C. J. and Barber, D. G. (2001). On the relationship between spatial patterns of sea-ice type and the mechanisms which create and maintain the North Water (NOW) polynya. *Atmosphere-Ocean*, 39(3):327–341.
- Neubacher, E. (2009). *Oxygen and nitrogen cycling in sediments of the southern North Sea*. PhD thesis, Queen Mary, University of London.

- Nicholson, D., Emerson, S., and Eriksen, C. (2008). Net community production in the deep euphotic zone of the subtropical North Pacific gyre from glider surveys. *Limnology and Oceanography*, 53(5, part 2):2226–2236.
- Nixon, S. (1982). Remineralization and nutrient cycling in coastal marine ecosystems. In Neilson, B. J. and Cronin, L. E., editors, *Estuaries and Nutrients*, pages 111–138. Humana Press, New York, NY.
- Orsi, A. H. and Wiederwohl, C. L. (2009). A recount of Ross Sea waters. *Deep Sea Research Part II: Topical Studies in Oceanography*, 56(13-14):778–795.
- Osborn, T. J. (2011). Winter 2009/2010 temperatures and a record-breaking North Atlantic Oscillation index. *Weather*, 66(1):19–21.
- Otto, L., Zimmerman, J. T. F., Furnes, G. K., Mork, M., Saetre, R., and Becke, G. (1990). Review of the physical oceanography of the North Sea. *Netherlands Journal of Sea Research*, 26(2-4):161–238.
- Painting, S. J., Devlin, M. J., Rogers, S. I., Mills, D. K., Parker, E. R., and Rees, H. L. (2005). Assessing the suitability of OSPAR EcoQOs for eutrophication vs ICES criteria for England and Wales. *Marine pollution bulletin*, 50(12):1569–84.
- Peloquin, J. A. and Smith, W. O. (2007). Phytoplankton blooms in the Ross Sea, Antarctica: Interannual variability in magnitude, temporal patterns, and composition. *Journal of Geophysical Research*, 112(Humana Press):1–12.
- Pena, M., Katsev, S., Oguz, T., and Gilbert, D. (2010). Modeling dissolved oxygen dynamics and hypoxia. *Biogeosciences*, 7:933–957.
- Perry, M. J., Sackmann, B. S., Eriksen, C., and Lee, C. M. (2008). Sea-glider observations of blooms and subsurface chlorophyll maxima off the Washington coast. *Limnology and Oceanography Special Issue on Autonomous and Lagrangian Platforms and Sensors (ALPS)*, 53(5 part 2):2169–2179.

- Pörtner, H. O. and Knust, R. (2007). Climate change affects marine fishes through the oxygen limitation of thermal tolerance. *Science*, 315(5808):95–7.
- Postma, H. and Zijlstra, J. (1988). *Ecosystems of the world, Vol. 27. Continental shelves*. Elsevier, Amsterdam, illustrate edition.
- Powell, T. (1995). Physical and biological scales of variability in lakes, estuaries, and the coastal ocean. In Powell, T. M. and Steele, J. H., editors, *Ecological time series*, chapter Part II, pages 119–138. Springer US, New York, NY.
- Queste, B. Y., Fernand, L., Jickells, T. D., and Heywood, K. J. (2013). Spatial extent and historical context of North Sea oxygen depletion in August 2010. *Biogeochemistry*, 113(1-3):53–68.
- Queste, B. Y., Heywood, K. J., Kaiser, J., Lee, G. a., Matthews, A., Schmidtko, S., Walker-Brown, C., and Woodward, S. W. (2012). Deployments in extreme conditions: Pushing the boundaries of Seaglider capabilities. In *2012 IEEE/OES Autonomous Underwater Vehicles (AUV)*, pages 1–7. IEEE.
- Rabalais, N. N., Levin, L. A., Turner, R. E., Gilbert, D., and Zhang, J. (2010). Dynamics and distribution of natural and human-caused coastal hypoxia. *Biogeosciences*, 7:585–619.
- Rabalais, N. N., Turner, R. E., Diaz, R. J., and Justić, D. (2009). Global change and eutrophication of coastal waters. *ICES Journal of Marine Science*, 66(7):1528–1537.
- Rabalais, N. N., Turner, R. E., and Wiseman, W. J. (2002). Gulf of Mexico hypoxia, A.K.A "The Dead Zone". *Annual Review of Ecology and Systematics*, 33(1):235–263.
- Reddy, T. E. and Arrigo, K. R. (2006). Constraints on the extent of the Ross Sea phytoplankton bloom. *Journal of Geophysical Research*, 111(C07005):1–8.
- Reid, P., Lancelot, C., Gieskes, W., Hagmeier, E., and Weichart, G. (1990). Phytoplankton of the North Sea and its dynamics: A review. *Netherlands Journal of Sea Research*, 26(2-4):295–331.

- Rodwell, M., Rowell, D., and Folland, C. (1999). Oceanic forcing of the wintertime North Atlantic Oscillation and European climate. *Nature*, 398:320–323.
- Rosenberg, R., Agrenius, S., Hellman, B., Nilsson, H. C., and Norling, K. (2002). Recovery of marine benthic habitats and fauna in a Swedish fjord following improved oxygen conditions. *Marine ecology progress series*, 234:43–53.
- Rosenberg, R., Hellman, B., and Johansson, B. (1991). Hypoxic tolerance of marine benthic fauna. *Marine Ecology Progress Series*, 79:127–131.
- Ruardij, P., Van Haren, H., and Ridderinkhof, H. (1997). The impact of thermal stratification on phytoplankton and nutrient dynamics in shelf seas: a model study. *Journal of Sea Research*, 38(3-4):311–331.
- Rudnick, D. L. and Cole, S. T. (2011). On sampling the ocean using underwater gliders. *Journal of Geophysical Research*, 116(C08010).
- Rudnick, D. L., Davis, R. E., Eriksen, C., Fratantoni, D. M., and Perry, M. J. (2004). Underwater gliders for ocean research. *Marine Technology Society Journal*, 38(1):48–49.
- Sackmann, B. S., Perry, M. J., and Eriksen, C. (2008). Seaglider observations of variability in daytime fluorescence quenching of chlorophyll-a in Northeastern Pacific coastal waters. *Biogeosciences Discussions*, 5(4):2839–2865.
- Sathyendranath, S., Stuart, V., Nair, A., Oka, K., Nakane, T., Bouman, H., Forget, M. H., Maass, H., and Platt, T. (2009). Carbon-to-chlorophyll ratio and growth rate of phytoplankton in the sea. *Marine Ecology Progress Series*, 383:73–84.
- Scarlet, R. (1975). A data processing method for salinity, temperature, depth profiles. *Deep Sea Research and Oceanographic Abstracts*, 22(7):509–515.
- Scavia, D. and Donnelly, K. A. (2007). Reassessing hypoxia forecasts for the Gulf of Mexico. *Environmental science & technology*, 41(23):8111–7.

- Sedwick, P. N. and DiTullio, G. R. (1997). Regulation of algal blooms in Antarctic Shelf Waters by the release of iron from melting sea ice. *Geophysical Research Letters*, 24(20):2515–2518.
- Sedwick, P. N., Marsay, C. M., Sohst, B. M., Aguilar-Islas, A. M., Lohan, M. C., Long, M. C., Arrigo, K. R., Dunbar, R. B., Saito, M. A., Smith, W. O., and DiTullio, G. R. (2011). Early season depletion of dissolved iron in the Ross Sea polynya: Implications for iron dynamics on the Antarctic continental shelf. *Journal of Geophysical Research*, 116(C12019).
- Sharples, J., Ross, O., Scott, B., Greenstreet, S., and Fraser, H. (2006). Inter-annual variability in the timing of stratification and the spring bloom in the North-western North Sea. *Continental Shelf Research*, 26(6):733–751.
- Simpson, J., Hughes, D., and Morris, N. (1977). The relation of seasonal stratification to tidal mixing on the continental shelf. *Deep-Sea Research*, 24:327–340.
- Skogen, M. D. and Moll, A. (2005). Importance of ocean circulation in ecological modeling: An example from the North Sea. *Journal of Marine Systems*, 57(3-4):289–300.
- Smith, W. O., Asper, V. L., Tozzi, S., Liu, X., and Stammerjohn, S. E. (2011a). Surface layer variability in the Ross Sea, Antarctica as assessed by in situ fluorescence measurements. *Progress In Oceanography*, 88(1-4):28–45.
- Smith, W. O. and Comiso, J. C. (2008). Influence of sea ice on primary production in the Southern Ocean: A satellite perspective. *Journal of Geophysical Research*, 113(C5S95):1–19.
- Smith, W. O. and Gordon, L. I. (1997). Hyperproductivity of the Ross Sea (Antarctica) polynya during austral spring. 24(3):233–236.
- Smith, W. O., Marra, J., and Hiscock, M. (2000). The seasonal cycle of phytoplankton biomass and primary productivity in the Ross Sea, Antarctica. *Deep Sea Research Part II*, 47:3119–3140.

- Smith, W. O., Shields, A. R., Dreyer, J. C., Peloquin, J. A., and Asper, V. L. (2011b). Interannual variability in vertical export in the Ross Sea: Magnitude, composition, and environmental correlates. *Deep Sea Research Part I: Oceanographic Research Papers*, 58(2):147–159.
- Smith, W. O., Shields, A. R., Peloquin, J. A., Catalano, G., Tozzi, S., Dinniman, M., and Asper, V. L. (2006). Interannual variations in nutrients, net community production, and biogeochemical cycles in the Ross Sea. *Deep Sea Research Part II: Topical Studies in Oceanography*, 53(8-10):815–833.
- Stössel, A., Yang, K., and Kim, S. (2002). On the role of sea ice and convection in a global ocean model. *Journal of physical oceanography*, 32:1194–1208.
- Stramma, L., Johnson, G. C., Sprintall, J., and Mohrholz, V. (2008). Expanding oxygen-minimum zones in the tropical oceans. *Science*, 320(5876):655–8.
- Stramma, L., Prince, E. D., Schmidtko, S., Luo, J., Hoolihan, J. P., Visbeck, M., Wallace, D. W. R., Brandt, P., and Körtzinger, A. (2012). Expansion of oxygen minimum zones may reduce available habitat for tropical pelagic fishes. *Nature Climate Change*, 2(1):33–37.
- Stramma, L., Schmidtko, S., Levin, L. A., and Johnson, G. C. (2010). Ocean oxygen minima expansions and their biological impacts. *Deep Sea Research Part I: Oceanographic Research Papers*, 57(4):587–595.
- Suratman, S., Jickells, T. D., Weston, K., and Fernand, L. (2008). Seasonal variability of inorganic and organic nitrogen in the North Sea. *Hydrobiologia*, 610(1):83–98.
- Tengberg, A., Almroth, E., Hall, P. O. J., Kononets, M., Nilsson, M., and Viktorsson, L. (2010). Use of a Seaguard and Fast Response Optodes in the Study of Oxygen Dynamics in the Baltic Sea. Technical Report 979, Aanderaa Data Instruments, Bergen.
- Tengberg, A. and Hovdenes, J. (2013). Updated information on long-term stability and accuracy of Aanderaa oxygen optodes. Inform-

- ation about multipoint calibration system and sensor option overview. Technical report, Aanderaa Data Instruments, Bergen.
- Tengberg, A., Hovdenes, J., Andersson, H. J., Brocandel, O., Diaz, R. J., Herbert, D., Arnerich, T., Huber, C., Körtzinger, A., Khripounoff, A., Rey, F., Rønning, C., Schimanski, J., Sommer, S., and Stangelmayer, A. (2006). Evaluation of a lifetime-based optode to measure oxygen in aquatic systems. *Limnology and Oceanography: Methods*, 4(1964):7–17.
- Tett, P., Gowen, R., Mills, D. K., Fernandes, T., Gilpin, L., Huxham, M., Kennington, K., Read, P., Service, M., Wilkinson, M., and Malcolm, S. (2007). Defining and detecting undesirable disturbance in the context of marine eutrophication. *Marine pollution bulletin*, 55(1-6):282–97.
- Thomas, H., Bozec, Y., De Baar, H. J. W., Elkalay, K., Frankignoulle, M., Schiettecatte, L., Kattner, G., and Borges, A. V. (2005). The carbon budget of the North Sea. *Biogeosciences*, 2(1):87–96.
- Thomas, H., Bozec, Y., Elkalay, K., and de Baar, H. J. W. (2004). Enhanced open ocean storage of CO<sub>2</sub> from shelf sea pumping. *Science*, 304(5673):1005–1008.
- Thompson, C., Couceiro, F., Fones, G., Helsby, R., Amos, C. L., Black, K., Parker, E., Greenwood, N., Statham, P., and Kelly-Gerreyn, B. (2011). In situ flume measurements of resuspension in the North Sea. *Estuarine, Coastal and Shelf Science*, 94(1):77–88.
- Ting, M., Kushnir, Y., Seager, R., and Li, C. (2009). Forced and Internal Twentieth-Century SST Trends in the North Atlantic. *Journal of Climate*, 22(6):1469–1481.
- Turner, R. E., Rabalais, N. N., and Justić, D. (2006). Predicting summer hypoxia in the northern Gulf of Mexico: riverine N, P, and Si loading. *Marine pollution bulletin*, 52(2):139–48.
- Turrell, W., Henderson, E., Slessor, G., Payne, R., and Adams, R. (1992). Seasonal changes in the circulation of the northern North Sea. *Continental Shelf Research*, 12(2-3):257–286.

- Uchida, H., Kawano, T., Kaneko, I., and Fukasawa, M. (2008). In Situ Calibration of Optode-Based Oxygen Sensors. *Journal of Atmospheric and Oceanic Technology*, 25(12):2271–2281.
- University of Washington (2012). Seaglider Fabrication Center: <http://www.seaglider.washington.edu/>.
- Vaillancourt, R. D., Walker-Brown, C., Guillard, R. R. L., and Balch, W. M. (2004). Light backscattering properties of marine phytoplankton: relationships to cell size, chemical composition and taxonomy. *Journal of Plankton Research*, 26(2):191–212.
- van der Molen, J., Aldridge, J. N., Coughlan, C., Parker, E. R., Stephens, D., and Ruardij, P. (2012). Modelling marine ecosystem response to climate change and trawling in the North Sea. *Biogeochemistry*, 113(1-3):213–236.
- Van Engeland, T., Soetaert, K., Knuijt, A., Laane, R., and Middelburg, J. J. (2010). Dissolved organic nitrogen dynamics in the North Sea: A time series analysis (1995-2005). *Estuarine, Coastal and Shelf Science*, 89(1):31–42.
- Van Raaphorst, W., Malschaert, H., and Van Haren, H. (1998). Tidal resuspension and deposition of particulate matter in the Oyster Grounds, North Sea. *Journal of Marine Research*, 56(1):257–291.
- Vaquer-Sunyer, R. and Duarte, C. M. (2008). Thresholds of hypoxia for marine biodiversity. *Proceedings of the National Academy of Sciences of the United States of America*, 105(40):15452–7.
- Vermaat, J. E., McQuatters-Gollop, A., Eleveld, M. A., and Gilbert, A. J. (2008). Past, present and future nutrient loads of the North Sea: Causes and consequences. *Estuarine, Coastal and Shelf Science*, 80(1):53–59.
- Vested, H., Baretta, J. W., Ekebjærge, L., and Labrosse, A. (1996). Coupling of hydrodynamical transport and ecological models for 2D horizontal flow. *Journal of Marine Systems*, 8(3-4):255–267.

- Vichi, M., Pinardi, N., and Masina, S. (2007). A generalized model of pelagic biogeochemistry for the global ocean ecosystem. Part I: Theory. *Journal of Marine Systems*, 64(1-4):89–109.
- Vichi, M., Ruardij, P., and Baretta, J. W. (2004). Link or sink: a modelling interpretation of the open Baltic biogeochemistry. *Biogeosciences*, 1(1):79–100.
- Weston, K., Fernand, L., Mills, D. K., Delahunty, R., and Brown, J. (2005). Primary production in the deep chlorophyll maximum of the central North Sea. *Journal of Plankton Research*, 27(9):909–922.
- Weston, K., Fernand, L., Nicholls, J., Marca-Bell, A., Mills, D. K., Sivyer, D. B., and Trimmer, M. (2008). Sedimentary and water column processes in the Oyster Grounds: a potentially hypoxic region of the North Sea. *Marine environmental research*, 65(3):235–49.
- Weston, K., Jickells, T. D., Fernand, L., and Parker, E. R. (2004). Nitrogen cycling in the southern North Sea: consequences for total nitrogen transport. *Estuarine, Coastal and Shelf Science*, 59(4):559–573.
- Williams, P. and Jenkinson, N. (1982). A transportable microprocessor-controlled precise Winkler titration suitable for field station and shipboard use. *Limnology and Oceanography*, 27(3):576–584.
- Wunsch, C. (2010). Observational Network Design for Climate. In Hall, J., Harrison, D. E., and Stammer, D., editors, *Proceedings of OceanObs'09: Sustained Ocean Observations and Information for Society (Vol. 1)*, volume 1, pages 440–449, Venice, Italy. European Space Agency Publication.
- Zhang, J., Gilbert, D., Gooday, A. J., Levin, L., Naqvi, S. W. A., Middelburg, J. J., Scranton, M., Ekau, W., Peña, A., Dewitte, B., Oguz, T., Monteiro, P. M. S., Urban, E., Rabalais, N. N., Ittekkot, V., Kemp, W. M., Ulloa, O., Elmgren, R., Escobar-Briones, E., and Van der Plas, A. K. (2009a). Historical records of coastal eutrophication-induced hypoxia. *Biogeosciences*, 7:1443–1467.

Zhang, J., Gilbert, D., Gooday, A. J., Levin, L. A., Naqvi, W., Middelburg, J. J., Scranton, M., Ekau, W., Pena, A., Dewitte, B., Oguz, T., Monteiro, P. M. S., Urban, E., Rabalais, N. N., Ittekkot, V., Kemp, W. M., Ulloa, O., and Elmgren, R. (2009b). Natural and human-induced hypoxia and consequences for coastal areas: synthesis and future development. *Biogeosciences Discussions*, 6:11035–11087.



*Typography exists to honour content. [...] It is a craft by which the meaning of a text (or its absence of meaning) can be clarified, honoured and shared, or knowingly disguised.*

— Robert Bringhurst, 2004

#### COLOPHON

This document was typeset using the typographical look-and-feel classicthesis developed by André Miede. The style was inspired by Robert Bringhurst's seminal book on typography "*The Elements of Typographic Style*". classicthesis is available for both  $\text{\LaTeX}$  and  $\text{\LyX}$ :

<http://code.google.com/p/classicthesis/>

Happy users of classicthesis usually send a real postcard to the author, a collection of postcards received so far is featured here:

<http://postcards.miede.de/>

*Final Version* as of 4th April 2014 (classicthesis DRAFT).



## DECLARATION

---

I declare that the content of this thesis entitled *Hydrographic observations of oxygen and related physical variables in the North Sea and Western Ross Sea Polynya* was undertaken and completed by myself, unless otherwise acknowledged and has not been submitted in support of an application for another degree or qualification in this or any other university or institution.

*Norwich, United Kingdom, September 2013*

---

Bastien Yves Queste